(NASA-CP-10060-Pt-2) AIRBORNE WIND SHEAR N91-24140
DETECTION AND WARNING SYSTEMS: THIRD --THRU--
COMBINED MANUFACTURERS' AND TECHNOLOGISTS' N91-24156
CONFERENCE, PART 2 (NASA) 464 p CSCL 01C Unclas
G3/03 0003678

NASA Conference Publication 10060, Part 2
DOT/FAA/RD-91/2-II

Airborne Wind Shear Detection and Warning Systems

Third Combined Manufacturers' and Technologists' Conference

Compiled by
Dan D. Vicroy
and Roland L. Bowles
NASA Langley Research Center
Hampton, Virginia

Herbert Schlickenmaier
Federal Aviation Administration
Washington, D.C.

Proceedings of a conference sponsored by the
National Aeronautics and Space Administration
and the Federal Aviation Administration
and held in Hampton, Virginia
October 16–18, 1990

January 1991

NASA
National Aeronautics and
Space Administration

Langley Research Center
Hampton, Virginia 23665-5225

FOREWORD

The Third Combined Manufacturers' and Technologists' Conference was hosted jointly by NASA Langley Research Center (LaRC) and the Federal Aviation Administration (FAA) in Hampton, Virginia on October 16-18, 1990. The meeting was co-chaired by Dr. Roland Bowles of LaRC and Herbert Schlickenmaier of the FAA. Dan Vicroy of LaRC served as the Technical Program Chairperson and Carol Lightner of the Bionetics Corporation was the Administrative Chairperson.

The purpose of the meeting was to transfer significant ongoing results of the NASA/FAA joint Airborne Wind Shear Program to the technical industry and to pose problems of current concern to the combined group. It also provided a forum for manufacturers to review forward-look technology concepts and for technologists to gain an understanding of the problems encountered by the manufacturers during the development of airborne equipment and the FAA certification requirements.

The present document has been compiled to record the essence of the technology updates and discussions which followed each. Updates are represented here through the unedited duplication of the vugraphs, which were generously provided by the respective speakers. When time was available questions were taken form the floor; if time was not available questions were requested in writing. The questions and answers are included at the end of each presentation. A general question and answer session was conducted at the end of each day and is included at the end of report along with closing remarks.

TABLE OF CONTENTS

Part 1*

FOREWORD i

TABLE OF CONTENTS iii

SESSION I. -- Terms of Reference

A. Airline Industry Intentions 3
Frank Tullo, Air Transport Association
B. Wind Shear Program in France
1) Overview 19
Bernard Ades, DGAC/SFACT
2) LIDAR Studies on Microbursts 29
Y. Aurenche and J.L. Boulay, ONERA
3) RADAR Performance Experiments 37
C. Le Roux, DGAC/STNA
4) MEGASODAR Experiment 57
Alain Donzier, REMTECH

SESSION II. -- Case Study

A. Integrated Data Analysis of July 7, 1990 Microburst 63
Dave Hinton, NASA Langley
B. Model Comparison of July 7, 1990 Microburst 81
Dr. Fred Proctor, MESO

SESSION III. -- Flight Management

A. Microburst Avoidance Simulation Tests 107
Dr. John Hansman, MIT
B. Wind Shear Training Applications for 91/135 143
Capt. Ed Arbon, Flight Safety Foundation
C. Determining Target Pitch Angle 153
Herb Schlickenmaier, FAA
D. Probabilistic Reasoning for Wind Shear Avoidance 161
Dr. Robert Stengel, Princeton University
Alex Stratton, Princeton University

SESSION IV. -- Sensor Fusion & Flight Evaluation

A. Integration of Weather Sensing Devices 177
Jim Daily, Honeywell Sperry
B. NASA Langley Flight Test Program 201
Mike Lewis, NASA Langley

SESSION V. -- TDWR Data Link / Display

A. TDWR Information on the Flight Deck 227
Dave Hinton, NASA Langley
B. Orlando Experiment 243
Dr. Steve Campbell, MIT Lincoln Laboratory

---

* Published under separate cover.

PRECEDING PAGE BLANK NOT FILMED

C. Integration of the TDWR and LLWAS Wind Shear Detection System 263
Larry Cornman, National Center for Atmospheric Research
D. A Status Report on the TDWR Efforts in the Denver Area 299
Wayne Sand, National Center for Atmospheric Research
E. Thermodynamic Alerter for Microbursts 351
Dr. Peter Eccles, MITRE

SESSION VI. -- Heavy Rain Aerodynamics

A. Status of Heavy Rain Tests 367
Gaudy Bezos, NASA Langley
B. Heavy Rain Field Measurements 395
Ed Melson, NASA Wallops
C. Estimate of Heavy Rain Performance Effect 425
Dan Vicroy, NASA Langley

SESSION VII. -- 2nd Generation Reactive Systems

A. Status of Sundstrand Research 453
Don Bateman, Sundstrand
B. Temperature Lapse Rate as an Adjunct to Wind Shear Detection 479
Terry Zweifil, Honeywell Sperry

Part 2

SESSION VIII. -- Airborne LIDAR

A. NASA Langley / Lockheed Research Status 509
Russel Targ, Lockheed
B. Continuous Wave Laser 527
Dr. Loren Nelson, OPHIR Corporation
C. Status of 2 Micron Laser Technology Program 555
Mark Storm, NASA Langley
D. Avionic Laser Multisensor Program at Litton Aero Products 577
Rod Benoist, Litton

SESSION IX. -- Airborne Passive Infrared

A. Status of NASA's IR Wind Shear Detection Research 589
Dr. Burnell McKissick, NASA Langley
B. Status of Turbulence Prediction Systems' AWAS III 609
Pat Adamson, Turbulence Prediction Systems
C. Status of Colorado State Universities' IR Research 637
Dr. Pete Sinclair, Colorado State University

SESSION X. -- Airborne Doppler Radar / Industry

A. Status of General Motors Hughes Electronics Research 681
Dr. Brian Gallagher, Delco
Mark Selogie, Hughes
B. Saberliner Flight Test 714
Bruce Mathews, Westinghouse
C. Status of Bendix Research 755
Daryal Kuntman, Bendix
D. Status of Collins Research 767
Roy Robertson, Collins

SESSION XI. -- Airborne Doppler Radar / NASA

A. Clutter Modeling of the Denver Airport and Surrounding Areas 785
   Steve Harrah, NASA Langley
   V. Delnore, Lockheed
   R. Onstott, ERIM

B. Radar Simulation Program Up-grade & Algorithm Development 837
   Charles Britt, RTI

C. Signal Processing Techniques for Clutter Filtering & Wind Shear Detection 869
   Dr. Ernest Baxa, Clemson University
   M. Deshpande, VIGYAN Corp.

D. Airborne Radar Simulation Studies of the Denver July 11, 1988 Microburst 913
   Charles Britt, RTI
   E. M. Bracalente, NASA Langley

E. Description, Characteristics, & Testing of the NASA Airborne Radar 937
   W. R. Jones, NASA Langley
   O. Altiz, Rockwell International
   P. Schaffner, NASA Langley
   J. H. Schrader, RTI
   H. J. C. Blume, NASA Langley

GENERAL QUESTIONS AND ANSWERS 981

CLOSING REMARKS 987

APPENDIX - List of Attendees 991

Session VIII. Airborne LIDAR

PRECEDING PAGE BLANK NOT FILMED

Session VIII. Airborne LIDAR

N91-24141

NASA Langley / Lockheed Research Status
Russel Targ, Lockheed

PRECEDING PAGE BLANK NOT FILMED

RDD

Lockheed
LMSC-F415048

CLASS

COHERENT LIDAR AIRBORNE SHEAR SENSOR

WINDSHEAR AVOIDANCE

OCTOBER 1990

Prepared by

RUSSELL TARG

Electro-Optical Sciences Directorate
Research & Development Division
LOCKHEED MISSILES & SPACE COMPANY, INC.
3251 Hanover Street
Palo Alto, California 94304

THE CLASS PROGRAM

The coherent lidar airborne shear sensor (CLASS) is an airborne CO_2 lidar system being designed and developed by Lockheed Missiles & Space Company, Inc. (LMSC) under contract to NASA Langley Research Center. The goal of this program is to develop a system with a 2- to 4-kilometer range that will provide a warning time of 20 to 40 seconds, so that the pilot can avoid the hazards of low-altitude windshear under all weather conditions. It is a predictive system, which will warn the pilot at time T about a hazard that the aircraft will experience at some later time, $T + \tau$. The ability of the system to provide predictive warnings of clear-air turbulence will also be evaluated.

In order to validate the performance of CLASS, LMSC, together with NASA Langley Research Center, will conduct a 1-year flight-evaluation program. In this program, we will measure the line-of-sight wind velocity from a wide variety of windfields. Measurements made by airborne lidar will be compared with measurements of the same windfields obtained by an airborne radar, an accelerometer-based reactive wind-sensing system, and a ground-based Doppler radar. The success of the airborne lidar system will be determined by its correlation with the windfield as indicated by the onboard reactive system, which indicates the winds actually experienced by the NASA Boeing 737 aircraft.

THE WINDSHEAR PROBLEM

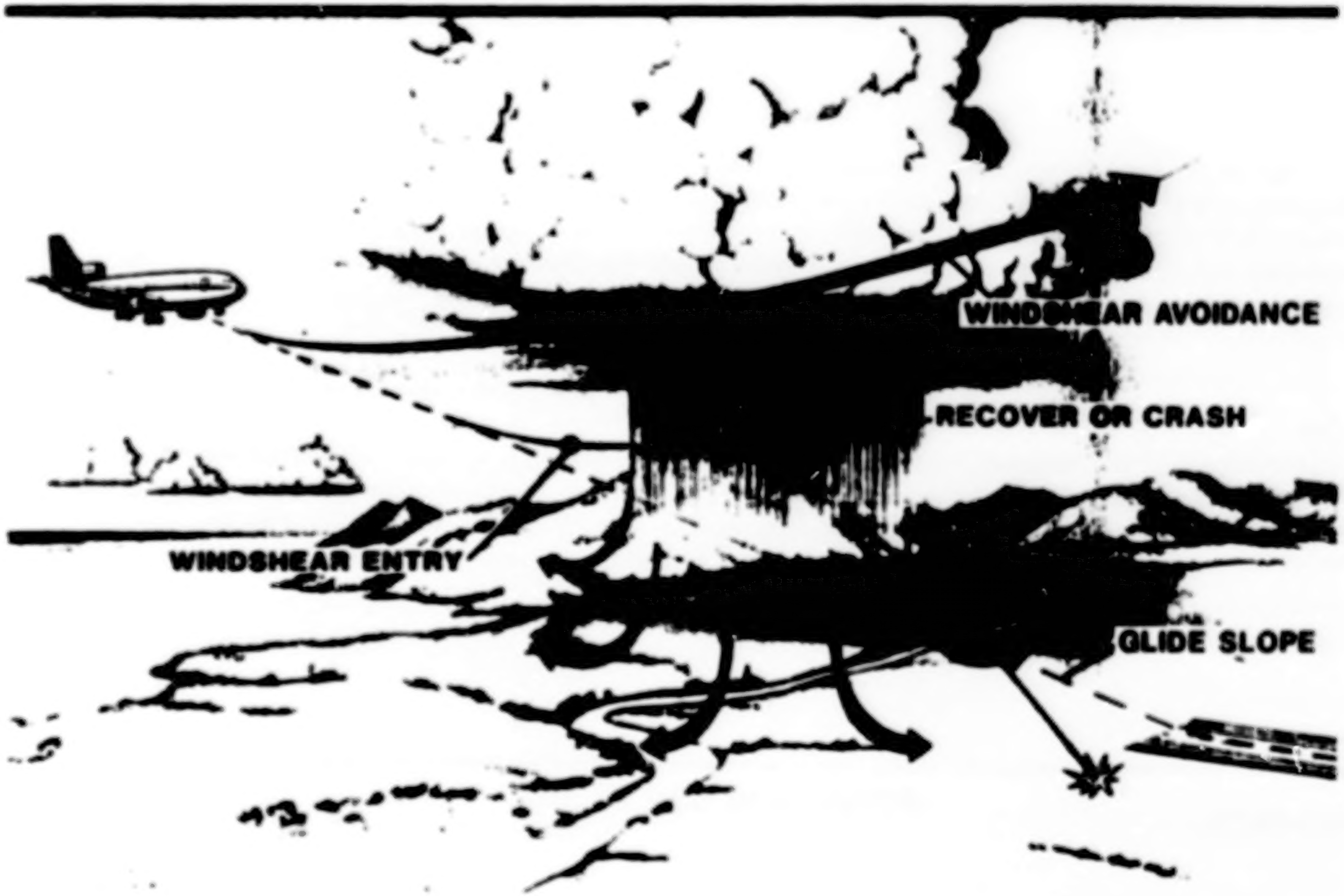
WINDSHEAR AVOIDANCE
RECOVER OR CRASH
WINDSHEAR ENTRY
GLIDE SLOPE

ORIGINAL PAGE IS
OF POOR QUALITY

AIRBORNE WINDSHEAR DETECTION: GENERAL REQUIREMENTS

- MEASURE LINE-OF-SIGHT COMPONENTS OF WIND VELOCITY FROM AIRCRAFT
- DETECT THUNDERSTORM DOWNBURST EARLY IN ITS DEVELOPMENT
- EMPHASIZE AVOIDANCE RATHER THAN RECOVERY
- RESPOND IN REAL TIME WITH LOW FALSE-ALARM RATE
- MONITOR APPROACH PATH, RUNWAY, AND TAKEOFF PATH
- OPERATE IN BOTH RAIN AND CLEAR-AIR CONDITIONS
- OPERATE RELIABLY WITH MINIMUM MAINTENANCE IN AIRCRAFT ENVIRONMENT

TECHNICAL REQUIREMENTS

The pilot should have as much time as possible to make an informed decision as to whether he will land or go around. If we consider an approach velocity of 100 meters per second (approximately 200 miles per hour), then a 3-kilometer look-ahead range will give the pilot a 30-second warning of a windshear hazard ahead. From our conversations with airline and military pilots, it appears that 30 seconds is an optimum warning time. A longer time is not appropriate since windshear formation is dynamic and changes on a time scale of about 30 seconds. Lockheed has designed the Coherent Lidar Airborne Shear Sensor (CLASS) to meet these requirements.

The CLASS system can give the pilot information about the windshear threat from his present position, extending 3 kilometers ahead. This can be conveniently accomplished by measuring and displaying ten 300-meter segments of the flight path.

To make a land/no-land decision, it is sufficient to measure wind velocity to an accuracy of 1 meter per second (approximately 2 miles per hour). The CLASS flight computers will continuously update the windshear display and alert the pilot by auditory signals if there is a windshear hazard. CLASS does not require the pilot to monitor the sensing equipment or display.

Sensing Range	**2 to 4 km or more**
Range Resolution	**0.3 km**
Velocity Resolution	**approximately 1 m/s**
Advance Warning Time	**20 to 40 s**

SYSTEMS SPECIFICATIONS RATIONALE

DESIGN ELEMENT	SELECTION	REASON
WAVELENGTH	10.6 μm	EYE SAFETY/MATURITY
LASER TYPE	RF-WAVEGUIDE	RELIABILITY
PULSE ENERGY	10 mJ	4 km RANGE
PULSE DURATION	2 μs	300 m RES./<1 m/s VELOCITY ERROR
PULSE REPETITION RATE	100 Hz	COVERAGE/PULSE AVERAGING
DETECTOR	PV HgCdTe	QUANTUM NOISE LIMITED PERFORMANCE
COOLING	LIN. MECH. REFRIG.	NO EXPENDABLES
TELESCOPE DIAMETER	15 cm	APPROPRIATE FOR 4-km RANGE
TELESCOPE TYPE	OFF-AXIS PARABOLOID	COST
SCANNING CAPABILITY	50° NOMINAL	MICROBURST GEOMETRY
SIGNAL PROCESSOR	POLY-PULSE PAIR	EXPERIMENTAL FLEXIBILITY
LASER LIFETIME	>2000 h	DEMONSTRATE OPERATIONAL PERFORMANCE

DOPPLER WIND VELOCITY MEASUREMENT

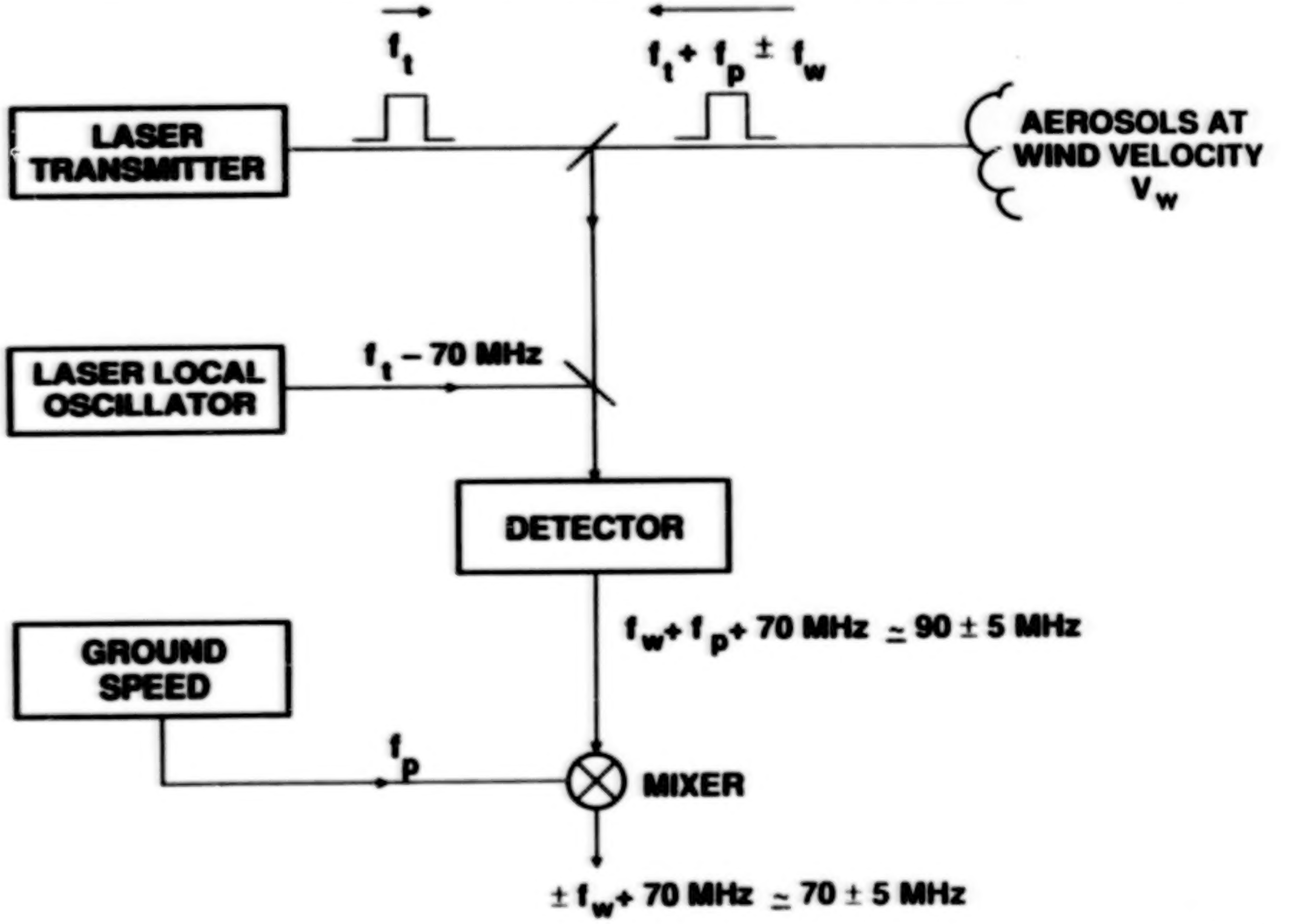

LASER TRANSMITTER

f_t

$f_t + f_p \pm f_w$

AEROSOLS AT WIND VELOCITY V_w

LASER LOCAL OSCILLATOR

$f_t - 70$ MHz

DETECTOR

$f_w + f_p + 70 \text{ MHz} \simeq 90 \pm 5 \text{ MHz}$

GROUND SPEED

f_p

MIXER

$\pm f_w + 70 \text{ MHz} \simeq 70 \pm 5 \text{ MHz}$

X00047/001PGM

CLASS LASER WINDSHEAR DETECTOR BLOCK DIAGRAM

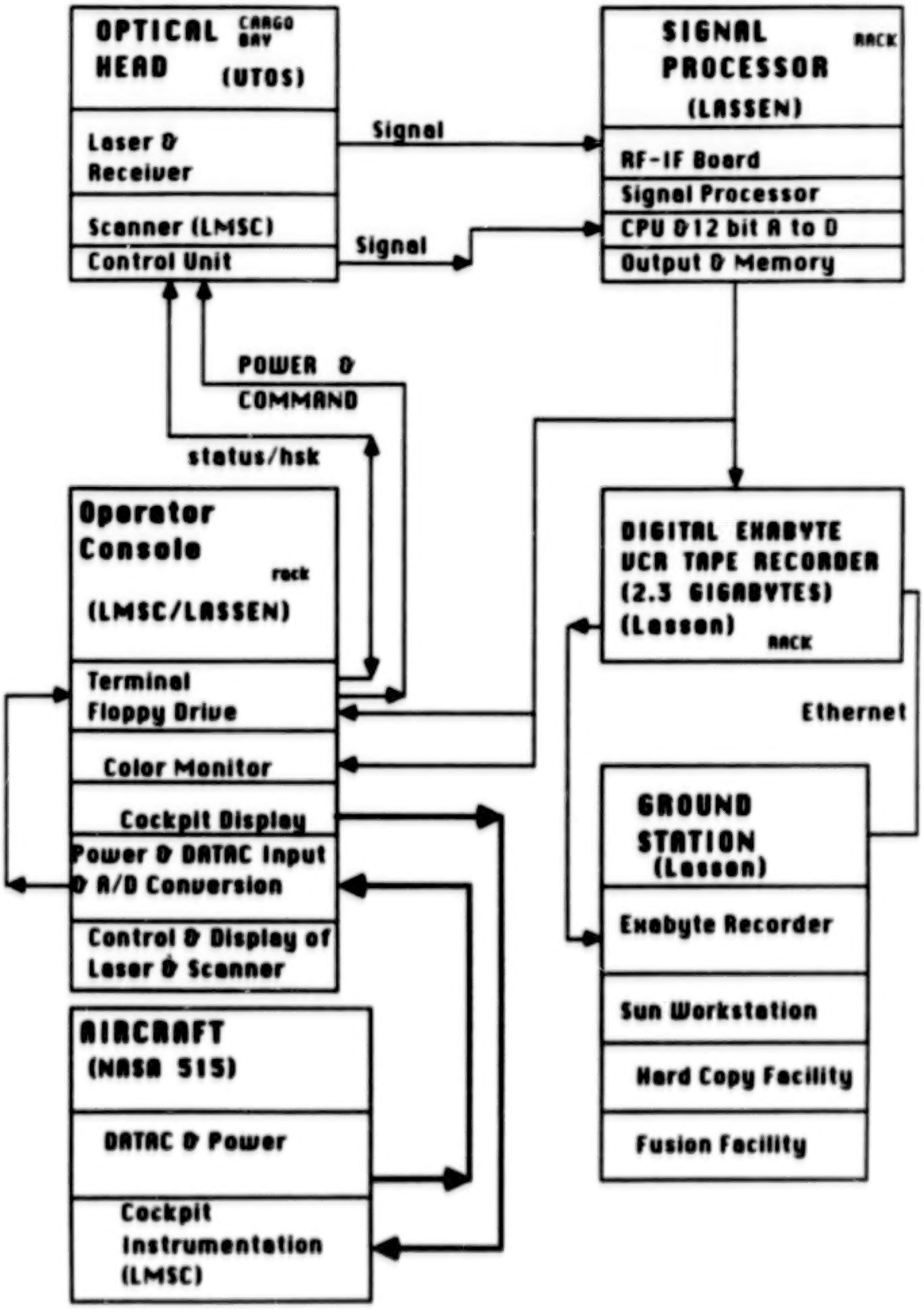
OPTICAL HEAD CARGO BAY (UTOS)
Laser & Receiver
Scanner (LMSC)
Control Unit
Signal
Signal
SIGNAL PROCESSOR RACK (LASSEN)
RF-IF Board
Signal Processor
CPU & 12 bit A to D
Output & Memory
POWER & COMMAND
status/hsk
Operator Console rack (LMSC/LASSEN)
Terminal Floppy Drive
Color Monitor
Cockpit Display
Power & DATAC Input & A/D Conversion
Control & Display of Laser & Scanner
DIGITAL EXABYTE VCR TAPE RECORDER (2.3 GIGABYTES) (Lassen) RACK
Ethernet
GROUND STATION (Lassen)
Exabyte Recorder
Sun Workstation
Hard Copy Facility
Fusion Facility
AIRCRAFT (NASA 515)
DATAC & Power
Cockpit Instrumentation (LMSC)

BLOCK DIAGRAM USING PULSED LASER

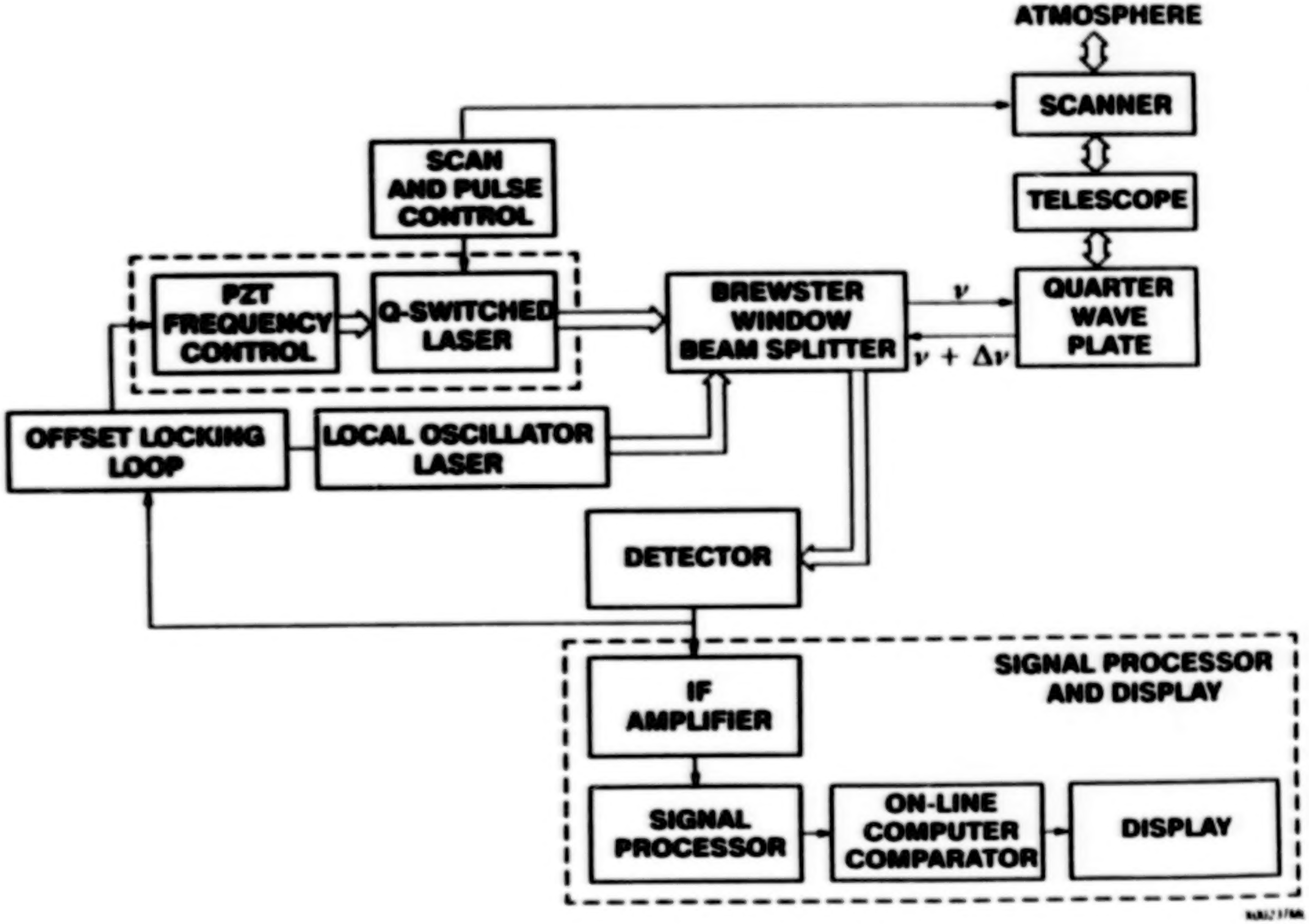

ATMOSPHERE

SCANNER

TELESCOPE

QUARTER WAVE PLATE

SCAN AND PULSE CONTROL

PZT FREQUENCY CONTROL

Q-SWITCHED LASER

BREWSTER WINDOW BEAM SPLITTER

ν

$\nu + \Delta\nu$

OFFSET LOCKING LOOP

LOCAL OSCILLATOR LASER

DETECTOR

SIGNAL PROCESSOR AND DISPLAY

IF AMPLIFIER

SIGNAL PROCESSOR

ON-LINE COMPUTER COMPARATOR

DISPLAY

CLASS MECHANICAL DESIGN SYSTEM SOLID MODEL

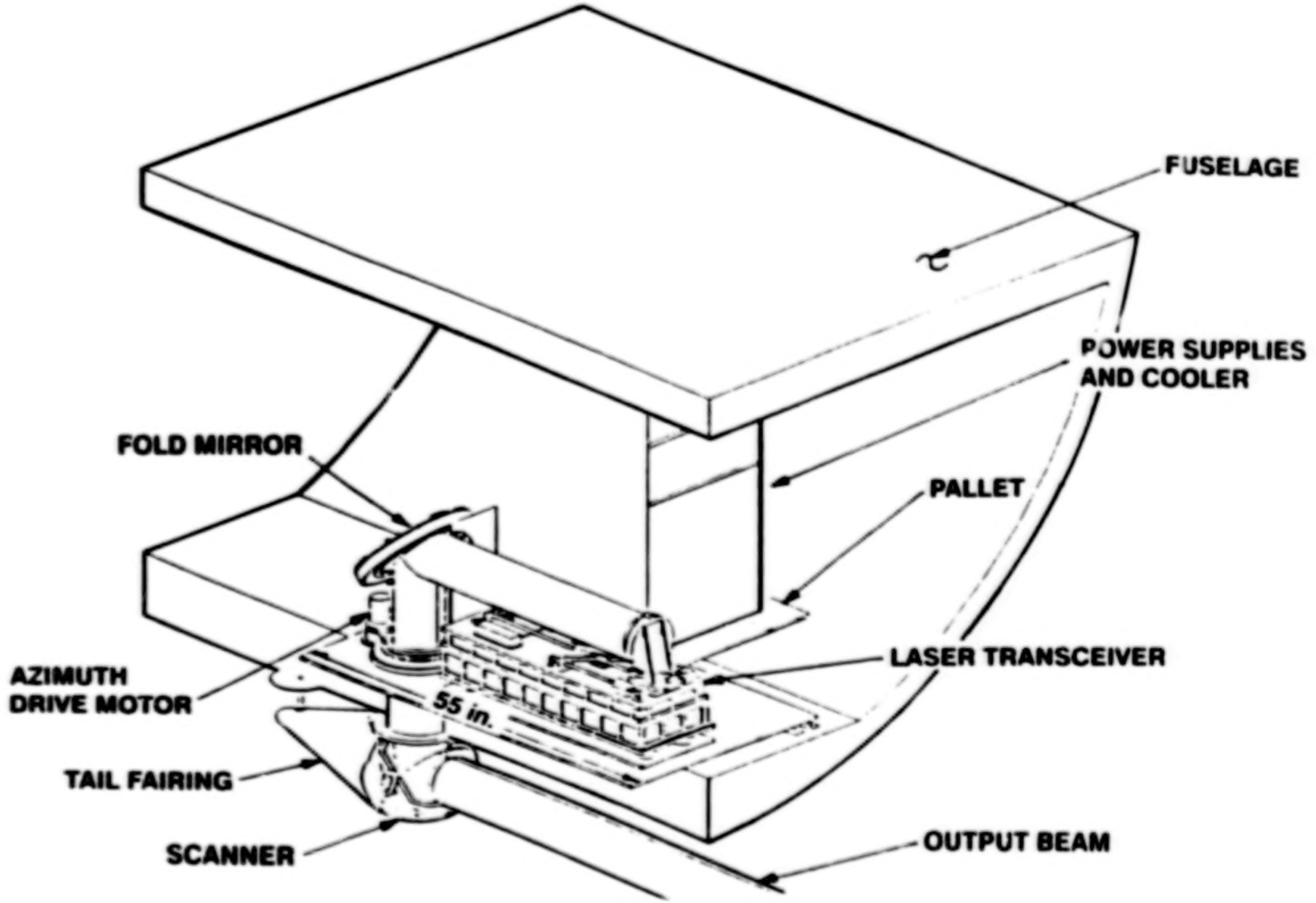
FUSELAGE
POWER SUPPLIES AND COOLER
FOLD MIRROR
PALLET
LASER TRANSCEIVER
AZIMUTH DRIVE MOTOR
55 in.
TAIL FAIRING
SCANNER
OUTPUT BEAM

MAXIMUM RANGE VERSUS PULSE ENERGY
NOAA LIDAR MEASURED MAY 24, 1990

3-PULSE AVERAGE, 10.6-μm LIDAR 0.9-deg ELEVATION ANGLE

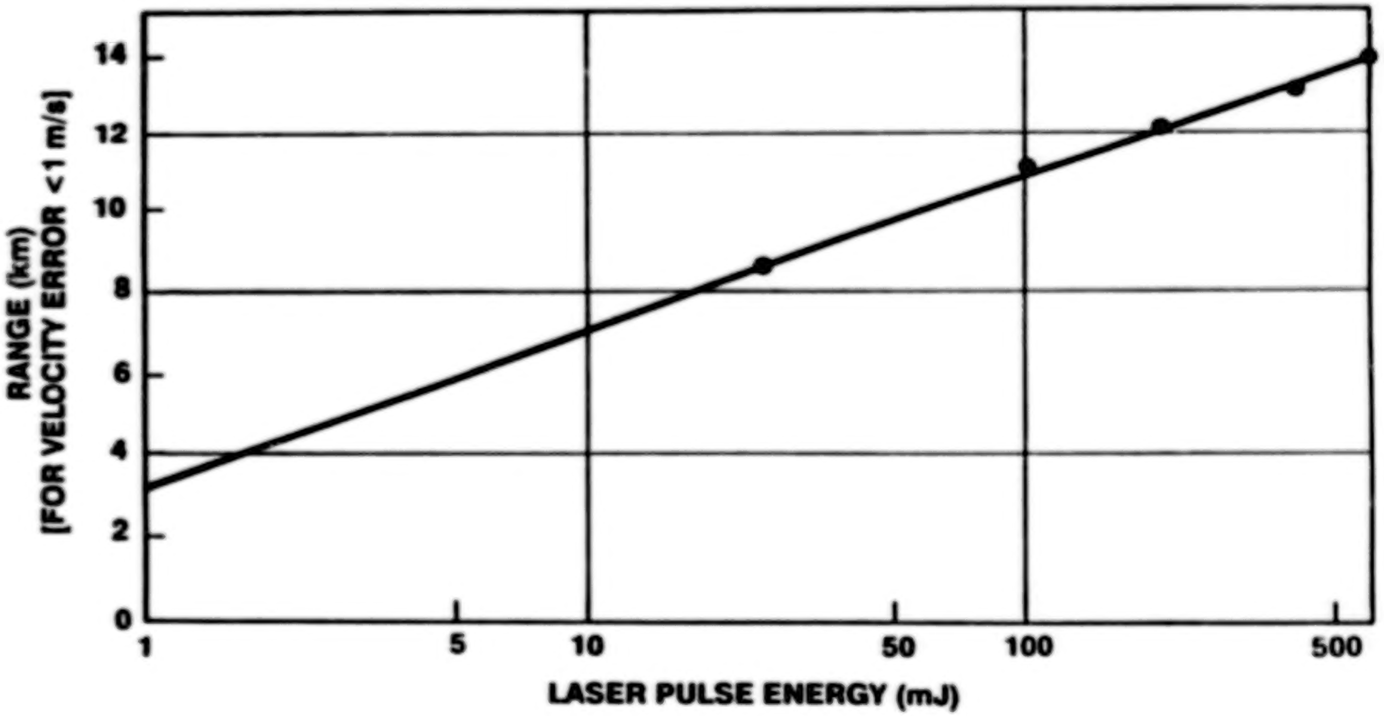

VELOCITY ERROR VS. RANGE
10 MICRON, CLASS LIDAR, 10 mJ
15 CM MIRROR, 1 DB/KM EXTINCTION

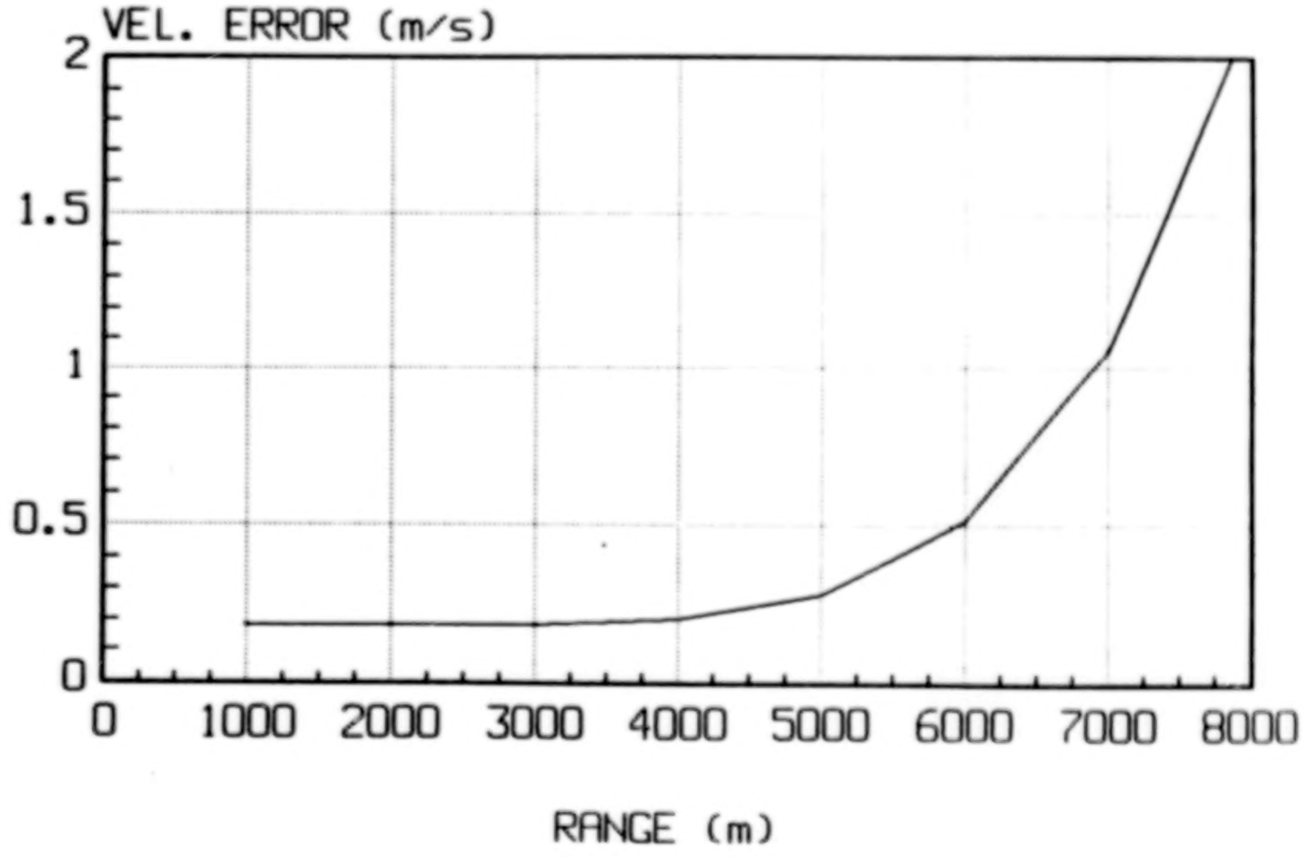

RANGE-AZIMUTH DISPLAY FOR A 30-KNOT "DRY" DENVER/STAPLETON MICROBURST, ILLUMINATED BY A 5-mJ CO_2 LIDAR 4 km FROM THE MICROBURST CORE

a. RADIAL WIND VELOCITY CONTOURS

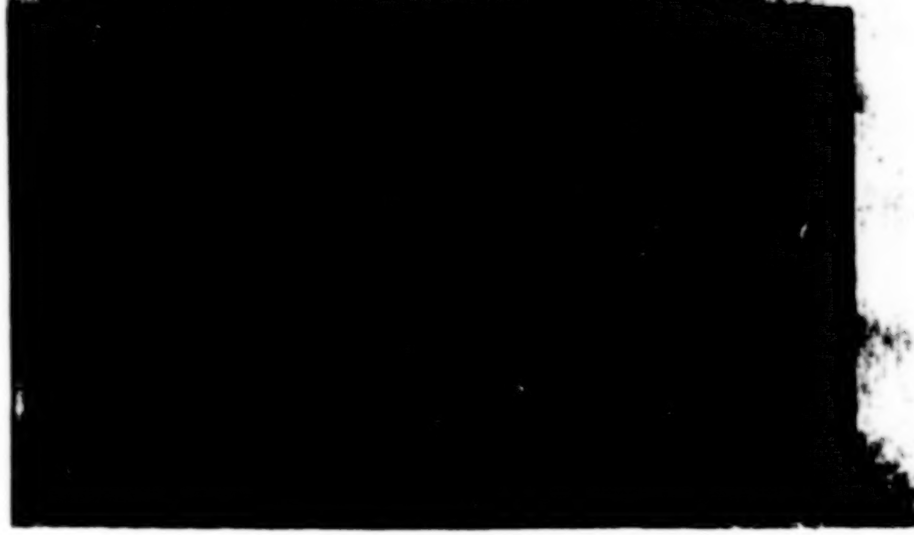

b. HAZARD INDEX
(RED = HAZARD INDEX (F-FACTOR) > 0.1)

ORIGINAL PAGE IS
OF POOR QUALITY

RANGE IN RAIN OF A 10.6-μm SYSTEM WITH A 10-mJ CO_2 LIDAR

It is well known that the 10.6-micron radiation from CO_2 lasers is attenuated by rain, and that will limit the usefulness of such systems in conditions of heavy rain. A systems analysis of an integrated windshear detection and avoidance system will take this into account. The figure shows the effects of rain on range, and indicates that a 10 millijoule CO_2 lidar is able to penetrate rain of moderate levels for a sufficient distance to give a warning of 10 to 20 seconds to a pilot flying into a potentially dangerous situation.

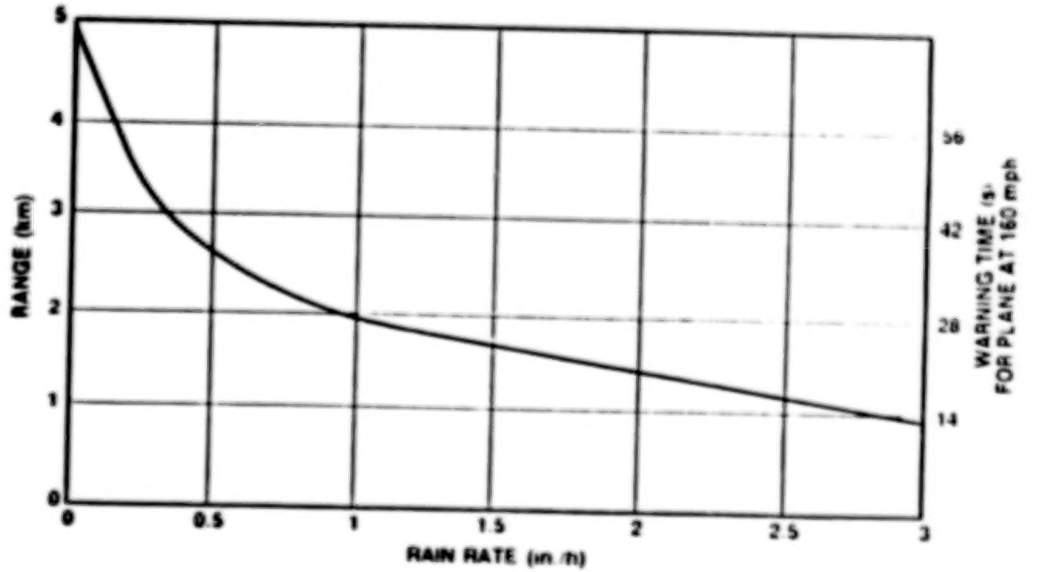

ATTENUATION DUE TO FOG

The data shown here illustrate the measured attenuation experienced by lasers of three different wavelengths. The critical fact to notice is that as the fog increases in density to the point where the red laser, with a 0.63-μm wavelength, is attenuated by more than 40 decibels, the CO_2 laser, at 10.6-μm wavelength, has less than 3-decibel loss.

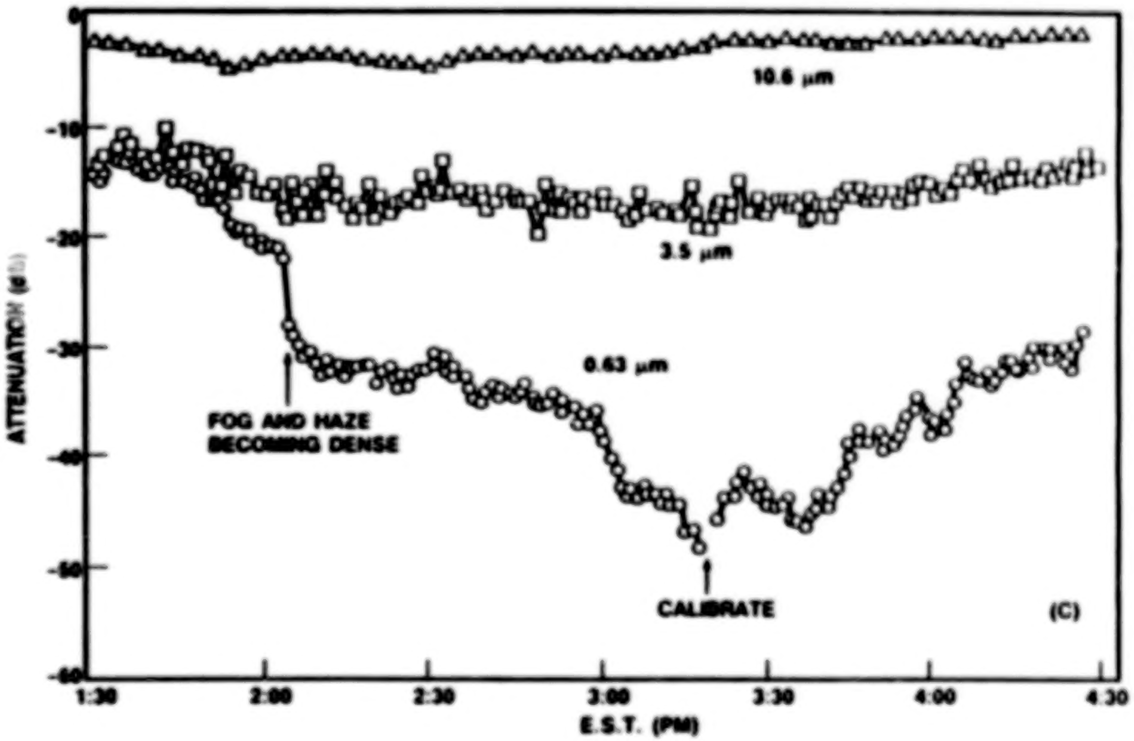

NASA Langley / Lockheed Research Status - Questions and Answers

Q: JAMES MEGAS (Northwest Air Lines) - What do you feel the cost of an operational coherent pulsed LIDAR would be? What are the trade offs that you feel could be made to reduce the cost?

A: RUSSEL TARG (Lockheed) - The price will be negotiated between our assessment of what it takes to make it and what the airlines find a conceivably acceptable price. I think that's probably the way the price of everything is determined. From our initial inquiries, what it appears is that there's a minimum price under which we think it can't be made and a maximum price above which the airlines wouldn't conceivably pay. We will price this thing some place within there assuming that that's possible. To be serious, for the thing to be ready to be installed into an airplane, it has to be manufactured and installed for about $100,000 or less. That's going to be a high price for the airlines and a challenging price for the manufacturer. At that price it seems to cause equal pain for everybody so it's probably the right price. The big systems that go into the airborne LIDAR are the laser, the photo detector, the scanner and the signal processor. We're going to have to take appropriately big bites out of each of those systems in accordance with what they presently cost to produce. Consequently, in order to even think about putting a LIDAR system into an airplane, the price of the laser has to be greatly reduced from the one of a kind system that we're presently using. We're so late in the day I think this is probably not a good time to go into the kinds of trades that we would do. I can say that choosing between a CO_2 system and a 2 micron system is not a big effect in the ultimate price of the system. There are several different components which I enumerated before in addition to the electronics to hold them all together. So I think that a 100k target is what we'll be looking at and that will be a challenge for any manufacturer in my opinion.

Q: BRUCE MATTHEWS (Westinghouse) - What are the impacts on range and performance of things other than rain? (Rain was already addressed). What are the impacts from fog, dust, smog and other aerosols?

A: RUSSEL TARG (Lockheed) - For the ten micron system the impact of fog is minimal. There have been experiments at Bell Labs measuring the performance of a lighthouse system in fog such as would attenuate a visible beam by 10^5 attenuation and the attenuation for the fog was essentially nil. So I would say that although you could create a fog situation presumably, and I have not seen more detailed data than Bell Labs had, but fog is not a significant problem for the 10 micron LIDAR system. Somebody else is going to have to comment about the 2 micron because I'm ignorant of that. Dirt and dust in the air enhances a performance of all the LIDAR systems so all things being equal this system will work better in Los Angeles than it would in Boulder. Dirty air is a friend of the CO_2 system.

Q: JOE YOUSSEFI (Honeywell) - Will the landing gear be in the way? Will it be a problem for the LIDAR as installed on the NASA aircraft? Are you going to compensate for aircraft attitude, pitch and roll?

A: RUSSEL TARG (Lockheed) - Yes, the landing gear will be a problem, it's right in our field of view. Luckily during the experimental phase of the program we're always going to conduct our experiment wheels up. So during the course of the experiment the landing gear will not be a problem. Presumably on a commercial aircraft we will be located up front, forward of the landing gear, so our scan will not be interfered with by landing gear. And the answer to the second question is affirmative. We will compensate for pitch and roll in real time as the information is given to us by the DATAC. Our two axis ball scanner is all programmed and has the capability to compensate for pitch and roll.

Q: ED LOCKE (Thermo Electron Technologies) - What's the frequency stability of the CO_2 laser?

A: RUSSEL TARG (Lockheed) - It is 200 kilohertz, which is just what you would require in order to maintain the measurement capability that we're looking for which is a meter per second.

Q: TERRY ZWEIFEL (Honeywell Sperry) - Do you anticipate any problems with the optical alignment with the wild temperature swings the airplane might see in G loadings during landing and stuff? Is that going to be a problem?

A: RUSSEL TARG (Lockheed) - The laser that we're building is actively frequency stabilized and is bolted down to a very rugged frame which I showed in the illustration. It's also actively water cooled to provide additional frequency stabilization. I don't anticipate any temperature fluctuations to cause a problem for the system. It's built so that it has a very high frequency loop, that is, we're feeding back at greater than a kilohertz rate so we think that any motion of the airplane will be very small indeed compared to the speed of the feed back loop controlling the laser frequency stability.

ROLAND BOWLES (NASA Langley) - That airplane is carrying so much equipment that we are really having some air conditioner burdens on it. That system will be basically cabin ambient down there and we may very well bit the bullet on that airplane and really upgrade the air conditioning system on it. You must remember, we're not building product runs for consumption in a civil system. The NASA role in this program is to prove the feasibility of the technology. We leave it to you airlines and manufacturers to work out the market place dynamics.

Session VIII. Airborne LIDAR

N91-24142

Continuous Wave Laser
Dr. Loren Nelson, OPHIR Corporation

THIRD ANNUAL MANUFACTURER'S AND TECHNOLOGISTS'
AIRBORNE WIND SHEAR REVIEW BRIEFING

NASA LANGLEY RESEARCH CENTER
October 17, 1990

CONTINUOUS WAVE LASER FOR WIND SHEAR DETECTION

Dr. Loren Nelson
OPHIR Corporation
3190 S. Wadsworth Blvd.
Lakewood, CO 80227
(303) 986-1512

ABSTRACT

We present results of our development of a continuous-wave heterodyne carbon dioxide laser which has wind-shear detection capabilities. This development was sponsored by the FAA under their SBIR program under contract number DTRS-57-87-C-00111.

The goal of the development was to investigate the lower cost CW (rather than pulsed) lidar option for look-ahead wind shear detection from aircraft. The device also has potential utility for ground based wind-shear detection at secondary airports where the high cost ($6,000,000) of a Terminal Doppler Weather Radar (TDWR) system is not justifiable. The CW-Lidar system presented here was fabricated for a hardware cost of less than $100,000.

Details of the design and fabrication of the OPHIR CW 10.6μ heterodyne doppler lidar wind shear detector are presented. Shot noise limited heterodyne signal detection has been attained. Field wind observations from the CW-Lidar are presented. The OPHIR CW-Lidar was operated at Stapleton Airport (Denver, CO) on an intermittent basis during the months of August and September 1990. The look angle of the device was up the landing glide-slope of an active runway. No wind shear events occured during our observation period. The 3.5 watt CW output power of our propotype sensor is shown to be marginal for achieving reliable sensor echo returns during clear air at Stapleton. When the air is filled with blowing dust or precipitation particles, echo spectra peaks of 10 to 30 db can be observed and velocity resolved. The best way to increase sensitivity of our proof-of-concept prototype further is by changing from our single-channel scanning spectral analyzer to a FFT or multi-channel spectral analyzer. A multiplex advantage of 500X should result, improving sensitivity by 13.5 db with the same integration time. The proof-of-concept prototype is difficult to maintain in optical alignment, and would require significant redesign to become airworthy. A more practical near-term utilization may be in ground based use at secondary airports to monitor possible wind shear hazards.

The final two viewgraphs, presented for related general interest, illustrate a new commercial capability to monitor supercooled water aircraft icing conditions above airports. Our subsidiary (Radiometrics Corporation) markets a millimeter wave device which can be used to remotely monitor aircraft icing conditions. We detected and quantified such conditions at the time of the Stapleton AP icing related crash of the Federal Express Cessna 208 N80FE at 0240Z on Feb 27, 1990. Our data set has been presented to the NTSB for use in their investigation.

PRECEDING PAGE BLANK NOT FILMED

1. DISCUSSION - VIEWGRAPH 1

This viewgraph briefing will discuss the development and field testing of a cost-effective heterodyne continuous wave (CW) wind-shear doppler lidar. The CW output power is 3.5 watts at 10.6µ through an 8" telescope.

This research was sponsored by the FAA under their SBIR Contract Number DTRS-57-87-C-00111.

We will discuss proof-of-concept prototype hardware design, field testing at Stapleton AP, and conclusions drawn from the research.

AIRBORNE WIND SHEAR REVIEW
NASA LANGLEY RESEARCH CENTER
OCTOBER 17, 1990

CW LASER FOR WIND SHEAR DETECTION

- Dr. Loren Nelson
- OPHIR Corporation
- 3190 S. Wadsworth Blvd.
- Lakewood, CO 80227
- (303) 986-1512

FAA SBIR CONTRACT NO. DTRS-57-87-C-00111

- Prototype Hardware Design
- Field Testing (Stapleton AP)
- Conclusions

2. DISCUSSION - VIEWGRAPH 2

A functional diagram of the CW heterodyne lidar is shown. By using an acousto-optic modulator at 27.1 Mhz offset, we can see wind both toward and away from the lidar in this heterodyne system. The detector is a liquid nitrogen cooled Mercury Cadmium Telluride photovoltiac sensor. The spectrum analyzer is a commercial single-scanning channel spectrum analyzer. Sweep time is 0.2 seconds, and 5 sweeps are averaged before display. There are 500 digitized data records written to disk during each sweep. Sweep length is +/- 3.7 Mhz, centered on 27.1 Mhz. This corresponds to a velocity range of +/- 10 m/s. Some runs were also made at a velocity range of +/- 25 m/s.

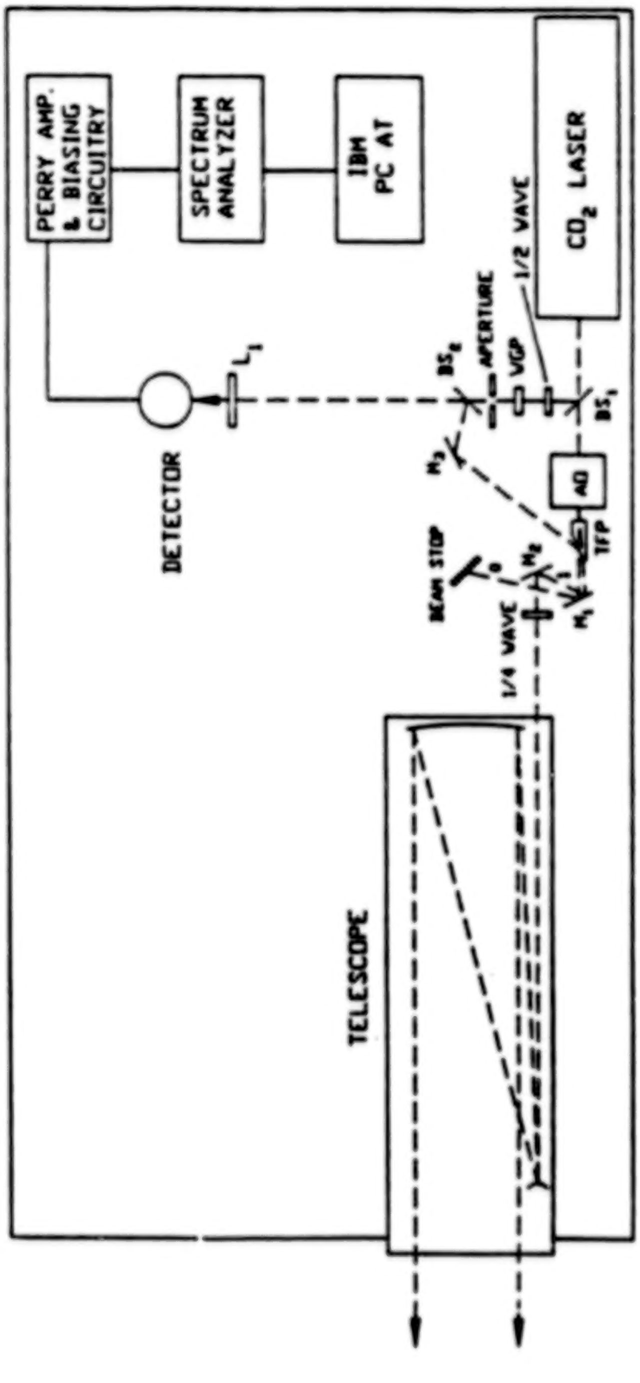
PERRY AMP. & BIASING CIRCUITRY
SPECTRUM ANALYZER
IBM PC AT
CO_2 LASER
1/2 WAVE
APERTURE
VGP
BS_2
BS_1
L_1
DETECTOR
M_3
AO
TFP
M_2
M_1
BEAM STOP
1/4 WAVE
TELESCOPE

3. DISCUSSION - VIEWGRAPH 3

Illustrates the location and orientation of the lidar van and beam during tests at Stapleton AP.

OPHIR CW WIND-SHEAR LIDAR

- LOCATION DURING STAPLETON AP TESTS

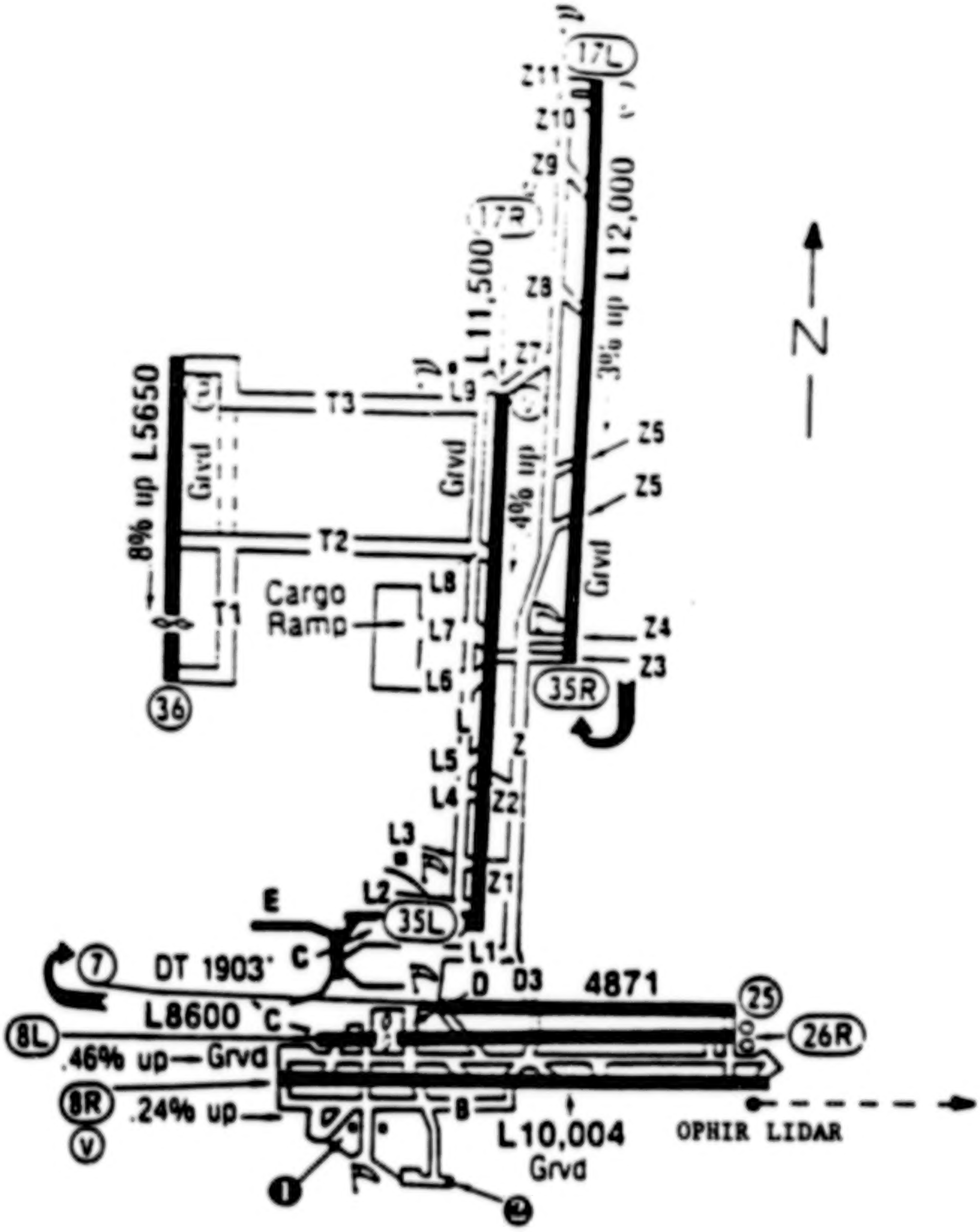

17L
Z11
Z10
Z9
17R
L11,500
Z8
Z7
3% up L12,000
N
L9
T3
.8% up L5650
Grvd
Grvd
Z6
Z5
4% up
Grvd
T2
L8
Cargo Ramp
T1
L7
Z4
L6
Z3
36
35R
L
Z
L5
L4
Z2
L3
Z1
L2
E
35L
C
L1
7
DT 1903'
D
D3
4871
25
L8600
C
8L
26R
.46% up—Grvd
8R
.24% up
B
V
L10,004
Grvd
OPHIR LIDAR
1
2

4. DISCUSSION - VIEWGRAPH 4

A color photograph of the Lidar Portable Van on location at Stapleton Airport.

ORIGINAL PAGE IS
OF POOR QUALITY

5. DISCUSSION - VIEWGRAPH 5

Data from functionality testing of the Lidar at Stapleton AP. Each successive trace is a 500 point spectrum analyzer scan of a +/- 10 m/s velocity range. Traces are separated vertically by 10 db. The lidar is viewing a segment of a rotating wheel calibrator about 100 yards away. As the wheel speed is changed, the location of the velocity spectral peak moves with it.

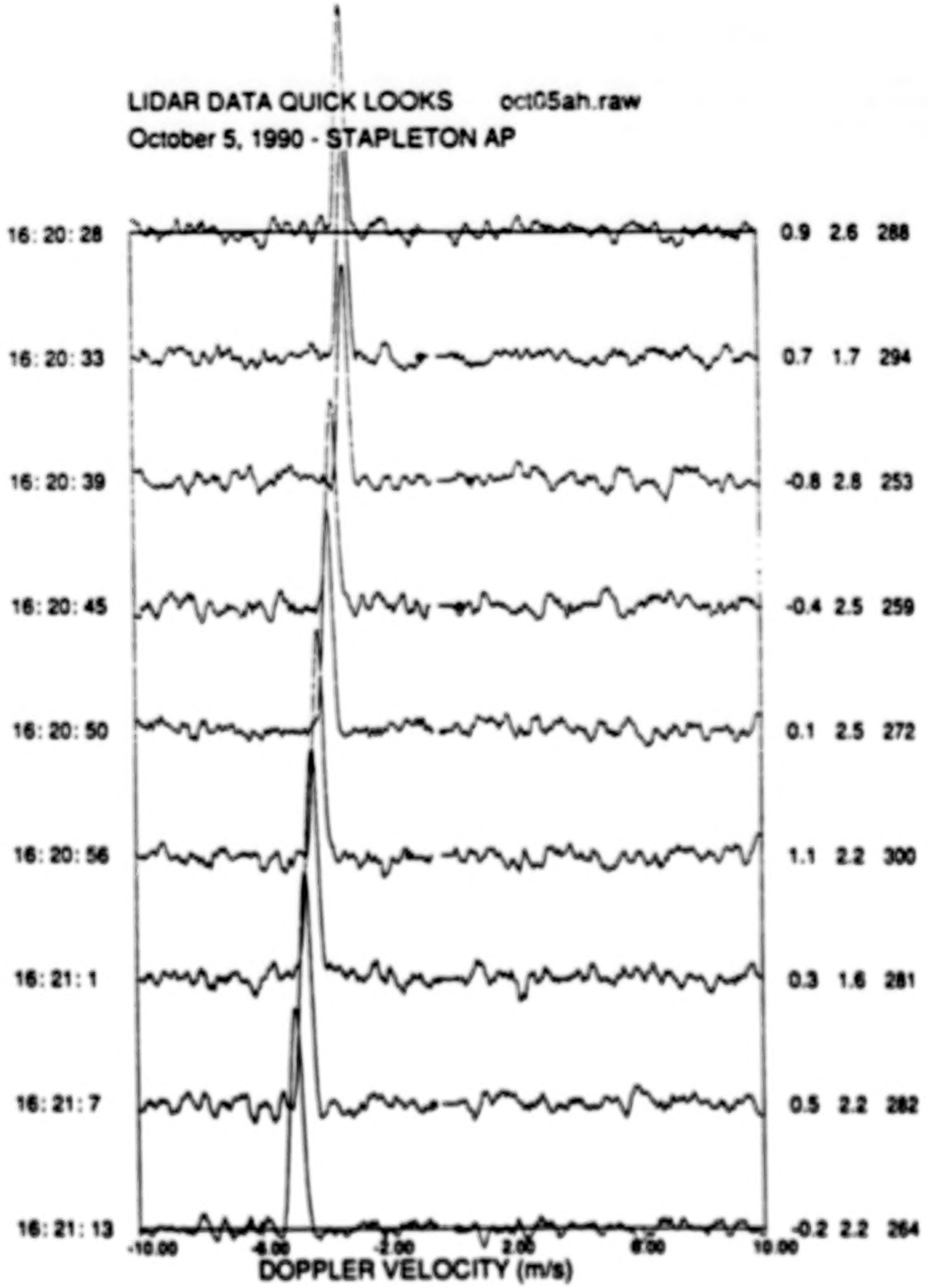LIDAR DATA QUICK LOOKS oct05ah.raw
October 5, 1990 - STAPLETON AP
16:20:28
0.9 2.6 288
16:20:33
0.7 1.7 294
16:20:39
-0.8 2.8 253
16:20:45
-0.4 2.5 259
16:20:50
0.1 2.5 272
16:20:56
1.1 2.2 300
16:21:1
0.3 1.6 281
16:21:7
0.5 2.2 282
16:21:13
-0.2 2.2 264
-10.00
-6.00
-2.00
2.00
6.00
10.00
DOPPLER VELOCITY (m/s)

6. DISCUSSION - VIEWGRAPH 6

A larger portion of this same calibration wheel experiment. Spectral intensity is contoured showing the changing wheel velocity both toward and away from the lidar. The central section blanked out is not observable with this system due to zero velocity stray light and modulator noise pickup.

LIDAR DATA VELOCITY CONTOURS oct05.raw

View Rotating Wheel Segment Calibrator

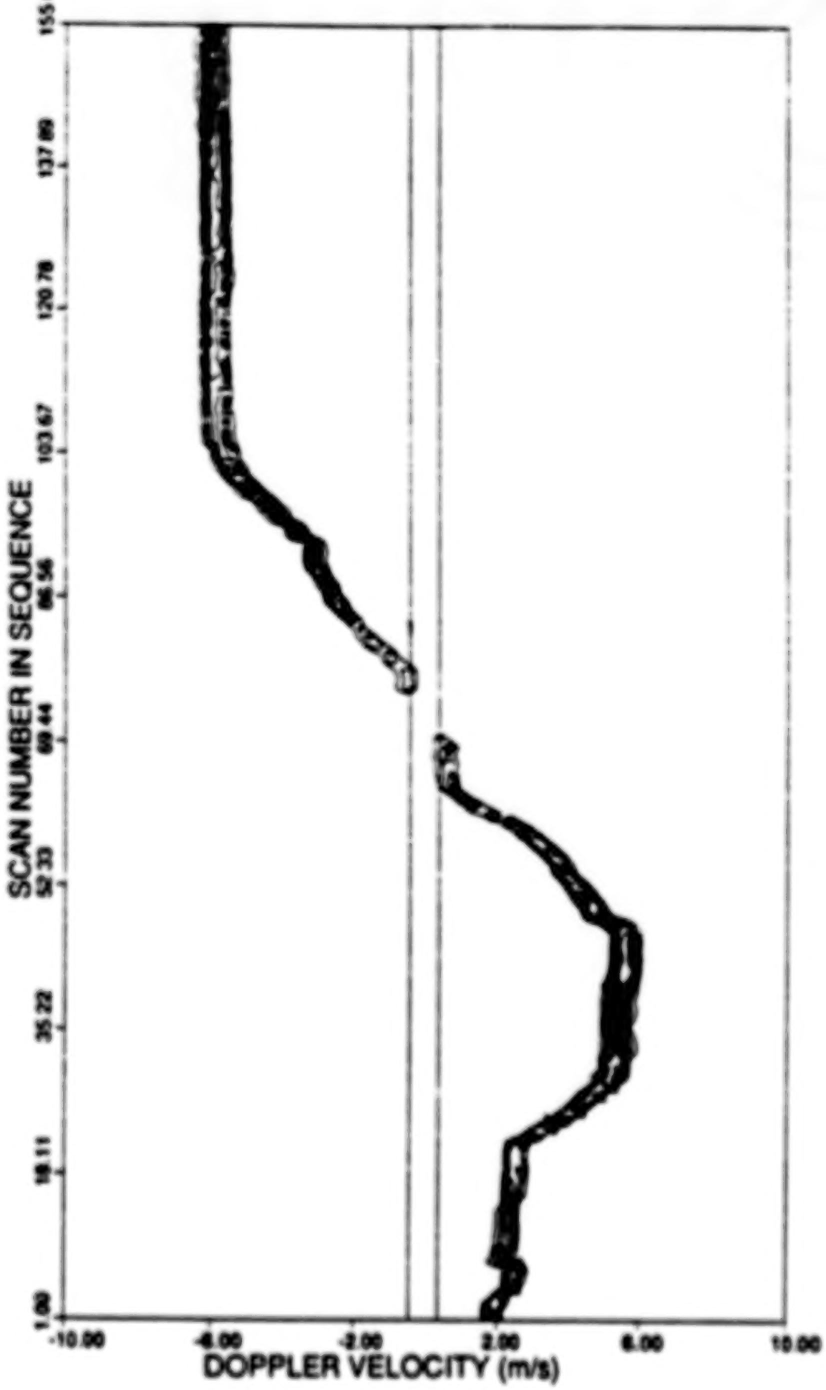

7. DISCUSSION - VIEWGRAPH 7

A comparion of lidar monitored wind velocity (solid) as compared to the along-beam wind component of a co-located anemometer (dashed).

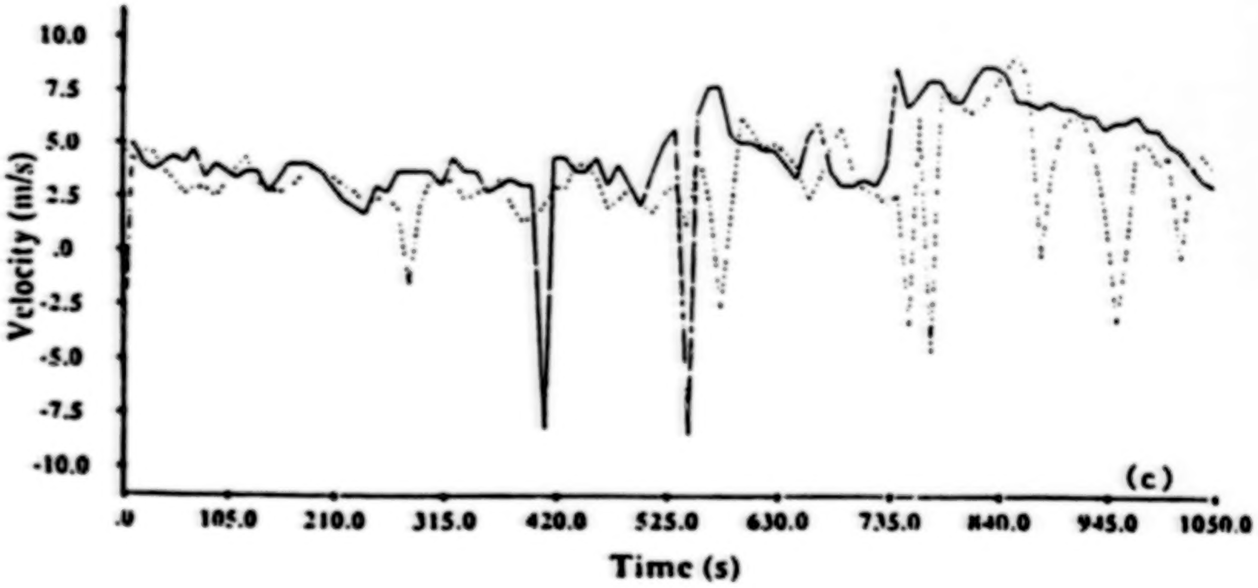
10.0
7.5
5.0
2.5
.0
-2.5
-5.0
-7.5
-10.0
Velocity (m/s)
.0
105.0
210.0
315.0
420.0
525.0
630.0
735.0
840.0
945.0
1050.0
Time (s)
(c)

8. DISCUSSION - VIEWGRAPH 8

A sample spectral intensity gray scale plot of the lidar return from natural wind. The wind velocity changes from -2.5 m/s to zero during the course of the experiment.

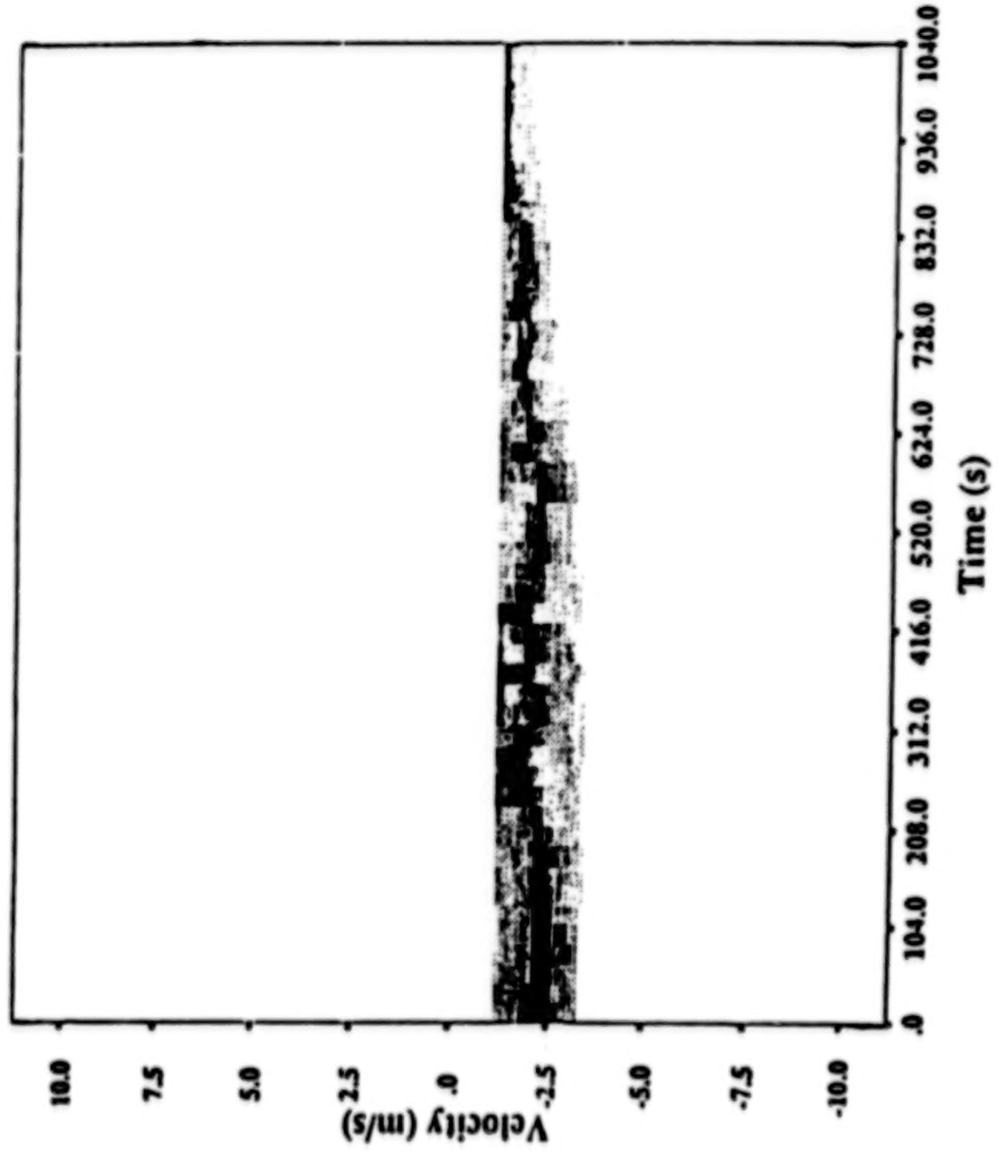
Velocity (m/s)
10.0
7.5
5.0
2.5
.0
-2.5
-5.0
-7.5
-10.0
Time (s)
.0
104.0
208.0
312.0
416.0
520.0
624.0
728.0
832.0
936.0
1040.0

9. *DISCUSSION - VIEWGRAPH 9*

A similar plot showing light and meandering wind where velocity toward and away from the lidar was simultaneously observed within the beam length. This illustrates that the system can record wind shears if they occur within the beam.

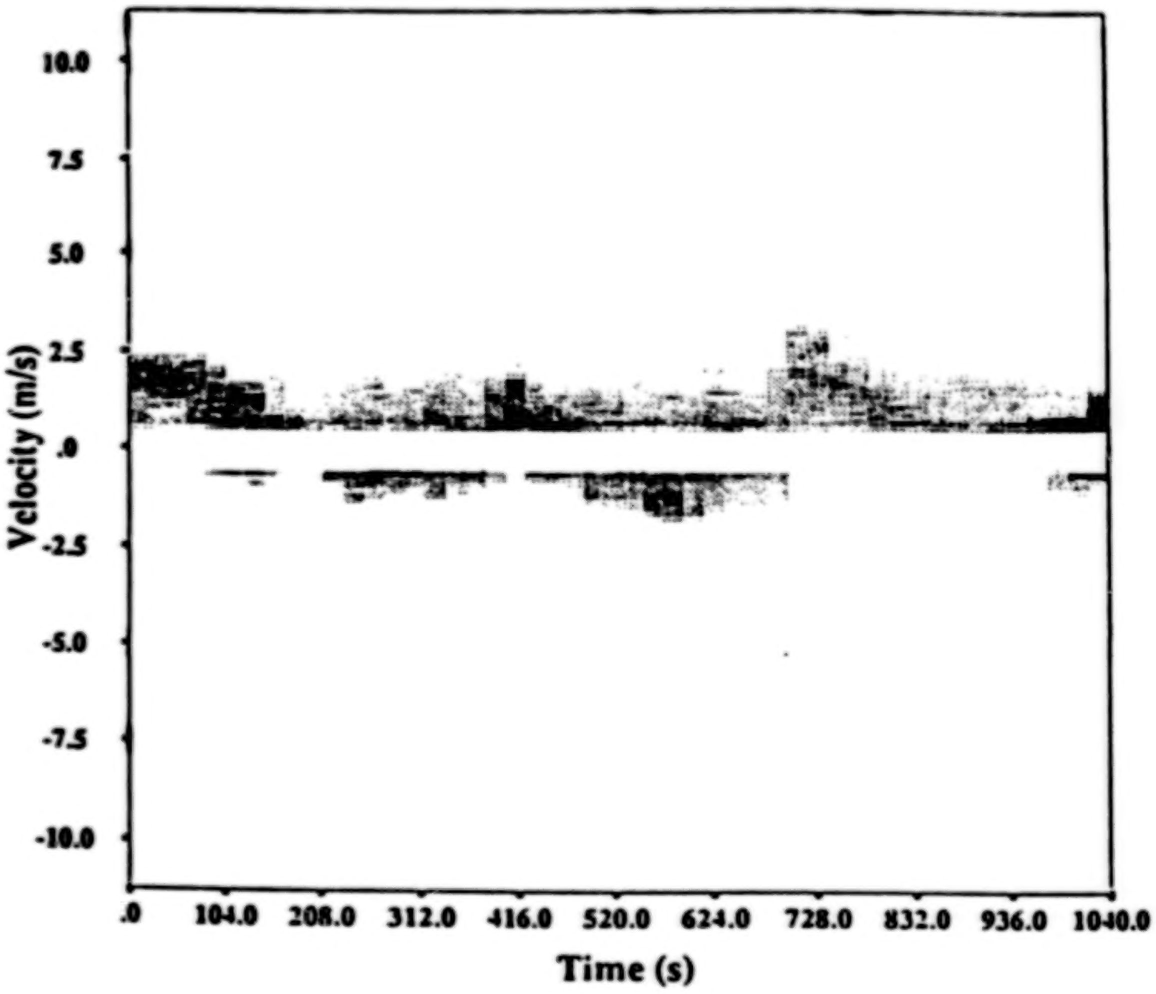
10.0
7.5
5.0
2.5
.0
-2.5
-5.0
-7.5
-10.0
Velocity (m/s)
.0
104.0
208.0
312.0
416.0
520.0
624.0
728.0
832.0
936.0
1040.0
Time (s)

10. DISCUSSION - VIEWGRAPH 10

Conclusions drawn from this research effort.

CONCLUSIONS

- COST EFFECTIVE HARDWARE DEMONSTRATED
  - 3.5 watt CW 10.6μ output power
  - Wind can be remotely monitored
  - Divergent winds can be seen
- STAPLETON AP TESTS
  - Intermittent Testing Aug and Sept 1990
  - No wind shear events occured
  - Sensitivity marginal in clear air
  - Sensitivity adequate in dust or precipitation
- PROTOTYPE DESIGN STATUS
  - Proof-of-concept prototype is difficult to align, bulky
  - 13.5db signal processing sensitivity improvement possible
  - Airborne use requires significant redesign
  - Possible ground-based utility at secondary airports

11. DISCUSSION - VIEWGRAPH 11

The last two viewgraphs relate to a different meteorological sensor for airport safety use. They are presented very briefly here for general interest. Ophir's subsidiary corporation, Radiometrics Corporation, has developed and is now internationally marketing a millimeter wave radiometer that is useful in geodetic surveying, weather forecasting, and radio-astronomy. It can also be configured to be capable of monitoring aircraft icing conditions above airports.

Viewgraph 11 is a copy of an illustrative handout about the sensor.

RADIOMETRICS MICROWAVE WATER VAPOR RADIOMETER

If you are involved in precise geodetic measurement, meteorology, or long-baseline astronomy, you should be aware of the newly available RADIOMETRICS Corporation Microwave Water Vapor Radiometer. This commercially available, transportable instrument can be used in the following applications:

- Weather forecasting and modification
- Sea level measurement for climactic change
- Remote sensing of geophysical resources
- Measuring strains in the earth's surface and detecting plate tectonic motion
- Forecasting aircraft icing
- Very Long Baseline Interferometry (VLBI)

Standard output measurements include:

- Sky brightness temperature (degrees Kelvin)
- Total precipitable water (in millimeters)
- Total liquid water (in millimeters)
- Excess path length (vapor refractive error in centimeters)

Unique design features include:

- Fast start-up
- Quasi-optical lens components
- Low power requirements (17 watts)
- Internal noise diode calibration sources
- Gaussian Horn-Lens antenna (5° beam width)
- Sky brightness temperature accuracy of 0.5 K
- Mountable on standard surveying instrument tripod
- Complete internal autocalibration every 10 seconds
- Dual wavelength measurement (23.8 GHz and 31.4 GHz)
- Automatic elevation scanning along single selected azimuth
- Portability (15 kilograms in a 45×28×74 centimeter package)
- Internal microprocessor control for automated measurement

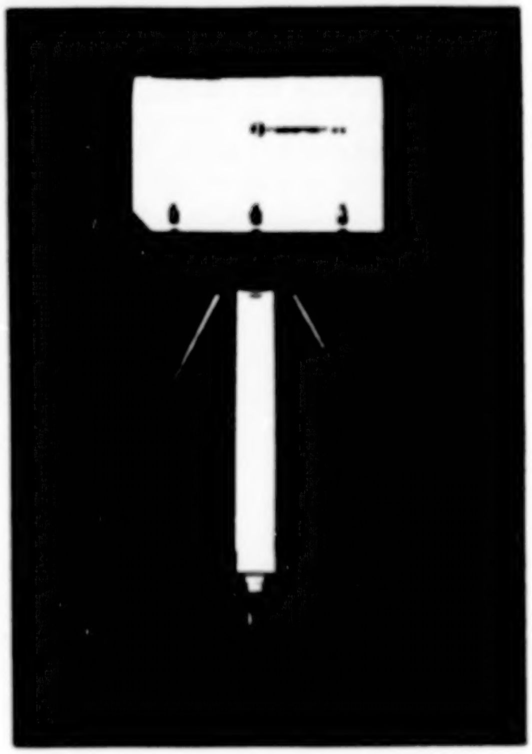

FUTURE DEVELOPMENTS

Plans include the addition of several passive 50-60 GHz oxygen channels to allow atmospheric temperature profiling as well as atmospheric moisture measurements from a single instrument package.

For more information concerning this instrument, please contact RADIOMETRICS Corporation at

3190 So. Wadsworth Blvd., Suite 100; Lakewood, Colorado 80227, U.S.A. Office hours are from 8:00 a.m. to 5:00 p.m. MST.

Telephone (303) 986-8558
24-Hour Telefax (303) 986-2257

radiometrics
CORPORATION

ORIGINAL PAGE IS
OF POOR QUALITY

12. DISCUSSION - VIEWGRAPH 12

On Feb 27, 1990 at 0240 Zulu the Federal Express Cessna 208 N80FE crashed upon landing at Stapleton in an icing related incident.

Radiometrics was operating its WVR-1000 Radiometer 30 miles away in Boulder, Colorado during this period of time. A data trace showing a time history of sensed supercooled liquid water amount (icing tendancy) aloft is shown. The time of the crash at Stapleton 30 miles away is shown as a dot. It can be seen that the crash occured at the beginning of a severe icing condition episode aloft as observed by the IR-2000. This data has been provided to the NTSB. We present it here for general interest since it may eventually prove to be a new method to monitor hazardous icing conditions aloft during aircraft airport approach and landing.

Radiometrics Corp. WVR-1000 Radiometer

at Boulder on February 27-28, 1990

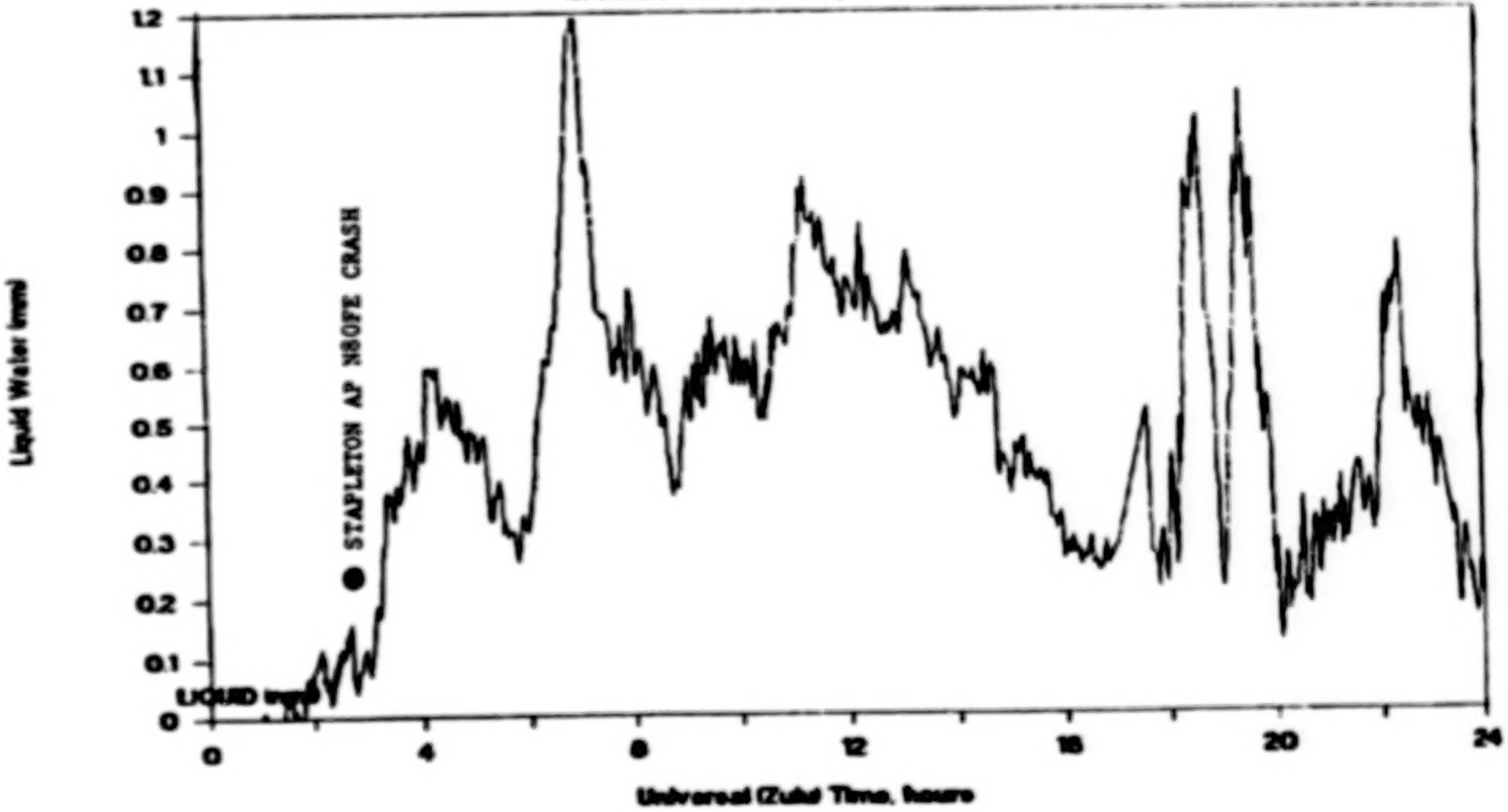

ORIGINAL PAGE IS
OF POOR QUALITY

Continuous Wave Laser - Questions and Answers

Q: JACQUES MANDLE (SEXTANT Avionique) - What are the characteristics of your telescope; type and aperture; variable or fixed focussing distance?

A: LOREN NELSON (OPHIR Corporation) - The telescope was an off axis Doll-Kirkman telescope, 8 inches in aperture. That type was chosen in order to minimize the spicular reflection from the internal optical components of the scope. The focusing distance was adjustable manually between the range of 200 meters to infinity and the data you saw was taken at a setting of 500 meters.

Q: PETER SINCLAIR (Colorado State University) - With reference to the millimeter wave radiometer, what water vapor spectral line does the instrument employ and why was that frequency selected?

A: LOREN NELSON (OPHIR Corporation) - At the end of the presentation I briefly indicated that the Radiometrics WVR-1000 millimeter wave radiometer had detected an icing condition which was related to the February '90 Stapleton crash of an aircraft. Water vapor has a single purely rotational line at 23 GHz, the nearest closest line being at 183. We operate on the wings of the 23 GHz line, specifically at 23.8 GHz. That specific wave length was chosen for three reasons, one of which is, at that wave length the pressure dependence of the line broadening is altitude independent so we can use the same attenuation coefficient at all altitudes in the atmosphere. A second reason is by ICAO International Treaty, 23.8 GHz is an internationally protected band where nobody is allowed to radiate energy. Since we're looking at very weak emission on the order of 30 degrees Kelvin brightness temperature, that becomes important. And the third reason is, that 23.8 GHz has a specific relation to our second channel at 31.4 and that let's us use a patented technique to half the cost of the instrument. We measure at 23.8, which is a water vapor absorption line, we measure at 31.4, which is a water vapor window. Where there is a square law relation to the absorption of liquid water the two equations can then be solved to come out with the liquid water line interval and the water vapor line interval.

Q: GAUDY BEZOS (NASA Langley) - I am interested in more information on the sensor that measured the super-cooled liquid water content. How and where was the sensor mounted, was it at ground level? What were the liquid water content values measured?

A: LOREN NELSON (OPHIR Corporation) - The sensor happened to be at our research facility in Boulder, Colorado, which was 30 miles away from the Stapleton Airport. It was mounted at ground level looking vertically, in a vertical acceptance beam. The sensor is about the size of a large mailbox and mounts on a standard surveying tripod. It's also capable of scanning in azimuth and elevation. The values weren't purely liquid water content, but are precipitable liquid water. The liquid that would be obtained if all of the water in a vertical column was squished down to a liquid layer at the bottom. They were on the order of one centimeter of liquid water.

Session VIII. Airborne LIDAR

N91-24143

Status of 2 Micron Laser Technology Program
Mark Storm, NASA Langley

STX
ST SYSTEMS CORPORATION
28 RESEARCH DRIVE, HAMPTON, VIRGINIA 23666 • (804) 865-1214

October 17, 1990

Status of 2 Micron Laser Technology Program

Mark Storm*, ST Systems Corporation (STX)
28 Research Drive
Hampton, Virginia 23666

This paper describes the status of 2 micron lasers for windshear detection. Theoretical atmospheric and instrument system studies by Russell Tang and Rowland Bowles have demonstrated that the 2.1 micron Ho:YAG lasers can effectively measure windspeeds in both wet and dry conditions with accuracies of 1 m/sec. Two microns laser transmitter technology looks very promising in the near future but several technical questions remain. Ho:YAG laser would be small compact and efficient requiring little or no maintenance. Since the Ho:YAG laser is diode laser pumped and has no moving part, the lifetime of this laser should be directly related to the diode laser lifetimes which can perform in excess of 10,000 hours. Ho:YAG efficiencies of 3-12% are expected but laser demonstrations confirming the ability to Q-switch this laser are required. Coherent laser operation has been demonstrated for both CW and Q-switched lasers.

1577 Spring Hill Road
Suite 500
Vienna, VA 22180
(703) 827-6600

4400 Forbes Blvd.
Lanham, MD 20706
(301) 794-5000

9701 J. Philadelphia Ct.
Lanham, MD 20706
(301) 306-1100

109 Massachusetts Ave
Lexington, MA 02173
(617) 862-0405

1900 Garden Road
Suite 130
Monterey, CA 93940
(408) 373-7292

Status of 2-Micron Laser Technology Program

Presented to the:

Third Combined Manufacturers' and Technologists'
Airborne Wind Shear Review Meeting, Hampton, Va.

October 17, 1990

Mark E. Storm
STX/NASA Langley

OUTLINE

1.0 Introduction
    - Requirements for Coherent Lidar
    - Laser approach

2.0 Single-Frequency Ho:Tm:YAG
    - Laser performance
    - Frequency Tuning
    - Heterodyne detection

3.0 2-micron laser issues:
    - Efficiency Considerations
    - Crystal Spectroscopy

4.0 Injection Seeding Experiment
    - Coherent Technology Results

5.0 Summary and Prospects for a Windshear Transmitter.

Laser Requirements for a Windshear Transmitter

Single-Frequency, Q-switched

Laser energy: 5-10 mJ

Repetition rate: 150-300 Hz

Laser Bandwidth: 1.0 MHz

Compact, Efficient, Reliable- 200+ hours of maintenence free operation.

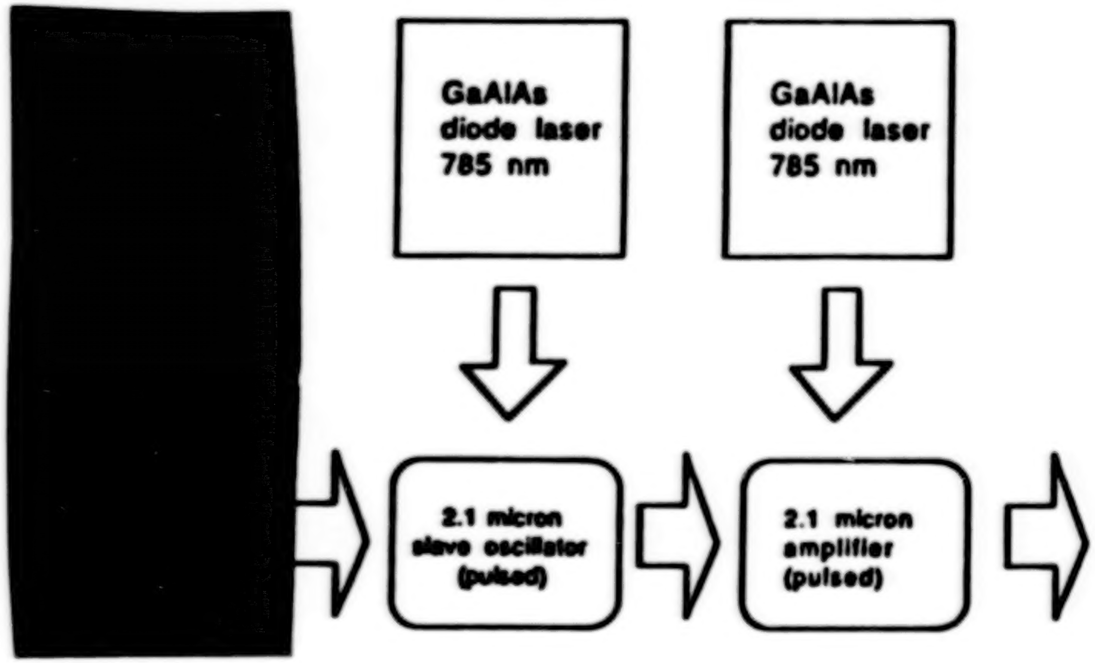
[redacted]
GaAlAs
diode laser
785 nm
GaAlAs
diode laser
785 nm
2.1 micron
slave oscillator
(pulsed)
2.1 micron
amplifier
(pulsed)

WINDSHEAR TRANSMITTER

ORIGINAL PAGE IS
OF POOR QUALITY

RESEARCH GOAL:

SINGLE-MODE LASER FOR INJECTION LOCKING
OF Q-SWITCHED, 2-MICRON LASER.

APPROACH:

FABRY-PEROT
PLANO-PLANO
DIODE-LASER PUMPED

ACHIEVEMENTS:

- SINGLE-MODE LASING OF HO:TM:YAG
- 10 mW optical power at 2.091microns
- 68% slope efficiency, QE.= 1.8, 4% optical-optical
- 31 GHz [4.5 Angstroms] Temperature Tuning
- Demonstrated Heterodyne Detection

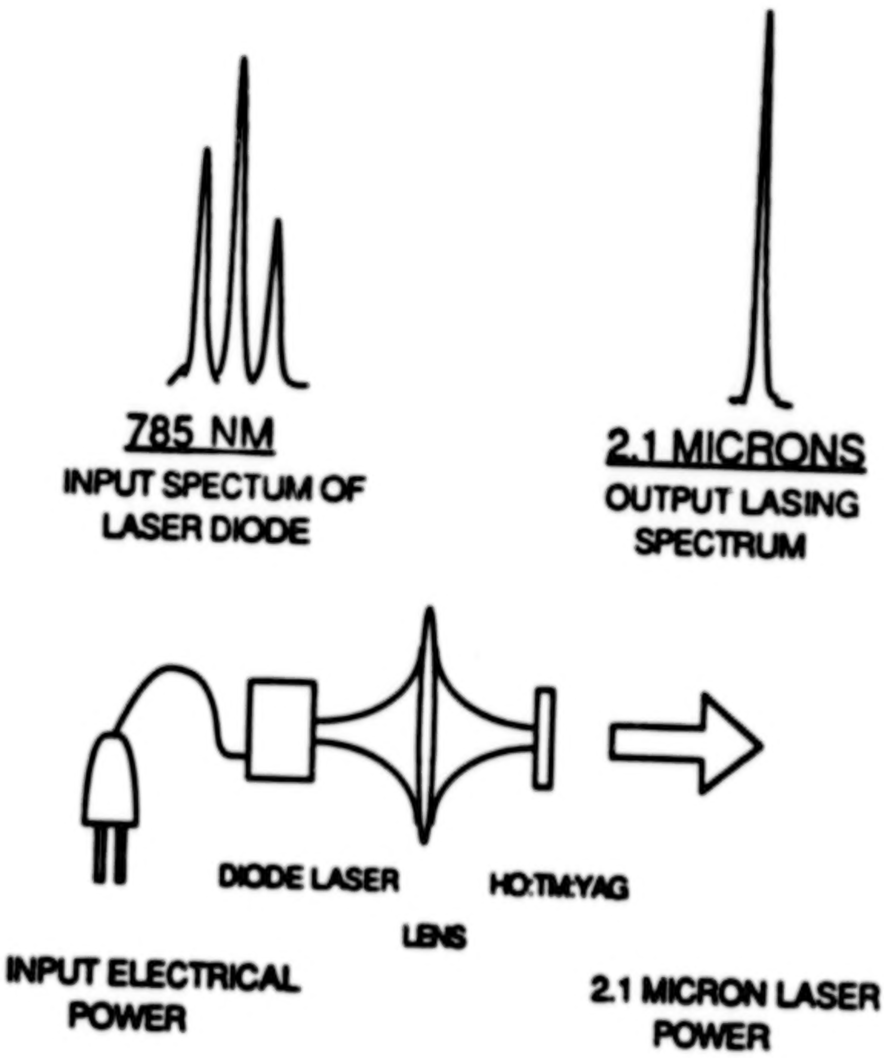

785 NM
INPUT SPECTUM OF LASER DIODE
2.1 MICRONS
OUTPUT LASING SPECTRUM
DIODE LASER
HO:TM:YAG
LENS
INPUT ELECTRICAL POWER
2.1 MICRON LASER POWER

SINGLE-FREQUENCY HO:TM:YAG LASER

SINGLE FREQUENCY HO:TM:YAG

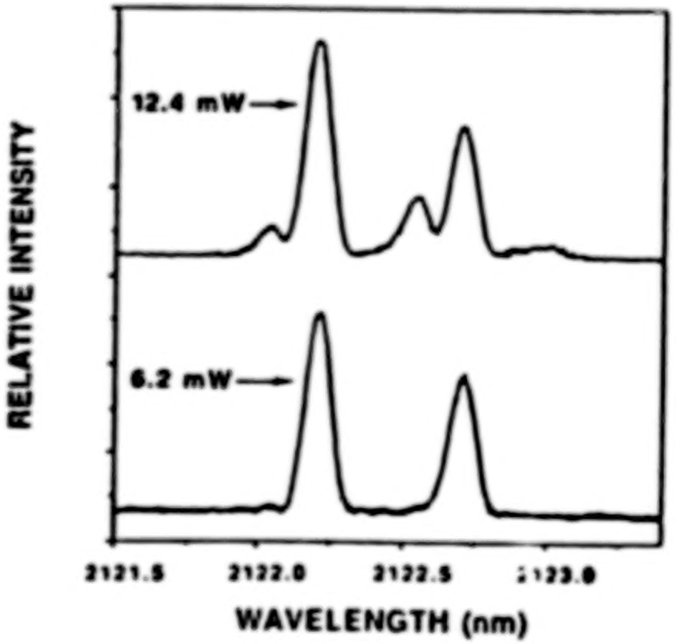

Fig. 1. Multimode lasing spectra of 2.5-mm thick Planoconvex Ho:Tm:YAG at two different laser output powers.

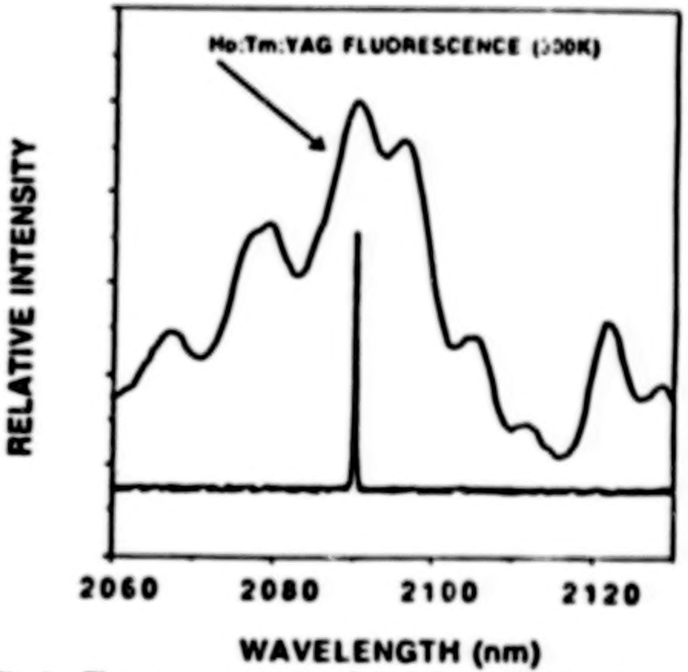

Fig. 2. Fluorescence spectra and single-longitudinal-mode lasing spectrum of a 1-mm thick Ho:Tm:YAG.

MULTIMODE LASING

SINGLE MODE LASING

SINGLE FREQUENCY HO:TM:YAG

FREQUENCY VS. TEMPERATURE
Ho:Tm:YAG

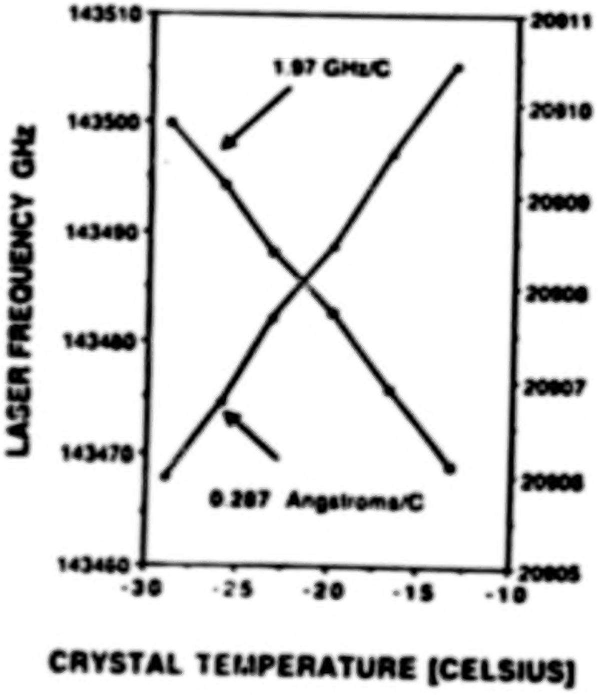

TEMPERATURE TUNING

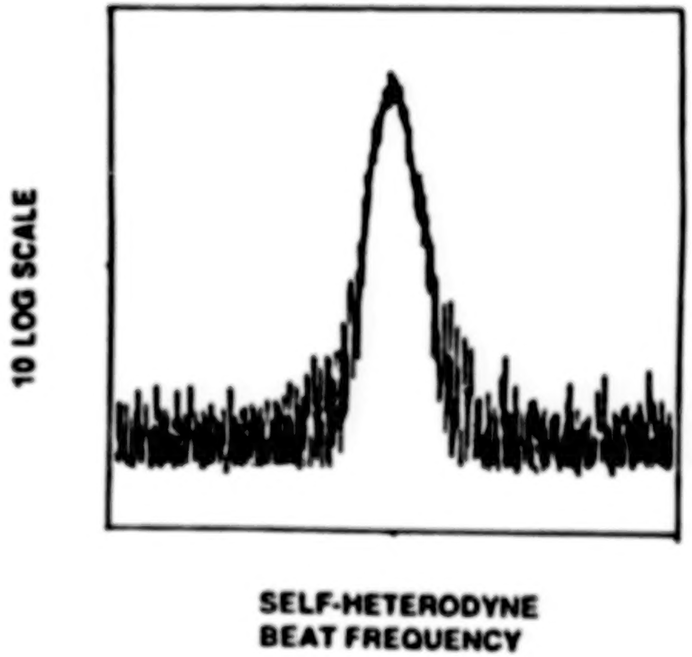

HETERODYNE SIGNAL

Single-Frequency Laser Power

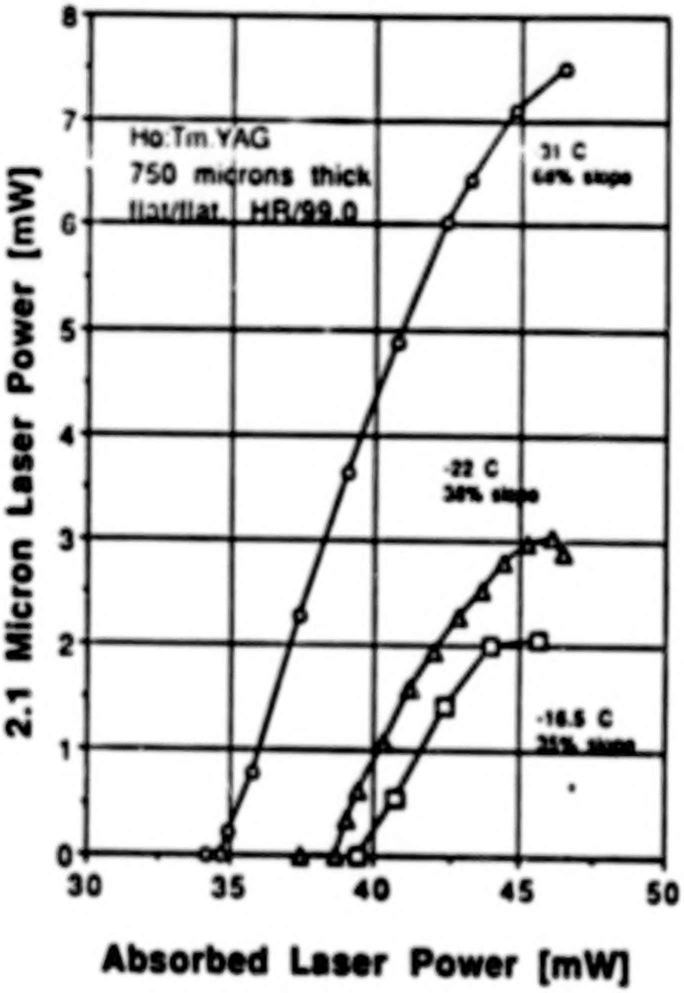

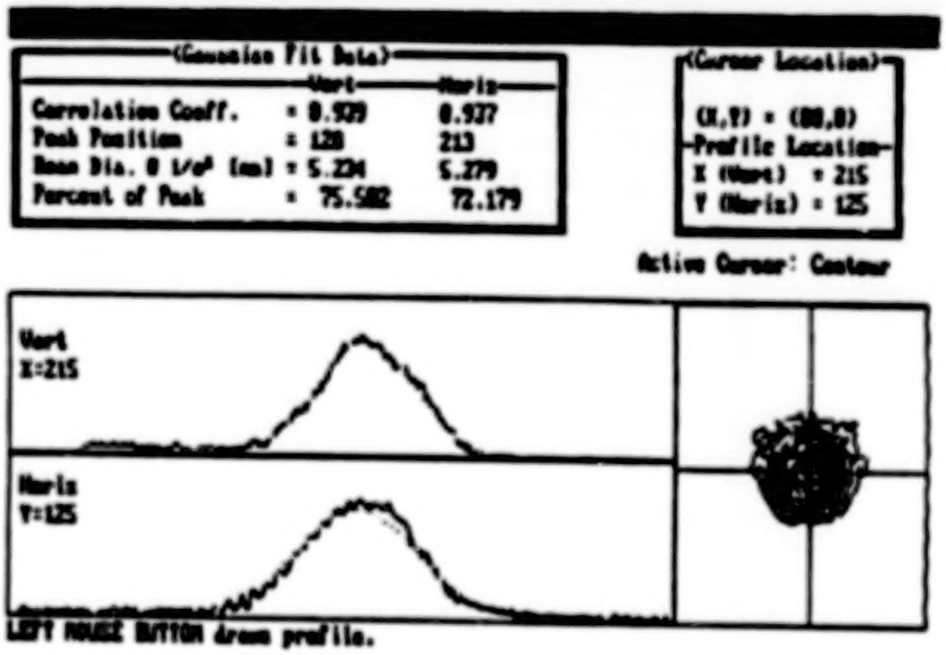

```
<Gaussian Fit Data>
                             Vert      Horiz
Correlation Coeff.        = 0.939     0.937
Peak Position             = 128       213
Beam Dia. @ 1/e² (mm)     = 5.234     5.279
Percent of Peak           =  75.582    72.179

<Cursor Location>
(X,Y) = (80,0)
Profile Location
X (Vert)  = 215
Y (Horiz) = 125

Active Cursor: Contour
```

```
LEFT MOUSE BUTTON draws profile.
```

SINGLE-MODE SPACIAL PROFILE : TEMoo

ORIGINAL PAGE IS
OF POOR QUALITY

NO ________

National Aeronautics and
Space Administration

ORIGINAL PAGE IS
OF POOR QUALITY

2 MICRON LASER EFFICIENCY

$$\eta_{\text{laser}} = \eta_{\substack{\text{diode}\\ \text{laser}}} \underbrace{\eta_{\text{absorption}}\;\eta_{\substack{\text{energy}\\ \text{transfer}}}}_{\text{SPECTROSCOPIC}} \underbrace{\eta_{\substack{\text{Q-switch}\\ \text{optical}\\ \text{extraction}}}}_{\substack{\text{LASING}\\ \text{DYNAMICS}}}$$

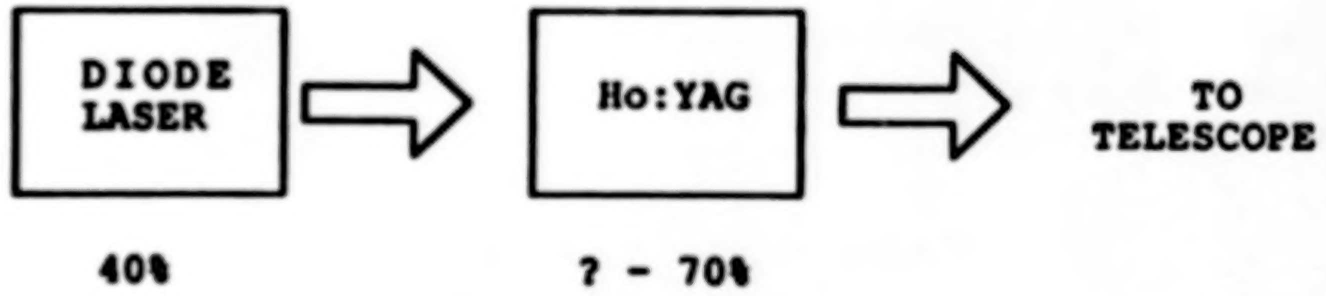

2-micron Laser Efficiency

	Present	Projected
Diode Laser	.50	.50
Optical Coupling	.80	.90
Absorption Effic.	.50	.65
Energy Transfer	.95	.95
Optical Extraction	.30	.60
Q-switching	.55	.80
Total Efficiency	.03	.13

Multi-mode Lasing Spectrum

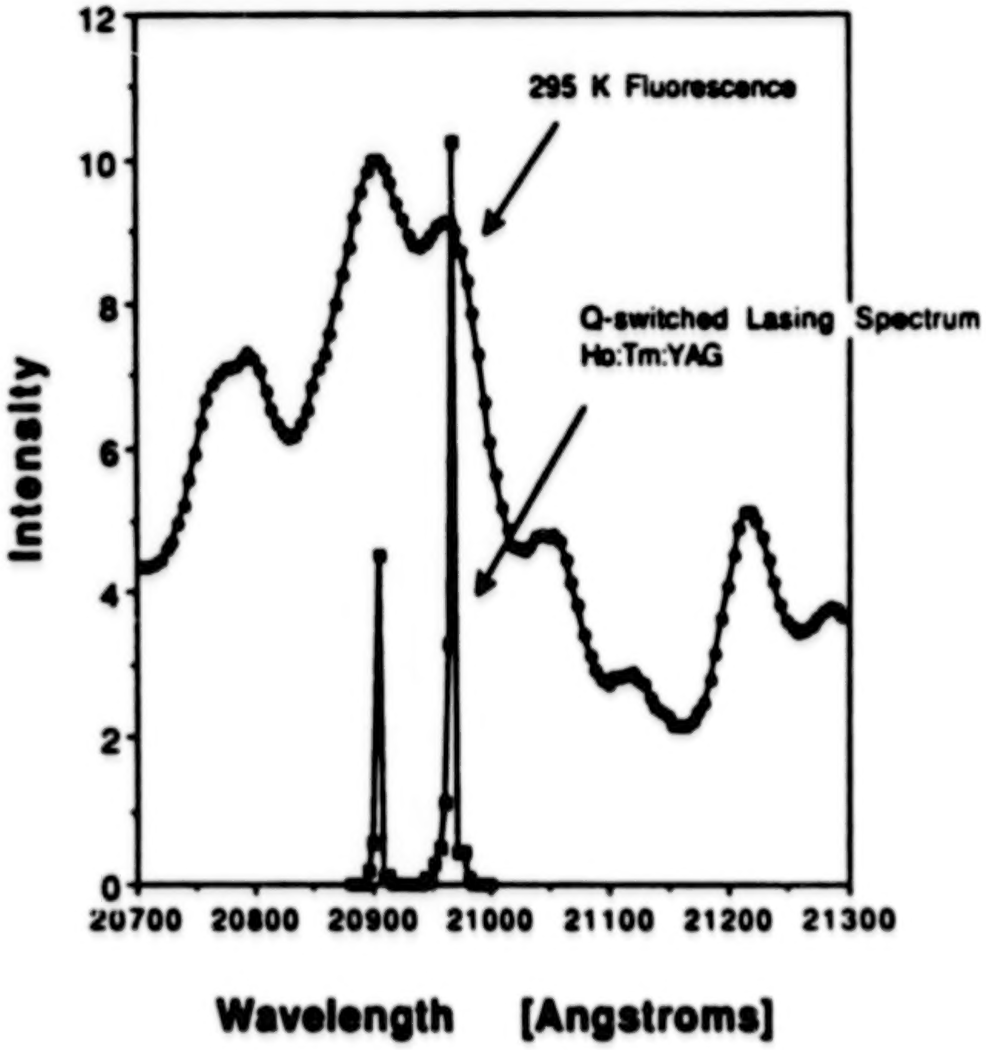

Coherent Technology Inc.

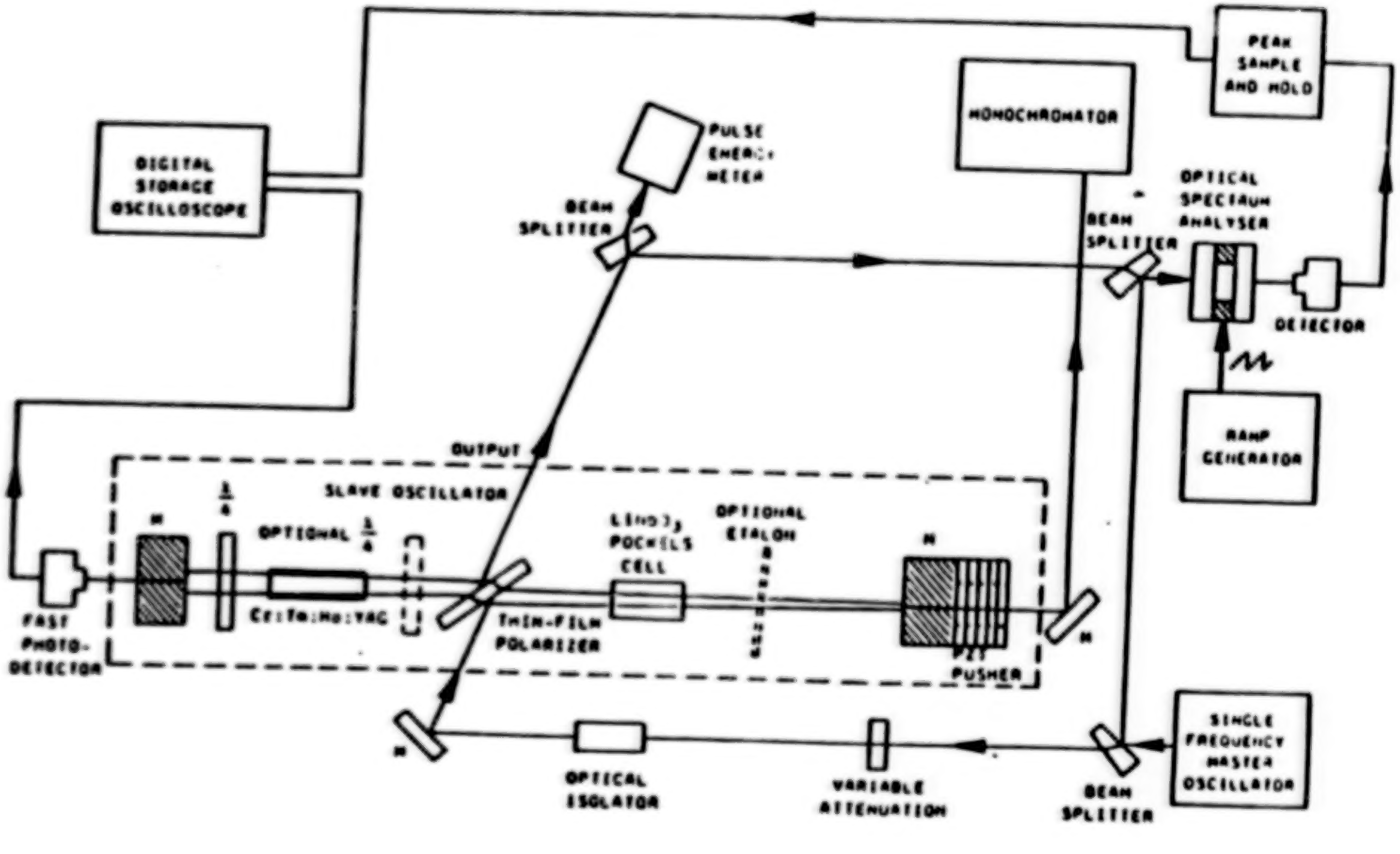
DIGITAL STORAGE OSCILLOSCOPE
PULSE ENERGY METER
BEAM SPLITTER
MONOCHROMATOR
PEAK SAMPLE AND HOLD
BEAM SPLITTER
OPTICAL SPECTRUM ANALYSER
DETECTOR
RAMP GENERATOR
OUTPUT
SLAVE OSCILLATOR
M
λ/4
OPTIONAL λ/4
Cr:Tm:Ho:YAG
FAST PHOTO-DETECTOR
THIN-FILM POLARIZER
LiNbO3 POCKELS CELL
OPTIONAL ETALON
M
PZT PUSHER
M
M
OPTICAL ISOLATOR
VARIABLE ATTENUATION
BEAM SPLITTER
SINGLE FREQUENCY MASTER OSCILLATOR

Injection Locked , Q-switched , 2-micron Laser

Coherent Technology Inc.

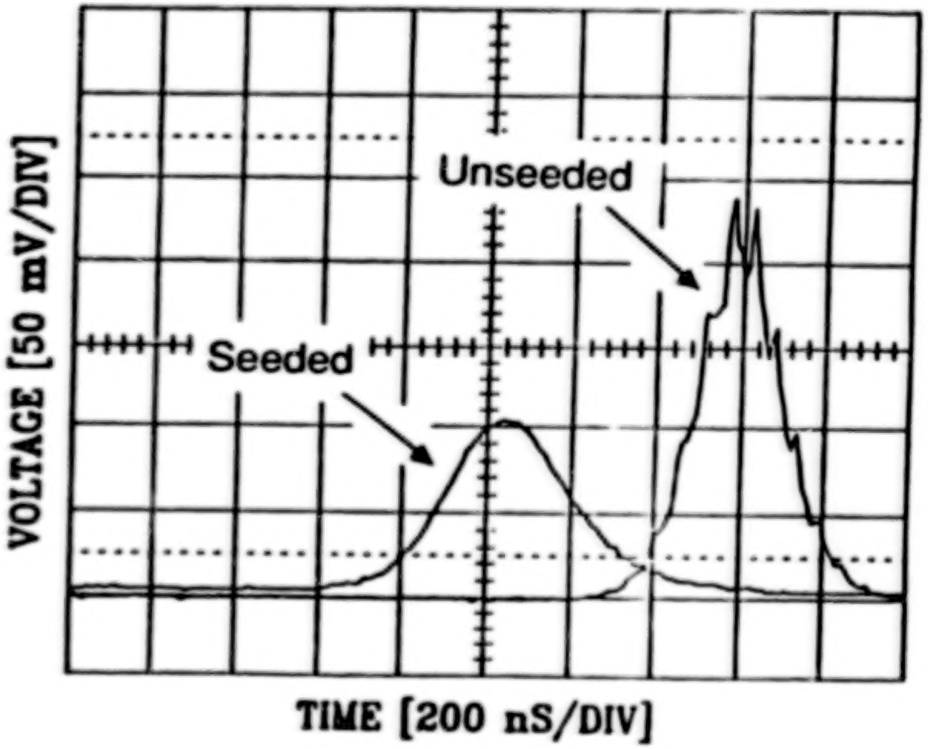

2-Micron Accomplishments for Coherent Transmitter

-CW, single-frequency demonstrated.
Storm,Kane

-Pulsed, single frequency demonstrated in flashlamp-pumped, injection control experiment.
Henderson

-Heterodyne detection demonstrated in self-heterodyne experiment.
Storm

Future Demonstrations Necessary for Windshear Laser

-Efficient energy scaling to 10 mJ level for Q-switched operation.
  - -Diode laser pumped
  - -100 Hz min. rep. rate

LASER DIODE PUMPED REMOTE SENSING DEVELOPMENT

Cr doped flashlamp
pumped laser

Tm:Ho
laser

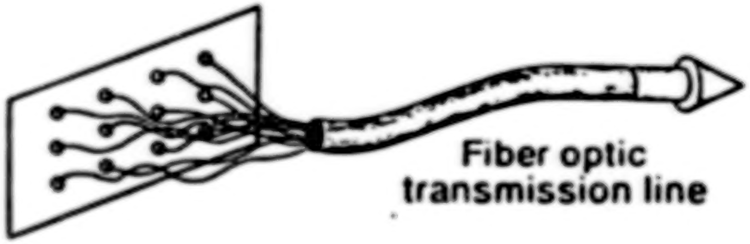

Fiber optic
transmission line

Laser diode
array bank

Rare earth
eye - safe
laser

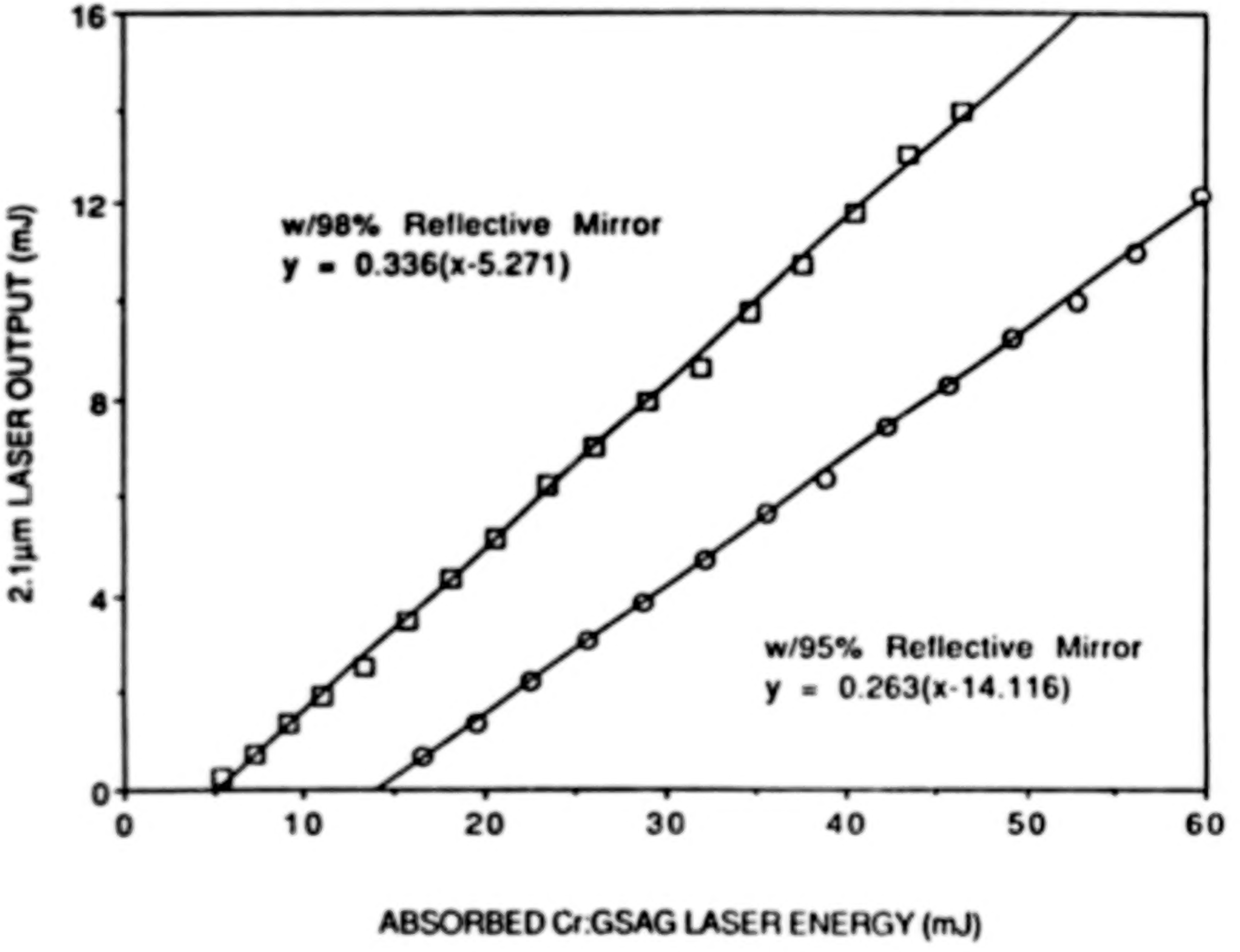

OUTPUT VS. ABSORBED ENERGY FOR ROOM TEMPERATURE
Cr:GSAG (Gd3 Sc2 Al3 O12) PUMPED RARE EARTH LASER

Session VIII. Airborne LIDAR

N91-24144

Avionic Laser Multisensor Program at Litton Aero Products
Rod Benoist, Litton Aero Products

Litton

Aero Products

AVIONIC LASER MULTISENSOR PROGRAM AT LITTON AERO PRODUCTS

Dave Bjorndahl, Chief Scientist of APD
Rod Benoist, Project Manager
Farzin Amzajerdian, Principal Investigator

DESCRIPTION OF LITTON AERO PRODUCTS

Litton

Aero Products

- LITTON AERO PRODUCTS
  - COMMERCIAL AVIONICS
  - 600 EMPLOYEES
  - LOCATED IN MOORPARK, CALIFORNIA
  - WORLDWIDE PRODUCT SUPPORT

- CURRENT PRODUCTS OF AERO PRODUCTS DIVISION
  - ATTITUDE AND HEADING REFERENCE SYSTEMS
  - INERTIAL NAVIGATION SYSTEMS
  - OMEGA AND GPS NAVIGATION SYSTEMS

- OTHER LITTON DIVISIONS CAPABILITIES
  - AVIONICS DISPLAYS
  - FIBER OPTIC DATA BUSES
  - MILITARY LASER SYSTEMS

AVIONIC LASER MULTISENSOR PROGRAM

Litton

Aero Products

- LONG RANGE PROJECT GOALS
  - NEW PRODUCT DEVELOPMENT OF A FORWARD LOOKING AVIONIC WIND VELOCIMETER BASED ON LASER TECHNOLOGY
  - PREDICTIVE WINDSHEAR DETECTOR
  - MULTIFUNCTIONAL CAPABILITY

- THIS FISCAL YEAR GOALS
  - COMPLETE EXPERIMENTAL BREADBOARD DEVELOPMENT USING SOLID STATE HOLMIUM LASER
  - PERFORM FIELD MEASUREMENTS OVER DIFFERENT ATMOSPHERIC CONDITIONS
  - COMPLETE ATMOSPHERIC MODELS AND SYSTEM WINDSHEAR PERFORMANCE ANALYSIS
  - DEFINE REQUIREMENTS OF OTHER POTENTIAL AVIONIC FUNCTIONS

Litton

COHERENT DOPPLER LASER RADAR

Aero Products

- POTENTIAL AVIONIC APPLICATIONS
  - WINDSHEAR DETECTION
  - WINDS ALOFT MEASUREMENT FOR CRUISE FUEL SAVINGS
  - CLEAR AIR TURBULENCE DETECTION
  - WAKE VORTEX DETECTION
  - ALTIMETERY
  - GROUND VELOCITY MEASUREMENT
  - OBSTACLE AVOIDANCE
  - RUNWAY VISUAL RANGE
  - AIR DATA PARAMETERS (TRUE AIR SPEED, ANGLE OF ATTACK, ANGLE OF SIDESLIP)
  - PRESSURE ERROR MEASUREMENT
  - CRUISE GUST ALLEVIATION
  - CLOUD TOP IDENTIFICATION

Litton

BREADBOARD SYSTEM DEVELOPMENT

Aero Products

- ASSEMBLY OF BREADBOARD LIDAR IS NEARING COMPLETION
- CONSTRUCTED A ROOF TOP TEST SITE SUITABLE FOR ATMOSPHERIC BACKSCATTERING AND WIND VELOCITY MEASUREMENTS
- DEVELOPED SYSTEM CALIBRATION PROCEDURE USING DIFFUSE HARD TARGETS

Litton AVIONIC LASER MULTISENSOR PROGRAM

Aero Products

FUTURE WORK

- PERFORM FIELD MEASUREMENTS AT APD AND OTHER LOCATIONS OVER DIFFERENT ATMOSPHERIC CONDITIONS (FOG, RAIN, ...)
- DEFINE REQUIREMENTS OF AVIONIC FUNCTIONS OTHER THAN WINDSHEAR DETECTION
- DESIGN AND BUILD FLYABLE PROTOTYPE SYSTEM

AVIONIC LASER MULTISENSOR PROGRAM

Litton

Aero Products

SUMMARY

- HOLMIUM SOLID STATE LASER RADAR IS A PROMISING TECHNOLOGY FOR AVIONIC APPLICATIONS
    - DIODE PUMPING AND SINGLE FREQUENCY OPERATION HAVE BEEN DEMONSTRATED
- AVIONIC LIDAR OFFERS POTENTIAL FOR MULTIFUNCTIONAL CAPABILITY IN ADDITION TO WINDSHEAR DETECTION
    - SAFETY AND REVENUE ENHANCEMENT

Litton AVIONIC LASER MULTISENSOR PROGRAM

Aero Products

- APD WOULD LIKE TO ESTABLISH A DIALOG WITH GOVERNMENT AGENCIES, AIRLINES, AND AIRFRAME MANUFACTURERS TO DISCUSS
  - APPLICATIONS
  - INSTALLATION QUESTIONS
  - SYSTEM/USER INTERFACE AND DISPLAYS

Avionic Laser Multisensor Program at Litton Aero Products
Questions and Answers

Q: MIKE McCLENDON (American Airlines) - How long until a flying prototype? How long will the evaluation last? How long until a production system? How much dollars?

A: ROD BENOIST (Litton Aero Products) - Each year we do a project plan which looks at these numbers and I'll tell you what our plan is. Basically we see a prototype as being an 18 month project and then the production system another 18 months. So you're looking at from a kick off of about three years to production. In terms of dollars, I certainly listened very interestedly to what Dr. Targ had to say and wouldn't disagree with him at all on any point. We have a very aggressive target price though of $50,000. It's a target. So we're probably looking at 3 to 4 years to production and we're not kicked off on a prototype right now. However, an order for 100 systems, 1000 systems would probably do it.

Session IX. Airborne Passive Infrared

Session IX. Airborne Passive Infrared

N91-24145

Status of NASA's IR Wind Shear Detection Research
Dr. Burnell McKissick, NASA Langley

NASA's EXPERIENCE WITH INFRARED WIND SHEAR DETECTION

by

Burnell T. McKissick
NASA, Langley Research Center
Hampton, VA 23665

Third Combined Manufacturers' and Technologists'
Airborne Windshear Review Meeting
Radisson Hotel, Hampton
October 16-18, 1990

EARLY EXPERIENCE TO PRESENT

"Can ambient air temperature changes lead to the detection of hazardous wind shear conditions"

- Fawbush and Miller (1954) - Peak Gust = $7 + 3.06\,T - 0.007\,T^2 - 0.00284\,T^3$
- Foster (1958) - $W_o = -(-\,gz\delta T_c/T_m)^{1/2}$
- Kuhn and others (late 1970's) - infrared radiometer flown on NASA Learjet (1982)
- Proctor (mid-1980's) - microburst modeling: $u_{max} = -\,2.5\Delta T$
- Adamson (mid 1980's) - development of a FLIR for wind shear detection
- IR is an integral part of the NASA/FAA wind shear detection and warning progam

NASA SBIR NAS1-18637 WITH TURBULENCE PREDICTION SYSTEMS

Phase I (1987)

- Determined that a FLIR is feasible for wind shear detection
- FLIR has considerable commercial potential

Phase II (1989)

- Production of a prototype FLIR, AWAS I
- Installation of AWAS I on NASA 515
- 4.89 hours of flight test in 1989 and early 1990
- Production of an advanced FLIR, AWAS III
- Installation of AWAS III on UND Cessna Citation
- Recording of microburst penetrations in Orlando, FL and Denver, CO
- Installation of AWAS III on NASA 515 in fall of 1990
- Future test flights at LaRC and Denver, CO

QUANTITIES MEASURED BY AWAS I

NEAR FIELD TEMPERATURE - Approx. 100 meters ahead of the aircraft

FAR FIELD TEMPERATURE - Up to 6 or more kilometers ahead of the aircraft. Dependent on humidity.

DELTA TEMPERATURE - Spectral measurement of near field minus far field temperatures

THERMAL F-factor - A hazard index based on temperature

TEMPERATURE +/- ONE STANDARD DEVIATION

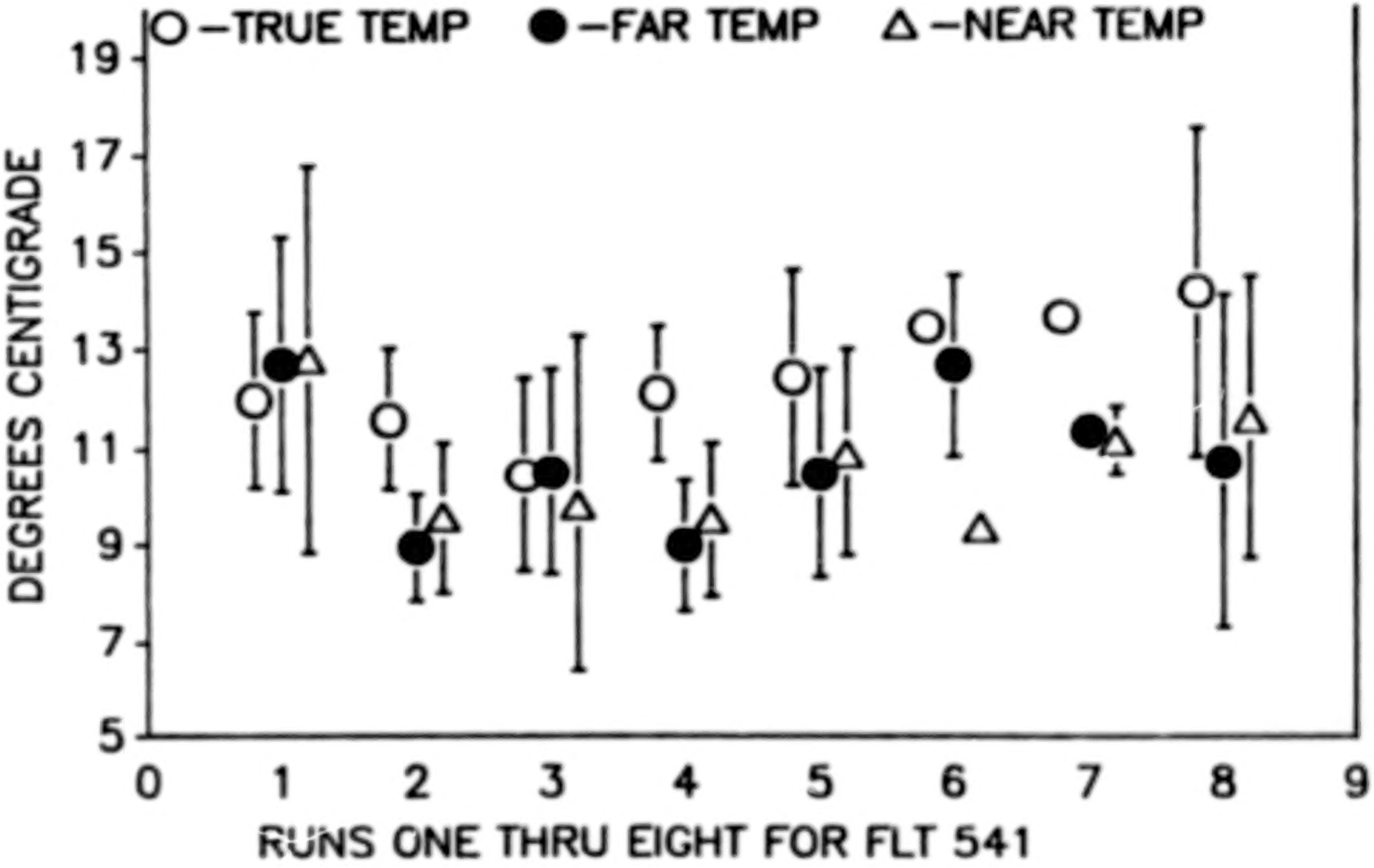

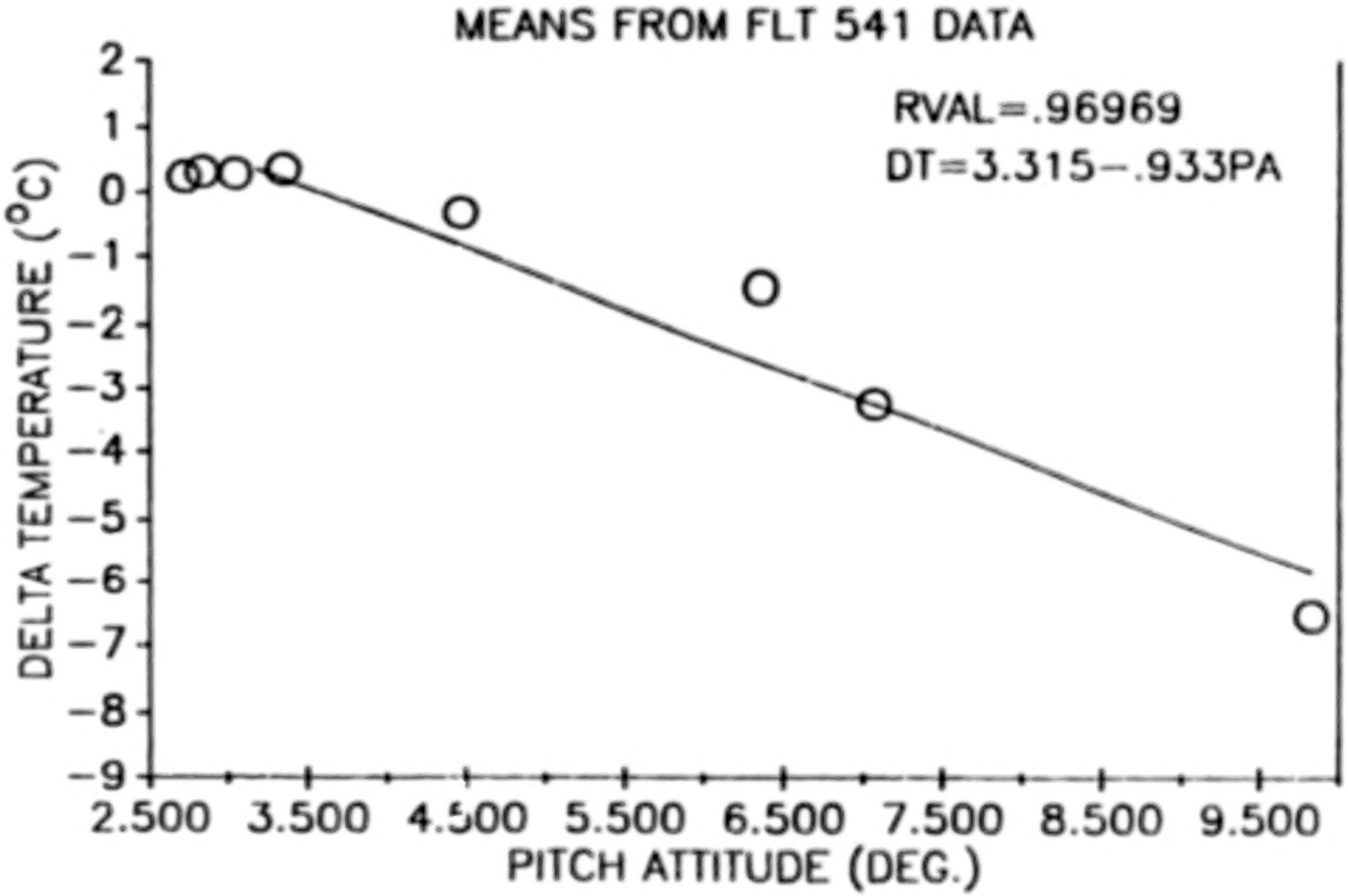
MEANS FROM FLT 541 DATA
RVAL=.96969
DT=3.315−.933PA
2
1
0
−1
−2
−3
−4
−5
−6
−7
−8
−9
DELTA TEMPERATURE (°C)
2.500
3.500
4.500
5.500
6.500
7.500
8.500
9.500
PITCH ATTITUDE (DEG.)

FLT 551 TURBULENCE ENCOUNTER

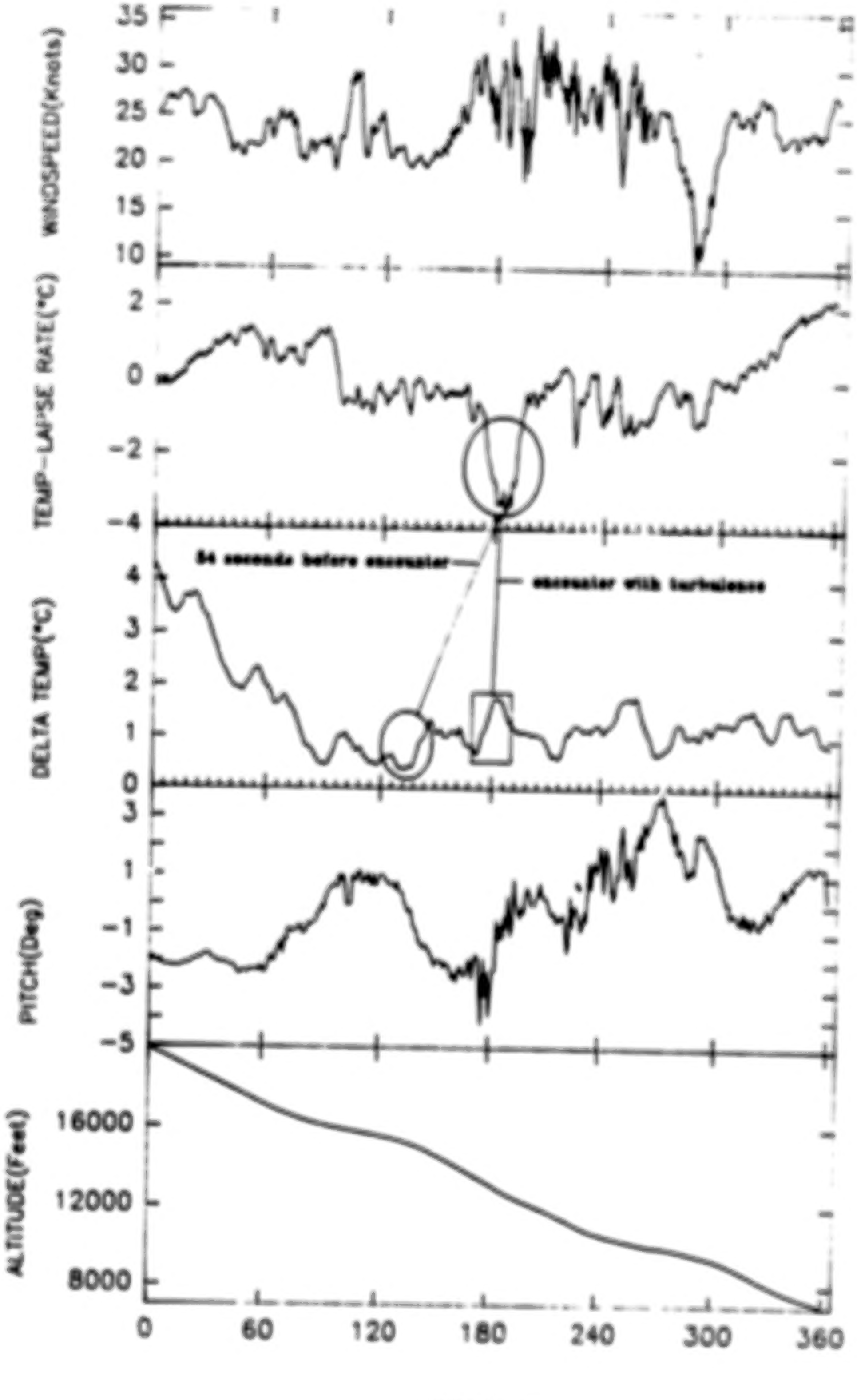

TIME SERIES MODEL FOR FLIGHT 551

DT(t): Infrared measurement of temperature difference at time t

ΔT(t): $T(t) - T(t + 54)$; difference of air temp. 54 seconds apart

$\theta(t)$: pitch attitude at time t

B : shift operator; $B^K X(t) = x(t - k)$

E(t) : Residual error from modelling

$$(1 - \Sigma a_k B^k) DT = \Sigma b_k B^k \theta + \Sigma c_k B^k \Delta T + E$$

Model $R^2 = .98$

estimated look distance 9.6 km

Advance detection time is 54 seconds

Average ground speed of 346.09 knots

Altitude ranged from 19,921 feet to 7,079 feet

CONCLUSION FROM NASA 737 FLIGHTS

- Prototype Infrared sensor measures temperature
- Temperature measurement is affected by pitch
- Look ahead distance of approximately 9.6 km or look ahead time of 54 seconds at high altitude for Flight 551

AWAS III MNEMONICS

LLWS1 - Predictive thermal F-factor

LLWSR - In situ thermal F-factor

FHAZF - In situ winds F-factor

ORLANDO EXPERIMENT 7/7/90

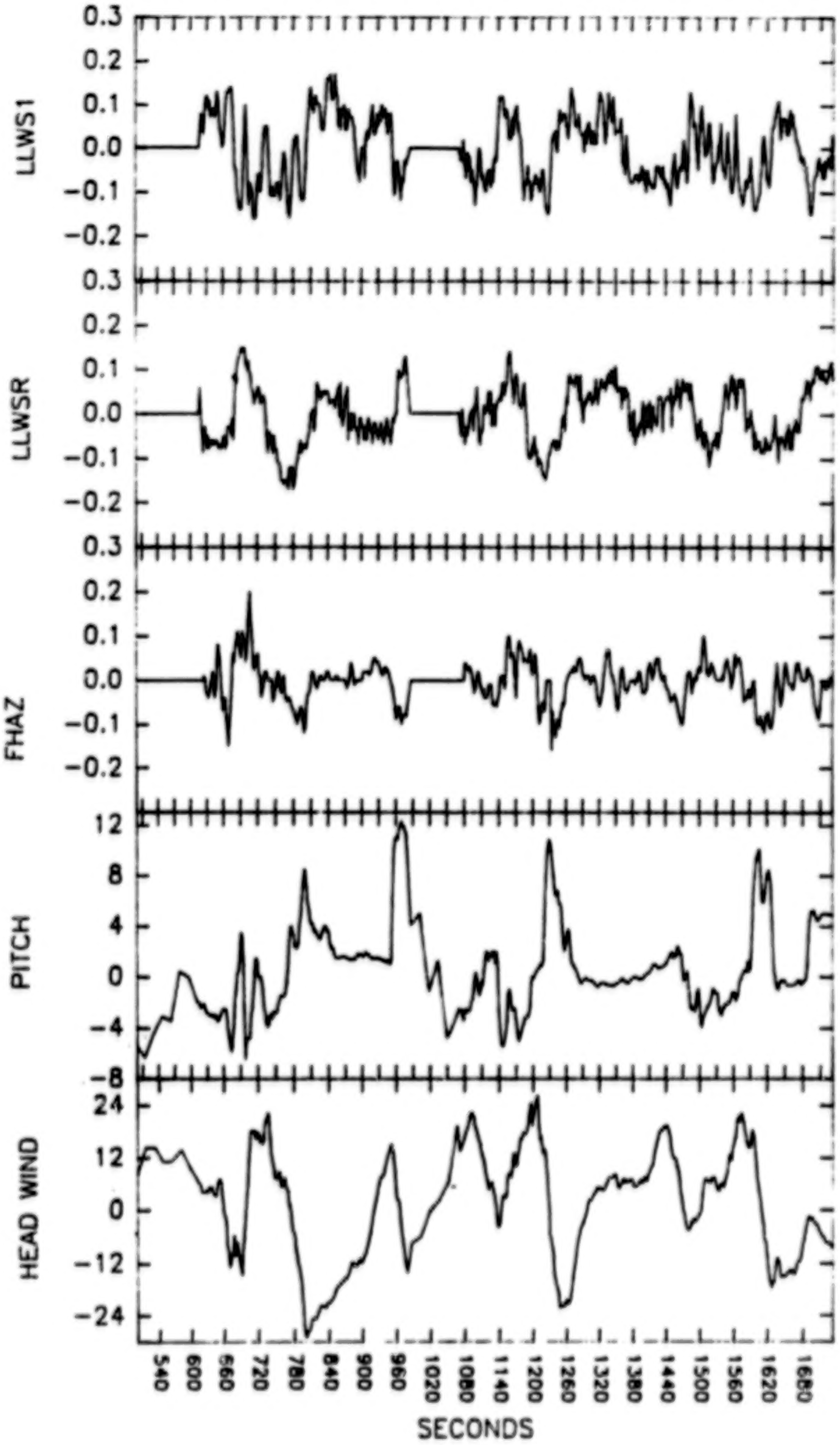

CROSSCORRELATIONS OF LLWS1 VS. LLWSR

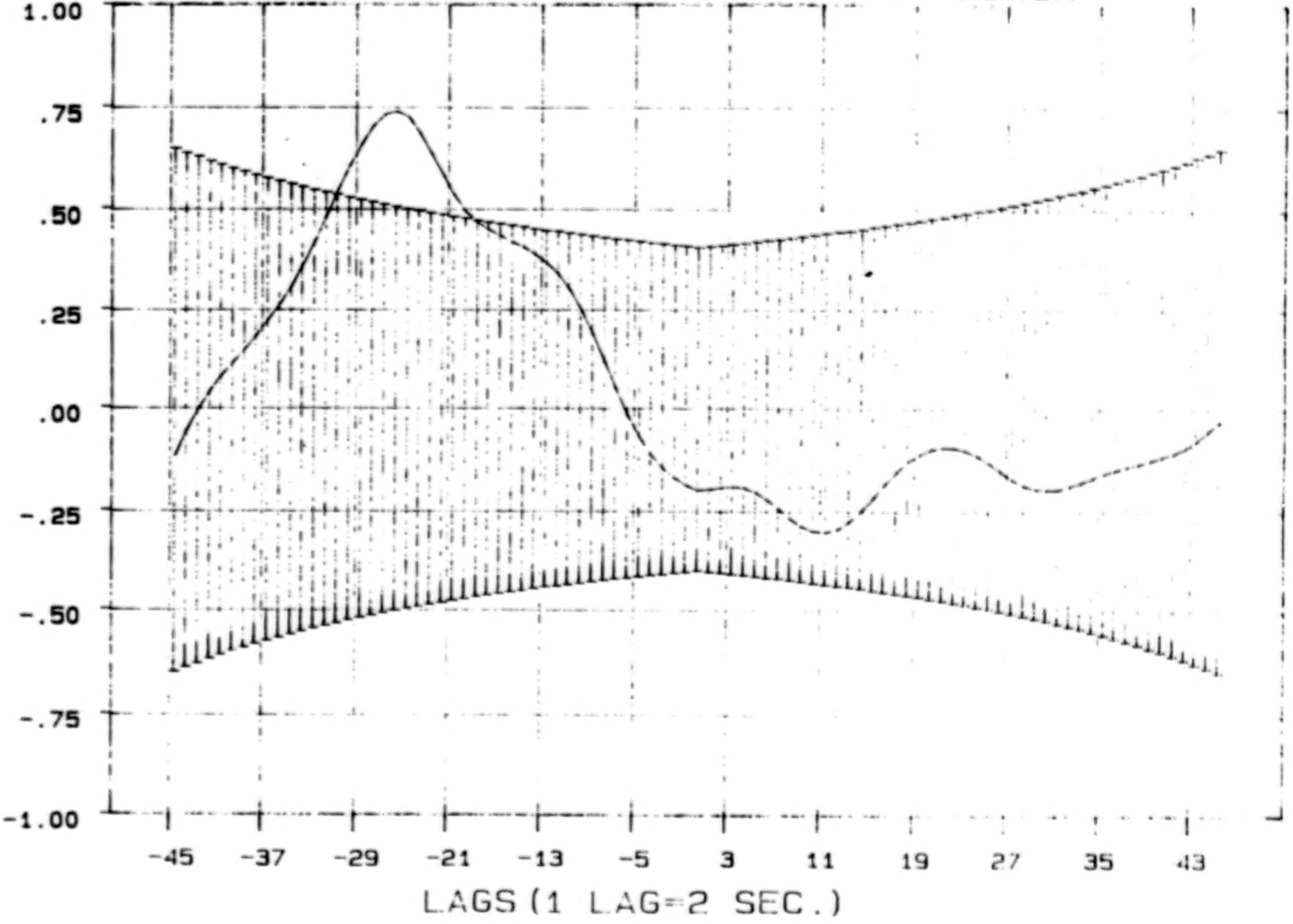

ORIGINAL PAGE IS
OF POOR QUALITY

CROSSCORRELATIONS OF LLWS1 VS. FHAZF

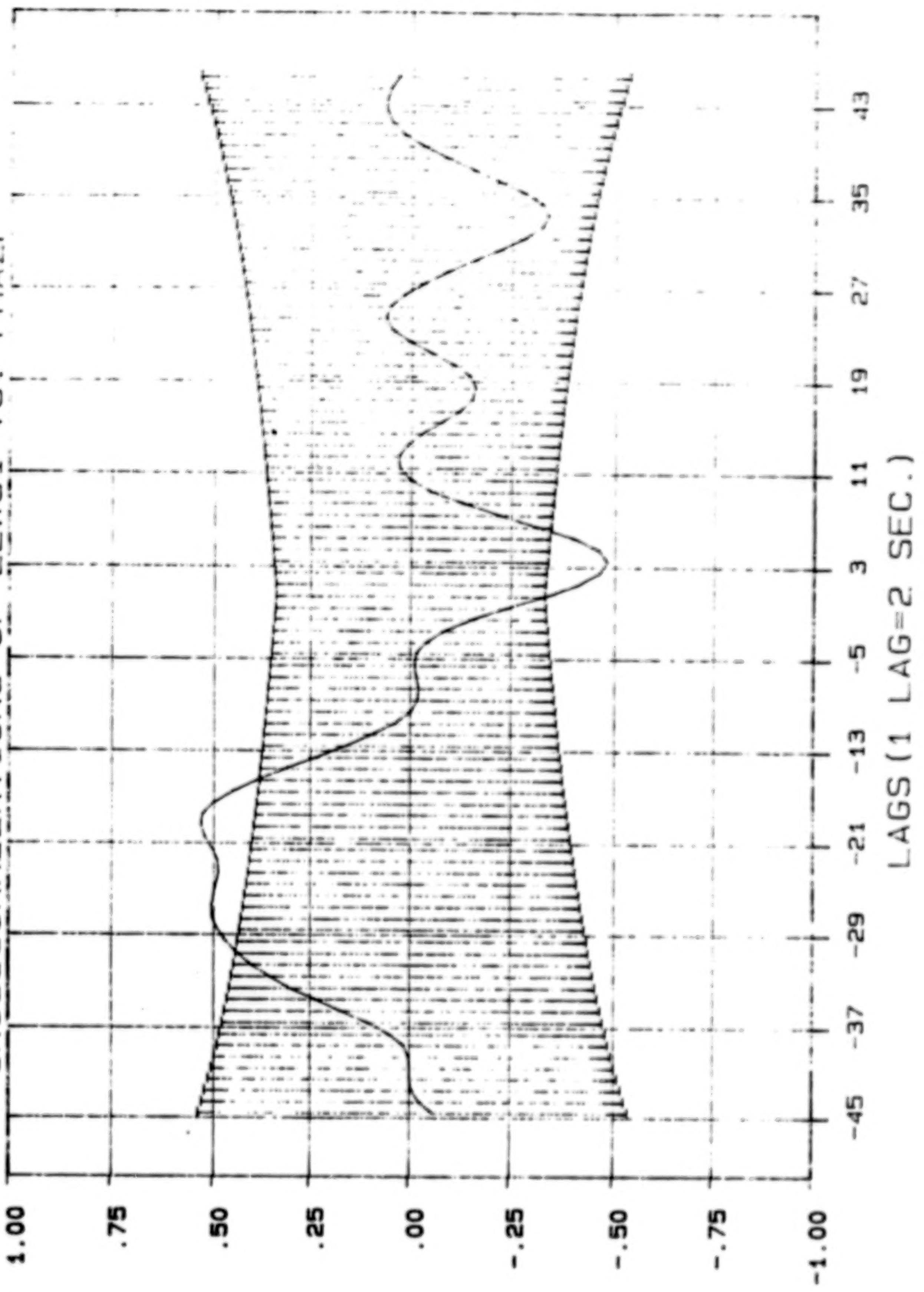

ORIGINAL PAGE IS
OF POOR QUALITY

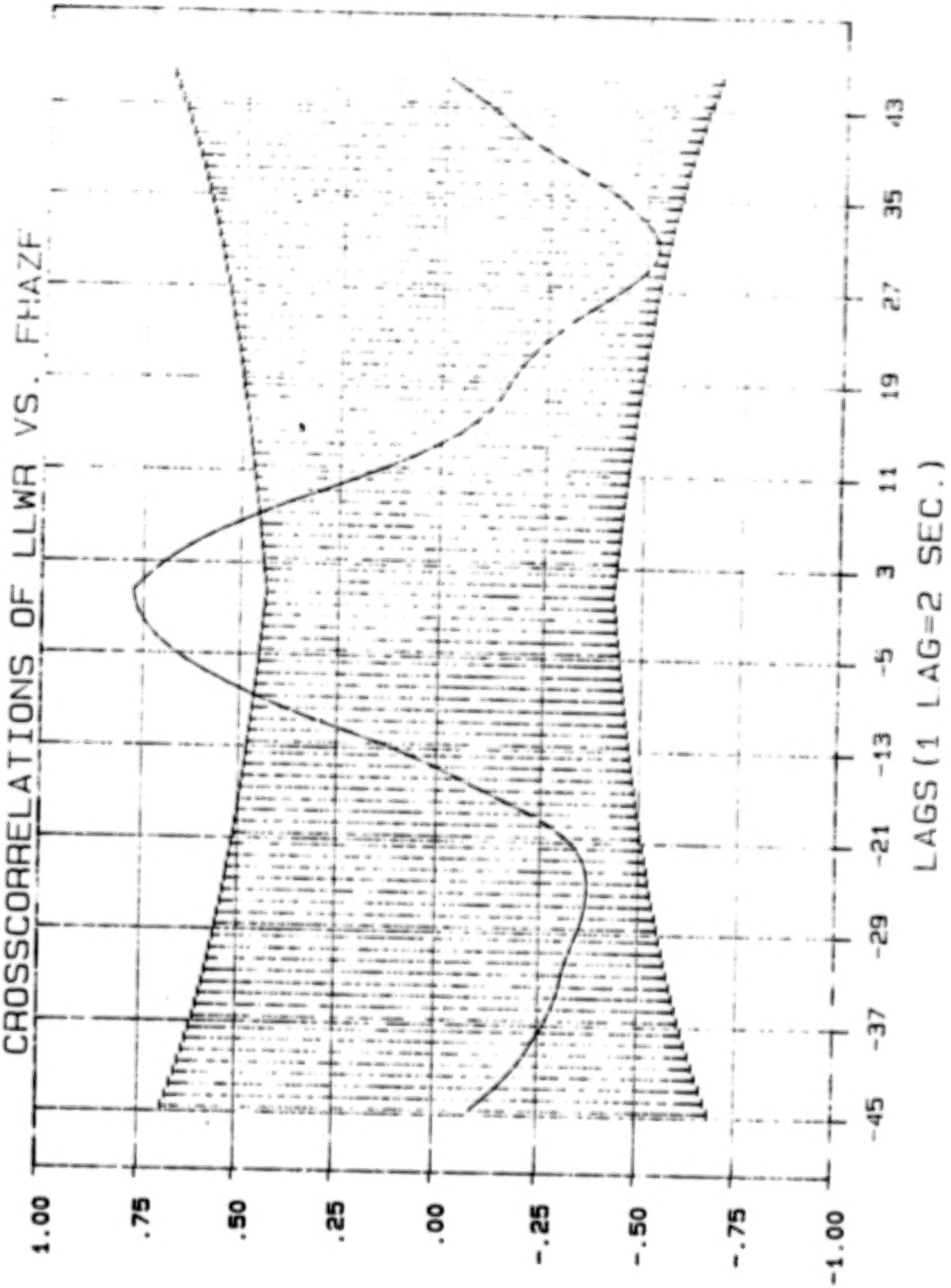

CROSSCORRELATIONS OF LLWR VS. FHAZF

ORIGINAL PAGE IS
OF POOR QUALITY

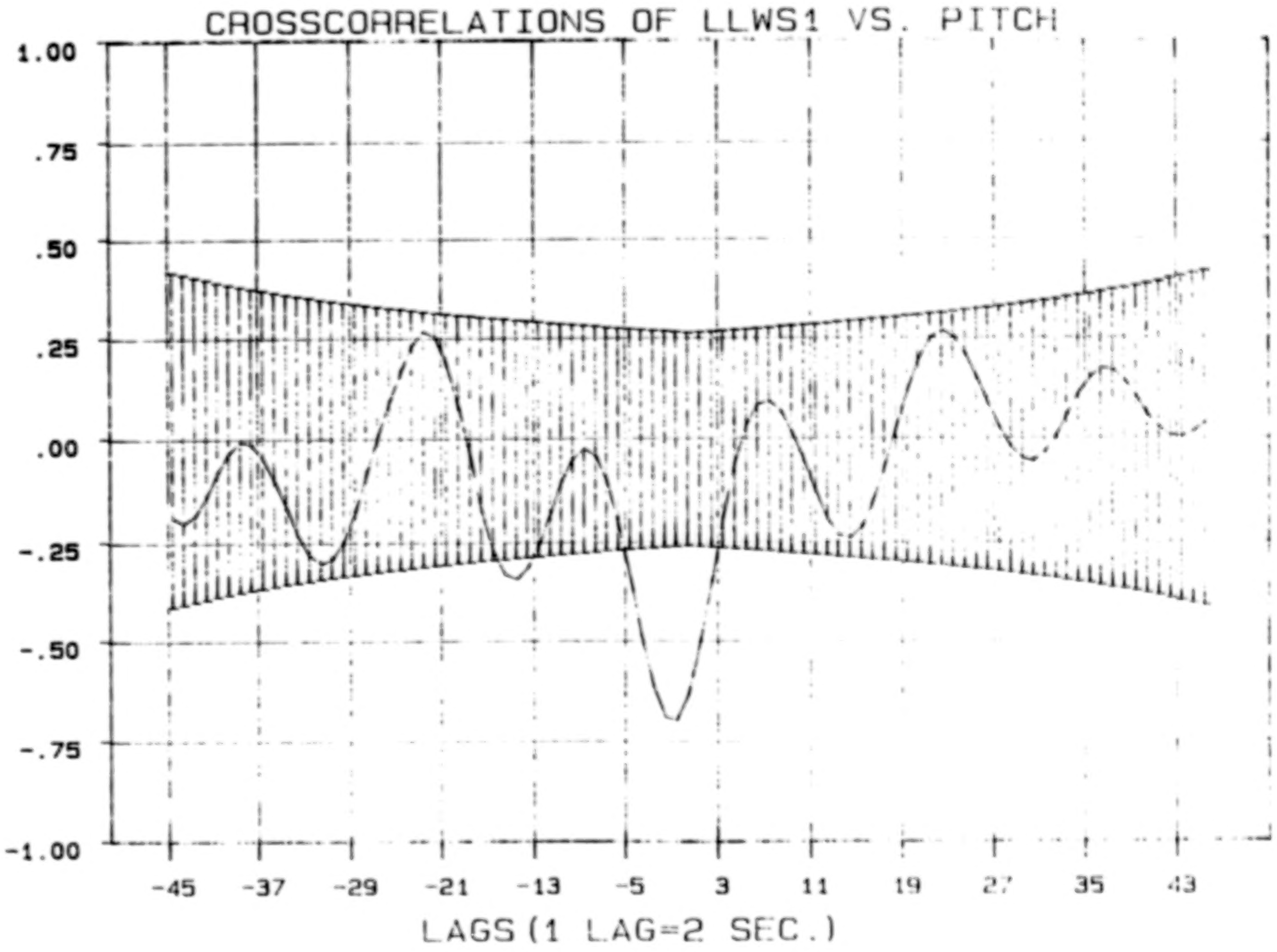

ORIGINAL PAGE IS
OF POOR QUALITY

TIME SERIES ANALYSIS OF ORLANDO 7-7-90 EVENT

$$(1 - \Sigma a_k B^k) F_T(t) = \Sigma b_k B^k F_{TI}(t + 23) + \Sigma c_k B^k \theta(t) + \mathrm{E}_T(t)$$

where F_T= thermal look-ahead F-factor

F_{TI} =thermal in situ F-factor

θ= pitch attitude

E_T = residual error from modeling

Model R^2 =.996

Estimated look distance 4.659 km

Advance detection time of 46 seconds

Average ground speed of 196.838 knots

Altitude ranged from 1843 to 393 ft.

CONCLUSIONS ON ORLANDO 7-7-90

F_T correlates with F_{TI}
F_T correlates with F
F_{TI} correlates with F
F_T correlates with θ

AWAS III showed an advance warning time of 46 sec for the first pass through the 7-7-90 event at Orlando, FL

SUMMARY

Atmospheric temperature changes and microbursts can be detected with forward looking infrared devices

NASA and Industry are continuing research (Orlando, LaRC and Denver) that will lead to the validation of windshear detection via infrared technology

Status of NASA's IR Wind Shear Detection Research
Questions and Answers

Q: MIKE TAYLOR (Boeing) - Will a lightning flash or a series of flashes in the infrared sensors field of view cause a temperature anomaly similar to a microburst event?

A: BURNELL McKISSICK (NASA Langley) - Lightning flashes tend to be too local. They are very small events. The temperature anomaly that is sensed by infrared, the one that is really detectable from the standpoint of wind shear hazards, is a reduction in temperature drop. Lightning wouldn't be that. If you could sense one, it would be like a spike, I would think, a rise in temperature. Also being very local, I don't think it would be something you could sense from infrared.

Session IX. Airborne Passive Infrared

N91-24146

Status of Turbulence Prediction System's AWAS III
Pat Adamson, Turbulence Prediction Systems

Status of
Turbulence Prediction Systems
AWAS III

H. Patrick Adamson

Turbulence Prediction Systems

Advance Warning Airborne System (AWAS)

- AWAS I 1987
- AWAS II 1988
- AWAS III 1990

Funded in part by NASA SBIR Contracts

Flight Tests

- **AWAS I** Piper Apache , Cessna Citation II & NASA B 737
- **AWAS II** Cessna Citation II
- **AWAS III** Cessna Citation II, MD 80 & NASA 737

FAA CERTIFICATION

- AWAS II STC: 1 Installation
- AWAS III STC: 4 Installations
  Production model
  Platform Independent STC

PASSIVE INFRARED SYSTEM RECORDS THE FIRST EVER VALIDATED IN-FLIGHT PREDICTION OF A MICROBURST

H. PATRICK ADAMSON
TURBULENCE PREDICTION SYSTEMS
3131 INDIAN ROAD
BOULDER, COLORADO 80301

Paper Presented at SAE S7 Meeting
Cincinnati, Ohio
October 8, 1990

ABSTRACT

On July 7, 1990, a passive infrared system flown on the University of North Dakota Cessna Citation II atmospheric research aircraft achieved the first ever advance warning of an in-flight windshear encounter.

The Cessna, following vectors from a ground based Terminal Doppler Weather Radar (TDWR) operated by MIT and NASA, intentionally flew towards a known windshear. The infrared system on the aircraft recorded the detection of the windshear with a 35 second advance warning.

The aircraft continued to fly into the windshear to record the encounter. The aircraft was equipped with a: 1) Turbulence Prediction Systems (TPS) passive infrared Advance Warning Airborne System (AWAS), 2) inertial navigational system (INS), and 3) air data measurement device. The data recorded in-flight by the infrared system was later compared to and found to agree with the data recorded by the TDWR and the in-situ air data.

Background and Introduction

The hazard to aircraft resulting from an unexpected encounter with low-level windshear is well established. In studies using flight simulators, it was proven that the amount of warning time provided to the flight crew was the most significant factor in ensuring a successful recovery from a microburst encounter.[1] The AWAS-III, which is the third generation system and is in the process of FAA certification, provides advance warning by sensing the temperature signature of a microburst ahead of the aircraft. A number of studies have demonstrated that there is a reliable relationship relating the severity of the microburst hazard to the change in temperature between the ambient air and the microburst.[2] The AWAS senses this change in temperature and through the use of a proprietary algorithm, constructs a hazard index.[4]

When this index exceeds a pre-determined level, an alert is provided to the flight crew through an aural warning and the illumination of a red warning lamp in the cockpit.

The following describes the performance of the AWAS during the approach to and the penetration of a severe microburst in Orlando, Florida. To judge this performance, the data recorded by the AWAS is compared to that recorded by the in-situ aircraft sensors and by the ground based TDWR.

Significant advance warning (10 seconds or more) prior to a microburst encounter has not been available until now. The Turbulence Prediction Systems (TPS) Advance Warning Airborne System (AWAS), a passive infrared spectrometer, provided the first ever verified advance warning (more than 35 seconds) of a severe windshear event. This historic event occurred on July 7th, 1990.

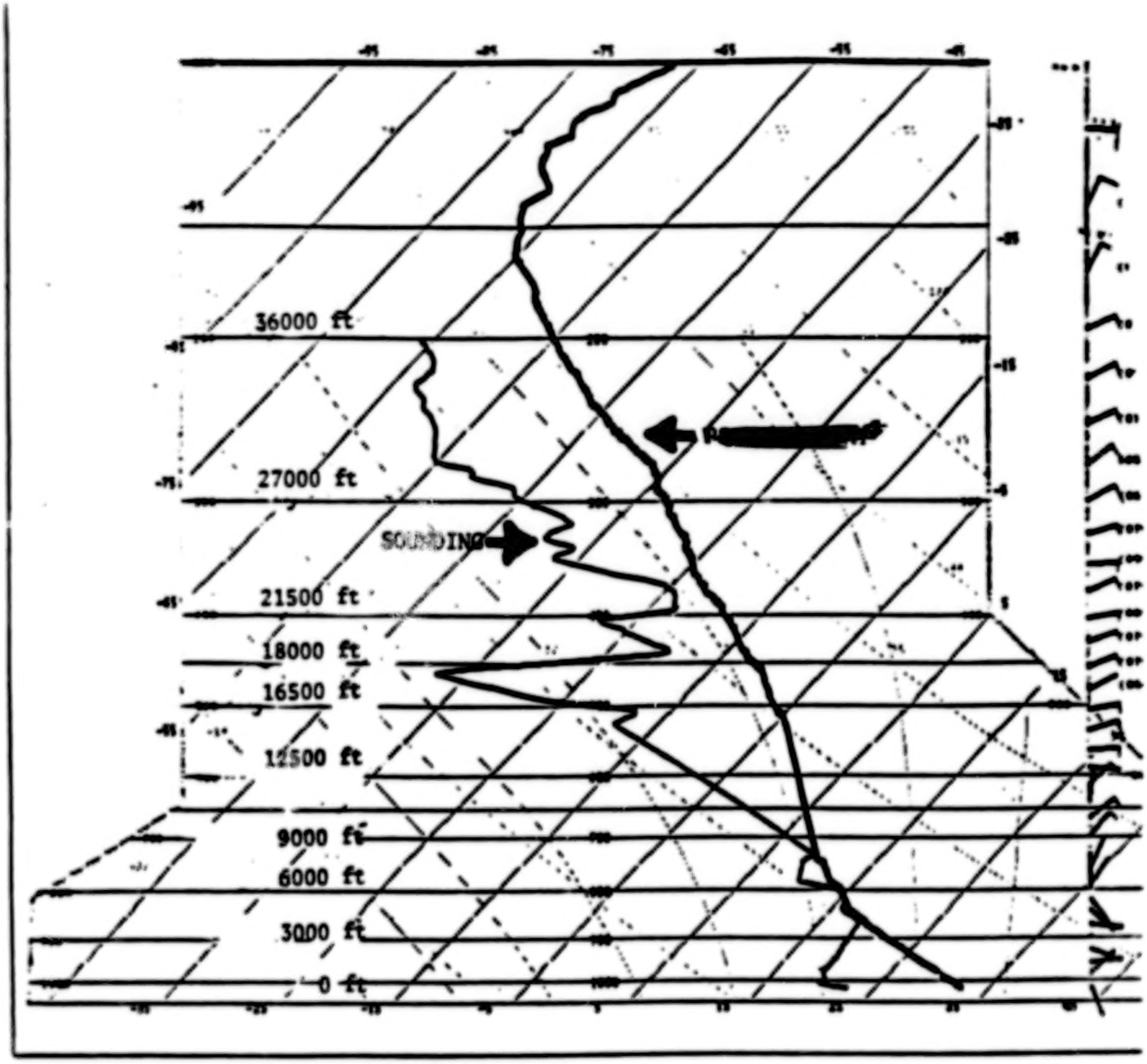

RAWINDSONDE Data - Figure 1

Massachusetts Institute of Technology Lincoln Laboratory (MIT) conducted a RAWINDSONDE (sounding) of the air over Orlando at 16:50 GMT, approximately two hours before the microburst developed. This sounding revealed a very wet layer of air from 18,000 to 23,000 feet. Just below this wet air was a layer of dry air extending down from 18,000 feet to the 9,000 foot level. Another dry layer also existed below the 6,000 foot level. This type of configuration in the upper atmosphere, i.e., a wet layer with underlying dry layers is believed to constitute the conditions which favor the formation of wet microbursts.[3]

FRED REMER
UND FLIGHT SCIENTIST NOTES

14:31:30 Engine start. A cell is developing just to the northeast of the airport. There are towering cumulus all quadrants. Plan is to get up early and hope a cell drifts over the airport. Planning on successive ILS 17 approaches. The 1753 Z ATIS is 4,500 SCT, 25,000 bkn, visibility 12 miles, temperature 95, dew point 71, wind 110 @ 4 kts, altimeter 30.03". Crew: Kent Streibel, Frederickson, Remer, Copp.

14:43:55 Airborne. Climbing out to the south. ATC is taking us high (6000 ft.).

14:50:10 Downwind for ILS 17. The storm is situated over the approach end of Runway 17. It is 60 dbZ. Lots of anvil. Lots of precipitation.

14:51:07 The storm is starting to produce a microburst at the surface. It is just off our left wing. We are trying to keep the approach short so we can penetrate.

14:52:09 FL-2 observes a 25 knot divergence over the approach end of Runway 17. We are on final and heavy precipitation is obscuring the view of the airport.

14:57:29 Climbing out after penetration. Strong downdraft in precipitation and increasing tailwind as we exited the precipitation. Excellent study. Down air was 15 m/s.

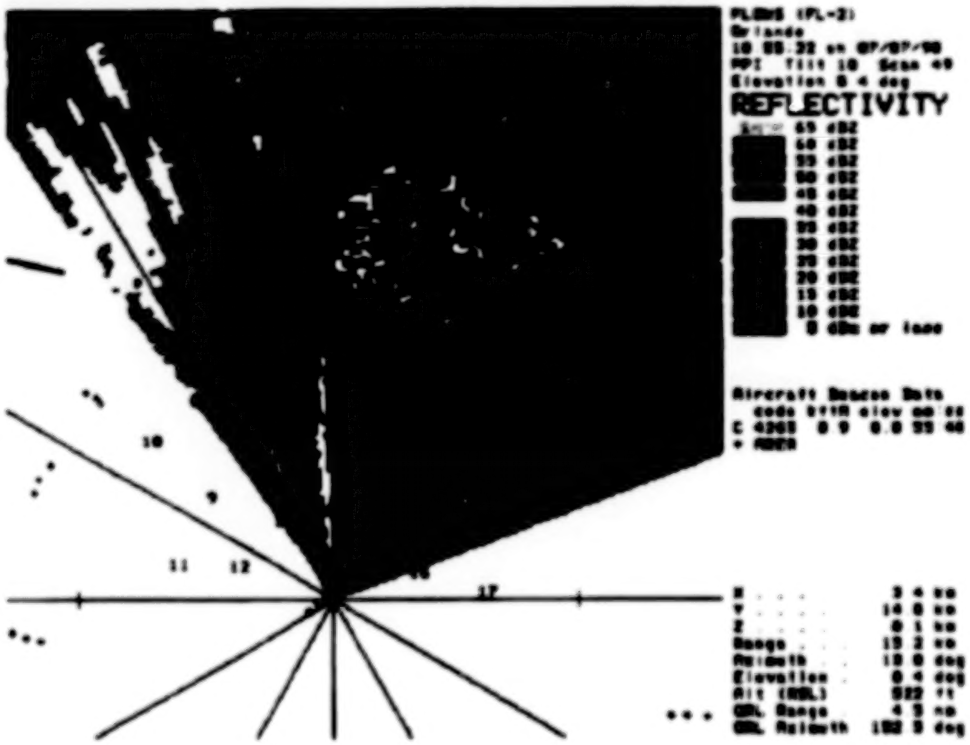

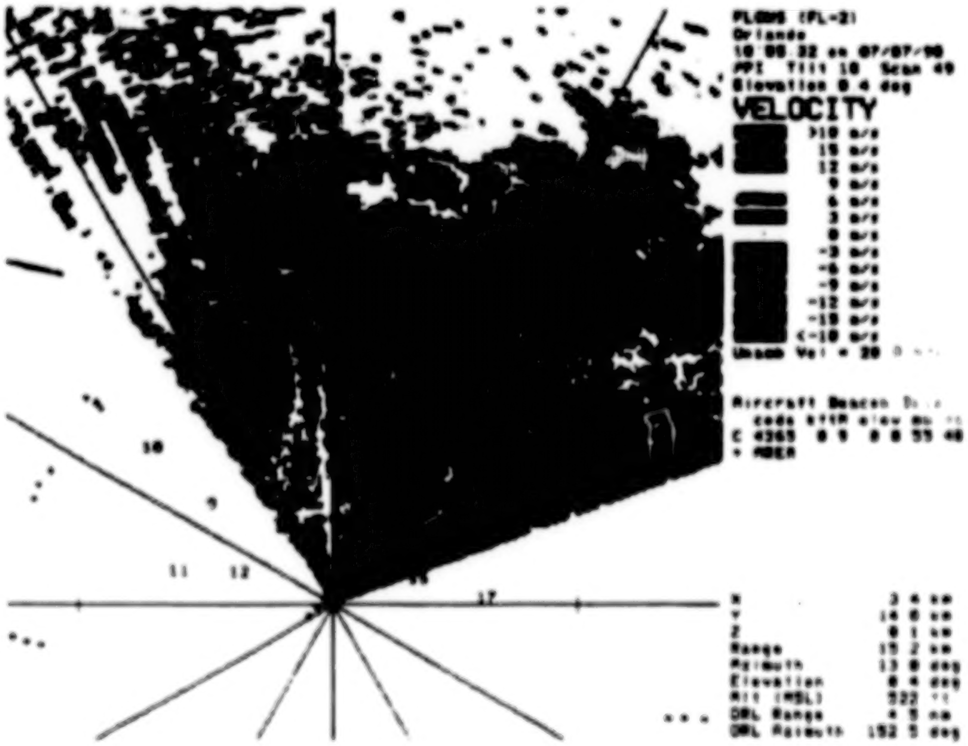

ORIGINAL PAGE IS
OF POOR QUALITY

TDWR Data - Figure 2

(pictured on previous page)

The TDWR scans provided by MIT clearly show a well developed microburst just north of the airport with a measured wind divergence of 23 m/s or about 50 kts. over a distance of approximately 3 miles. The peak TDWR windshear index calculated by Bowles/Hinton was 0.15.[5] The peak horizontal windshear occurred near the center of the microburst at about 1.5 kts/sec. with a peak downdraft of 1000 feet per minute. The beacon from the aircraft (indicated by the letter "C" in the scan) shows that the sequences and related aircraft altitudes were in agreement for both the TDWR and the aircraft sensors. The reflectivity scan represents the rain rate per hour. A 60 dBz reading is greater than 9.98 inches per hour. The velocity scan represents the horizontal winds. The minuses represent winds blowing toward the TDWR while the positive readings represent winds blowing away from the TDWR. The horizontal windshear occurs between the positive and negative readings. A reading of -12 m/s indicates a horizontal wind of approximately 24 knots.

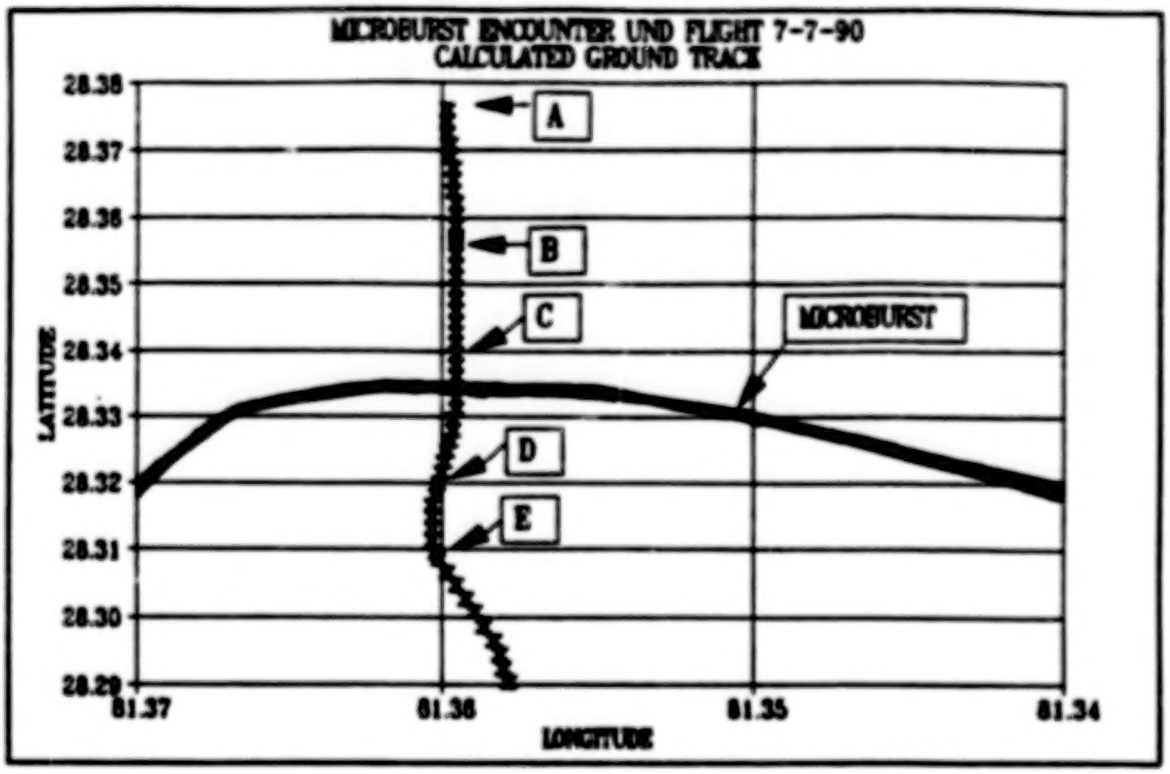

Ground Track - Figure 3

The Cessna Citation II was stabilized on an approach path toward the developing microburst in time to allow the AWAS to view the microburst for 90 seconds prior to penetration. When the aircraft was 90 seconds from penetration, the microburst (which was almost 3 miles in diameter) occupied approximately 40 degrees of the field of view. Since the AWAS has a field of view of only two degrees, the AWAS sensed the event throughout the entire approach.

The five letters, A through E, depicted in all of the graphs represent the following:

	LOCAL	GMT	SECONDS
A: Start of Stabilized Flight	14:54:29	18:54:29	53669
B: First AWAS Peak	14:55:02	18:55:02	53702
C: First AWAS Alert	14:55:22	18:55:22	53722
D: Second AWAS Alert Condition	14:55:42	18:55:42	53742
E: Peak Inertial Hazard	14:55:57	18:55:57	53757

Flight scientist notes indicate that at 14:50:10 (53410 sec) the TDWR is indicating that the storm detected near Runway 17 has a reflectivity of 60 dbZ. This corresponds to a rain rate of greater than 9.98 inches per hour. ATC reports at 14:54:24 (53664 sec) a divergence of 40 knots.

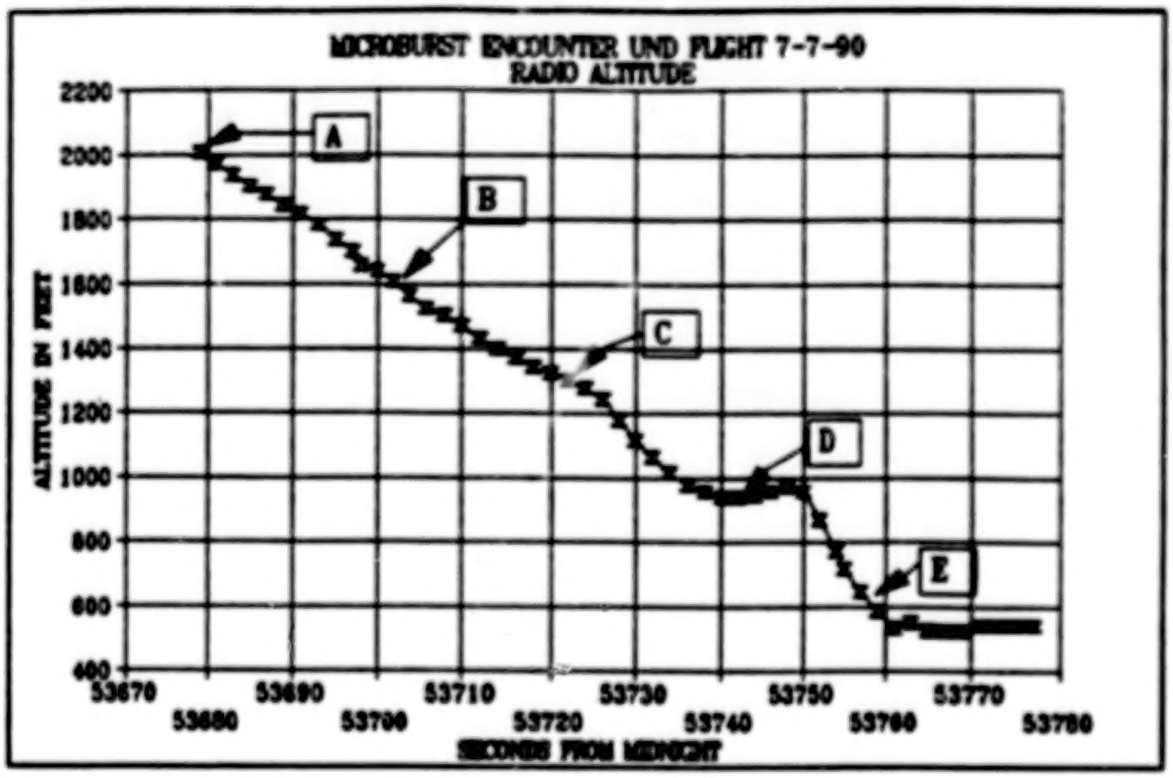

Altitude Profile - Figure 4

While approaching the microburst, the aircraft maintained a 3.5 degree glide slope. The aircraft (just before point 'D') leveled off while penetrating the microburst. Later it continued its glide path until it leveled off at approximately 500 feet.

The microburst maximum shear occurred at point 'E', where the combination of the horizontal and vertical winds combined @ ~650' AGL. The pilot countered the threat with increased throttle and continued through the event.

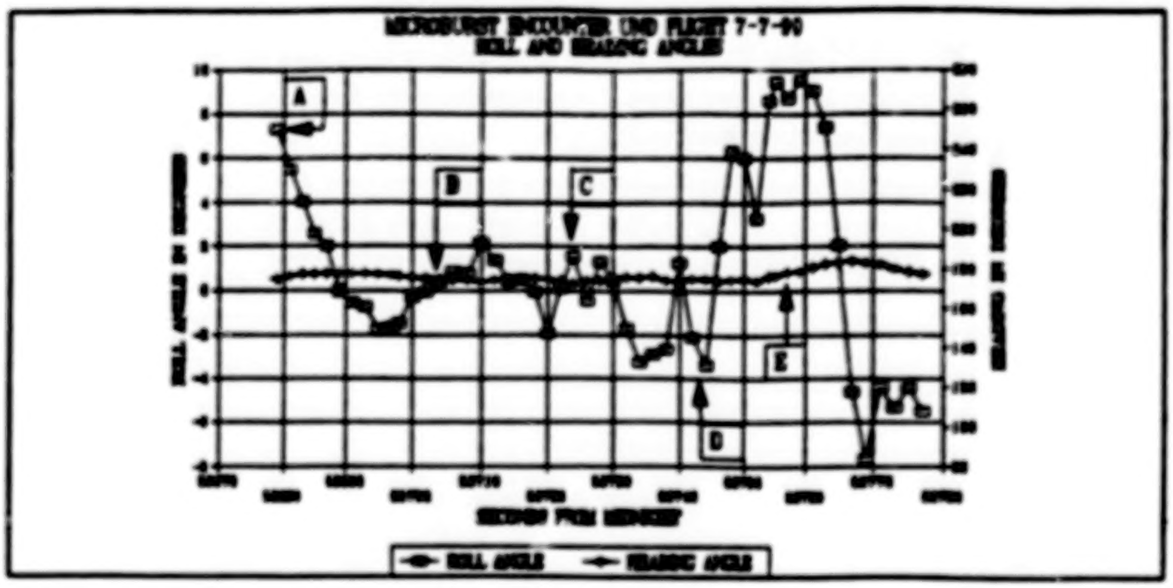

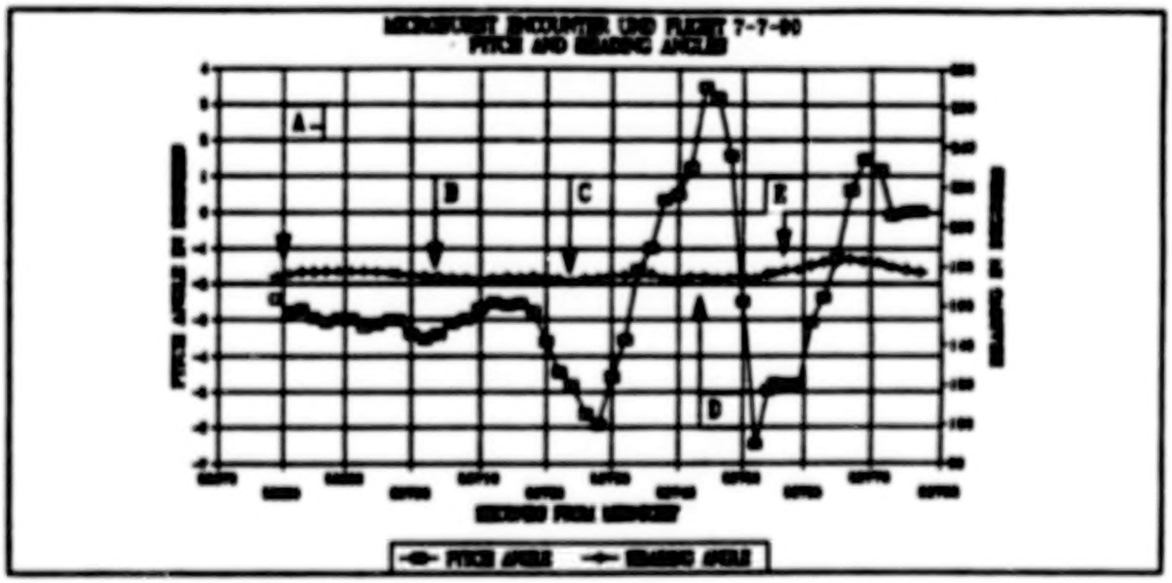

Roll, Pitch, and Heading Profiles - Figure 5 and 6

A constant heading is important for a predictive system because it is necessary to be observing the atmosphere in the expected flight path. The heading, as indicated in Figure 5, was constant throughout the approach to and the penetration of the microburst encounter.

The roll profile had a maximum deviation of 10 degrees during the encounter with the microburst. Roll angles varied from +2 to -4 degrees prior to penetration. During maximum shear, the greatest roll moment occurred (+10 to -5).

ORIGINAL PAGE IS
OF POOR QUALITY

The increasing changes in pitch as the aircraft approached the microburst is indicative of the increasing turbulence encountered. The greatest changes (-6 to +4) occurred on penetration of the microburst.

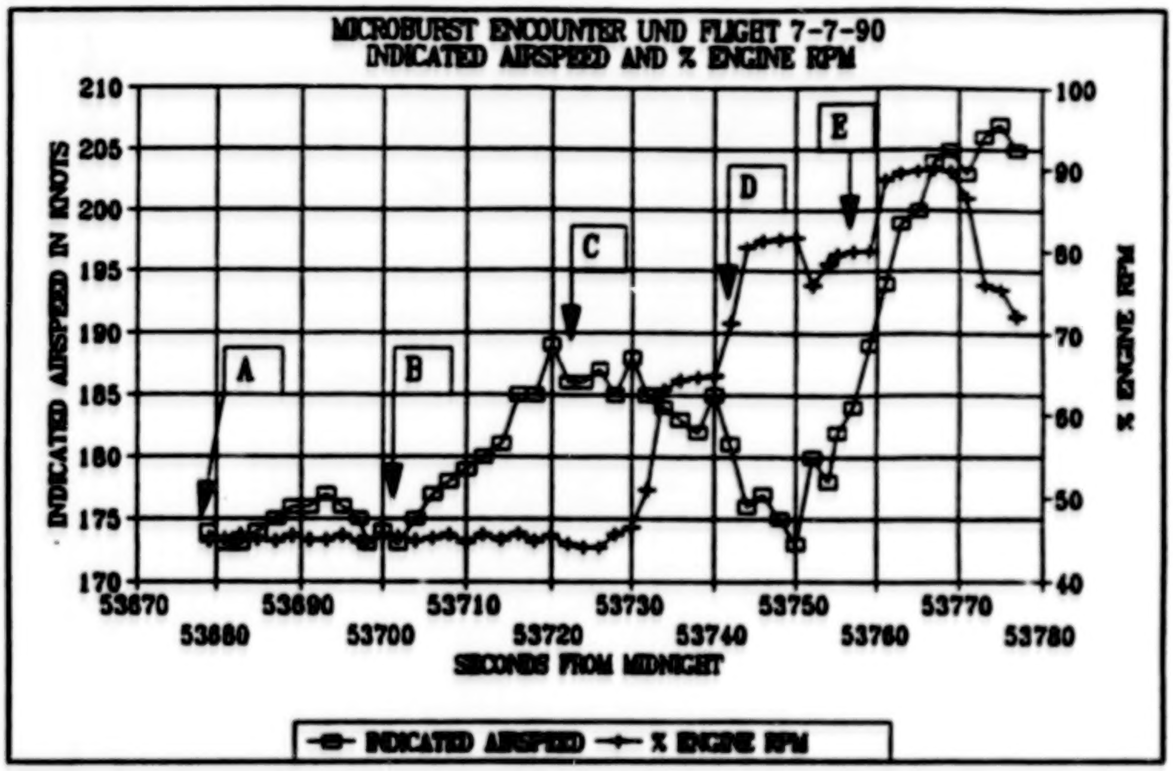

Airspeed and Thrust Profile - Figure 7

In preparation for penetrating the microburst, the pilot increased airspeed by 10 knots going from 175 to 185 knots. The pilot then leveled out the descent angle and increased the engine RPM by 20%, going from 45 to 65%.

During initial penetration (prior to point 'D'), the aircraft recorded a substantial reduction in performance. Even though the pilot increased engine thrust, the airspeed decreased by 10 knots. A significantly greater decrease in performance could be expected in an aircraft with less power capacity, i.e., a lower thrust to weight ratio.

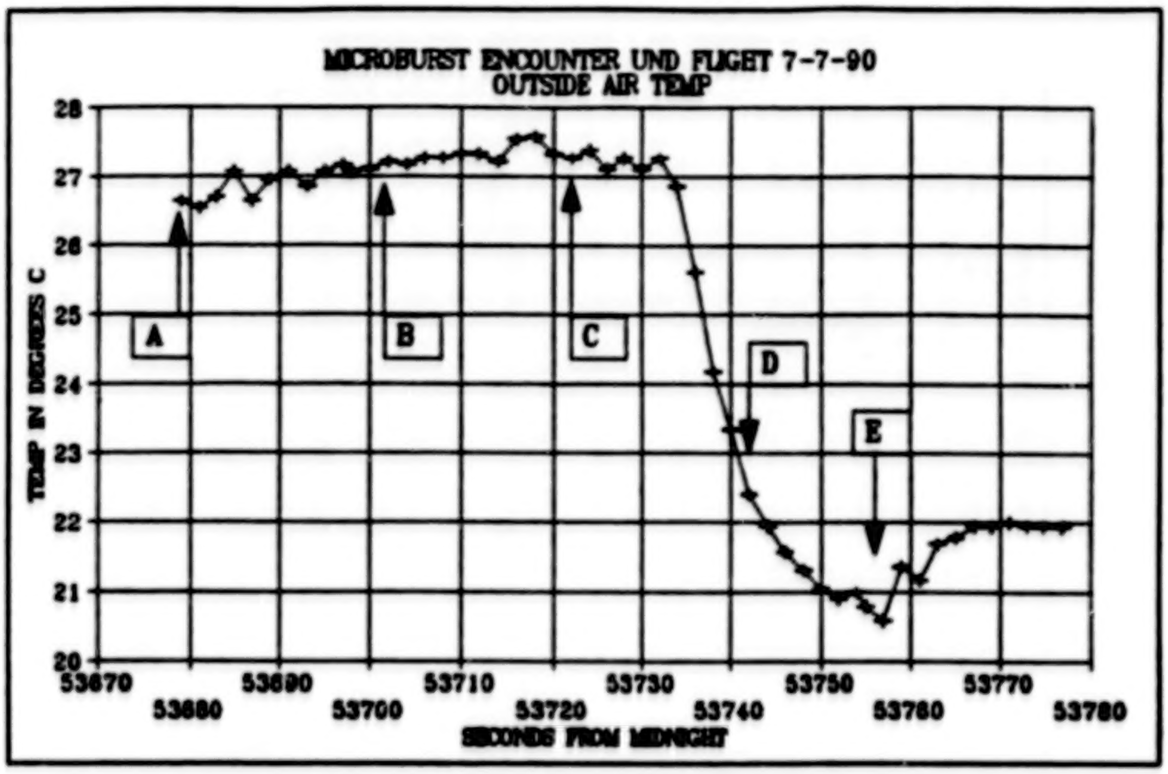

Outside Air Temp Profile - Figure 8

The outside air temperature profile obtained from the standard Citation instrument indicates a 6° C temperature decrease existing between the edge of the microburst and the maximum shear. This is the temperature change that is remotely sensed by the infrared system.

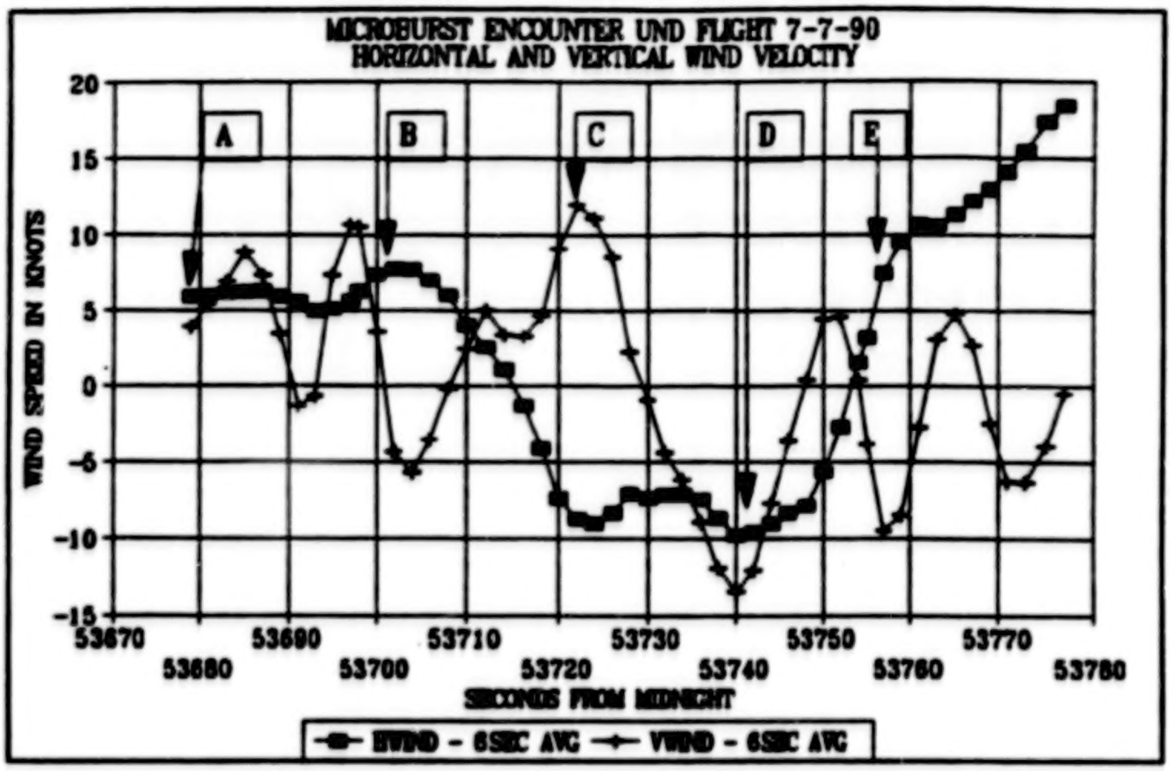

Horizontal and Vertical Wind Profile - Figure 9

These winds were calculated from the on-board INS sensor as the Cessna approached and passed through the microburst. While some degradation of the wind data was probably introduced by the turbulent flight, the major wind features of a typical microburst were recorded. The horizontal winds first shift from a slight tail wind to a performance increasing head wind as the microburst is approached. This occurs several seconds before point 'C'. This performance increasing head wind shifts rapidly to a tail wind near the axis of the microburst at point 'E'. The vertical winds indicate a major down draft beginning at 'C' and continuing throughout most of the event.

It should be noted that the maximum shear occurs with the combination of the horizontal wind and the second vertical downdraft at point 'E'. It is this combination of a changing horizontal wind (decreasing performance) and a downdraft that maximize the hazard to the aircraft.

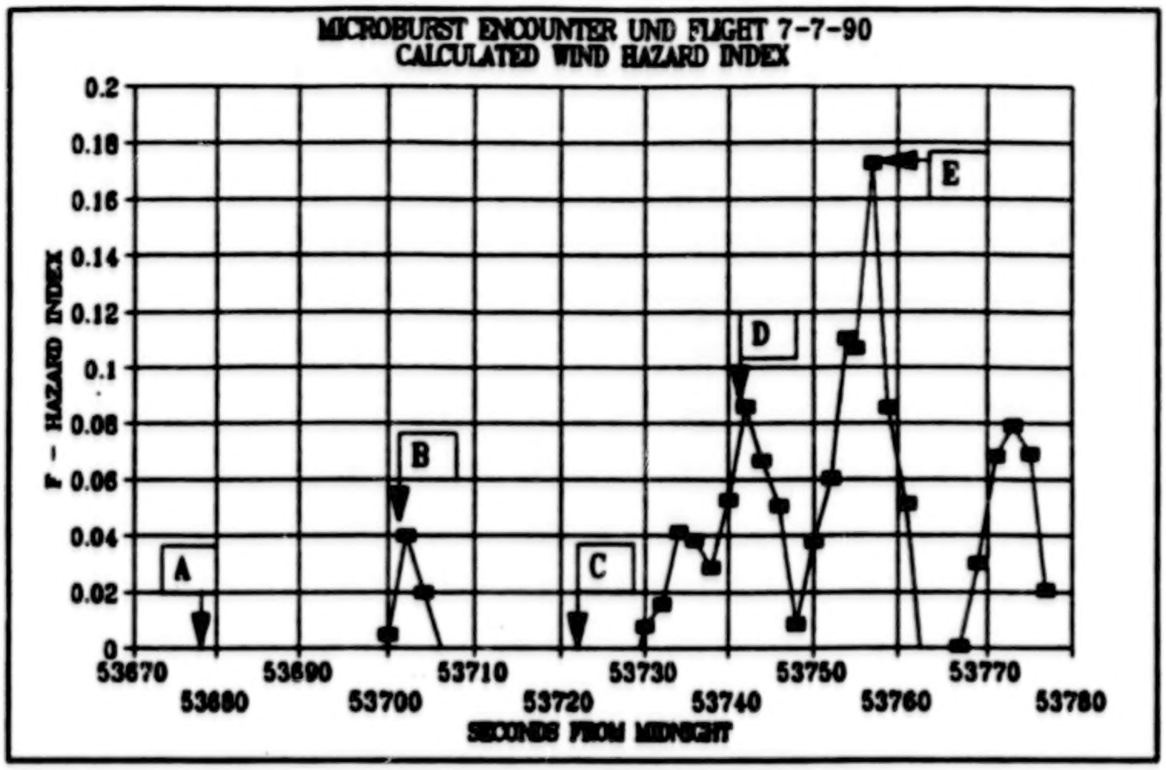

Hazard index F (threat) - Figure 10

The hazard index (F) represents the threat to the aircraft. F multiplied by the acceleration due to gravity (g) represents the thrust in kts/second necessary to maintain level flight.

In this flight, the wind hazard index was calculated from the INS winds. The one hertz data from the UND aircraft was used for high fidelity information. The winds are averaged over a 6 second period in order to reduce the effects of atmospheric transients which may be turbulent but not sustained. The 6 second running average is used to compute the wind hazard index by the following equation[6]:

$$F = (dWH/dt)/g - VW/AS$$

where dWH/dt is the change per unit time in flight path wind velocity. The units are kts/sec:

g is acceleration due to gravity in kts/sec (19.04 kts/s)
VW is the vertical wind velocity in kts
AS is the air speed of the plane in kts

In the instance where F = 0.17, the thrust required to negate the threat is 3.24 kts/s (0.17 x 19.04). This is within the performance capabilities of the Cessna Citation II.

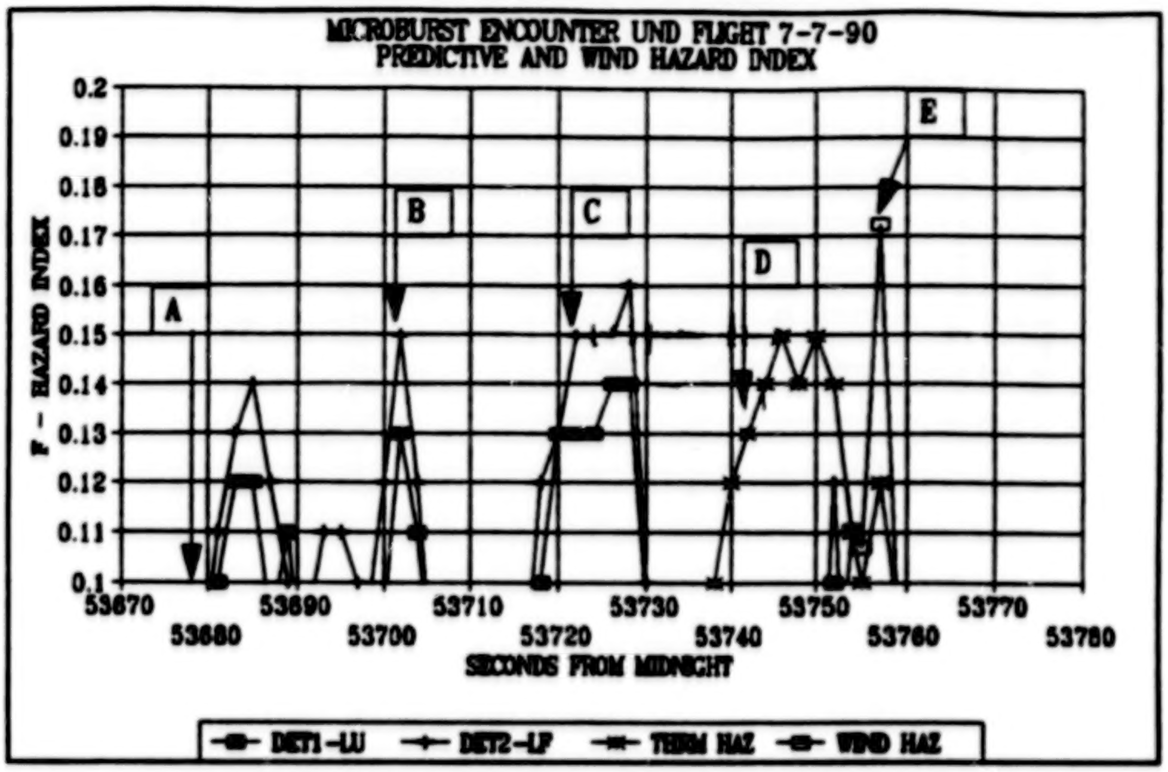

AWAS Performance vs In-Situ - Figure 11

The actual performance of the AWAS, in respect to accurately predicting the hazard to the aircraft, is provided in Figure 11. The only in-situ reference is at point 'E' indicating a hazard of 0.17.

The AWAS first sensed a hazard of 0.15 at point 'B'. Because this predicted threat was calculated above the altitude limit of 1500 feet, the alarm was not sounded. This did represent however, a potential predictive warning of 55 seconds.

The first AWAS infrared (IR) based predictive alert was recorded at point 'C'. Both aural and visual alerts were enabled at 1302 feet. This represented a predictive warning of 35 seconds.

At point 'D', the AWAS provided an alert based on outside air temperature (OAT). The use of this sensor provided a hazard of 0.13 and a 15 second warning.

The preset hazard thresholds in the AWAS are 0.15 for the IR and 0.13 for the OAT. The alerts were active at points 'B' and 'D' but because the present software inhibits aural and visual warnings at or above 1500' AGL, the alarms were inhibited at point 'B'.

AIRCRAFT VIDEO OF MICROBURST ENCOUNTER

A forward looking video camera mounted in the UND aircraft affords a pilot's eye view of the approach to the event. This video, along with flight scientist notes, is used as a confirmation tool- i.e. to identify pilot reactions, onset of rain, etc.

Conclusions:

TDWR F Index[5] = 0.15

In Situ F Index = 0.17

AWAS F Index = 0.15 55 seconds advance warning
0.16 35 seconds advance warning
0.~~15~~ 15 seconds advance warning
0.13

FAA Certification

FAA certification is in process. The application was filed in January 1990 and completion is expected in early 1991.

An FAA STC for AWAS-III installation on the UND Cessna Citation II was issued on 05/17/90. Research flights of the UND Citation since 05/17/90 will be used for Proof of Intended Function. Most recently the Citation has flown in the Orlando TDWR study (5/90 through 9/90) and in a Denver area dry microburst study (9/90). Numerous hazardous conditions occurred during these flights. The relevant flight and TDWR data is currently being analyzed by TPS, NASA Langley and UND Aerospace Sciences personnel.

An FAA STC for AWAS-III installation on American Airlines MD-80 (specifically DC-9-82 & 83) was issued 09/27/90.
The first of three AWAS-III installations was completed 09/27/90. Preliminary flight test data has been collected with actual commercial flight data expected soon. Data will be collected over 1000 flights to assist in operational aspects of certification.

BIBLIOGRAPHY

1 - Hinton, David A., 1990: "Relative Merits of Reactive and Forward-Look Detection for Windshear Encounters During Landing Approach for Various Microburst Escape Strategies", NASA Technical Memorandum 4158, DOT/FAA/DS-89/35.

2 - Proctor, F. H., 1989: "A Relationship Between Peak Temperature Drop and Velocity Differential in a Microburst", Preprint, 3rd International Conference on the Aviation Weather System, Anaheim, CA.

3 - Caracena, F. and Maier, M.W., 1987: "Analysis of a Microburst in the FACE Meteorological Mesonetwork in Southern Florida", American Meteorological Society.

4 - Adamson, H. P., 1988: "Airborne Passive Infrared System for the Advance Warning of Low-Level Windshear and Clear Air Turbulence: 1988 In-Service and Theoretical Work". AIAA/NASA/AFWAL Conference on Sensors and Measurements Techniques for Aeronautical Applications, 9/88, Atlanta, Georgia.

5 - Bowles, R. L. and Hinton, D. A., 1990: "Windshear Detection: Airborne System Perspective", Presented at WINDSHEAR-One Day Conference, London, England, 11/90.

6 - Bowles, R. L. and Hinton, D. A., 1990. Same as Above.

FUTURE ISSUES FOR PREDICTIVE LLWS SYSTEMS

- Define LLWS threat by type
- Define system requirements
- Define certification methodology
- SAE S-7 to instigate TSO effort

DEFINE LLWS THREAT BY TYPE

(Revise AC 0050)

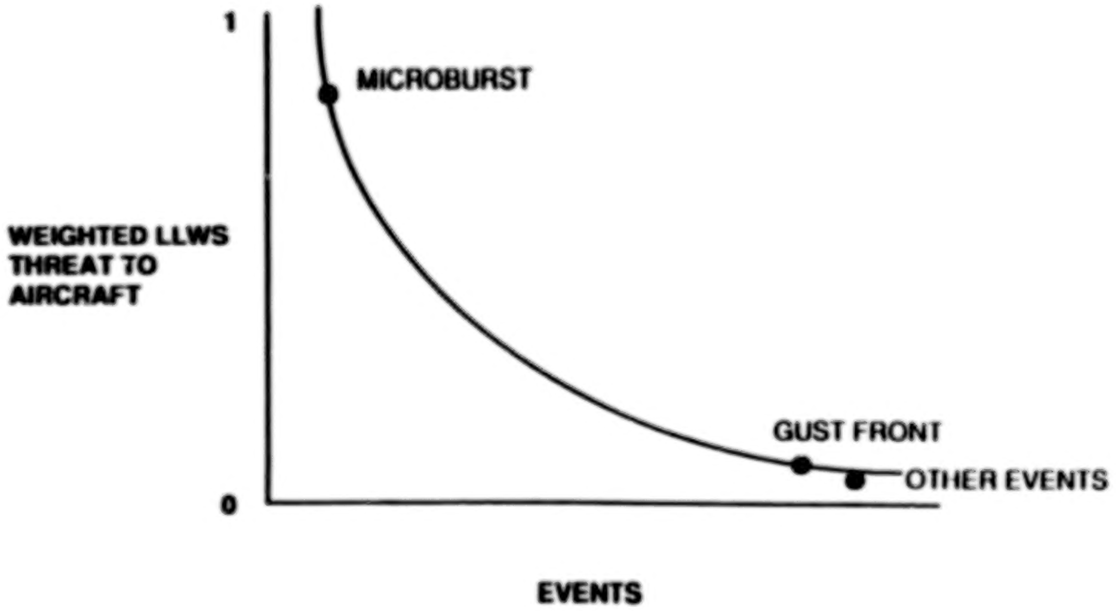

DEFINE SYSTEM REQUIREMENTS

- Min/Max warning time
- Approach corridor rain rate ≤ 40 dbz
- Wet and dry microburst detection
- Probability of detection
- Nuisance alert criteria

DEFINE CERTIFICATION METHODOLOGY

- Success criteria plan (ref AC25-12)
  - analysis
  - modelling data
  - flight data
  - combination of above
- Supporting documentation

Status of Turbulence Prediction System's AWAS III
Questions and Answers

Q: MARILYN WOLFSON (MIT Lincoln Laboratory) - Can your sensor be used to detect clear air turbulence? If so, do you have any data that shows its effectiveness?

A: PAT ADAMSON (Turbulence Prediction Systems) - Yes. We'll be doing clear air turbulence tests in the American Airlines program. I forgot to mention it in the talk. We expect to get six minutes warning at high altitude in clear air turbulence.

Q: MIKE GALE (American Airlines) - Based on the positive reaction by the "scientific community" to the 35+ second predictive warning of the AWAS III in relatively heavy rainfall on 7/7/90, has the question regarding IR penetration distance been laid to rest?

A: PAT ADAMSON (Turbulence Prediction Systems) - I don't know if it has been laid to rest. From my perspective we certainly look through some of the rain. We're still trying to analyze how far through the rain we looked. One of the things we hope to get out of the UND sensor is the rain rate from the aircraft. So we'll get some numbers from that work.

ROLAND BOWLES (NASA Langley) - I'll answer the same question that was addressed to Pat because I think it was addressed to both of us. Data is data. If Pat has no problem, anybody that wants it can take it home with them. My conclusion is I saw the performance increase on the back side of the microburst right in the rain core. From best estimates anywhere from 5 to 6 inches per hour, maybe as high as 7 inches per hour of rain, that's pretty wet . Objectively it looked like it saw through it. So, I'll share that data with anybody.

UNKNOWN - Would you share it with the Long Beach Aircraft Certification Office?

ROLAND BOWLES (NASA Langley) - Any time they are ready.

HERB SCHLICKENMAIER (FAA) - We're in the throws of putting together a briefing for Long Beach of not only this meeting but some of the technical topics that they might want to review with us as well. Guice Tinsley is also interested in coming down here with his team, as soon as funds are available to travel, to get a review of what this meeting did and what happened.

Session IX. Airborne Passive Infrared

N91-24147

Status of Colorado State Universities' IR Research
Dr. Pete Sinclair, Colorado State University

An Airborne FLIR Detection and Warning System for Low Altitude Wind Shear

Peter C. Sinclair
Department of Atmospheric Science
Colorado State University
Fort Collins, CO

Peter M. Kuhn
ARIS, Inc.
Fort Collins, CO

October 18, 1990

To be published in:

The Journal of Applied Meteorology
November 1990

Abstract

There is now considerable evidence to substantiate the causal relationship between low altitude wind shear (LAWS) and the recent increase in low-altitude aircraft accidents. The National Research Council (1983) has found that for the period 1964 to 1982, LAWS was involved in nearly all the weather related air carrier fatalities. However, at present, there is no acceptable method, technique, or hardware system that provides the necessary safety margins, for spatial and timely detection of LAWS from an aircraft during the critical phases of landing and takeoff. The Federal Aviation Administration (FAA) has addressed this matter (Federal Registry, 1988) and supports the development of an airborne system for detecting hazardous LAWS with at least a one minute warning of the potential hazard to the pilot. One of the purposes of this paper is to show from some of our preliminary flight measurement research that a forward looking infrared radiometer (FLIR) system can be used to successfully detect the cool downdraft of downbursts (microbursts/macrobursts) and thunderstorm gust front outflows that are responsible for most of the LAWS events. The FLIR system provides a much greater safety margin for the pilot than that provided by reactive designs such as inertial-air speed systems that require the actual penetration of the MB before a pilot warning can be initiated. Our preliminary results indicate that an advanced airborne FLIR system could provide the pilot with remote indication of MB threat, location, movement, and predicted MB hazards along the flight path ahead of the aircraft.

In a proof-of-concept experiment, we have flight tested a prototype FLIR system (non-scanning, fixed range) near and within Colorado MB's with excellent detectability. The results show that a minimum warning time of one-four minutes (5-10 km), depending on aircraft speed, is available to the pilot prior to MB encounter. Analysis of the flight data with respect to a modified 'Hazard Index' indicates the severe hazard that the apparently weak and innocuous MB's present to both the commercial transport pilots as well as the much larger number of pilots who fly the smaller general aviation and executive aircraft.

1. Introduction

Over the past few years the importance of low altitude wind shear (LAWS) from thunderstorm outflows and downbursts to aviation safety has resulted in the development of several new detection techniques and warning systems. The driving force for this atmospheric research had its roots in the sobering statistics of LAWS related accidents. The 1975 Eastern Airlines accident at Kennedy Airport (Fujita, 1985) provided much of the impetus for this initial research and development work.

The National Transportation Safety Board (NTSB) statistics show that 1987 was the worst year for air travel since 1974 with 31 aircraft accidents claiming 231 lives. A number of these accidents were related to low altitude wind shear (LAWS)[1] incidents during the approach or takeoff phases. In addition, a study conducted by the National Research Council (1983) for the period 1964 to 1982 showed that LAWS was involved in nearly all the air carrier fatalities. Since 1982, the NTSB has studied three additional LAWS accidents, including the widely publicized Delta Airline microburst accident at Dallas/Fort Worth International Airport where 134 passengers and crew were killed. These studies do not include similar statistics for the largest aircraft segment of the country, i.e. private and executive aircraft or general aviation aircraft (GA). Because of their low-altitude operating regime GA aircraft have increased possibilities of encountering dangerous wind shear events. Aircraft with high airspeed and wind loading appear to be more sensitive to head/tail wind variations than aircraft with low airspeed and wing loading which are more sensitive to downdraft/updraft penetrations (Stengel, 1984). Our preliminary studies suggest that many small, private aircraft accidents, especially over high terrain are the result of LAWS generated by gust fronts (GF), and/or micro-macroburst (MB) activity.

Although, significant progress has been made in the development and testing of the TDWR[2] and the LLWAS[3] for large airport LAWS hazards (Mahoney, *et al.* 1989; Turnbull.

---

[1] LAWS as used in this proposal is a generic term which includes the wind shear/vertical motion fields produced by gust fronts (GF), and microbursts/macrobursts (MB).

[2] TDWR: Terminal Doppler Weather Radar (Research Applications Program, 1988)

[3] LLWAS: Low Level Windshear Alert System (Wilson and Flueck, 1986; Goff and Gramzow, 1989)

et al., 1989; Goff and Gramzow, 1989; McCarthy and Wilson, 1985; Campbell, *et al.*, 1989; Smythe, 1989), the FAA (Federal Registry, 1988) and other Federal agencies now recognizes that there is a need for an airborne low altitude wind shear system that will:

1. supplement the planned 47 airport deployment of LLWAS and TDWR warning systems, and
2. provide an on-board aircraft system that will indicate low altitude wind shear hazards at all airports for all commercial aircraft during the critical landing and takeoff phases.

The importance of an airborne system is manifested in its unique capability to search, in real-time, the airspace directly ahead of the aircraft for suspected LAWS/MB activity during the entire approach to or departure from all runways at any airport. Figure 1 schematically depicts a possible LAWS/MB scenario for the landing (LDG) and takeoff (T/O) phases that involve a MB penetration. The foward looking infrared radiometer (FLIR) system remotely monitors the cold downdraft region of the MB vertical core as the aircraft descends along the glide slope toward the runway. Prior to and during takeoff, the aircraft FLIR system can scan vertically and horizontally ahead of the aircraft to detect MB activity. Airborne inertial systems must first sense positive deviations above the glide slope due to an increase in headwinds or vertical motions (R_{L_1}) before corrective action can be initiated (Fig. 1). Further penetration into the MB to R_{L_2} are needed by these reactive systems to completely assess the MB intensity and safety of flight. A similar situation develops for aircraft departures through a MB at locations R_{T_1} and R_{T_2}. It is well recognized that severe MB wind fields are capable of bringing down any commercial or private aircraft now flying. Consequently, aircraft inertial systems do not provide adequate warning for avoidance or escape of severe LAWS/MB situations. Even in nonsevere situations they do not provide avoidance capability and may be marginal in providing a timely alert to the pilot and/or flight control system. In essence they are a reactive not a predictive flight safety system.

2. The Forward-Looking Infrared Radiometer (FLIR) System

a. Instrumentation

Our objective has been to determine the applicability of a prototype infrared (IR) system for airborne, advance detection of thunderstorm downbursts which lead to low altitude wind shear (Fig. 2). The IR sensing system is a precision radiation thermometer with an instantaneous field of view (IFOV) of 2 deg. and special filters for sensing in the 13 to 15 micrometer portion of the atmospheric molecular spectrum of CO_2. The radiometer is mounted (forward pointing) under the wing of a small atmospheric research aircraft (Fig. 3). The wing suspension strut and instrument pod for the radiometer are located such that the radiometer IFOV is outside the propellor arc.

A highly efficient onboard data acquisition system provides the data processing and calculation of Doppler winds, gust gradient observations (3-axis gust probe system) together with all standard meteorological parameters (Sinclair and Purdom, 1989, 1983). An advanced, high accuracy DME/LORAN-C navigation system allows precise positioning of the aircraft with respect to the location of advance shear detection and subsequent shear encounter. The central processing unit (MASSCOMP multi-bus computer) provides data sampling (25–100 samples sec^{-1}), storage, calculation, and graphical display in quasi-real-time. All data sampled is initially stored on hard disk (80 megabytes) and then it is dumped to a compact, cassette type tape for final storage prior to landing. Post flight data processing is accomplished on the airborne computer and then dumped to a printer/graphics ground system. During the research flight the computer also provides current graphical display of all the parameters for real-time display and control of the flight operations.

b. Atmospheric Physics of Microburst Detection

Previous work by several authors has shown that there is a demonstrated relationship between the temperature difference across a shear-producing gust front or downburst outflow and the wind speed and direction of the gust front outflow. The larger temperature differences appear to produce higher wind shear or peak gusts. Fawbush and Miller (1954), Foster (1958), and Proctor (1989) have provided a physical basis for predicting surface peak gusts caused by thunderstorm density currents. Temperature drops of 5°C may readily accompany peak gusts of 17 m s^{-1} while those of 15°C are associated with peak gusts of approximately 40 m s^{-1} (Fig. 4). The more recent work by Proctor (1989) involving MB modeling tends to corroborate these earlier results of Fawbush and Miller and Foster for non-frontal thunderstorms. For example, Proctor's results show a maximum deviation from earlier data of approximately −4 m s^{-1} at a temperature drop (ΔT) of approximately 6°C. At other ΔT values the surface wind gust values are also slightly lower with both data sets indicating nearly identical peak winds at $\Delta T = 16°C$.

On the other hand, however, Fujita (1985) has shown that 40% of NIMROD and JAWS microbursts are warmer than their enviroment at the surface. The outflow is then not strictly analogous to a relatively cold gravity or density current, although it initially may have a similar momentum structure. As a result, the temperature anomaly across the leading edge of the outflow at the surface may not always indicate a cool gravity current outflow with a known temperature drop vs. maximum wind gust relationship. Thus, a FLIR temperature sensing-wind shear predictor system that looks at the surface outflow region would give confusing results much of the time. In addition, infrared observations of the surface outflow during the landing approach would also include a ground surface heat source term that would swamp the MB outflow signal. Consequently, our present FLIR system has an IFOV that intercepts the MB in a horizontal plane (Fig. 1). Thus, as the aircraft descends, successively lower regions of the MB vertical core are remotely sensed by the FLIR system. Below approximately 300 m AGL, the FLIR system will at some point intercept the MB outflow region. However, the FLIR system is designed to provide a warning signal to the pilot long before this low altitude-low speed situation develops. Consequently, the FLIR detected temperature anomalies will normally not include those positive anomalies that may be measured in the surface layer. If positive temperature anomalies exist significantly above the surface layer, then the MB will in all probability not be a flight hazard.

In some of our previous research [Kuhn *et al.* (1983), Kuhn and Sinclair (1987), Sinclair and Kuhn (1989)] low level penetrations of downbursts and microbursts indicated that the magnitude of the time rate of change of temperature difference ($\frac{\Delta T}{\Delta t}$) was indicative of gust front intensity. These results suggested that the criterion for potential shear warning was $-0.5°C/s$. For larger negative values of $\frac{\Delta T}{\Delta t}$, the algorithm applied to the radiometer output predicts gust front shear to also increase. Note we are continuing our FLIR measurements in order to increase the number of MB penetrations from which statistical and dynamical formulations can be developed between the MB temperature anomaly and the low altitude wind shear intensity.

In a horizontally uniform temperature field, both the near filter channel of the radiometer, or the static air temperature measured at the aircraft, and the forward, long-range sensing filter channel of the radiometer sense the same temperature. As a cool MB is approached, the long range channel begins to sense a cooler temperature well before the aircraft reaches the gust front, and the near channel senses the warmer static temperature at the aircraft until the cool downdraft or gust front is penetrated (Fig. 1). At this point both radiometers sense the same temperature for a period of time. No alert for LAWS is produced until the temperature difference between the forward sensed temperature and the aircraft temperature reaches the predetermined negative threshold (ΔT) and/or negative rate threshold ($\frac{\Delta T}{\Delta t}$).

The width of the FLIR radiometer filter pass band, $\Delta\nu$, is an important consideration in designing the optics of the FLIR LAWS radiometer (Caracena, *et al.*, 1981). Theoretical considerations show that narrow pass bands give the best spatial discrimination of thermal perturbations, while broad pass bands produce the strongest corresponding perturbation signal in the radiometer output.

Radiation in the atmospheric molecular spectrum of carbon dioxide (N_E) and from the target (N_T) that reaches the radiometer optics detector may be expressed as

$$N = N_E + N_T [\text{watts cm}^{-2}\text{sr}^{-1}]$$

or

$$N = \int_{\nu}\int_{x} B(\nu,T)\phi(\nu)\left(\frac{\partial\tau_{\Delta\nu}(u[CO_2])}{\partial x}\right)dx\,d\nu + \int_{\nu} B(\nu,T_o)\phi(\nu)\tau_o(\nu)d\nu \qquad (1)$$

See Appendix 1 for explanation of symbols. The first term in Eq. (1) represents emitted radiance from the atmosphere (well-mixed CO_2) while the second term represents the target radiance transmitted through the atmosphere to the detector.

In the first term (N_E) of Eq. (1) the horizontal transmission may be expressed as

$$\tau_{\Delta\nu} = exp(-k_{\Delta\nu}q\rho x) \qquad (2)$$

where the product, $q\rho$, is the mean density of carbon dioxide gas. The weighting function distance in Eq. (1) is given by $\frac{\partial\tau_{\Delta\nu}}{\partial x}$ as a function of the horizontal path distance, x. Equation (2) may be differentiated with respect to distance, x, to give the logarithmic weighting function:

$$\frac{\partial\tau}{\partial \ln x} = \frac{\partial\tau}{\partial x}x = -k_{\Delta\nu}q\rho\tau x \qquad (3)$$

This term weights the radiance received from the target at the radiometer from distance increments in the direction of the target, such as a cold microburst or gust front where LAWS may exist. This weighting function thus characterizes the contribution of IR radiation in the wavelength range selected by the filter through portions of the atmosphere along the cone of acceptance of the IR sensor. The choice of the filter spectral band (determined by the cut-on and cut-off filter wavelengths) therefore determines the range or 'look distance' of the radiometer. The 'look distance' (L) is defined as the weighted mean distance ($\bar{x}$), i.e.

$$L \equiv \bar{x} = \frac{\int_0^{\infty}\frac{\partial\tau}{\partial x}x\,dx}{\int_0^{\infty}\frac{\partial\tau}{\partial x}dx} \qquad (4)$$

A detailed evaluation of Eq. (3) as a function of various horizontal distances, x, and altitudes (33 to 800 m) over various pass bands at 10 cm^{-1} intervals in the 667 to 710 cm^{-1} (14.99–14.08 μm) portion of the CO_2 spectrum (Fig. 5) provides a large matrix of logarithmic weighting functions. For our prototype IR detector system, we selected a weighting function centered near 700 cm^{-1} (14.29 μm) which results in a theoretical, fixed 'look-distance' of approximately 5.0 km (Fig. 6). This configuration would give approximately 100–140 seconds warning time to microburst and shear encounter for our aircraft penetration speeds. For transport aircraft which have approach speeds of approximately 150 mph, the warning time to MB penetration would be only slightly less, i.e. 75-105 seconds.

The second term (N_T) in Eq. (1) represents the target temperature which in this case refers to the cool downdraft or microburst at temperature (T_e). If the target is at or within the equivalent 'look distance', it will be easily detected. For targets beyond the 'look distance', the atmospheric transmittance [$\tau(\Delta\nu)$] will act to suppress the target radiance. The technique is to scan radially (in combination with azimuth scanning) with various filters [$\phi(\nu)$] until a particular 'look distance' provides a maximum change in radiance. This provides an estimate of the target distance from the FLIR system.

c. FLIR System Performance

To establish some confidence in the ability of the FLIR system to detect MB temperature anomalies of at least a few degrees centigrade, an analysis of the detection system noise equivalent radiance (NEN) and noise equivalent temperature difference (NEΔT) thresholds was accomplished. The FLIR system employs a hyperimmersed thermister bolometer detector in the front end of a precision radiation thermometer which has the following specifications:

$\omega \equiv$ solid angle intercept at detector, $[\Delta\phi(1-\cos\Delta\theta)]$; sr^{-1}
$\Delta\theta, \Delta\phi \equiv$ detector IFOV, (2.0°); where θ and ϕ are spherical coordinates
$\Delta f \equiv$ electronic bandwidth (1.0 Hz)
$T_f \equiv$ filter efficiency (0.68)
$T_l \equiv$ lens efficiency (0.44)
$k_e \equiv$ electronic system noise factor (1.2)
$A_o \equiv$ optics clear aperature (0.785 cm^2)
$A \equiv$ detector area ($0.25 \times 10^{-4}\text{cm}^2$)
$D^* \equiv$ detector detectivity ($3.0 \times 10^8\text{cm Hz}^{1/2}\text{W}^{-1}$)

From these system parameters the noise equivalent radiance (NEN) can be calculated,

$$NEN = \frac{\sqrt{A}\sqrt{\Delta f}k_e}{D^* A_o \omega T_f T_l}$$

or

$$NEN = 4.0 \times 10^{-6}\text{watts cm}^{-2}\text{sr}^{-1}.$$

The NEN provides a lower threshold at which the FLIR system can detect atmospheric radiant anomalies.

In terms of temperature thresholds, a compatible noise equivalent temperature difference (NETD) can also be obtained from the following expression:

$$NETD = \frac{\pi F \sqrt{\Delta f n}}{(\Delta\theta) A_d \epsilon \int_{\lambda_1}^{\lambda_2} \tau_a(\lambda) \tau_o(\lambda) D^*(\lambda) \left[\frac{\partial B(\nu, T_o)}{\partial T}\right]_{T_B} d\lambda}$$

where:

ϵ ≡ emissivity (1.0)
F ≡ sensor focal length (14 mm)
B ≡ Planck radiation law
T_o ≡ blackbody target temperature (292 K)
T_B ≡ background temperature (294 K)
τ_a ≡ atmospheric transmission (0.35)
τ_o ≡ optical transmission (0.30)

With these values of the system parameters, the noise equivalent temperature difference is:

$$NETD = 0.03\, K\, .$$

This NETD represents the necessary temperature difference between the MB target (292 K) and the environment (294 K) to produce a signal-to-noise ratio of unity (laboratory case, $\tau_a = 1.0$). For a real atmosphere with 350 ppm CO_2, 5 gm Kgm^{-1} water vapor, and the MB at a range of approximately 5 km, the NETD becomes:

$$NETD = 0.12\, K\, .$$

These results are compatible with the experimentally determined FLIR system sensitivity of ±0.1° K and accuracy of ±0.5° K.

These performance parameters will be improved significantly in a second generation FLIR design which employs a cooled, HgCdTe (Mercury-Cadmium-Telluride) detector that provides a NEN = 4.72×10^{-8} watts cm^{-2}sr^{-1}.

Atmospheric effects (absorbtion and scattering) act to degrade the FLIR system performance. We have assumed that the MB is essentially a black body radiating through an intervening FASCODE2 model atmosphere (Clough *et al.*, 1986) that absorbs (CO_2 and water vapor) and re-radiates as a black body. Background radiation is neglected since the MB lateral and vertical dimensions provides an essentially opaque (black) body that completely intercepts the IFOV of the FLIR system. Scattering by dry atmospheric aerosols is small compared to carbon dioxide and water vapor absorbtion. For example, the LOWTRAN 7 tropospheric aerosol model (Kneizys, *et al.*, 1988) for a mid-latitude MB situation indicates that neglect of aerosol scattering leads to a percentage error that is less than 0.2%.

This analysis of the FLIR system performance provided a quantitative foundation from which we concluded that MB's with at least a ΔT = 1°–2°C could be detected remotely through an absorbing atmosphere in the 12–15 μm infrared spectral passband. The results of several relatively 'weak' (ΔT = 2°C) MB penetrations also support the results of this system analysis and show that the FLIR system estimated accuracy of ±0.5°C is met or exceeded.

We have tested this basic concept under actual flight conditions and some of these measurement results are discussed in the following sections.

3. Preliminary Measurements and Observations

a. Verification of FLIR Detectability

The prototype FLIR radiometer was installed on the right wing of our atmospheric research aircraft, a Cessna T207. A highly efficient on-board data acquisition system (MASSCOMP computer) provides digital recording (25–50 sps) of doppler winds, 3 axis gust probe and strap-down gyro parameters, along with standard meteorological parameters (Sinclair and Purdom, 1989, 1984, 1983a,b; Sinclair, 1979, 1973).

Several flight tests of our present proof-of-concept system not only brought to light several new features of the microburst phenomena but provided, as well, a real microburst environment for preliminary testing of the forward-looking IR (FLIR) wind shear detection system (Sinclair and Kuhn, 1987, 1989). Two examples of these penetrations are discussed below in order to show the potential for further development of the present proof-of-concept detection system. The approach to the microburst penetration is depicted in Fig. 7 with the winds (V_H, w), the temperature difference (ΔT_r) between the microburst and the aircraft environment, and the FLIR temperature difference (ΔT_R) shown in Figs. 8 and 10. In these two MB penetrations the aircraft was flown in a constant attitude, constant power configuration which allowed altitude changes above and below the initial point. We believe these to be the first airborne measurements made near and within a microburst of vertical motion (w), horizontal wind (V_H), ΔT_s, and ΔT_R.

The important features of these penetrations are outlined below:

1) MB#1

(a) The penetration was begun at 1800 ft (549 m) AGL, 18 km south of the Cheyenne Ridge (Colorado-Wyoming border) on 11 August 1987 at approximately 1400 MST. The aircraft's true heading was approximately 270° at a true airspeed of 56 m sec^{-1}. The MB depiction in Fig. 7 is a reasonable facsimile of the penetration configuration. The four graphs in Fig. 8 represent (1) the atmospheric vertical motion (w) in m s^{-1}, (2) the horizontal wind (V_H) in degrees from true north (vertical lines) and knots, (3) the static (environmental) temperature (T_s) at the aircraft, and (4) the far field radiometric temperature minus the static temperature (T_s) measured at the aircraft (ΔT_R). The abcissa is the horizontal distance in kilometers from the initial point.

(b) The vertical motion field (w) shows the characteristic upward velocity of 1 m s^{-1} below the cloud on approach to the MB. The core of the MB occurs at approximately 10.0 km and is 'buried' within a heavy precipitation (HP) cor (Fig. 9) where the maximum vertical velocity of $w = -12.5$ m s^{-1} is reached. A secondary region of large vertical motion ($w = -8$ m s^{-1}) was also encountered in light precipitation (LP) prior to entering the MB core at $x \approx 7.5$ km. This secondary downdraft core is driven by the upstream flow field of the downstream vortex (Fig. 9). It is important to note that this secondary downdraft core was encountered primarily because of the selected aircraft penetration altitude and heading relative to the MB orientation. Other aircraft penetration headings and altitudes could have produced quite different secondary, as well as primary, downdraft structure due to the MB asymmetry and vortex circulation structure.

(c) The horizontal wind field (V_H) during most of the penetration indicates a headwind component of approximately 10 knots. Within the HP core of the MB the wind changes abruptly to a tailwind of 15–20 knots. This wind reversal (ΔV_H = 25–30 knots), coupled with the severe downdraft of the MB, provides a critical flight regime for aircraft maneuvering near the ground. Since this was a mid-level MB penetration (i.e. initially above the vortex flow field), the V_H wind field did not exhibit the classical strong headwind-tailwind sequence that is normally observed closer to the ground in the MB outflow region.

(d) The static temperature (T_s) measured at the aircraft represents the temperature variations near and within the MB with respect to a reference altitude ($z \approx 550$ m AGL), i.e. the initial altitude at $x = 0$. The process lapse rate required to reference the measured temperature from altitudes above and below this reference altitude was obtained from multi-level aircraft soundings near and within the MB. The temperature measurements indicate a sharp decrease at approximately $x \approx$ 5.5 km, just prior to entering the light precipitation (LP), Fig. 9. A maximum temperature deficit or change of $\Delta T_s \approx 2$°C occurs near the backside (upstream) of the MB core just outside of the HP in the rain-cooled region.

(e) The FLIR, ΔT_R data plot indicates a target acquisition at about 3.3 km or approximately 6.0 ~~8.0~~ km from the target which represents the rain-cooled core of the wet MB at $x \approx$ 9-10 ~~11.5~~ km. As pointed out above in the temperature (T_s) discussion, the maximum ΔT_s actually occurs on the upstream or backside of the MB. However, the FLIR measured ΔT_R of −2°C agrees with the in-situ ΔT_s of −2°C, and therefore a warning of impending MB penetration of [illegible] ~~at least~~ 2–3 minutes is available to the pilot of a jet transport type aircraft in the landing phase. At slower approach speeds, this warning time is significantly increased. It is important to note also, that because of the FLIR systems minimum detectability of approximately ±0.5°C, the first significant temperature decrease at $x \approx 5.5$ km of $\Delta T_s = 0.5$°C, was actually detected at approximately $x \approx 1.3$ km. Consequently, this rain cooled region of the LP region which proceeded the main core of the MB, may provide alert alarms prior to penetration of the MB core on particular aircraft penetration tracks. In any case, these preliminary measurements indicate that our FLIR system can detect the MB core through light precipitation.

The cross-over point where $\Delta T > 0$ does not mean that the wet MB is now warmer than the near field static temperature. What has happened is that some of the precipitation has been deposited on the radiometer optics. This water coating on the lens has resulted in the blockage of outside radiation to the detector. The detector then also views reflected energy from the heated black body reference cavity during this part of the chopper cycle. This results in an erroneously high temperature output which will eventually approach the 45°C cavity reference. Hence, the ΔT's will progressively increase in a positive direction as indicated for ≥ 5.7 km. We are testing several design modifications which will eliminate this precipitation contamination of the FLIR optics.

2) MB#2

On the same day, a second MB penetration was made over flat terrain just north of Fort Collins, CO (Figs. 10 and 11). The important features of this penetration are outlined below:

(a) The penetration was started at 1150 ft (350 m) AGL at approximately 1500 MST. The aircraft true heading was 200° at a true airspeed of 57 m $\sec^{-1}$. This MB configuration is similar to that depicted in Fig. 7, but with very little vortex roll-up of the outflow near the ground. The three graphs depict the same parameters as displayed in the first MB penetration (Fig. 8).

(b) The vertical motion field (w) in this case is primarily downward on approach to the wet MB. This is a result of the light rain encountered between z = 2.5 km and 5.0 km. The core of the wet MB is located at approximately 9.0 km and is 'buried' within the moderate precipitation (MP) core where the downward vertical motion reaches a maximum of $w \approx -14$ m s^{-1}. In this case, MB#2 had a much more extensive area of LP prior to penetration of the MB core which was approximately the same diameter as that of MB#1 (Figs. 9 and 11). Although the largest vertical motion ($w \approx -14$ m s^{-1}) was encountered within the MB core, the downward vertical motion was still strong just upstream from the MP in the rain-cooled region (Fig. 11). This region of downward motion appears to frequently occur on the upstream side, which appears to be a rain cooled region following the primary precipitation core of the MB.

(c) The horizontal wind field (V_H) during most of the penetration indicates a headwind component of approximately 10 knots. In this case, the wind begins to change within the core of the wet MB from southwesterly to a 5–10 knot northerly flow. While the effective headwind-tailwind component amounts to approximately 20–25 knots, the change takes place over a horizontal distance of 4–5 km. This change is more gradual in headwind-tailwind component ($\frac{\Delta V_x}{\Delta x} \approx 2.8 \times 10^{-3}$ sec^{-1}) than in MB#1 where essentially the same change occurred over a 1 km distance ($\frac{\Delta V_x}{\Delta x} \approx 13.8 \times 10^{-3}$ sec^{-1}). Note, that the shear ($\frac{\Delta V_x}{\Delta x}$) in MB#1 significantly exceeds the presently accepted minimum wind shear hazard of 2.5×10^{-3} sec^{-1} (Mahoney, *et al.*, 1989). Again, however, this is a mid-level MB penetration where the V_H wind field did not exhibit the classical headwind-tailwind sequence that is normally observed closer to the ground in the MB outflow regions.

(d) The temperature minimum of approximately 18.5°C occurs at z = 9.3 km (Fig. 10) which agrees well with the location of the maximum downward vertical motion of $w = -14$ m s^{-1} (Fig. 11). Thus, the total temperature deficit is approximately ΔT_s = 1.8°C. The T_s measurements indicate that the cool MB downdraft core begins at $z \approx 8.3$ km and extends to $z \approx 11.0$ km. Note, that the temperature returns slowly to a near constant environmental value of $T_e \approx 20.0$°C. This slow return of the temperature to a somewhat lower value on the upstream side of the MB is due primarily to the effect of the rain cooled region left in the 'wake' of the MB. Also, as in MB#1, there is a definite temperature decrease as the aircraft approaches or enters the precipitation regions. In MB#2, this initial temperature decrease occurs at $z \approx 5.2$ km while in MB#1 this same initial decrease of temperature occurs at $z \approx 5.5$ km. In both cases, this initial temperature decrease is associated with the approach to or encountering light precipitation (LP) preceding (or downstream of) the MB core. Penetration tracks from the upwind side of the MB would show a more gradual temperature decrease characteristic of the trailing 'wake' or rain-cooled region. On the other hand, cross-stream penetrations of the MB core may show neither of these temperature variations, especially in the case of asymmetric MB flow structure. Under particular conditions therefore, these temperature decreases may prove to be important precursors of MB presence and intensity further along the flight path. Numerical simulations of microbursts also indicate a temperature drop prior to penetration of the MB core, primarily during the increasing headwind portion of the penetration (Babcock and Droegemeier, 1989; Droegemeier and Babcock, 1989). This is easily explained in that in these cases the modeled penetration track is through the symmetrical outflow vortex roll-up which represents cooler air than the environment. However, as Proctor (1989) and others (Bedard and LeFebvre, 1986) have pointed out, the presence of a surface stable layer or warm boundary layer can greatly modify the temperature of the outflow (vortex) air—to the point, in some cases, where the increasing headwind may be warmer than the surrounding environment. In the two cases we have cited here the initial penetration flight track is just above the outflow and consequently the first temperature decrease is due to the LP region preceding the MB core.

(e) The FLIR, ΔT_R data plot suggests a MB target acquisition at $x \approx 3.0$ km or approximately 6.3 km from the MB core at $x \approx 9.3$ km (Fig. 10). In this case, the detail of the maximum ΔT_R is somewhat obscurred by the effect of the precipitation on the PRT-5 optics. In this case, the maximum temperature deficit ($\Delta T_s \approx 1.8$°C) also compares favorably with the maximum FLIR measurement of $\Delta T_R \approx 1.8°$-2.0°C. Again, a warning time of approximately 2 minutes is available for transport type aircraft and up to 4 minutes for smaller, general aviation aircraft. Furthermore, we believe that the MB was, in essence, initially detected at $x \approx 1.0$ km due to the cool downdraft in LP at $x \approx 5.2$ km. As in MB#1, this early detection of the cool downdraft preceding the MB core along this penetration track provides 1 minute plus alert signal at $x \approx 1.0$ km in addition to the 2 minute warning at $x \approx 5.0$ km of impending MB penetration.

b. Microburst Features Important to Flight Safety

1) Headwind/Tailwind—Vertical Motion Factor

Our flight research indicates, in agreement with previous events and research, that the low level penetration of a fully developed microburst (MB), which combines the effects of strong headwind/tailwind and vertical motion factors, can be very hazardous to the untrained pilot. However, this is not the only hazardous situation for the unsuspecting pilot. There are many more MB's that appear weak and innocuous to the pilot than there are those that can be easily distinguished by a trained pilot. Many of these so-called innocuous MB's are dry and therefore not easily detected by the proposed airport radars. However, these MB's are capable of producing vertical and horizontal flow fields that are still hazardous with respect to transport type aircraft landing and takeoff performance margins. Furthermore, pilots of smaller aircraft may well find that their aircraft landing/takeoff performance margins (climb rate, controllability, speed control, etc.) are significantly exceeded during these MB penetrations.

Consequently, in order to fully document this flight safety hazard, it is imperative that in-situ flight measurements by research aircraft be continued in a full range of MB types, at various altitudes and penetration headings with respect to the MB track. Our preliminary flight results indicate that in certain MB approach headings and altitudes the vertical motion field may provide a more hazardous flight regime than the headwind/tailwind factor. In other approach headings and MB configurations, the reverse may be true or both factors may be of near equal importance. The availability of in-situ measurements of this type by research aircraft will provide the air-truth needed for radar algorithm improvement, numerical modeling studies, and realistic aircraft simulation operation and training.

2) The Hazard Index

In order to put some of our preliminary measurements in perspective with the anticipated hazards of MB penetration, the hazard index (F) developed by Targ and Bowles (1988) is shown in Figs. 9 and 11, i.e.,

$$F = \frac{\dot{u}}{g} - \frac{w}{V}$$

along with a second hazard factor proposed by the authors,

$$F^{*} = F\left[1 + \frac{120\ \mathrm{m}}{A}\right]$$

where:

$\dot{u}$ ≡ Lagrangian change in the wind along the aircraft flight path
g ≡ acceleration of gravity
w ≡ vertical wind velocity component
V ≡ true airspeed of the aircraft
A ≡ altitude above ground level (AGL)

Positive values of F indicate aircraft performance loss (i.e. decreasing headwind or increasing tailwind and/or downdraft) while negative values of F indicate aircraft performance gain (i.e. increasing headwind or decreasing tailwind and/or updraft). The F factor is quantitatively related to the effect of wind shear/vertical motion on the aircraft energy state and the available rate of climb potential. We suggest an additional hazard index factor (F^*) which is represented by the second hazard index graph (Δ) in Figs. 9 and 11. It includes the additional hazard of the aircraft AGL altitude, i.e. the potential MB hazard is substantially increased for a low level aircraft penetration vs one at a higher altitude where recovery may be more probable. From our experience with general aviation aircraft, an altitude loss of 250–300 m is not unusual in our present penetration technique, i.e. constant attitude–constant power profile. Note, this altitude loss results in a maximum 7–10 degree flight path angle with the horizontal and thus does not significantly affect the hazard index (F) derivation approximations. As the aircraft approaches the ground due to aircraft performance loss within the MB ($F > 0$), the hazard index (F^*) increases significantly due to the altitude term $(1+\frac{120\,\mathrm{m}}{A})$. Thus, F^* is always greater than F depending on the aircraft altitude (AGL). For example, at critical altitudes below 120 m, F^* will be more than twice the value of F. An analysis of a wide range of commercial aircraft (light-to-medium weight) performance capabilities indicates that the hazard index factor (F^*) could be used to alert the pilot of the flight hazards of MB penetration, i.e.

MB Flight Hazards

No hazard: $F^* < 0.10$
Yellow alert: $0.10 \leq F^* < 0.20$
Red alert: $F^* \geq 0.20$

The yellow alert implies considerable caution must be exercised by the pilot to avoid unacceptable altitude/airspeed losses during MB penetration. The red alert indicates that MB penetration is not advised and appropriate abort and go-around procedures will be necessary. Consequently, in both MB#1 and MB#2 (Figs. 9 and 11), the hazard index [F or F^*] becomes significant (yellow and red alerts) from near the forward edge of the MB to an area just upstream of the rear precipitation boundary. This hazard region is generated primarily by the vertical motion term $(\frac{w}{V})$ and the ground proximity term $(1+\frac{120\,\mathrm{m}}{A})$. Only near the rear boundary of MB#1 (Fig. 9) does the wind shear term $(\frac{\dot{u}}{g})$ become more significant (at $x \approx 10.9$ km) than the vertical motion term ($\frac{w}{V}$). The general dominance of the term $\frac{w}{V}$ is important when one considers that most private-commercial aircraft have easily generated climb capabilities significantly less than the 8–15 m s^{-1} vertical motions measured in MB#1 and MB#2.

4. Conclusions

We anticipate that continued aircraft probing of microbursts of various sizes and intensities at different altitudes and relative penetration headings will yield significant information on MB structure and aircraft hazards [F, F^*]. This information coupled with the FLIR (ΔT_R) measurements will provide a data base from which alert and warning algorithms can be developed for second and third generation FLIR detection systems. These on-going and future studies will bring into sharper focus the importance of water vapor absorbtion, precipitation screening of MB infrared signals, and warm MB false alarms. The latter factor, warm MB's, is considered by many to be simply a manifestation of the disturbance of the warm, surface layer air by the MB outflow. As a result, ground surface temperature measurements could indicate a warm MB core which in reality may still be colder than its environment at an altitude of 50–100 m. This warm surface layer is usually below the FLIR scan volume and would therefore not become a false alarm factor. Additional measurements will provide a clearer and quantitative picture of the actual atmospheric processes responsible for the warm MB structure.

Acknowledgements. The research was supported by NSF Grant #ATM-84-20980 (Thunderstorm Outflow Studies), NOAA Grant #43-RANR-5-03966, and ARIS, Inc., Fort Collins, CO. The authors thank Becky Armstrong for preparation of the text and Judy Sorbie-Dunn for drafting the figures.

Appendix: Symbol and Acronym Table

N, B	radiance, w cm^{-2} sr^{-1} ($B \equiv$ blackbody radiance)
K	temperature, degrees Kelvin
$k_{\Delta\nu}$	CO_2 absorption coefficient, $cm^2 g^{-1}$
q	mass mixing ratio of CO_2, g g^{-1}
T	atmospheric temperature, K
T_o	Target temperature, K (Downburst volume)
u	optical thickness of CO_2 gas (g cm^{-2})
w	vertical motion, m s^{-1}
x	horizontal distance, km
z	vertical distance, m
ΔT_R	temperature difference between FLIR sensed air temperature and the aircraft static temperature
$\frac{\Delta T_R}{\Delta t}$	time rate of change of forward looking IR air temperature minus static air temperature at aircraft, °C s^{-1}
ΔT_s	static temperature deficit between aircraft and microburst
$\Delta\nu$	optical filter band width, cm^{-1}
sr^{-1}	steradian
ν	wave number, cm^{-1}
λ	wavelength
τ	CO_2 transmittance, %
ρ	air density, g cm^{-3}, p/RT
$\phi(\nu)$	radiometer filter transmission, %
AGL	Above Ground Level
DME/LORAN–C	Distance Measuring System/Long Range Navigation System
IFOV	Instantaneous Field of View

References

Babcock, M.R. and K.K. Droegemeier, 1989: Numerical simulation of microbursts: aircraft trajectory studies, Preprints, *Third International Conference on the Aviation Weather System*, Anaheim, CA, AMS, Boston, Jan 30–Feb 3.

Bedard, A.J., Jr. and T.J. LeFebvre, 1986: Surface measurements of gust fronts and microbursts during the JAWS project: statistical results and implications for wind shear detection, prediction, and modeling, NOAA Tech. Memo. ERL WPL-135, Wave Propagation Laboratory, Boulder, Colorado, 112 p.

Campbell, S.D., M.W. Merritt, and J.T. DiStefano, 1989: Microburst recognition performance of TDWR operational testbed, *Third International Conference on the Aviation Weather System*, Anaheim, CA, AMS, Boston, Jan 30–Feb 3.

Caracena, F., P.M. Kuhn, and R.L. Kurkowski, 1981: Design and preliminary tests of an IR-airborne LLWS remote sensing system, *AIAA Paper 81–0239*, January.

Clough, S.A., *et al.*, 1986: Atmospheric radiance and transmittance: FASCODE 2, *Proceedings of 6th Conference on Atmospheric Radiation*, Williamsburg, VA, AMS, Boston, MA, 141–144.

Droegemeier, K.K. and M.R. Babcock, 1989: Numerical simulation of microburst downdrafts: application to on-board and look-ahead sensor technology, Preprints, *AIAA Aerospace Sciences Conference*, Reno, NV, Jan. 9–12.

Fawbush, E.J., and R.C. Miller, 1954: A basis for forecasting peak wind gusts in non-frontal thunderstorms, *Bull. Amer. Meteor. Soc.*, **35**, 14–19.

Federal Registry, 1988: Airborne low-altitude wind shear equipment and training requirements, Volume 53, No. 187, Rules and Regulations, p. 37688. Department of Transportation, FAA, 14CFR Parts 121 and 135 [DOCET 19110: Ammendment Nos. 121–149, 135–27].

Foster, D.S., 1958: Thunderstorm gusts compared with computed downdraft speeds, *Mon. Wea. Rev.*, **86**, (3).

Fujita, T., 1985: The downburst, Department of Geophysical Sciences, University of Chicago, 122p.

Goff, C.R. and R.H. Gromsow, 1989: The Federal Aviation Administration's low level windshear alert system: a project management prospective, *Third International Conference on the Aviation Weather System*, Anaheim, CA, AMS, Boston, Jan 30–Feb 3.

Kneizys, F.X., *et al.*, 1988: Users Guide to LOWTRAN 7, Environmental Research Paper No. 1010, AFGL–TR–88–0177, Air Force Geophysics Lab., Hanscom AFB, MA.

Kuhn, P.M., R.L. Kurkowski, and F. Caracena, 1983: Airborne operation of an infrared low-level wind shear prediction system, *J. Aircraft*, **20**, 170–173.

Kuhn, P.M. and P.C. Sinclair, 1987: Airborne infrared wind shear detector performance in rain obscuration, *AIAA Paper, 25th Aerospace Conference*, Reno, NV, January.

National Research Council, 1983: Low altitude wind shear and its hazard to aviation. National Academy Press, Washington, D.C., 161 pp.

Mahoney, W., W. Wilson, K. Brishawn, and M.K. Poletovich, 1989: Microburst detection by TDWR: performance assessment, *Third International Conference on the Aviation Weather System*, Anaheim, CA, AMS, Boston, Jan 30–Feb 3.

McCarthy, J. and J.W. Wilson, 1985: The calssify, locate, and avoid wind shear (CLAWS) project at Denver's Stapleton International Airport: operational testing of terminal weather hazard warnings with an emphasis on microburst wind shear, Preprints, *2nd International Conference on the Aviation Weather System*, Montreal, Can., AMS, Boston, MA, 247–256.

Proctor, F.H., 1989: A relationship between peak temperature drag and velocity differential in a microburst, *Third International Conference on the Aviation Weather System*, Anaheim, CA, AMS, Boston, Jan 30–Feb 3.

Research Applications Program, 1988: Terminal doppler weather radar (TDWR): a briefing paper, Prepared for the Federal Aviation Administration by the Research Applications Program, National Center for Atmospheric Research, Boulder, CO.

Sinclair, P.C., 1973: Severe storm air velocity and temperature structure deduced from penetrating aircraft. *Preprints, 8th Conference on Severe Local Storms*. AMS, Boston, MA, Oct. 15–17.

Sinclair, P.C., 1979: Velocity and temperature structure near and within severe storms. *Preprints, 11th Conference on Severe Local Storms*, AMS, Boston, MA, Oct. 2–5.

Sinclair, P.C. and J.F.W. Purdom, 1983a: The genesis and development of deep convective storms, Final Report, NOAA Grant NA80AA-D-00056, CIRA, Colorado State University, Fort Collins, January.

Sinclair, P.C. and J.F.W. Purdom, 1983b: Shuttle recovery requirements and the development of arc cloud lines from the thunderstorm outflows, *Preprints, 9th Conference on Aerospace and Aeronautical Meteorology*, AMS, Boston, MA, June 6–9.

Sinclair, P.C. and J.F.W. Purdom, 1984: Aircraft penetrations of arc cloud lines, *Preprints, Conference on Sattellite/Remote Sensing and Applications*, AMS, Boston, MA, June 25–29.

Sinclair, P.C. and P.M. Kuhn, 1987: Forward looking airborne infrared wind shear sensor operation in precipitation. Final Report to NOAA, Environmental Research Laboratory, Boulder, CO, September.

Sinclair, P.C. and J.F.W. Purdom, 1989: Real-time data acquisition and interactive display system for a small, single-engine, atmospheric research aircraft. Submitted to *J. Atmos. Oceanic Tech.*

Sinclair, P.C. and P.M. Kuhn, 1989: Aircraft low level wind shear detection and warning system, *Third International Conference on the Aviation Weather System*, Anaheim, CA, AMS, Boston, Jan 30–Feb 3.

Smythe, G.R., 1989: Evaluation of the 12-station enhanced low level wind shear alert system (LLWS) at Denver Stapleton International Airport, *Third International Conference on the Aviation Weather System*, Anaheim, CA, AMS, Boston, Jan 30–Feb 3.

Stengel, R.F., 1984: Unsolved issues in wind shear encounters, NASA Conf. Publication, 2474: *Wind Shear/Turbulence Inputs to Flight Simulation and Systems Certification*. Langley Research Center, Hampton, VA, May 30-June 1.

Targ, R. and R.L. Bowles, 1988: Investigation of airborne lidar for avoidance of wind shear hazards, Preprints, *2nd Combined Maunfacturer's and Technology Airborne Windshear Review Meeting*, Williamsburg, VA, October 18–20.

Turnbull, D., J. McCarthy, J. Evans, and D. Zrnic, 1989: The FAA terminal doppler weather radar (TDWR) program, *Third International Conference on the Aviation Weather System*, Anaheim, CA, AMS, Boston, Jan 30–Feb 3.

Wilson, F.W., Jr., and J.A. Flueck, 1986: A study of the methodology of low altitude wind shear detection with special emphasis on the low level wind shear alert system concept, Final Report, DOT/FAA/PM-86/4. DOT/FAA, Program Engineering Maintenance Service, Washington, D.C., 101 pp. (Available through NTIS, Springfield, VA 22161).

Figure Captions

Fig. 1 LAWS/MB Detection Systems. R_L and R_T refer to reactive systems that require the aircraft to penetrate and react to the LAWS/MB circulation. Surface based single doppler radars (TDWR) have good surveilance capabilities but may not detect all MB's (dry) or winds at low altitudes. The FLIR system remotely monitors the cold downdraft region of the MB during landing and takeoff. Vertical scanning avoids intercept with ground surface and warm boundary layer air.

Fig. 2 Thunderstorm Microburst Detection by Scanning FLIR System. The forward scanning and ranging capabilities of the new FLIR system provides a 50–70 second warning of microburst penetration to the pilot of the approaching aircraft. Note that the FLIR system has an IFOV that intercepts the MB in a horizontal plane above the ground surface.

Fig. 3 Wing-mounted Forward-Looking Radiometer Pod. The radiometer FOV(±10°) is completely outside of the engine propellor arc. The radiometric measurements are supplemented with:

- Gust probe measurements of u', v', w'.
- Doppler (navigation) wind measurements of $\hat{u}, \theta$.
- Temperature and dewpoint measurements.
- Real-Time, Computer (MASSCOMP/Concurrent Systems) controlled data acquisition, data storage, and color graphical display.

Fig. 4 Relationship of Thunderstorm Peak Gust with Temperature Drop (ΔT) at the Surface (Fawbush and Miller, 1954).

Fig. 5 Transmittance of a 1,000-foot path in air at sea level containing 5.7 millimeters of precipitable water at a temperature of 79°F.

Fig. 6 CO_2 weighting functions for passbands 20 cm^{-1} wide about center frequencies labeled in the figure.

Fig. 7 Mid-Level Penetration of Wet Microburst with T207 Research Aircraft.

Fig. 8 MB#1; Variations of Vertical Motion (w), Horizontal Winds (V_H), Temperature (T_s), and Radiometric Temperature Difference (ΔT_R) During a Wet Microburst Penetration (see text for explanation and discussion).

Fig. 9 MB#1 Cross-Section of Flight Paths and Vertical Motion Field (w) With Respect to Distance (x) in km from the Initial Point at $z \approx 550$ m. The mean (layer) environmental wind [$V_H(c)$] and the MB translation velocity at mid-levels is labeled along with the depiction of heavy (HP) and Light (LP) precipitation. The lower graph shows the variability of the hazard factors F and F^* along the flight path (see text for further explanation).

Fig. 10 MB#2 Variations of Vertical Motion (w), Horizontal Winds (V_H), Temperature (T_s), and Radiometric Temperature Difference (ΔT) During a Wet Microburst Penetration (see text for explanation and discussion).

Fig. 11 MB#2; See Figure 9 and text for explanation.

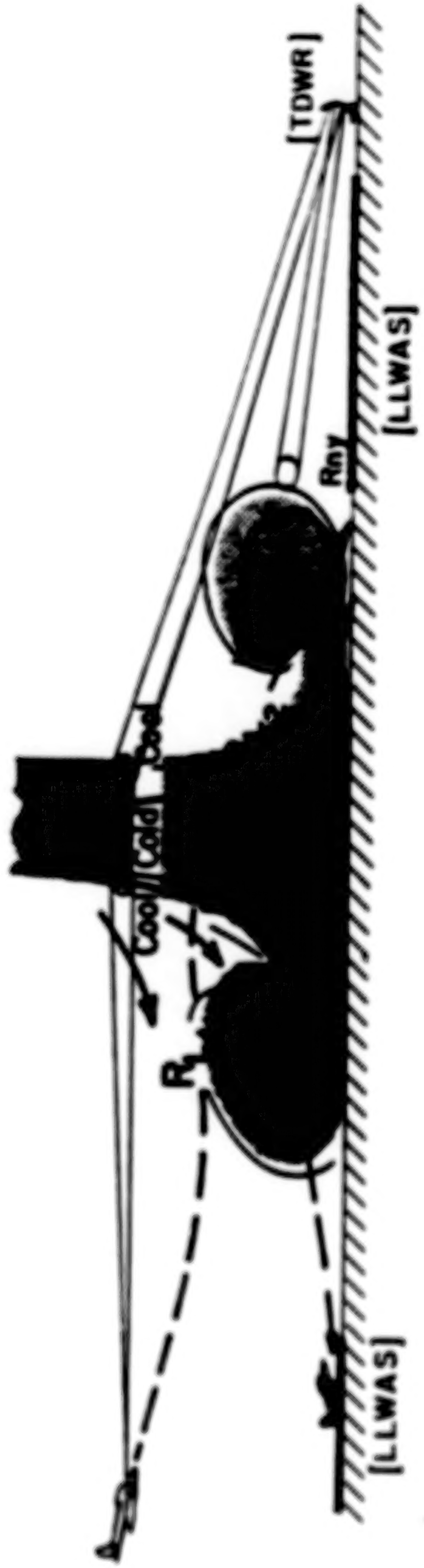
[TDWR]
[LLWAS]
Rny
Cool
Cold
Cool
R
[LLWAS]

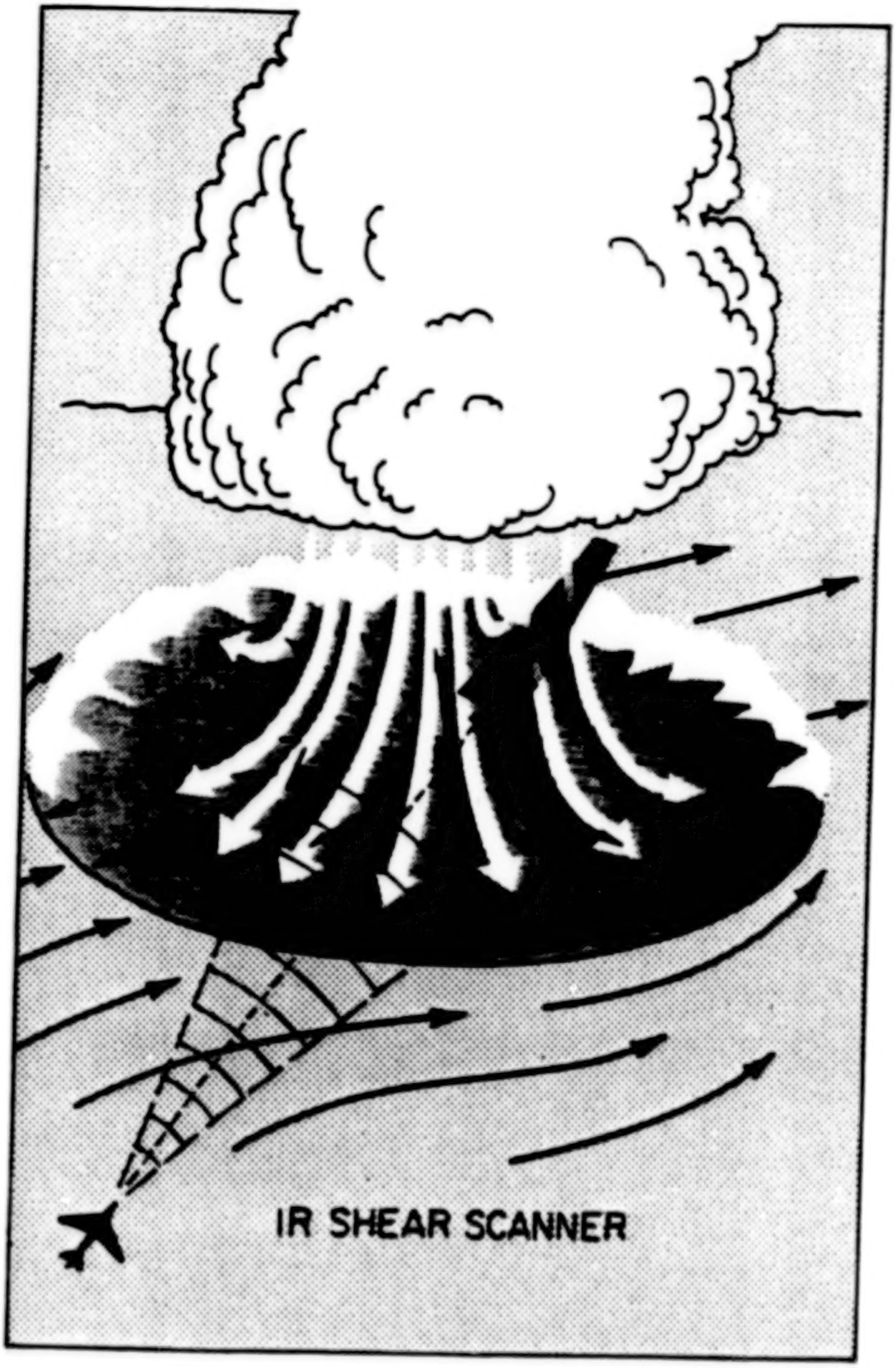
IR SHEAR SCANNER

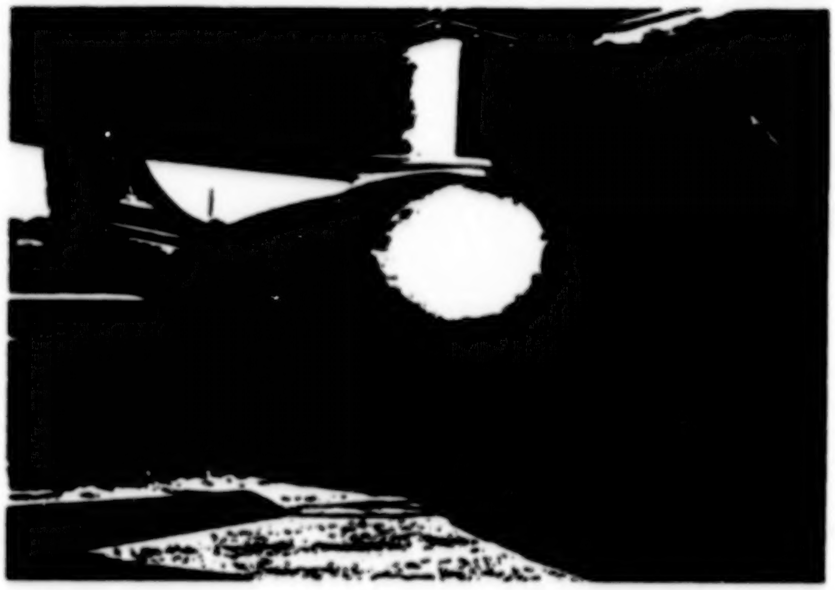

ORIGINAL PAGE IS
OF POOR QUALITY

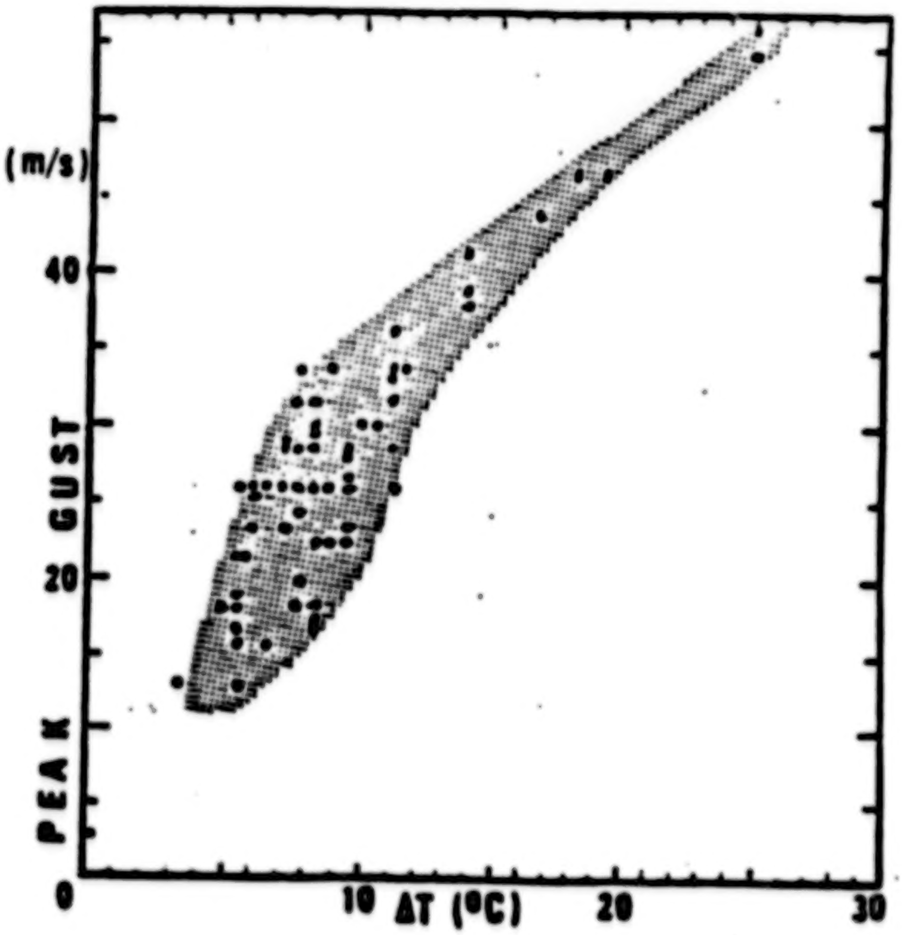
(m/s)
40
20
PEAK GUST
0
10
ΔT (°C)
20
30

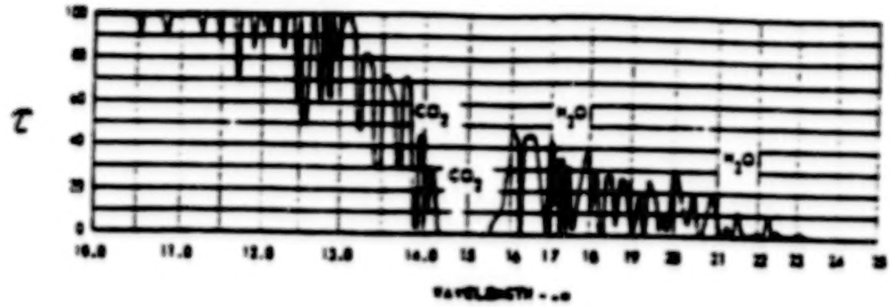
100
80
60
40
20
0
τ
CO_2
CO_2
H_2O
H_2O
10.0
11.0
12.0
13.0
14.0
15
16
17
18
19
20
21
22
23
24
25
WAVELENGTH - μ

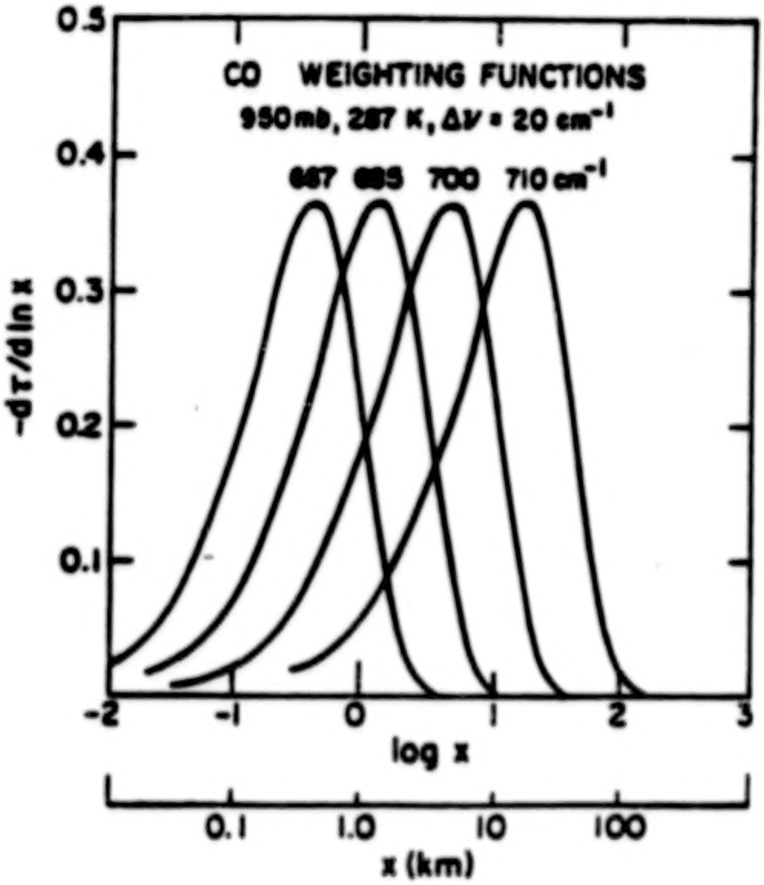
CO WEIGHTING FUNCTIONS
950mb, 287 K, $\Delta\nu$ = 20 cm^{-1}
667
685
700
710 cm^{-1}
0.5
0.4
0.3
0.2
0.1
$-d\tau/d\ln x$
-2
-1
0
1
2
3
log x
0.1
1.0
10
100
x (km)

670

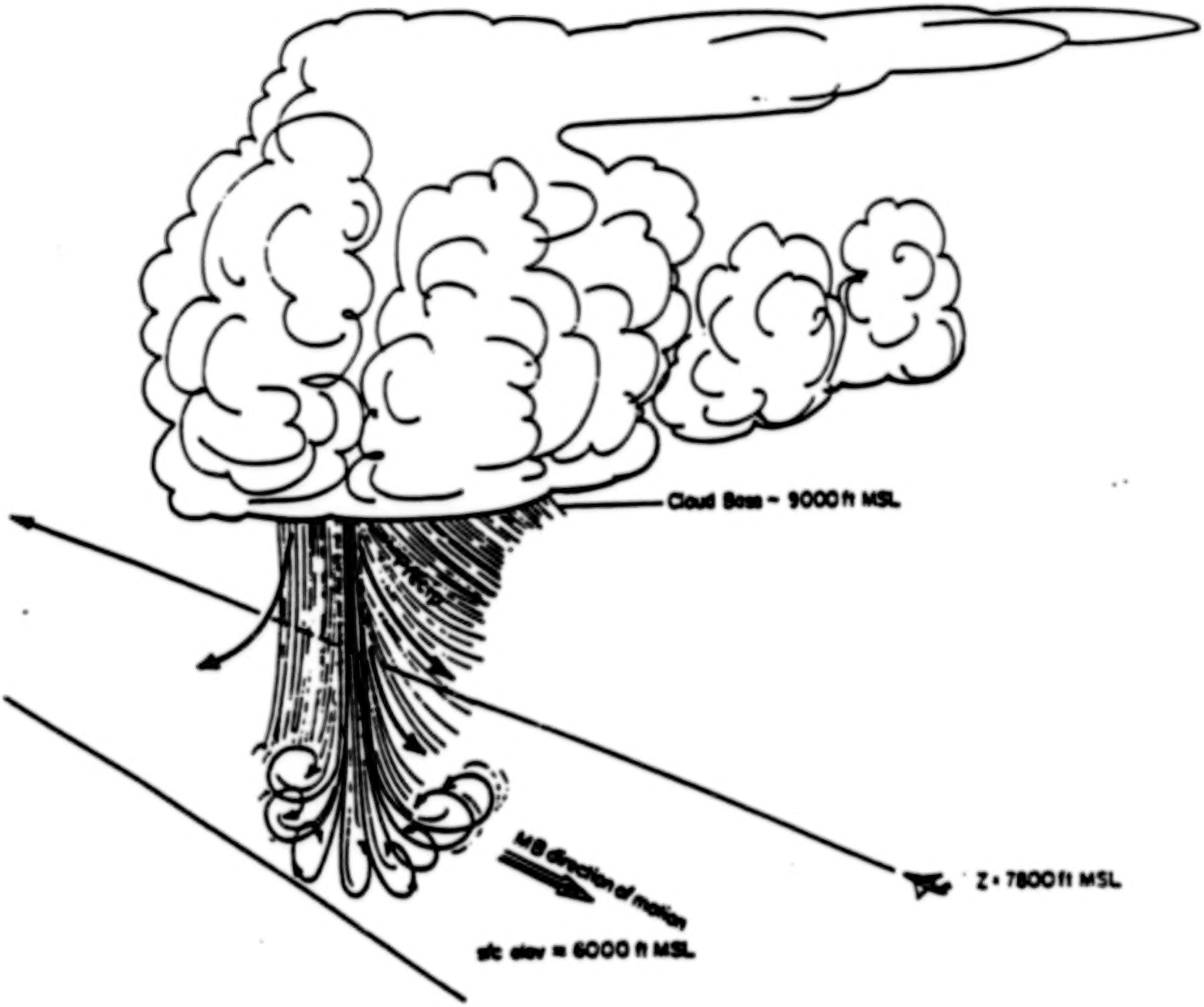
Cloud Base ~ 9000 ft MSL
MB direction of motion
Z = 7800 ft MSL
sfc elev = 6000 ft MSL

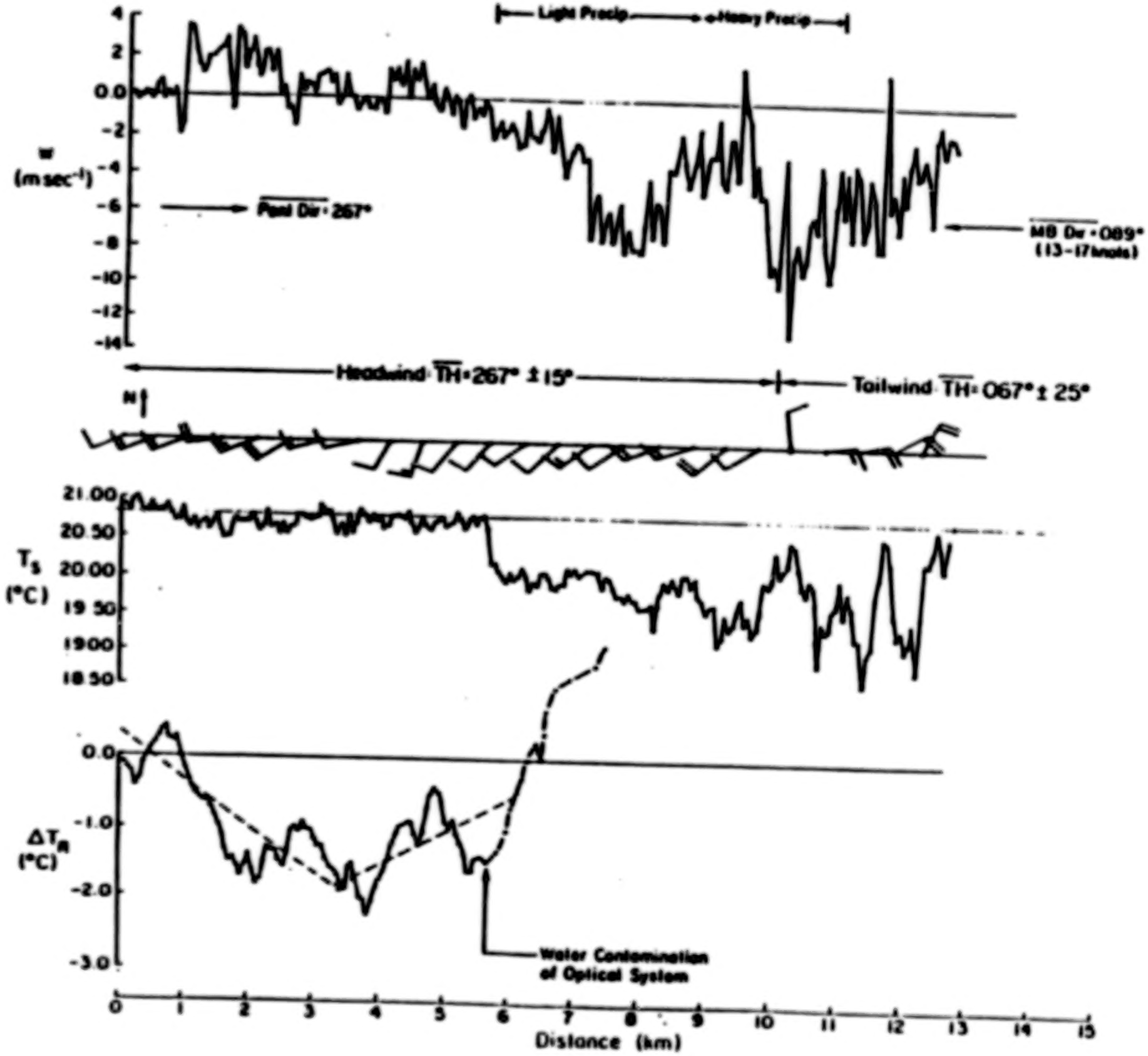
Light Precip
Heavy Precip
w
(m sec⁻¹)
4
2
0.0
-2
-4
-6
-8
-10
-12
-14
Past Dir = 267°
MB Dir = 089°
(13-17knots)
Headwind TH = 267° ± 15°
Tailwind TH = 067° ± 25°
N
T_s
(°C)
21.00
20.50
20.00
19.50
19.00
18.50
ΔT_R
(°C)
0.0
-1.0
-2.0
-3.0
Water Contamination
of Optical System
0
1
2
3
4
5
6
7
8
9
10
11
12
13
14
15
Distance (km)

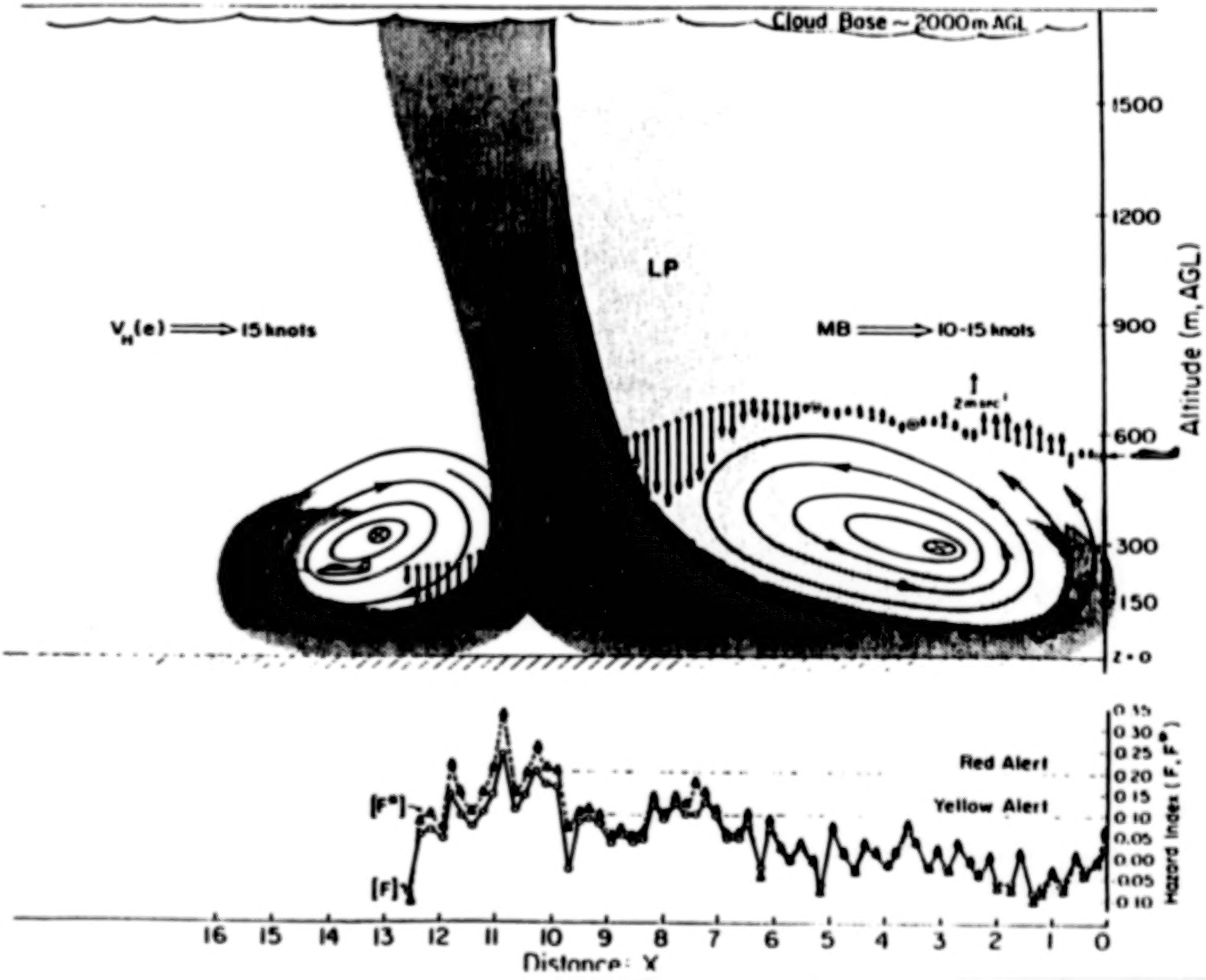
Cloud Base ~ 2000 m AGL
LP
$V_H(e)$ ⟹ 15 knots
MB ⟹ 10-15 knots
2 m sec^{-1}
Altitude (m, AGL)
1500
1200
900
600
300
150
z = 0
Red Alert
Yellow Alert
[F*]
[F]
Hazard Index (F, F*)
0.35
0.30
0.25
0.20
0.15
0.10
0.05
0.00
0.05
0.10
16
15
14
13
12
11
10
9
8
7
6
5
4
3
2
1
0
Distance: X

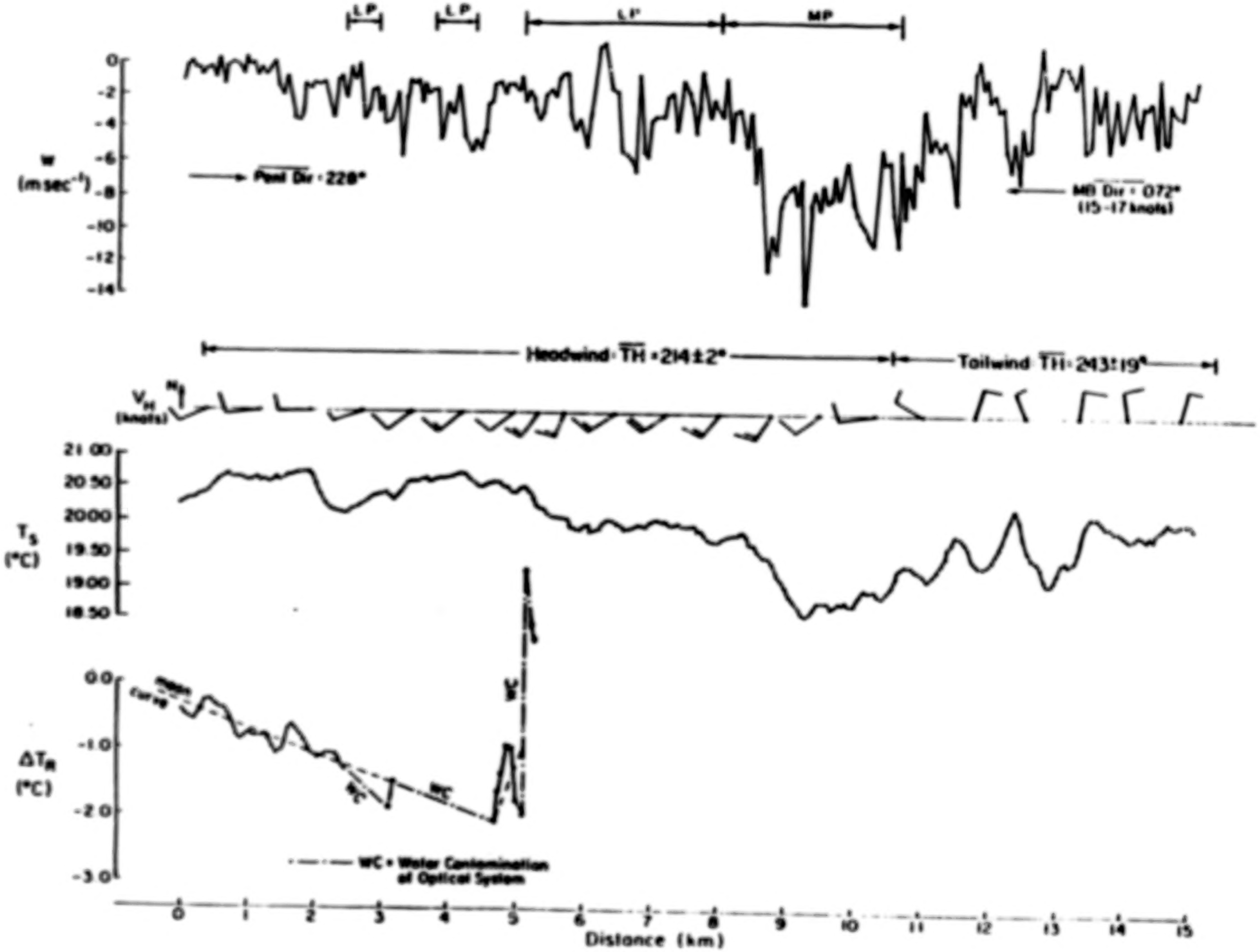
LP
LP
LP
MP
w
(msec⁻¹)
0
-2
-4
-6
-8
-10
-12
-14
Pent Dir = 228°
MB Dir = 072°
(15-17 knots)
Headwind TH = 214±2°
Tailwind TH = 243±19°
V_H
(knots)
21.00
20.50
20.00
19.50
19.00
18.50
T_S
(°C)
0.0
-1.0
-2.0
-3.0
ΔT_R
(°C)
Mean Curve
WC
WC
WC
WC = Water Contamination of Optical System
0
1
2
3
4
5
6
7
8
9
10
11
12
13
14
15
Distance (km)

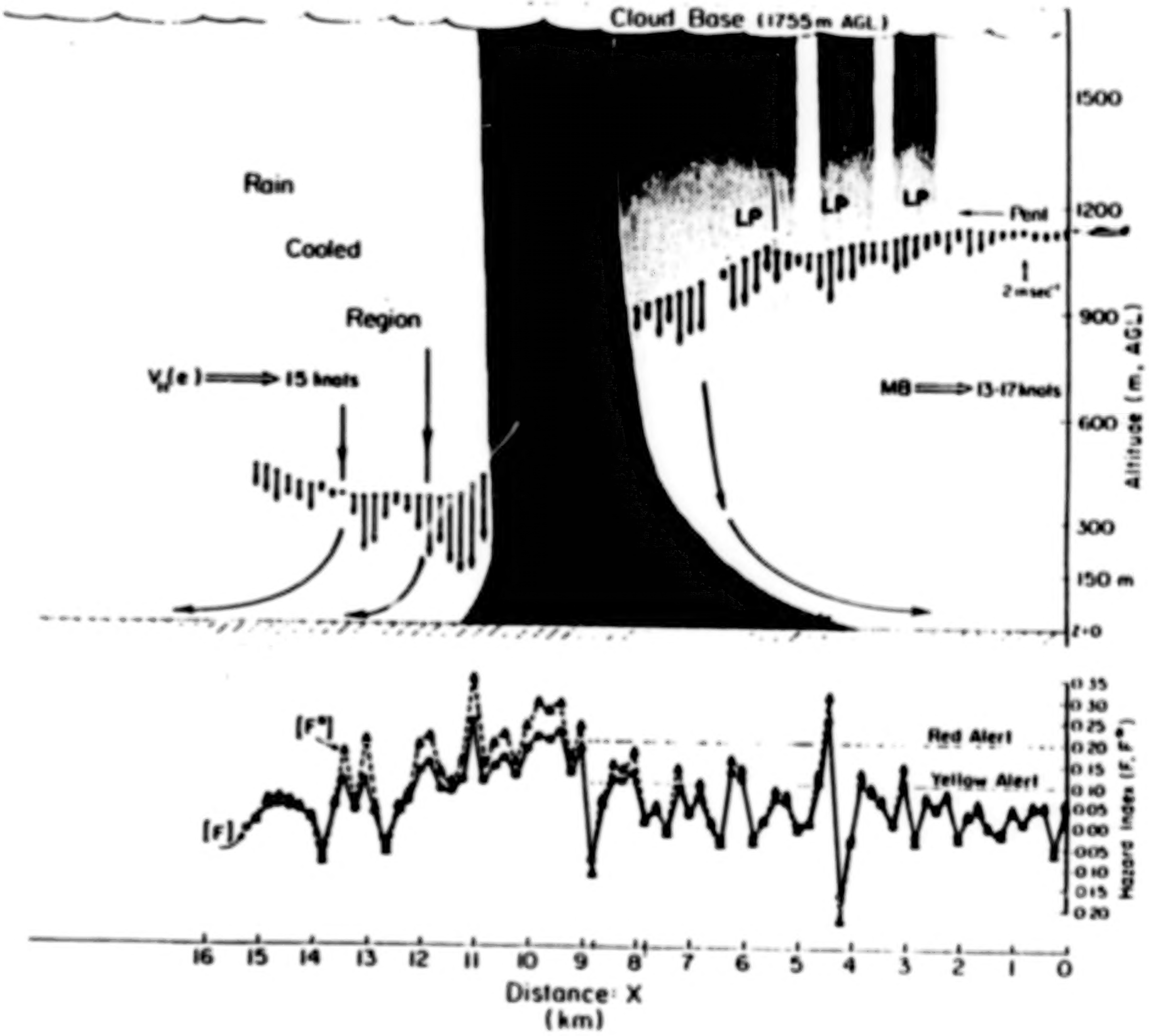
Cloud Base (1755 m AGL)
Rain
Cooled
Region
LP
LP
LP
Pent
2 m sec⁻¹
$V_h(e)$ ⟹ 15 knots
MB ⟹ 13-17 knots
1500
1200
900
600
300
150 m
z=0
Altitude (m, AGL)
[F*]
[F]
Red Alert
Yellow Alert
0.35
0.30
0.25
0.20
0.15
0.10
0.05
0.00
0.05
0.10
0.15
0.20
Hazard Index (F, F*)
16
15
14
13
12
11
10
9
8
7
6
5
4
3
2
1
0
Distance: X
(km)

Status of Colorado State Universities' IR Research
Questions and Answers

Q: DAVE HINTON (NASA Langley) - You discussed a microburst penetration technique for your Cessna that involved lowering the nose to increase or preserve airspeed, then trailing off this airspeed for potential energy at low altitude. I can understand doing this during intentional research penetrations begun at reasonable altitudes, but I am skeptical that this could be safely performed in an inverted encounter at low altitude, say 100 or 200 feet AGL. Are you advocating a pitch down technique for general aviation pilots?

A: PETE SINCLAIR (Colorado Stare University) - Yes. For intense microbursts with down-drafts of greater than 7 to 10 meters per second. The amount of pitch down, of course, will depend on the magnitude of the down-draft and the altitude above ground level.

Q: DAVE HINTON (NASA Langley) - Have you conducted any piloted simulation studies to determine the acceptability and viability of this procedure for GA pilots of average skill?

A: PETE SINCLAIR (Colorado Stare University) - Not yet, but I plan to enter our measured wind profiles into a flight simulator for development of GA flight procedures.

ROLAND BOWLES (NASA Langley) - It amazes me that people don't understand that you descend when you lower the nose of an airplane. It also surprises me that we talk about airspeed loss, dynamic pressure, forces on big lifting surfaces of 20 to 30% and realize that there is still the factors of 2 in lift coefficient by just getting the wing bite into the relative wind in the right way. It's not a very simple problem.

WAYNE SAND (NCAR) - I guess I have to respond a little bit. There is some foundation to what Peter is saying in this whole thing. It's a technique that actually has been proven by the sail plane people. They do this all the time to deal with rotor clouds when they're doing wave flights and all that sort of thing. The way they deal with it, to get through there as quickly as possible with the least altitude loss possible, is to go fast and to get the nose down. So I think that's the foundation for a lot of what he's saying and what he's trying to suggest. I think it's a long ways from proving that's the right way to do it. One of our people has gone through some calculations on that with this sort of thing in mind and actually came up with the same conclusion that you're probably better off in a light plane to get through there as quickly as you can however you do that, providing you have the ground clearance and all that sort of thing. I'm certainly not to the point of advocating that yet either. It is something to think about and it's one of the points that I think should be addressed.

ROLAND BOWLES (NASA Langley) - Sail planes don't have engines on them. One of the first rules is to get the thrust above the horizon.

UNKNOWN - Being both a sail plane pilot and a general aviation commercial sector pilot, I was just going to emphasize that in the sail plane arena the only option he's got to increase his forward speed, and therefore minimize the time in the shear, is by lowering his nose. That's the reason why we do that. However, in our sector, particularly the commercial sector, you have other options available. I think that Peter's goal is certainly worthwhile and that's to minimize the time in the shear. I think we can all agree that's a worthwhile objective but whether you lower the nose and go for the ground in order to do that or not is probably worth discussing.

DAVE HINTON (NASA Langley) - I'm also a sail plane pilot and I also understand wanting to put the nose down to get out of the sink as quickly as you can. But what works at 3000 feet may not work at 30. As anybody that has done any research on recovery procedures knows, you can't simply go for the optimal recovery technique and say fly it, there are other factors involved.

Session X. Airborne Doppler Radar / Industry

PRECEDING PAGE BLANK NOT FILMED

Session X. Airborne Doppler Radar / Industry

N91-24148

Status of General Motors Hughes Electronics Research
Dr. Brian Gallagher, Delco
Mark Selogie, Hughes

NASA/FAA
THIRD COMBINED MANUFACTURERS' AND
TECHNOLOGISTS' AIRBORNE WIND SHEAR
REVIEW MEETING

DELCO SYSTEMS OPERATIONS
DIVISION OF GENERAL MOTORS HUGHES ELECTRONICS

FORWARD LOOKING WINDSHEAR DETECTION PROGRAM
1989/1990 STATUS REPORT

Delco Systems
Operations

Brian J. Gallagher
October 18, 1990

DELCO SYSTEMS R&D PROGRAM ON FORWARD LOOKING WINDSHEAR DETECTION

COOPERATIVE EFFORT WITH HUGHES AIRCRAFT

- OBJECTIVES
- APPROACH
- PROGRESS
- CONCLUSIONS

Delco Systems
Operations

OBJECTIVES

Develop Predictive Windshear Detection System
Based on Passive IR Remote Sensing Technology

- Advance Warnings of 10 to 30 seconds
- Acceptable False Alarm Rate <10^-4
- Small, Lightweight, Affordable

- Original Objective was Stand Alone Sensor
- Integrated Sensor Approach Studied in 1989

APPROACH

- Inferential Approach Based on Temperature Differential of Downbursts Correlated with Vertical Velocity
- Sensor is Multi-Spectral Scanning Radiometer Operating in 10-14 micron Atmospheric Window
- Reliance on Measurement of Both Horizontal and Vertical Temperature Gradients of Atmosphere
- Primary Issue is Random Spatial Temperature Variations or Atmospheric Background 'Noise'

Delco Systems
Operations

EXTINCTION OF RADIANCE BY ABSORBING AND SCATTERING MEDIA

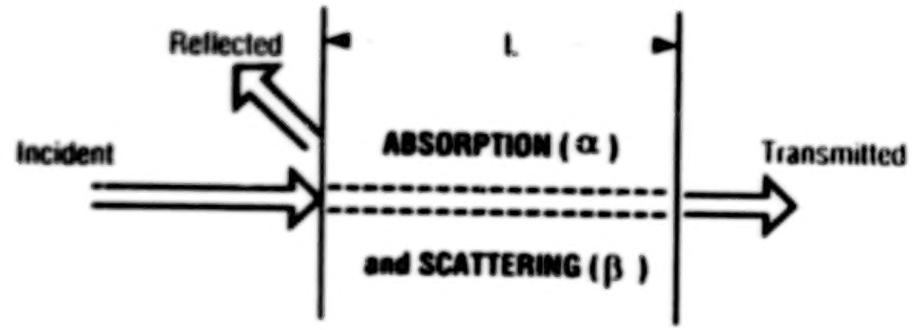
Reflected
L
Incident
ABSORPTION (α)
and SCATTERING (β)
Transmitted

σ = Absorption + Scattering = Extinction Coefficient (km^{-1})

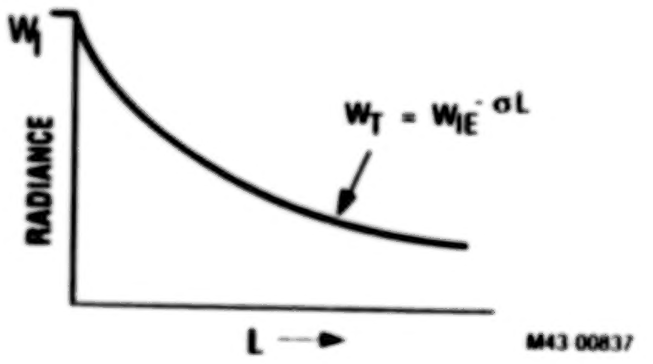

M43 00837

Delco Systems Operations

ATMOSPHERIC ABSORPTION IN FAR IR REGION

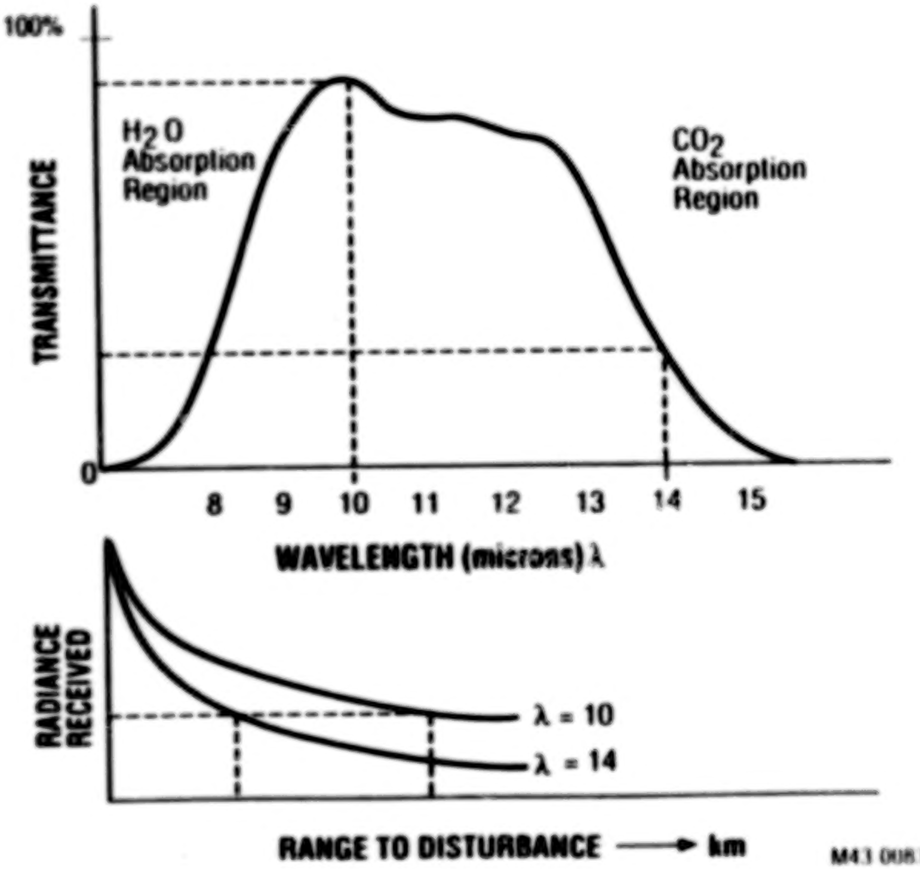

M43 008.16

INFRAMETRICS IMAGING RADIOMETER

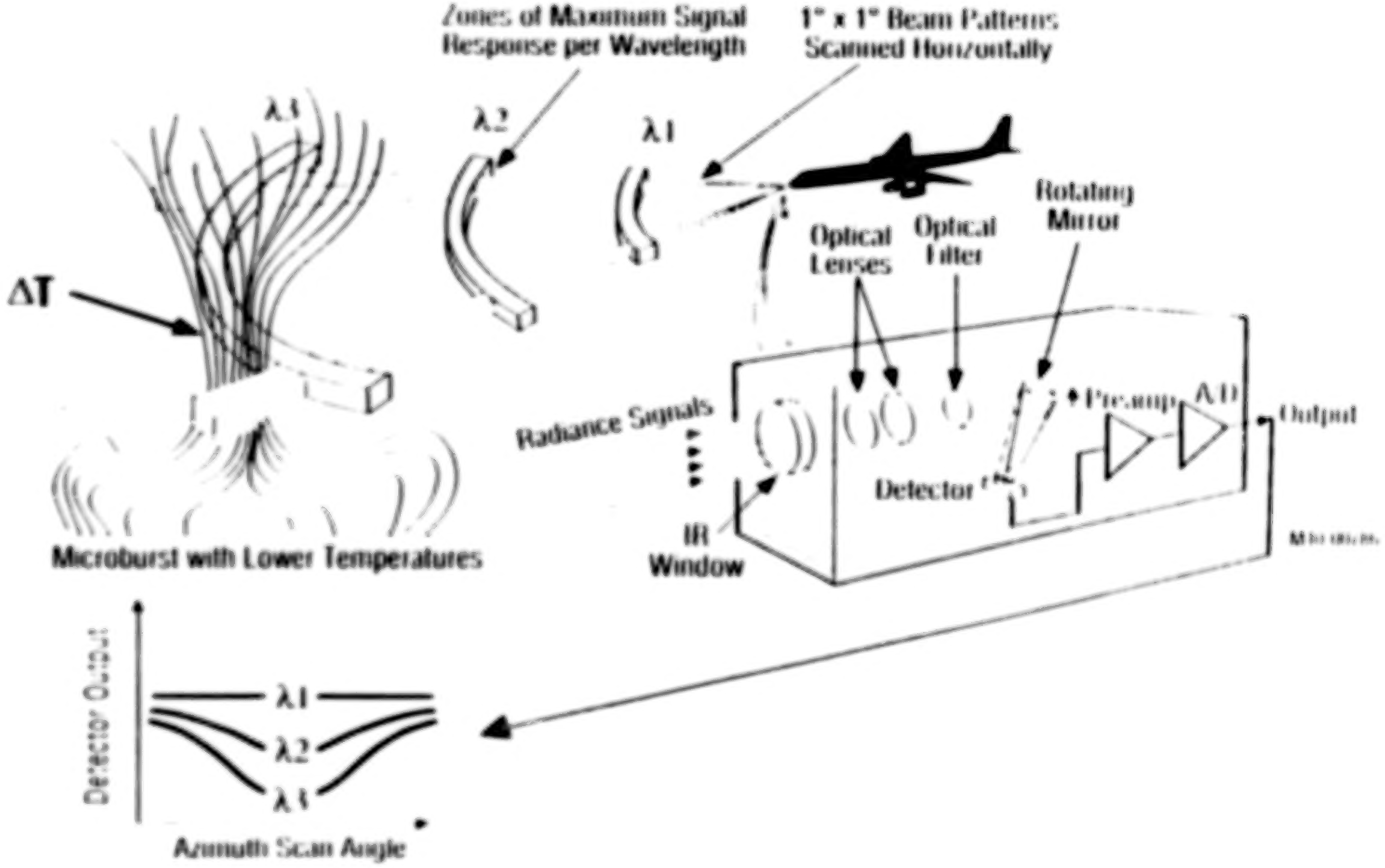
Zones of Maximum Signal Response per Wavelength
1° x 1° Beam Patterns Scanned Horizontally
λ3
λ2
λ1
ΔT
Optical Lenses
Optical Filter
Rotating Mirror
Preamp
A/D
Output
Radiance Signals
Detector
IR Window
Microburst with Lower Temperatures
Detector Output
λ1
λ2
λ3
Azimuth Scan Angle

BASIC RADIANCE SIGNAL EQUATION

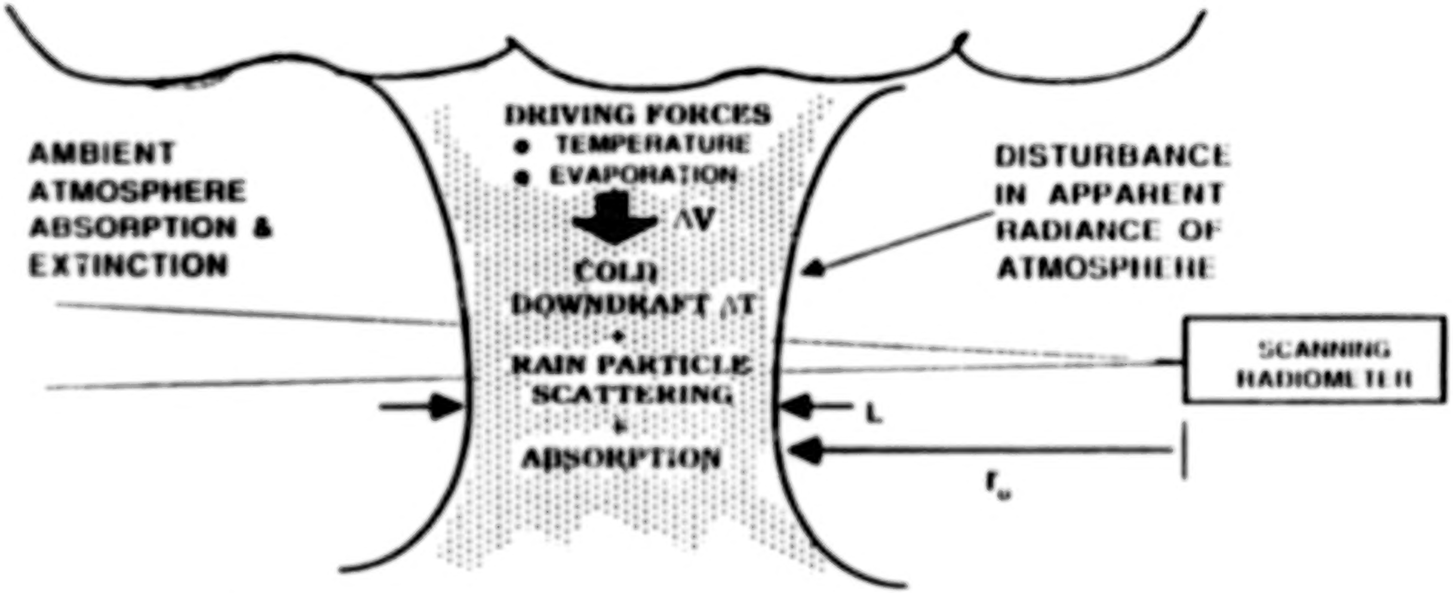

AMBIENT ATMOSPHERE ABSORPTION & EXTINCTION

DRIVING FORCES
- TEMPERATURE
- EVAPORATION

ΔV

COLD DOWNDRAFT ΔT
+
RAIN PARTICLE SCATTERING
&
ABSORPTION

DISTURBANCE IN APPARENT RADIANCE OF ATMOSPHERE

SCANNING RADIOMETER

PEAK SIGNAL RADIANCE AT λ_λ IN CO_2 ABSORPTION BAND

$$S_\lambda \cong G_\lambda W_{\lambda b} \frac{4\Delta T}{T} \underbrace{\left[1 - e^{-(\sigma_\lambda + \Delta\sigma) L}\right]}_{\text{emissivity}} \underbrace{e^{-\sigma_\lambda r_o}}_{\text{atmospheric transmission}}$$

ΔT proportional to ΔV

TOWER TEST PLAN

- Install test radiometer on 150-foot high control tower at Milwaukee airport to simulate airplane environment
- Collect atmospheric radiance data for different weather conditions during June and July 1989
- Reduce and analyze data using thermogram card and VAX computer programs
- Checkout computer algorithms, verify lapse rate measurements, and investigate atmospheric noise

ORIGINAL PAGE IS
OF POOR QUALITY

FLIGHT TEST PLAN

- Install test radiometer in modified nose cone of flight test aircraft with TV camera, video recorders, and controls
- Install test computer and monitors with in-flight data collection, display, analysis, and recording software
- Instrument aircraft with Kollman Research Systems Data Acquisition and Recording System
- Perform in-flight data collection and real-time analysis test flights during August and September 1989, under different weather conditions, and correlate with meteorological sounding data
- Reduce and analyze data and determine atmospheric noise distribution and lapse rates

APPROACH

EXPERIMENTAL RADIOMETER INSTALLED IN FLIGHT TEST AIRCRAFT

Delco Systems
Operations

ORIGINAL PAGE IS
OF POOR QUALITY

APPROACH

MODIFIED NOSECONE SHOWING INFRARED AND VISIBLE WINDOWS FOR RADIOMETER AND TV CAMERA

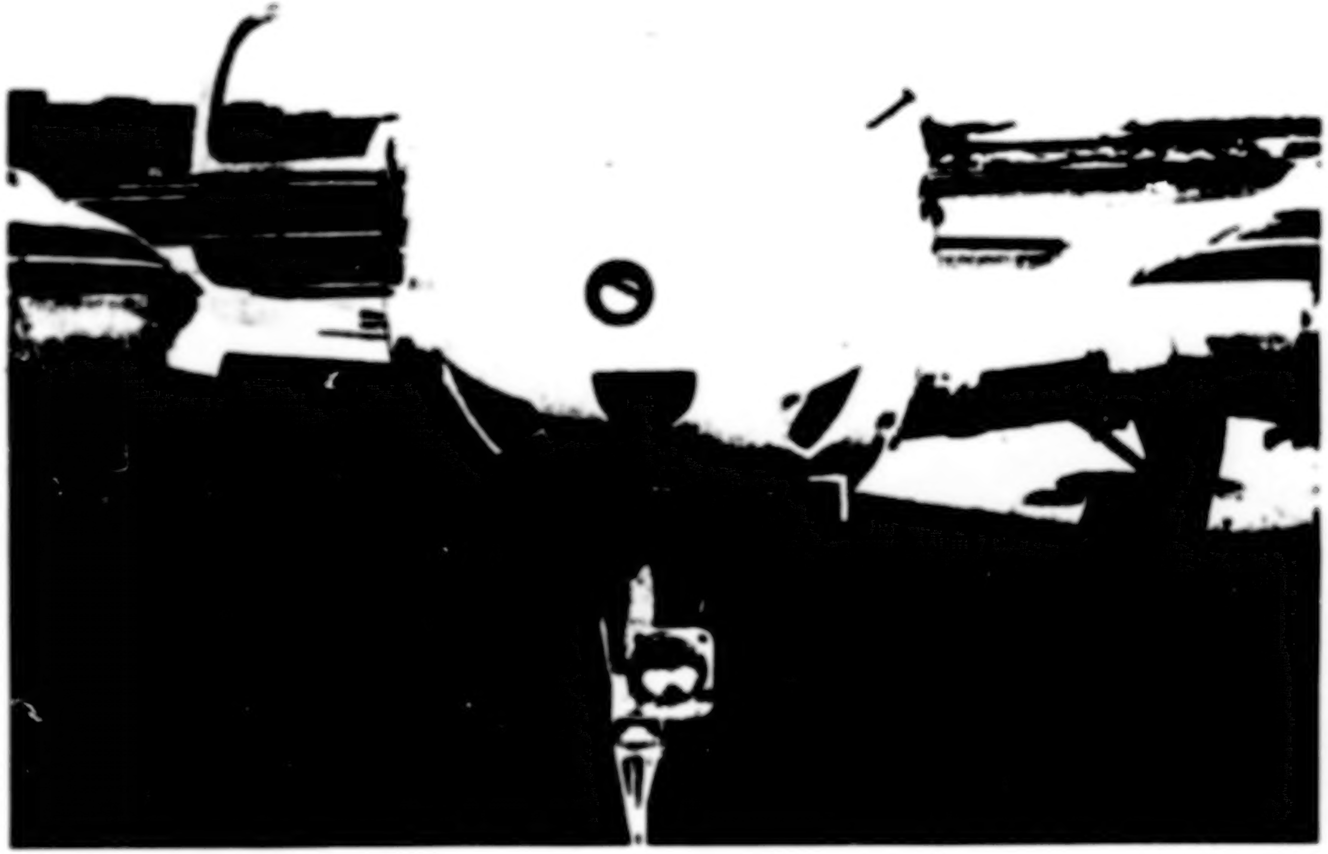

ORIGINAL PAGE IS
OF POOR QUALITY

APPROACH

FLIGHT TEST INSTRUMENTATION, DISPLAYS, AND OPERATING CONTROLS CONSOLE

ORIGINAL PAGE IS
OF POOR QUALITY

APPROACH

FLIGHT TEST DATA ACQUISITION AND DISPLAY CONSOLE

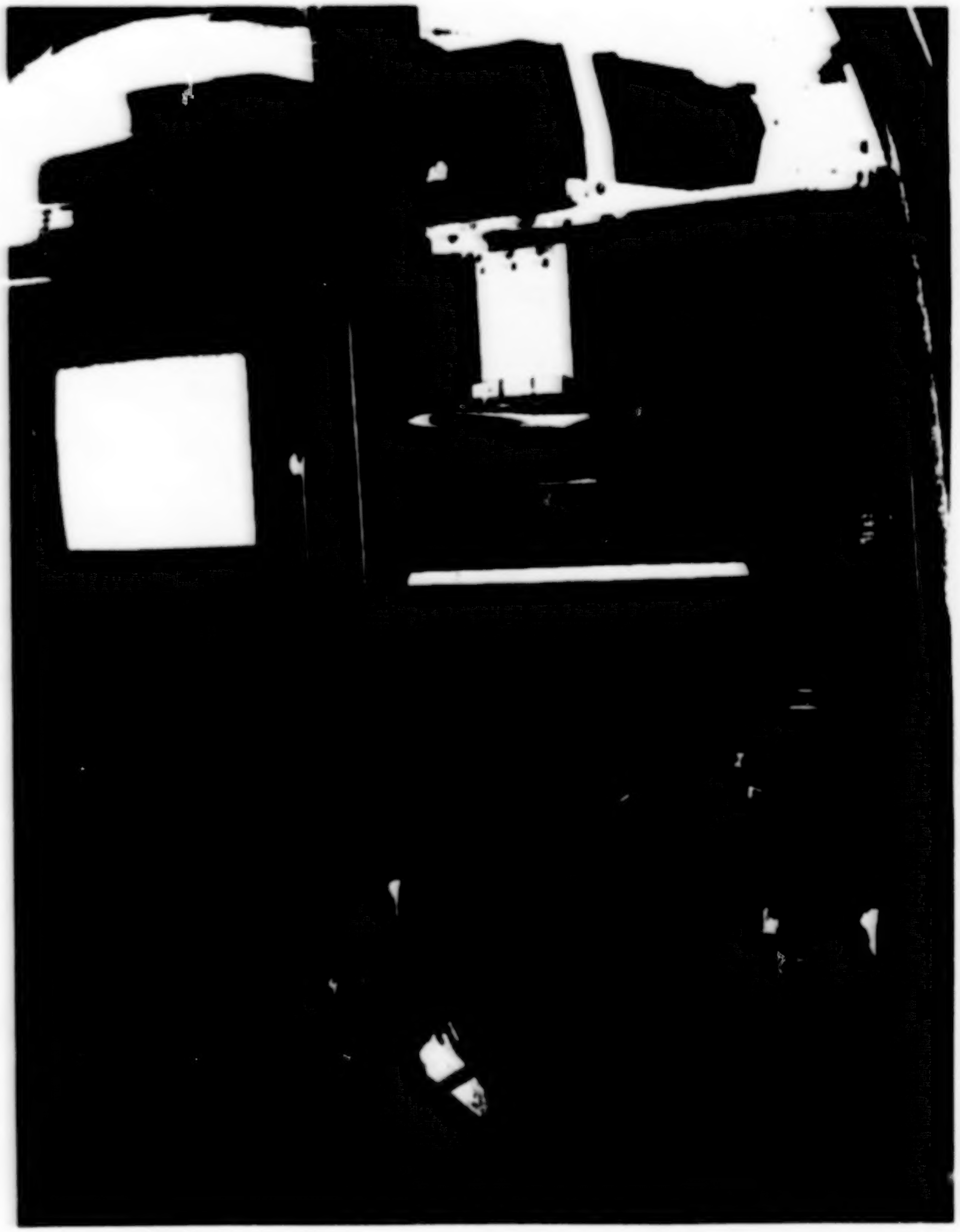

C-3

ORIGINAL PAGE IS
OF POOR QUALITY

Delco Systems Operations

DATA ACQUISITION SYSTEM DISPLAY

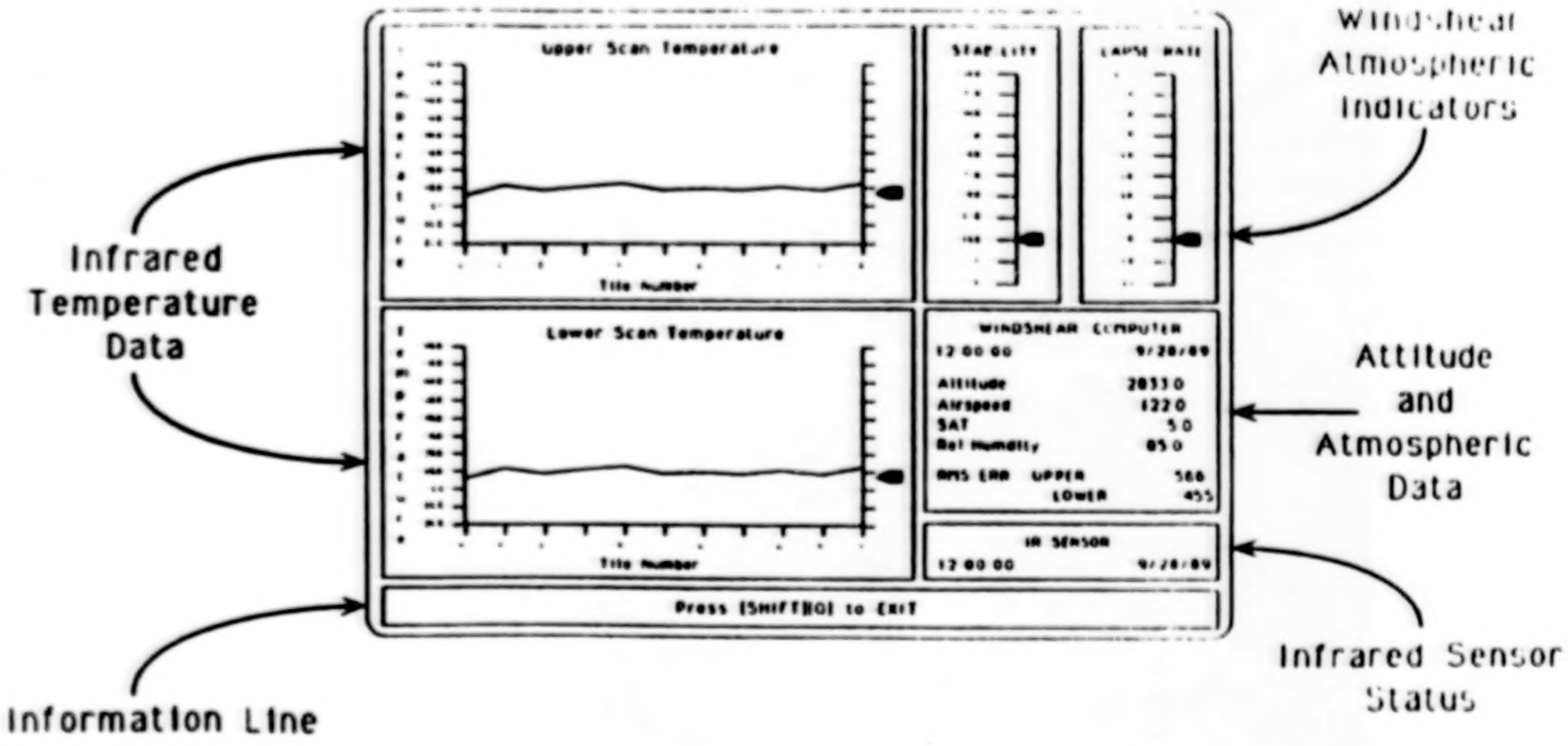
Upper Scan Temperature
Tile Number
Lower Scan Temperature
Tile Number
STABILITY
LAPSE RATE
WINDSHEAR COMPUTER
12 00 00
9/20/89
Altitude 2033 0
Airspeed 122 0
SAT 5 0
Rel Humidity 65 0
RMS ERR UPPER 566
LOWER 455
IR SENSOR
12 00 00
9/20/89
Press [SHIFT][O] to EXIT
Infrared Temperature Data
Information Line
Windshear Atmospheric Indicators
Attitude and Atmospheric Data
Infrared Sensor Status

Delco Systems Operations

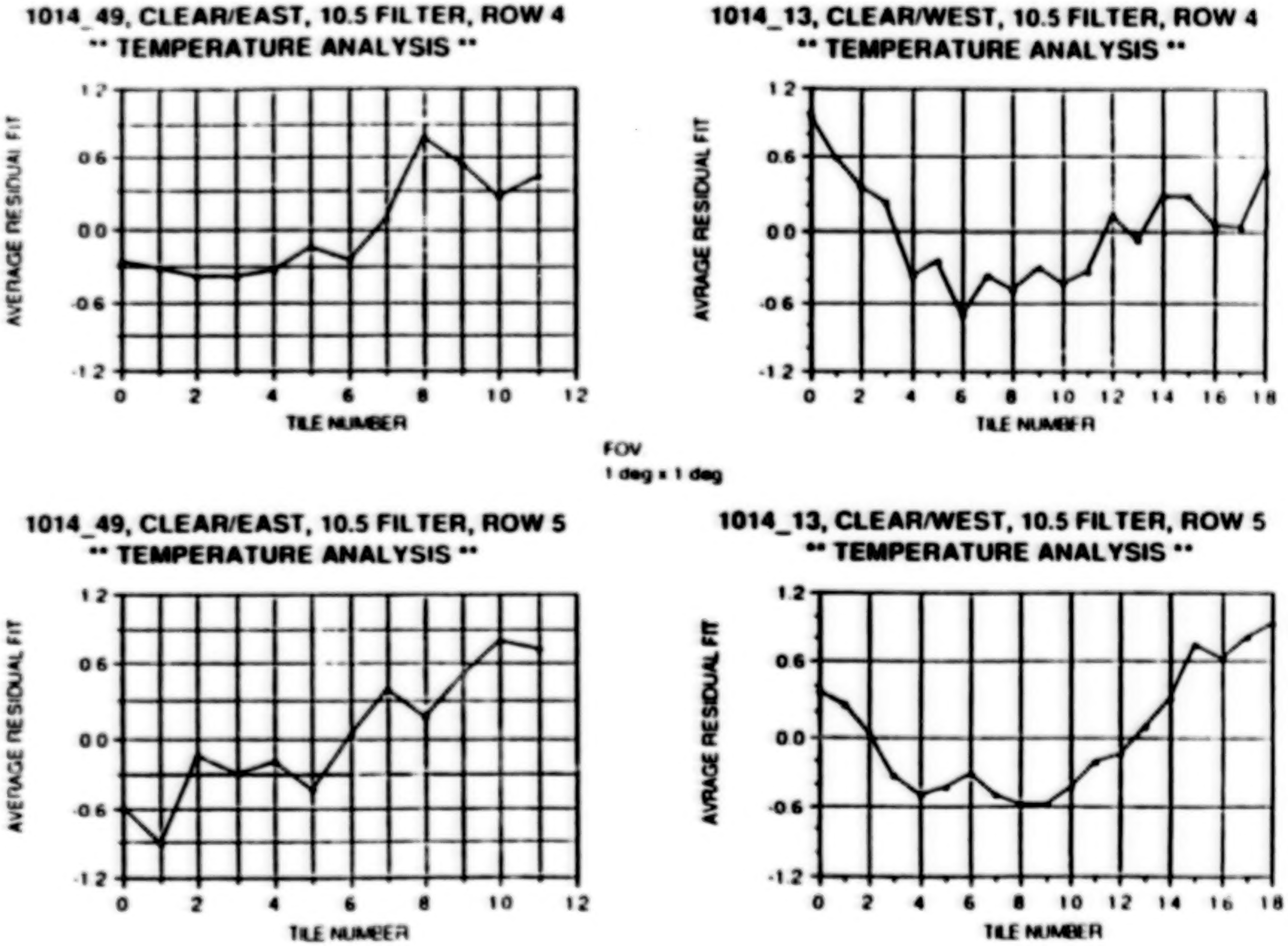

Linear Slope

Parabolic Slope

Examples of Data Showing Linear and Parabolic Slope

ORIGINAL PAGE IS
OF POOR QUALITY

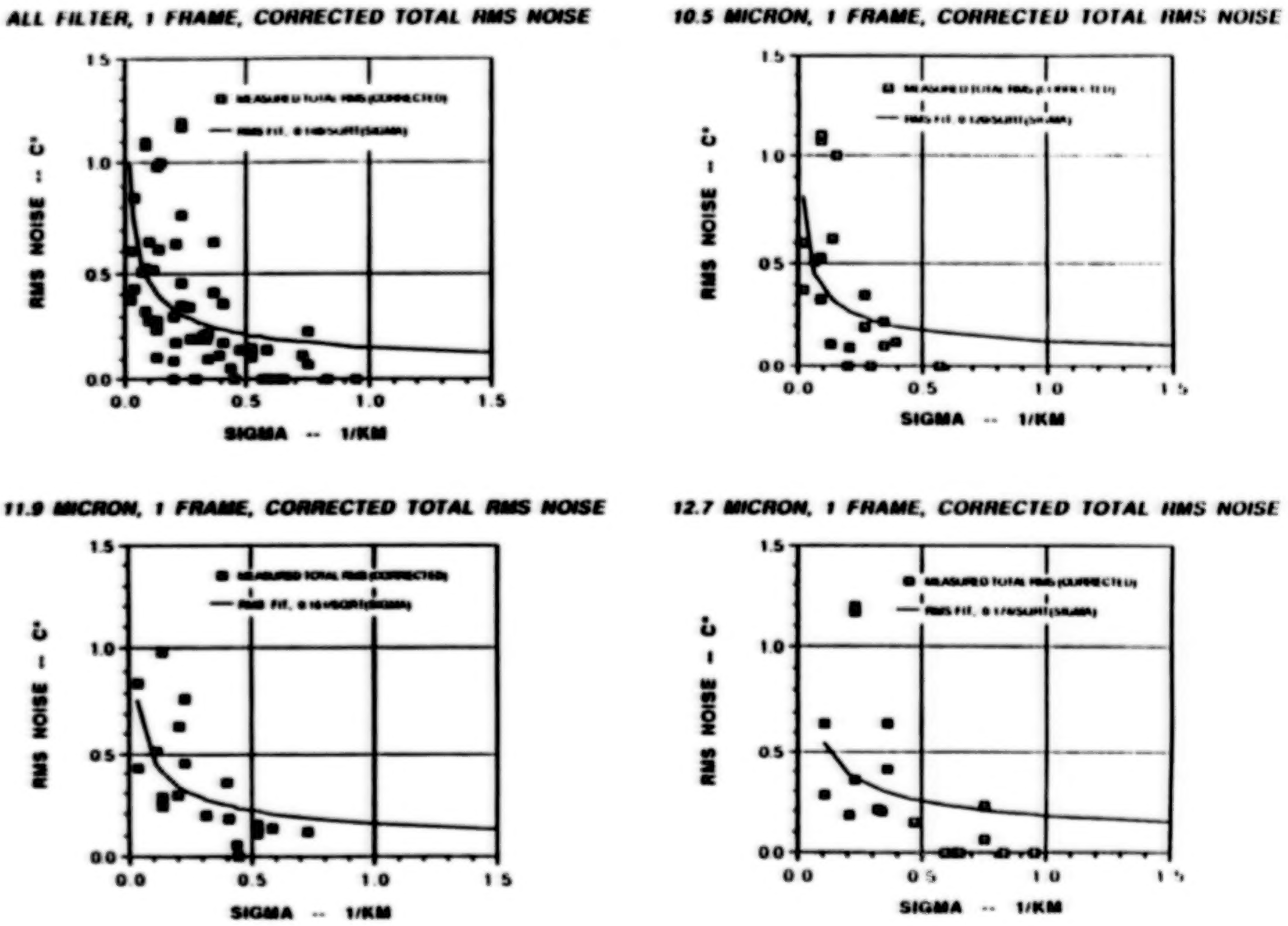

Corrected Total RMS Noise versus Extinction Factor

ORIGINAL PAGE IS
OF POOR QUALITY

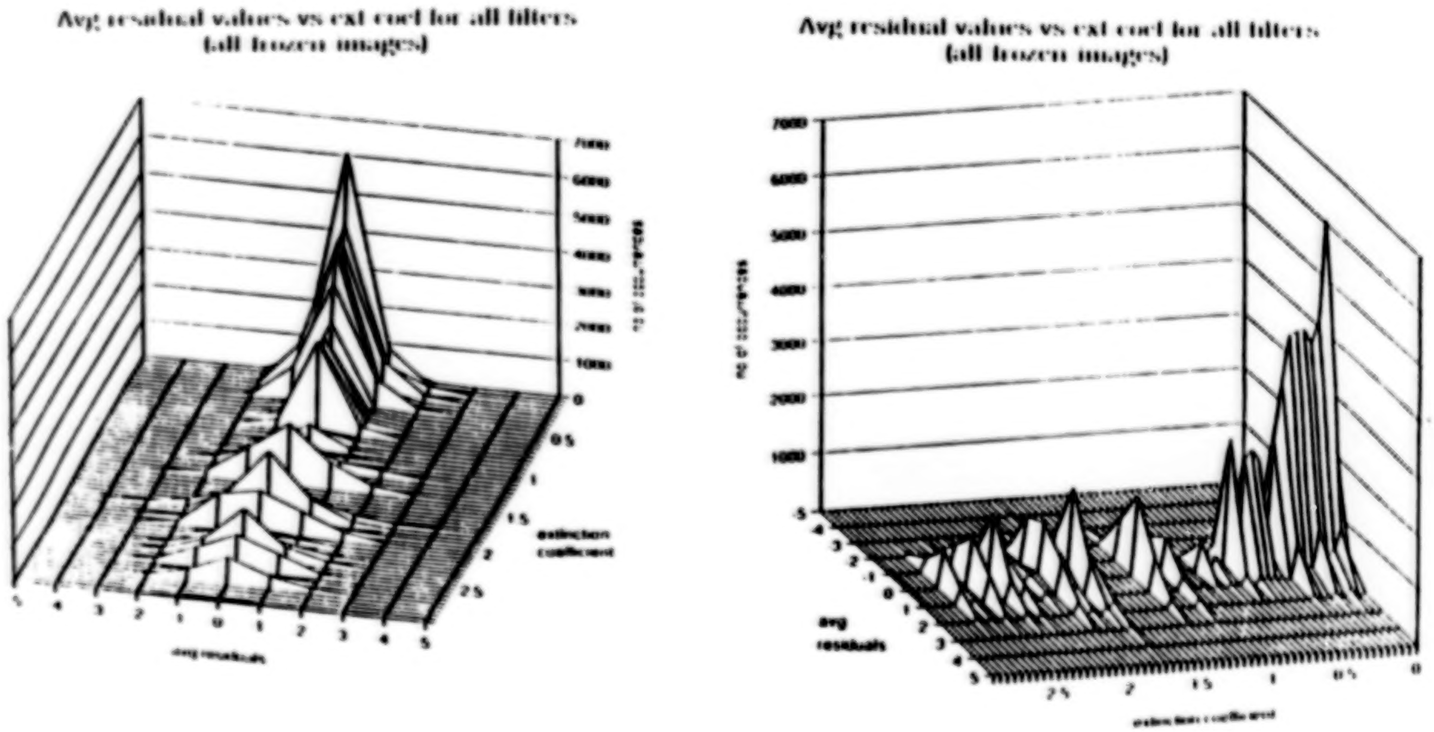

Frozen Image Total Residual Error Distributions

ORIGINAL PAGE IS
OF POOR QUALITY

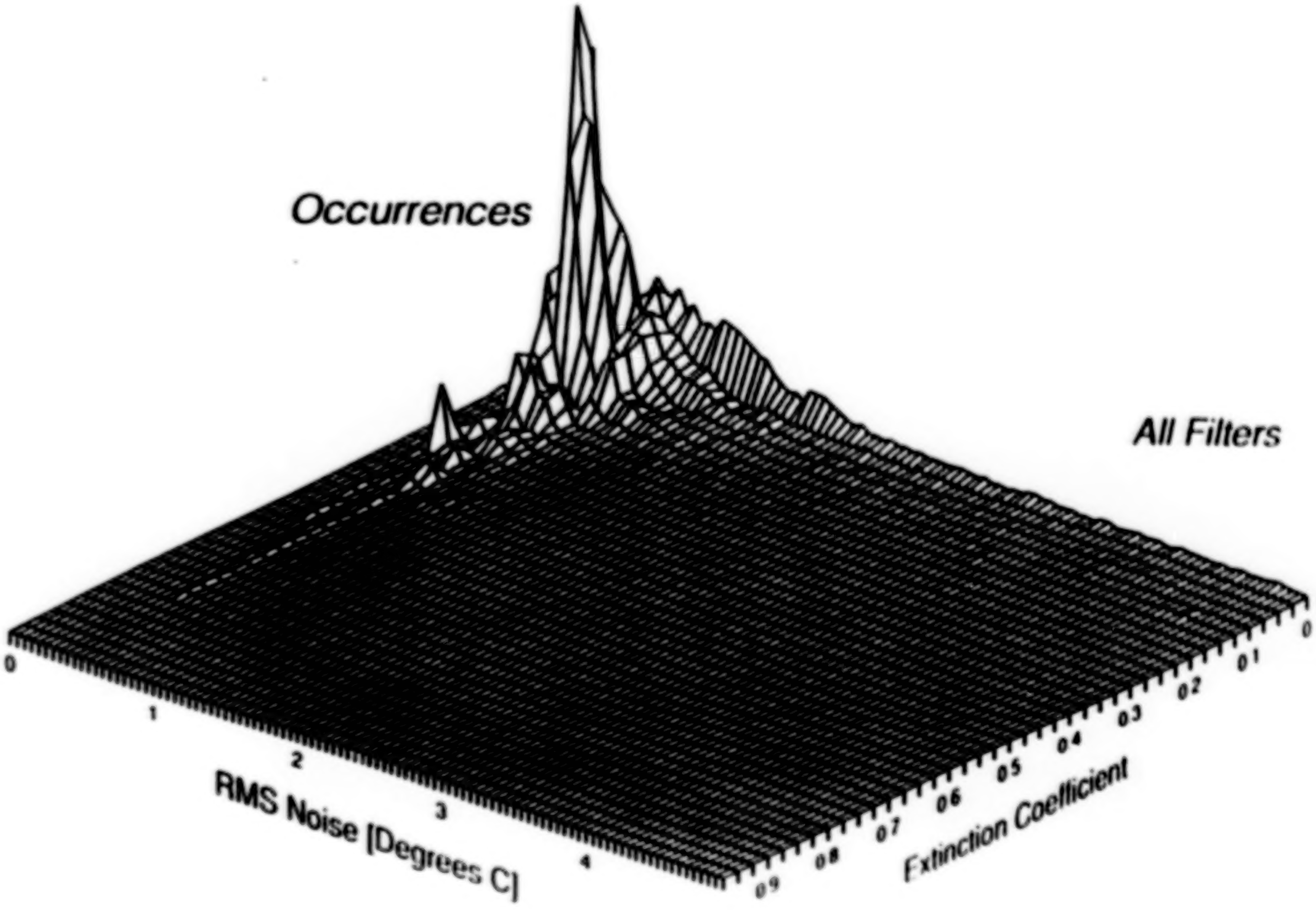

Atmospheric Noise - Corrected for Instrument Noise

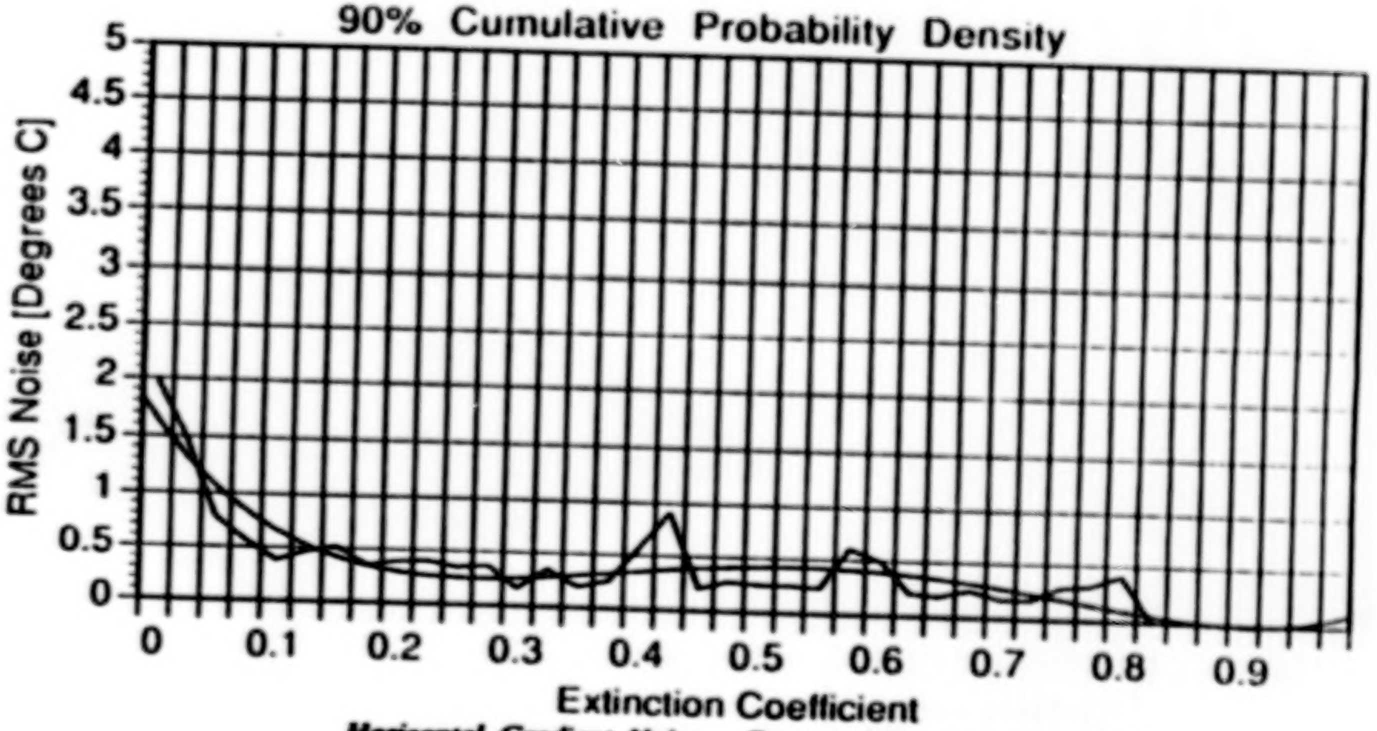

Horizontal Gradient Noise - Corrected for Instrument Noise

FROZEN IMAGE RMS NOISE SUMMARY

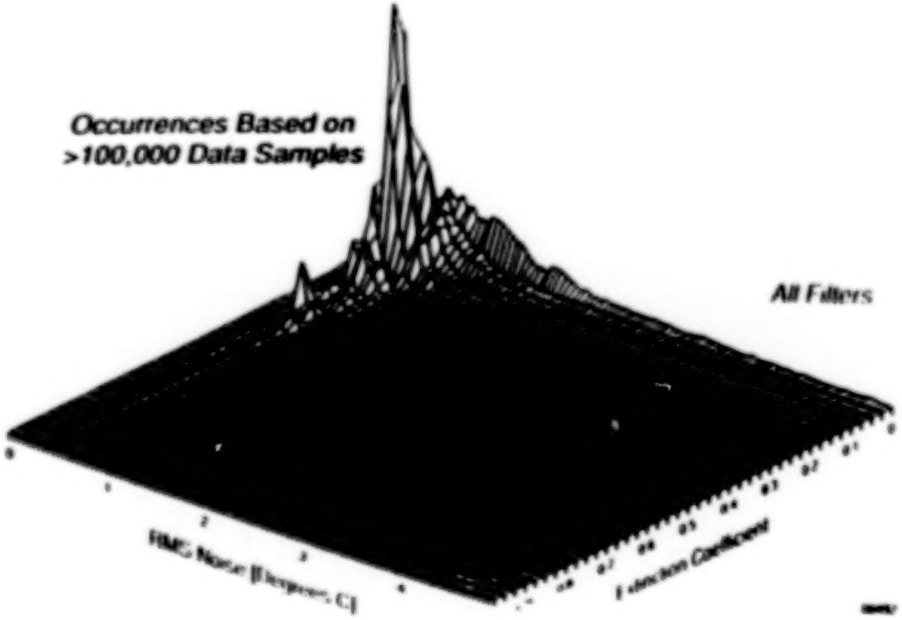

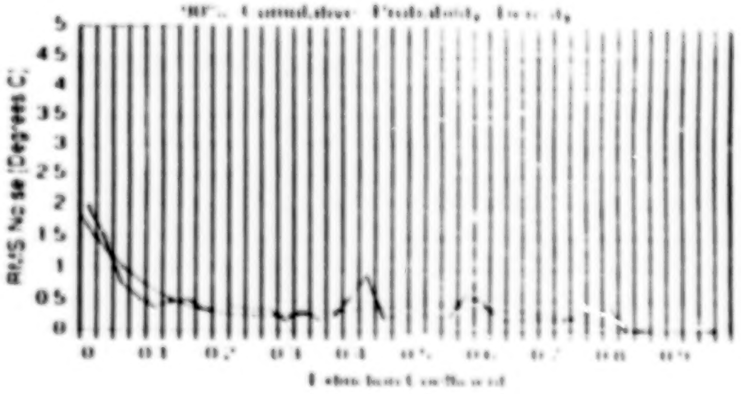

IR FILTER (micron)	APPROX σ (km^{-1})	APPROX RANGE (km)	LOW FREQUENCY SPATIAL NOISE (°C)
10.5	0.1	10	0.446
11.9	0.33	3	0.405
12.7	0.5	2	0.458
13.8	1.0	1	0.389

Delco Systems Operations

RESULTS OF ATMOSPHERIC SIGNAL, NOISE, AND RADIOMETER RESPONSE ANALYSIS

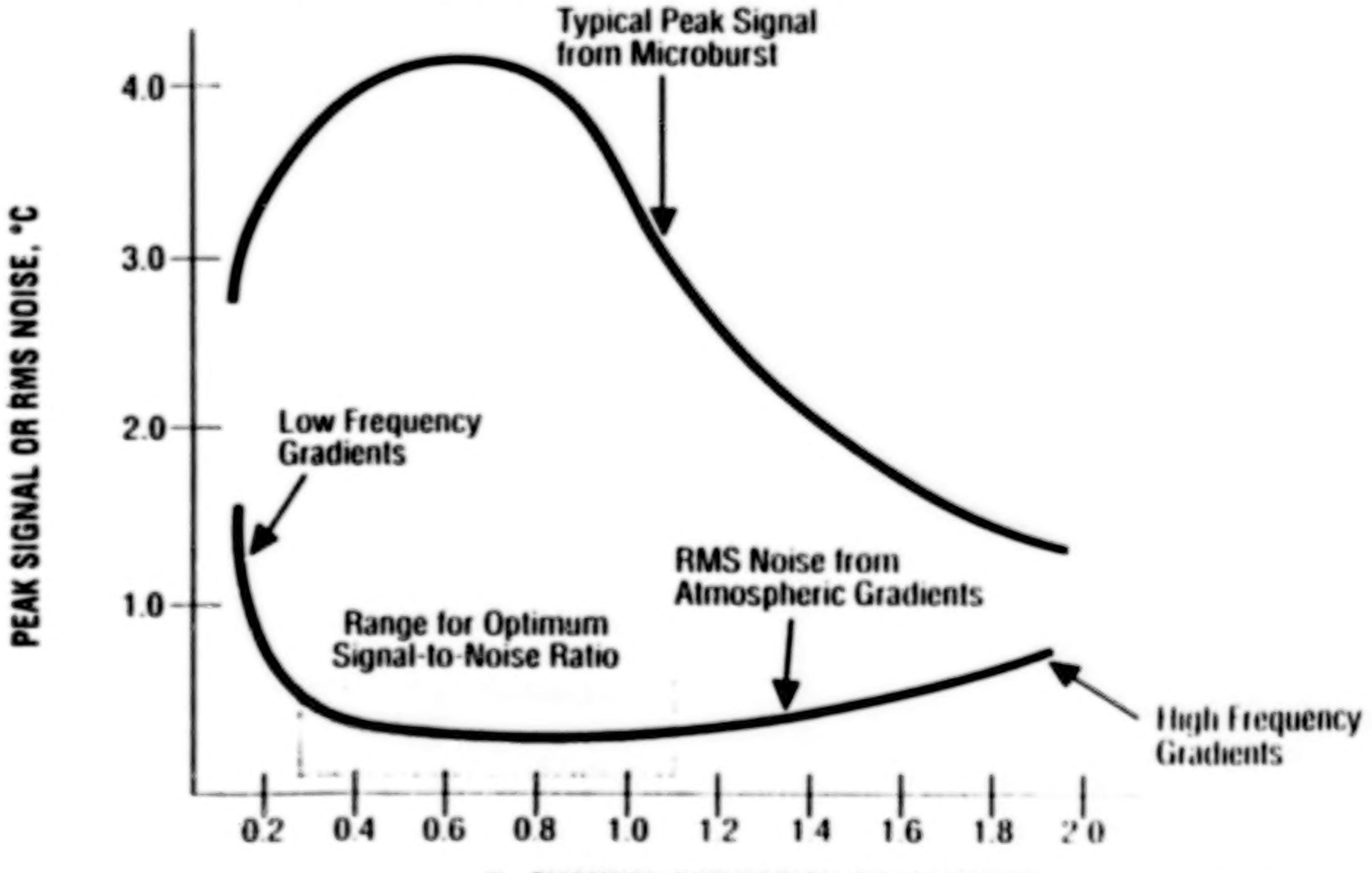

CONCLUSIONS

- In worst case, atmospheric low frequency noise appears twice as high as desirable for reliable detection of minimum velocity microbursts without false alarms (0.4°C instead of 0.2°C rms)
- Neural network study of University of Wisconsin-Milwaukee shows promise of significant noise reduction technique through adaptive filtering
- Forward Looking Windshear Detection using IR technology has definite potential as a complementary integrated sensor

RECOMMENDATIONS

- Need to correlate noise data with winds to determine how much "noise" is actually turbulence induced versus random background
- Low noise multispectral radiometer and real microburst data collection program essential for final concept verification
- Fusion of IR sensor data with Doppler radar, Ladar, and inertial sensor systems to reliably detect windshears and clear air turbulence should be pursued in future programs

DESIGN CONSIDERATIONS FOR AN AIRBORNE WINDSHEAR DETECTION RADAR

OCTOBER 18, 1990

HUGHES

DESIGN CONSIDERATIONS FOR AN AIRBORNE WINDSHEAR DETECTION RADAR

Hughes Aircraft Company

An airborne radar can be used to provide reliable forward looking windshear detection. The radar uses a direct measure of wind velocity to determine the hazard F-factor and issue a warning to the pilot. The radar measures wind velocity as a function of range and determines the presence of windshear if there is an abrupt change in wind direction over a short range interval. This change in wind direction is recognized by the radar as a distinct S-shaped curve in the range-velocity domain. The NASA windshear simulation has been used to verify the radar's ability to detect this S-shaped windshear curve.

In order to provide a useful alert to the pilot, the radar must provide at least 15-20 seconds of warning and provide this warning with a very low false alarm rate. In addition, the radar must have adequate range to penetrate the windshear to enough depth to discriminate dangerous shears from benign shears. Scan-to-scan correlation logic may be employed to lower the false alarm rate. The overall design issues involved in specifying a radar to detect windshear include its frequency, transmitter power, antenna beamwidth, coherent doppler processing, range resolution and interference rejection.

RADAR MEASURES WIND VELOCITY TO DETECT WINDSHEAR

HUGHES

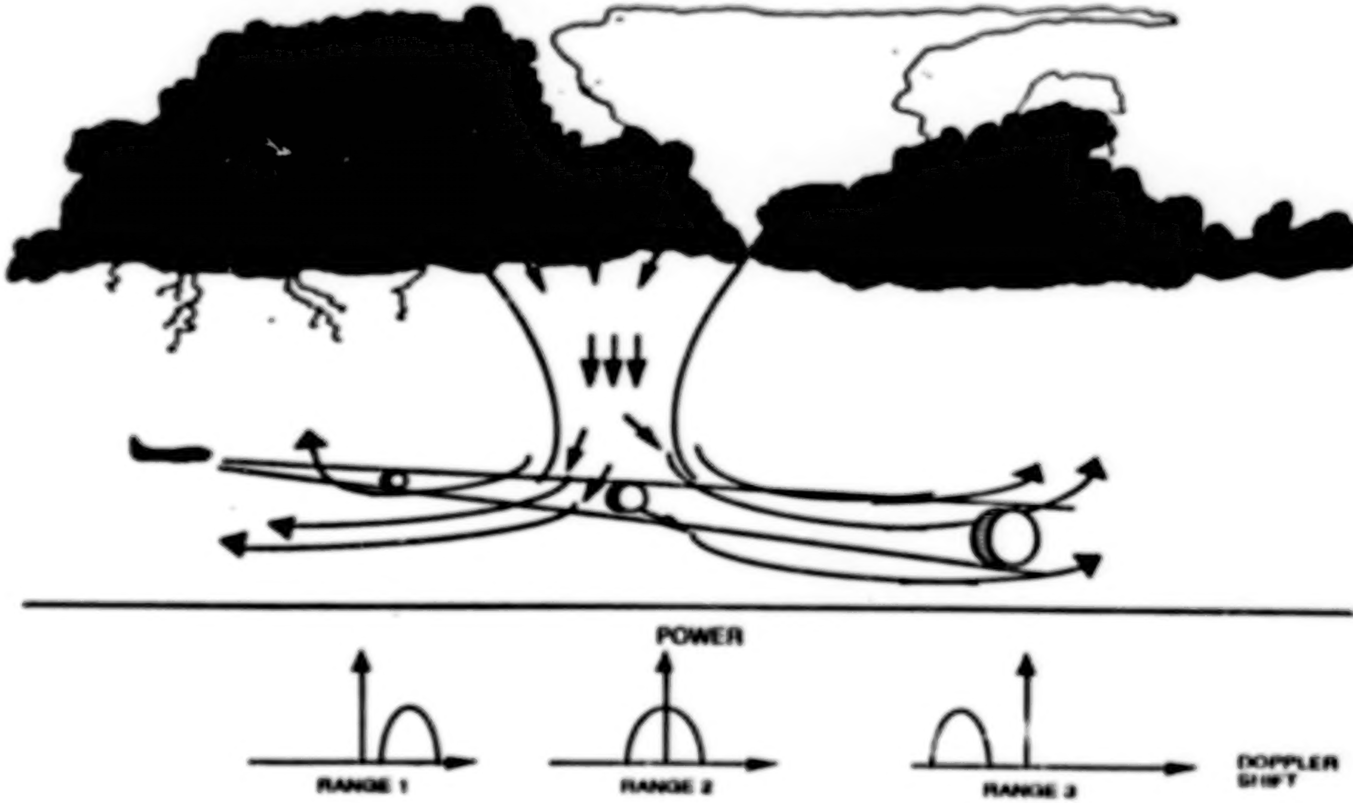
POWER
RANGE 1
RANGE 2
RANGE 3
DOPPLER SHIFT

- RADAR MEASURES RADIAL VELOCITY VS. RANGE

10/15/90

RADAR WINDSHEAR SIGNATURE

HUGHES

- RADAR GENERATES RANGE - VELOCITY MATRIX AT EACH BEAM POSITION

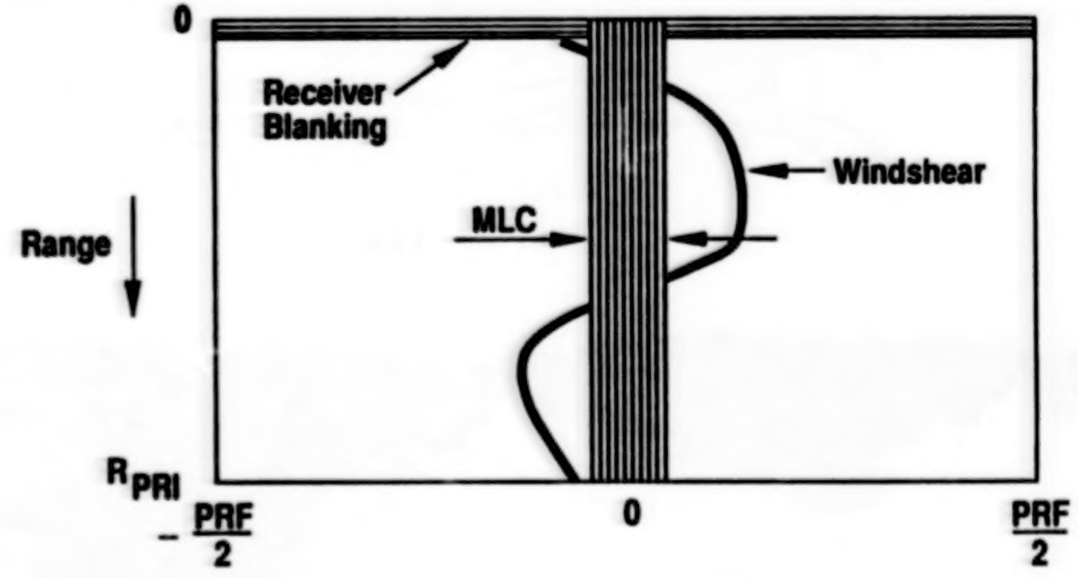
0
Receiver Blanking
Windshear
MLC
Range
R_{PRI}
$-\frac{PRF}{2}$
0
$\frac{PRF}{2}$

- RADAR DETECTS S-SHAPED WINDSHEAR SIGNATURE AND CALCULATES HAZARD F-FACTOR

10/18/90

TYPICAL WINDSHEAR PROFILE PREDICTED BY THE NASA SIMULATION

HUGHES

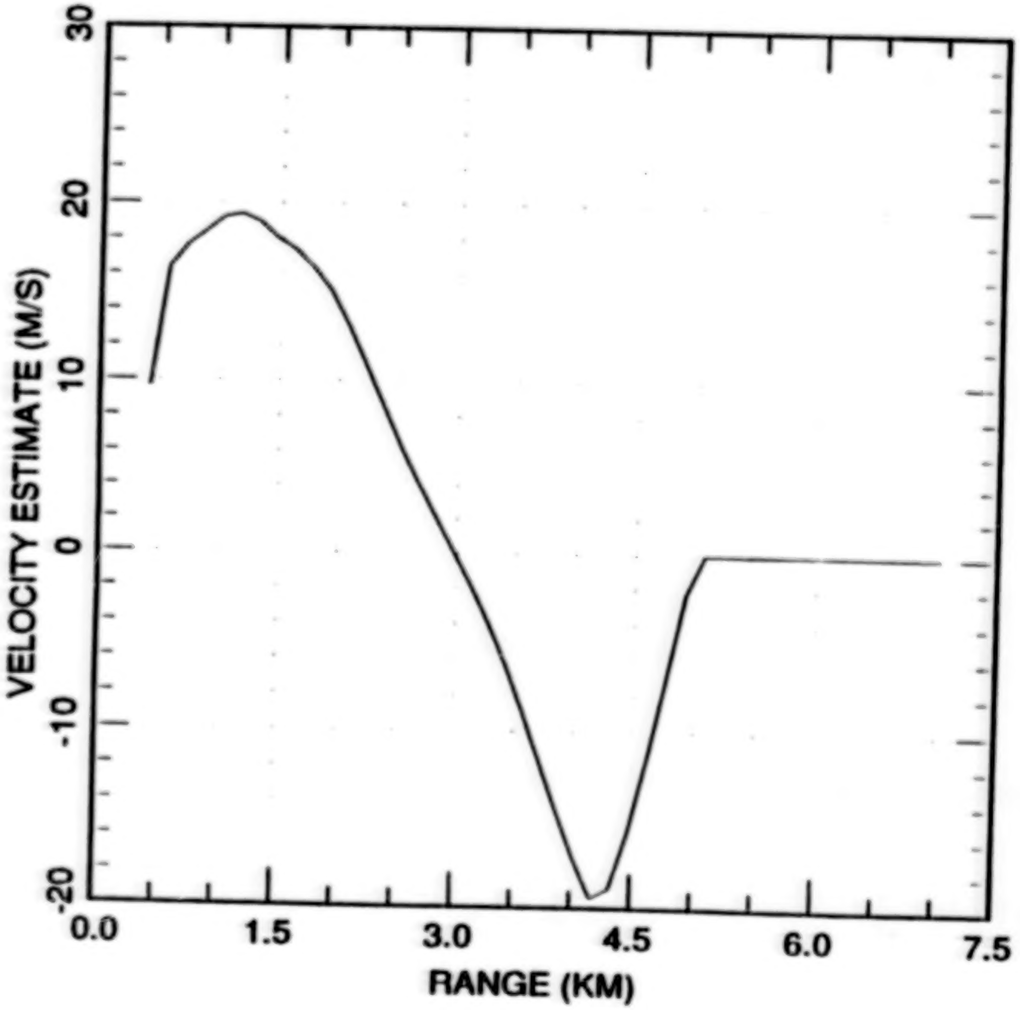

NO CLUTTER AND NO GMTS

WET MICROBURST (T11)

LOOKING STRAIGHT AHEAD ALONG GSL

WINDSHEAR DETECTION RANGE

HUGHES

DESIGN GOAL: PROVIDE THE PILOT WITH AT LEAST 15-20 SECONDS WARNING TIME WITH LOW FALSE ALARM RATE

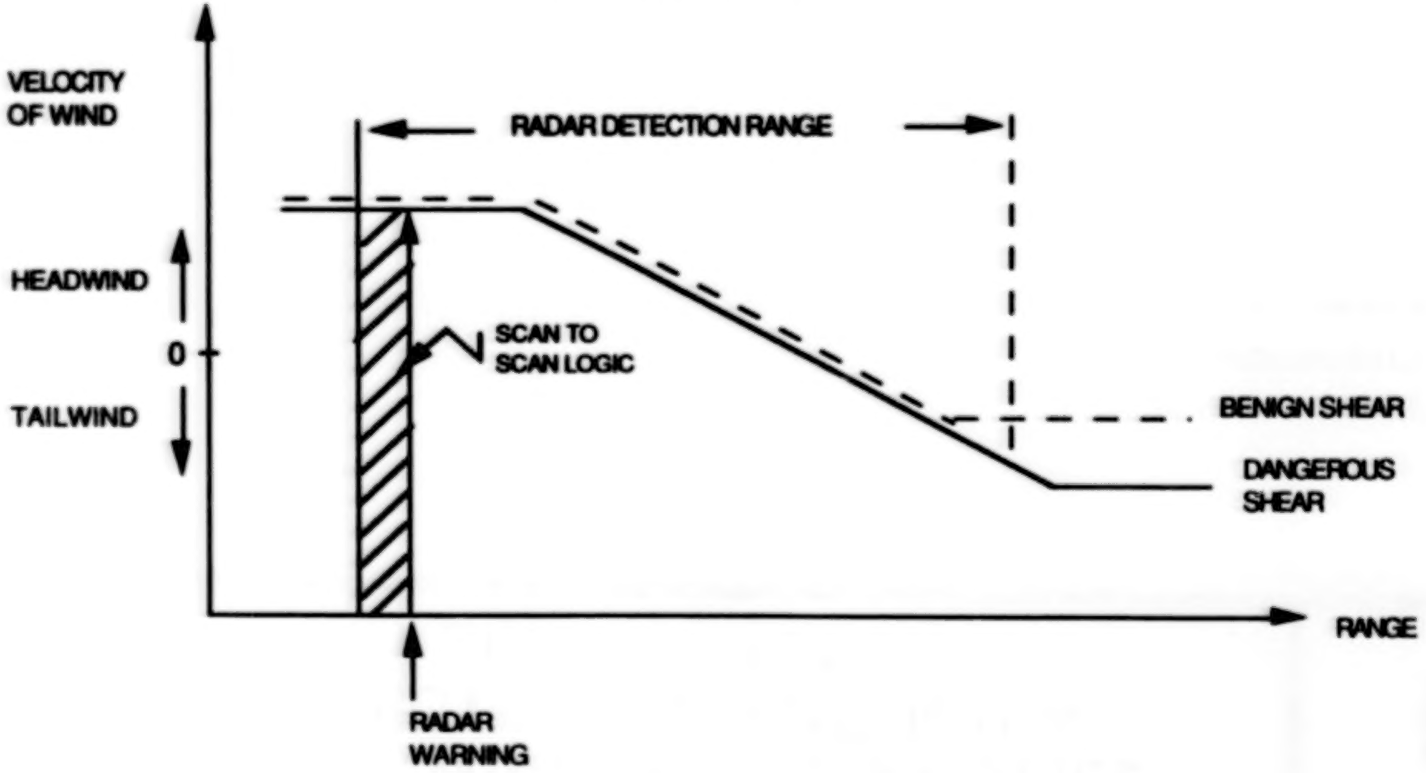

10/18/90

RADAR DESIGN ISSUES

HUGHES

MLS1012.1

- FREQUENCY
- TRANSMITTER POWER
- ANTENNA BEAMWIDTH
- COHERENT DOPPLER PROCESSING
- RANGE RESOLUTION
- INTERFERENCE REJECTION

Status of General Motors Hughes Electronics Research
Questions and Answers

Q: SUSAN KIM (Boeing) - You mentioned your goal is a targeted false alarm/nuisance rate of 1 per 10,000 flight. How do you plan to test/verify/achieve this rate?

A: BRIAN GALLAGHER (Delco) - We plan to achieve the rate through the discrimination techniques that we are developing which primarily rely on the horizontal temperature gradient. For example, angular size would be an important means of discriminating cold fronts, gust fronts, things that are non threatening. As far as verifying that, or testing that, that's a good question. I'll give you a pat answer. This is per discussions that we had with the FAA Los Angeles Certification Office. The answer is primarily through systems' simulations with "sufficient data to support the integrity of the simulation model." The question is what is sufficient data. And that data will be collected through flight tests and in-service evaluations that are being planned.

Q: SUSAN KIM (Boeing) - How do you define a false alarm?

A: BRIAN GALLAGHER (Delco) - Another word for a false alarm is a false alert. It's an alert which occurs when the design wind shear threshold conditions do not exist. An example that I could give is an atmospheric temperature gradient that emulates or masks or emulates a microburst without any turbulence whatsoever. Those things do exist out there and as a result we're going to have nonperfect systems.

Session X. Airborne Doppler Radar / Industry

Saberliner Flight Test
Bruce Mathews, Westinghouse

N91-24149

Sabreliner Flight Test

for

Airborne Windshear Forward Looking Detection and Avoidance Radar Systems

Bruce D. Mathews

Senior Engineer
Westinghouse Electric Co.
Electronic Systems Group
Radar Systems Engineering
Baltimore, Md.

Abstract

An important aspect in the design of an airborne radar for low level windshear avoidance is the false alarm/alert rate. To be used and trusted by pilots, any indications and/or displays of false hazards must be infrequent. A "clean scope" design aims to preserve detection performance and eliminate distracting false alarms. For lookdown radar, urban discretes and ground moving vehicle traffic dominate the false alarm design problem. Depending upon their relative location, spatial extent, and relative amplitude, these returns will compete with microburst windshear observables and may furnish false alarm candidates.

Westinghouse conducted a flight test with its Sabreliner AN/APG-68 instrumented radar to assess the urban discrete/ground moving vehicle clutter environment. Glideslope approaches were flown into Washington National, BWI, and Georgetown, Del. airports employing radar mode timing, waveform, and processing configuration plausible for microburst windshear avoidance. The perceptions, both general and specific, of the clutter environment furnish an empirical foundation for begining low false alarm detection algorithm development.

Sabreliner Flight Test

for

Airborne Windshear Forward Looking Detection and Avoidance Radar Systems

Bruce D. Mathews, Senior Engineer

Westinghouse Electric Corporation
Electronic Systems Group

[redacted]

- Objectives
- Expansion of Issues
- Design of Tests
- Details of Flights

ORIGINAL PAGE IS
OF POOR QUALITY

PRECEDING PAGE BLANK NOT FILMED

The next generation of commercial aviation weather radar may include a mode for forward looking detection of hazards due to low level windshear along the glideslope approach from a microburst for the purposes of detection and avoidance. This mode will dominate the design of the radar and will demand expertise in pulse Doppler radar technology. To succed in saving lives, this radar mode must be used and trusted by the pilots and be capable of sensing the presence of a hazard along the flight path prior to encountering the hazard. A hazard display should be a "clean scope", suppressing hazard indications from both mainbeam clutter and any ground moving discrete returns. Measures of a sensor to do this include its false alarm rate and minimum detectable hazard.

Concerns for defining this minimum detectable hazard for the airborne radar should include the temporal building of the hazard. To warn the first plane flying into a region just reaching a qualified hazard criteria is the objective. To wit, having a sensor which can detect/verify the presence of a mature microburst on-board a commercial airliner may be of less interest to the customer.

In our view, the NASA instrument radar will be capable of detecting and analysing existing microbursts opportunistically encountered or scouted. If NASA flight tests are able to encounter microbursts, the data collected will serve to verify/refine their/our understanding of the meteorological mechanisms which drive the microburst. This gives confidence in predicting the observables for radar (or other sensors) at the point in time of concern for a significant range of microbursts, significant enough to be considered an important increment to safety.

The other aspect of the sensor design, suppression of false alarms, begins with a characterization of the radar clutter environment for those many times when a microburst is not present.

Westinghouse
Technical Direction

1. Furnish a superior radar sensor to detect evolving microburst windshear along the approach glideslope

2. "Superior" means:
   - Low false alarm rate and a "clean scope" hazard display
   - Confident detection of minimal significant hazards, i.e.,
     - Minimal windblown rain RCS
     - Minimal Doppler speed

Westinghouse had some reservations on the feasibility and/or low cost realizability of a lookdown coherent radar mode for detecting slow and small RCS returns in the presence of dense urban clutter and ground moving vehicular traffic. These reservations could be evaluated by a flight test under realistic conditions.

Westinghouse is a world leader in the research and development of airborne radar and maintains a fleet of aircraft equipped with radars for those purposes.

Sabreliner Flight Test
for
Low Level Windshear
Hazard Detection Mode

Object:

1. To assess the impact of vertically extensive urban discretes on the operation of a microburst windshear mode

2. To observe the qualitative presence and extent of ground moving traffic in the airport approach environment

The Sabreliner is equipped for developing and improving airborne radar in a dynamic flight test environment. There is a capacity to arbitrarily configure the radar and program its processing. There is an ability to capture radar data at many different stages of the receive process, including A/D and FFT, complete with INS data on the aircraft position, movement, and orientation in navigation coordinates.

Sabreliner
AN / APG-68 Radar

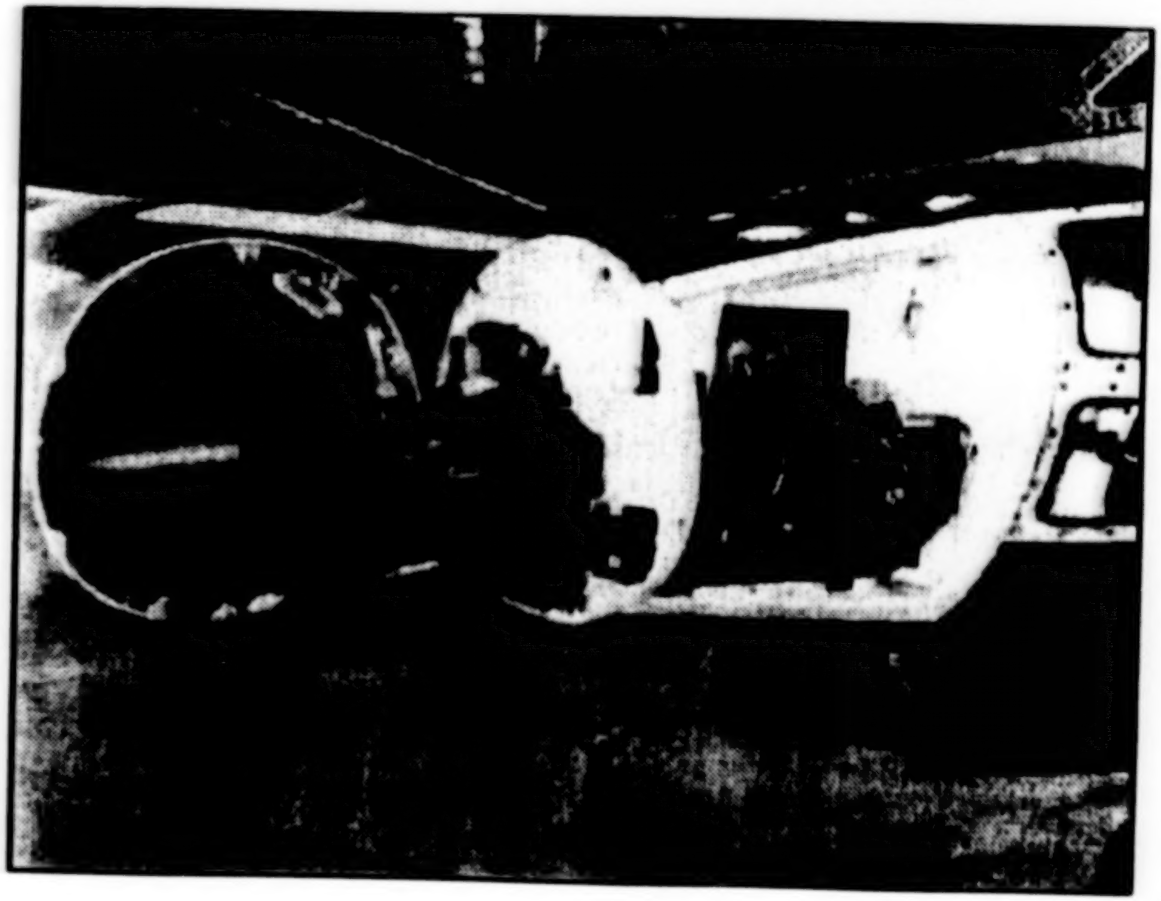

G903355.04 BD826

ORIGINAL PAGE IS
OF POOR QUALITY

Sabreliner Radar Furnishes Instrumentation and Capability Exceeding the Experiment

1. Programmable waveform and scan generation as desired. Choose from NASA range of PRFs.

2 . "Instrumentation" capacity:

- ERP exceeds anticipated / current weather radar products
- Spurious free dynamic range provides sensitivity exceeding product baseline
- Digital processing can mimic anticipated product waveform initial processing (programable pulsewidth and FFT)
- Data recording for range gated FFT is good match for expected product scope of interest
- Scan patterns and rates are programmable

Flight test data furnishes a foundation
for algorithm designs with empirically known clutter margins

Radar processing makes assumptions about targets. In the case of target location and velocity, the radar assumes the target return is from the direction that the mainbeam is pointing and that the Doppler velocity is relative to the ground clutter patch, also in that direction (clutter positioning). Large stationary urban discretes (e.g. hangers, gantries, skyscapers, etc.) pose a problem when

a) their returns lie above the noise level and
b) their direction is different from the direction of the mainbeam.

(when their direction is different from the direction of the mainbeam, the Doppler frequency of their return is different, i.e.

$$f_{Doppler} = 2[v/\lambda] \cos(\theta)$$

where

v = the speed of the aircraft
λ = the wavelength of the carrier, c/f_o
c = speed of light
θ = the angle between the line of sight to the object producing the return and the aircraft velocity vector.
f_o= rf carrier frequency)

Electronically positioning the return from mainbeam clutter to lie in the Doppler filterbank at zero velocity means that large returns from stationary objects could be interpretted at different velocities. For example, if the mainbeam is pointed along the velocity vector, a Dopper frequency

$$f_1 = 2\ v/\lambda$$

is interpretted as non-moving. A return from a building abeam of the aircraft returns at a Doppler frequency

$$f_2 = 0$$

If large enough in amplitude to be perceived through the sidelobes of the antenna, it would be interpretted to be at a Doppler velocity $-v$. Scatterers stationary on the ground returning from angles closer to the nose would be interpretted as slower opening targets and those farther off the nose would be interpretted as faster opening targets.

For the microburst windshear application, urban discretes perceived through the sidelobes can potentially "compete" at the ranges and Doppler speeds of tailwind outflows.

An objective of the Sabreliner flight test is to assess this problem by putting an instrumented radar of excessive measurement capability in an urban discrete stressing environment and observe the level of returns in the Doppler filterbank.

Urban Areas May Appear as Spatially Extensive Features at Doppler Frequencies Competing With Tailwind Outflows

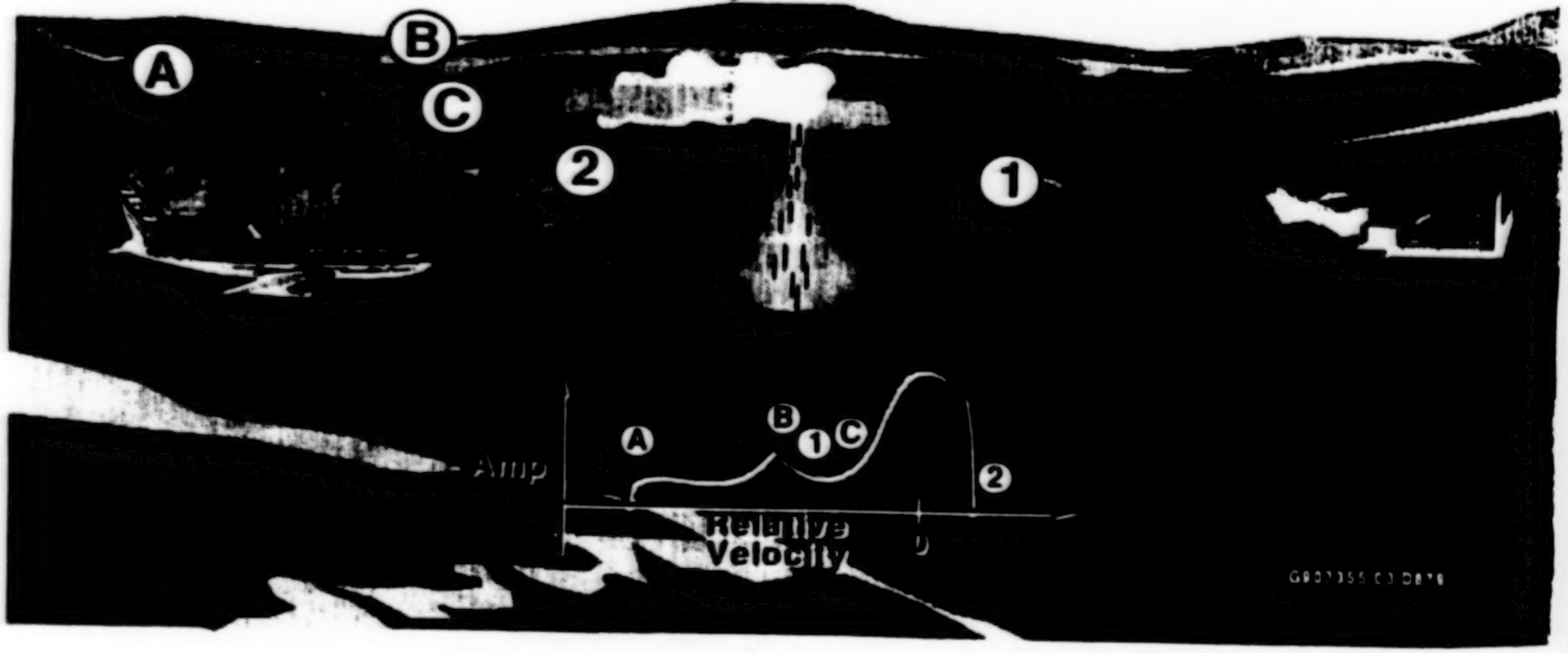
A
B
C
2
1
Amp
A
B
1
C
2
Relative Velocity
0

ORIGINAL PAGE IS
OF POOR QUALITY

Some airports in dense urban environments may have approach airspaces which do not conform to standards. High rise buildings, stacks, and towers in the proximity of the approach pose potential projecting sources of urban discretes at close ranges which may compete with tailwind outflows in the filterbank.

Urban Clutter May Project Vertically

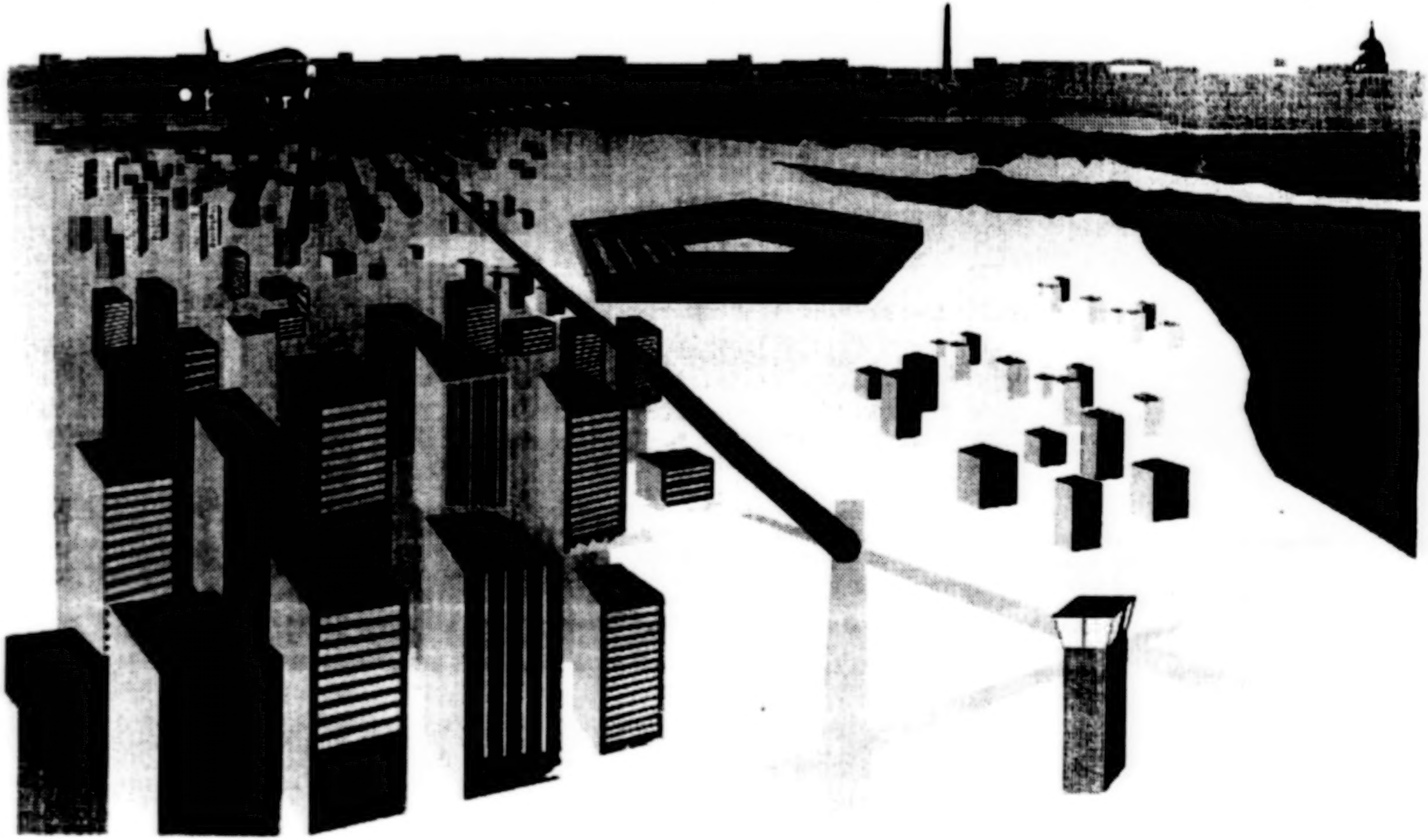

ORIGINAL PAGE IS
OF POOR QUALITY

Most airports are serviced by a network of roads which include high speed interstates. It is not uncommon for the glideslope to parallel and/or overfly such highways. Ground moving targets perceived by the radar through the sidelobes of the antenna may appear as small RCS targets distributed in range, Doppler, and space not unlike microburst windshear. An objective of the flight test was to assess qualitatively the perception of ground moving targets at the very close ranges in the sidelobes along the glideslope. This information will determine the complexity (i.e. there are additional/alternate means of rejecting returns not from the mainbeam direction) of the radar design for rejecting sidelobe and undesired movers.

Ground Movers May Be Extensive and Competing

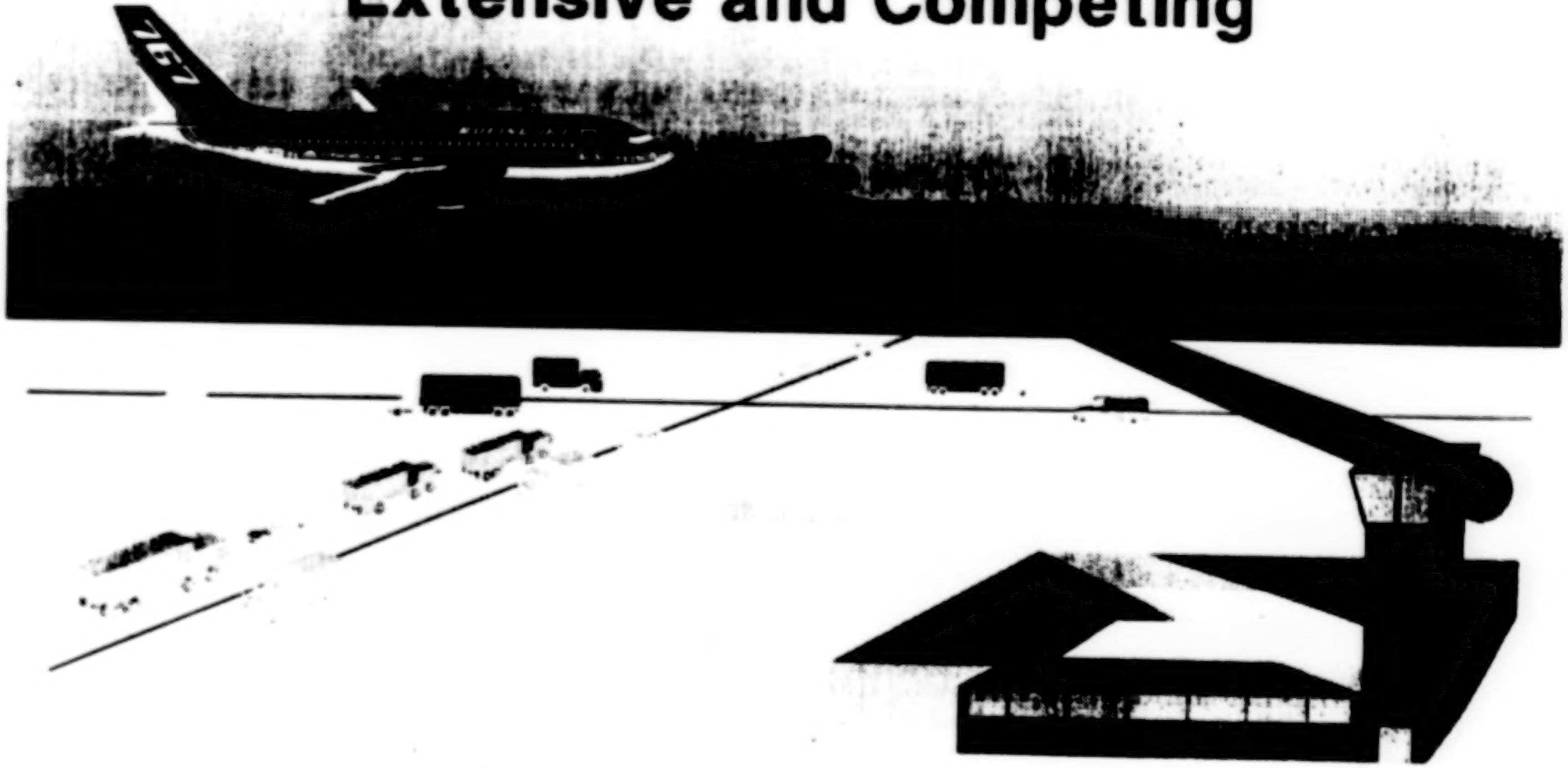

ORIGINAL PAGE IS
OF POOR QUALITY

A simple model for vehicular traffic can suggest the RCS of a number of vehicles in a range cell moving at high speeds. The model considers the individual vehicles to combine in a Rayleigh fashion. Presumably, at higher speeds, there will be some increased spacing between following vehicles.

A Model for RCS of Cells Containing Many Vehicles

(In a Range-Gated Doppler Cell)

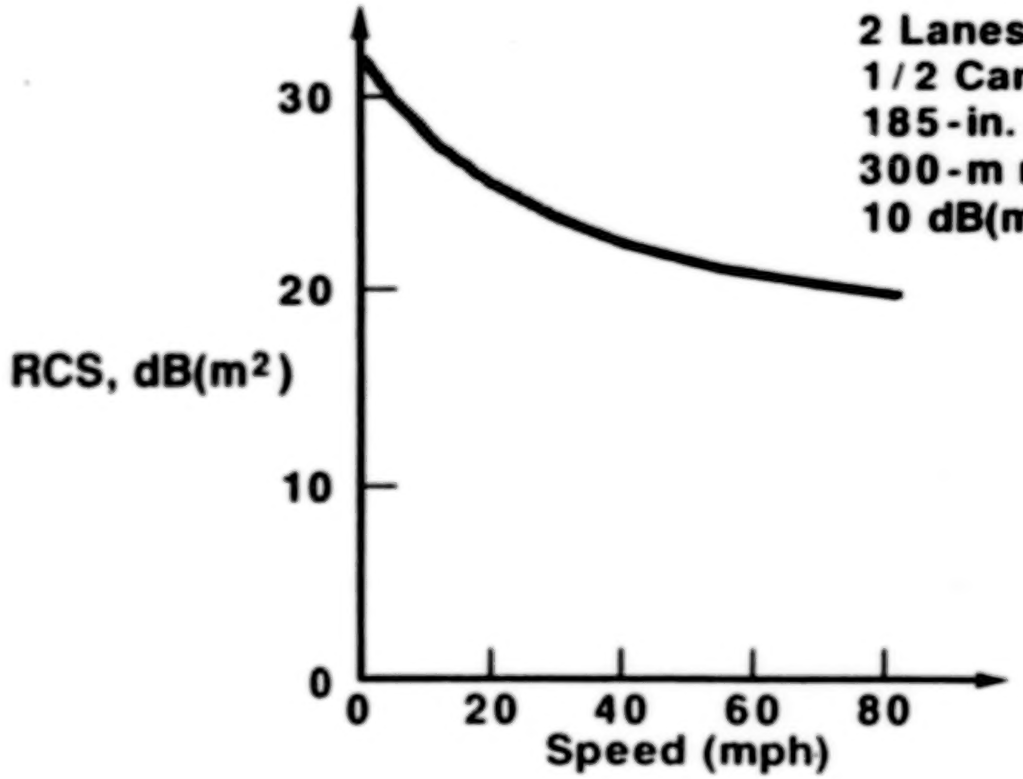

2 Lanes
1 / 2 Car Length / 10 mph
185-in. Car Length
300-m range gate
10 dB(m^2) Vehicle RCS, avg

The flight test must be designed to collect data which can be interpretted and addresses the issues raised. The PRF of the waveform was selected at 4KHz. to resolve vehicle traffic with ± 70 mph relative speeds. A 2 microsecond pulse allowed 16 range gates to be implemented, covering out in range 5.1 km. in unambiguous range. The second time around echo (STAE) range swath extends from 37.5 km. to 42.6 km. To determine whether, say, a moving target indication is from the sidelobes at unambiguous range or from the mainbeam at STAE ranges will require study of the elevation scan history (i.e. the change in illumination intensity at STAE ranges over the elevation contour is modest, but any peak sidelobes or mainbeam skirt effects will produce marked variation.)

The Results Must Be Comprehensible

(Use NASA Baseline Set of Parameters)*

1. **Doppler Ambiguity (±70 mph)**
   PRF $\geq 2(2\, v_{max}/\lambda)$
2. **Range Ambiguity**
3. **Angle Dependencies (Scan History)**

---

* Bracalante, et.al., "Airborne Doppler Detection of Low Altitude Windshear", AIAA/NASA/AFWAL Sensors and Measurement Technologies Conf., paper AIAA-88-4657, Sept 1988, Atlanta, Ga

Data was recorded for the approaches to three accessable airports.

Approaches to Georgetown, Delaware could easily be arranged with flight controllers. It posed a case benign in terms of second time around range ground moving target activity, urban clutter, and vehicular traffic around the airport. Instances or observations in the data should be easily interpretted from the features available from topographic maps.

The approaches to BWI in Linthicum, Maryland are relatively well know to Westinghouse personel. Although complex residential and road patterns abound, there is a general lack of pervasive complexity. The STAE ranges should include portions of azimuth scan including urban areas and high speed interstates. The final, low level approach to touchdown will over-fly representative worst case vehicular traffic in relative separable conditions.

The river approach to Washington National airport includes all the visions of hell to the imagination of an airborne radar engineer. There is a network of roads and freeways paralleling and underlying the approach with a deviance of high rise buildings, including the Washington Monument (height= 555 ft.). The STAE environment is generally rural and suburban but somewhat uncertain given the lag of updating maps to correspond to the development explosion.

Selected Airport Approaches for Data Collection

1. Benign
    - Georgetown, Delaware
        - Absence of urban clutter areas at unambiguous of STAE ranges minimal, isolatable ground moving traffic

2. Average
    - Baltimore Washington International Airport (BWI)
        - Approach includes a mix of resolvable clutter complexity; som vertically extensive clutter (Glen Burnie, radio towers, stacks ...; significant, radially lying interstates known for their speed

3. Worst Imaginable Case
    - Washington National Airport, D.C.
        - Approach glideslope overflys freeways and congested highways; Washington Monument, Crystal City and Pentagon; STAE is relatively benign (resolvable)

The data was collected in piggyback priority with other tests on the same flight. The first approach was at Washington National. The approach was from the north on a typical summer weekday early afternoon. Permission did not include landing or touch and go, so the route deviated to follow the Potomac river and included a nearly direct line on the Washington Monument within instrumented ranges at about 2000 ft. altitude.

The map scale has been chosen to emphasize the features of the map at the second time around echo (STAE) ranges. In general, the ±20° scan in azimuth about the aircraft nose illuminated a swath about the Patuxent River in Prince Georges County and Anne Aurundel County with little indicated highway or suburban complexity. As the approach turned directly south, the STAE swath extended beyond Prince Georges County into Charles County, the Potomac River, Virginia, and the Chesapeake Bay.

Approach to National Airport

STAE Scale

CHESAPEAKE

ORIGINAL PAGE IS
OF POOR QUALITY

The approach to Washington National overflies a dense highway network of perplexing design. The sidelobes of the antenna almost always will illuminate the George Washington Parkway at ranges of data collection.

The scan pattern for the mainbeam is a four elevation bar scan near the glideslope. Each bar is successively lower and covers ±20° in asimuth in about 1 second. The whole 4 bar sequence takes a little over 4 seconds.

The lowest bar of the scan pattern begins placing the mainbeam at or near the unambiguous ranges of level ground just about the time (i.e. altitude) of the approach toward the Washington Monument. The mainbeam skirt illuminates I-95 and describes a progressive increase in ground moving target amplitude data as each bar is scanned.

The turn to the south over the Jefferson Memorial illuminates within unambiguous ranges Anacostia and its usually relatively uncongested freeways southwest of the Suitland Parkway interchange and bridges.

The flight route closely followed a 3° glideslope until just opposite the Pentagon, over the river at about 600 ft. The flight down the river includes mainbeam illumination of both the Anacostia freeway and Crystal City.

Approach to Washington National Airport

(Unambiguous Range Scales and Detailed Features)

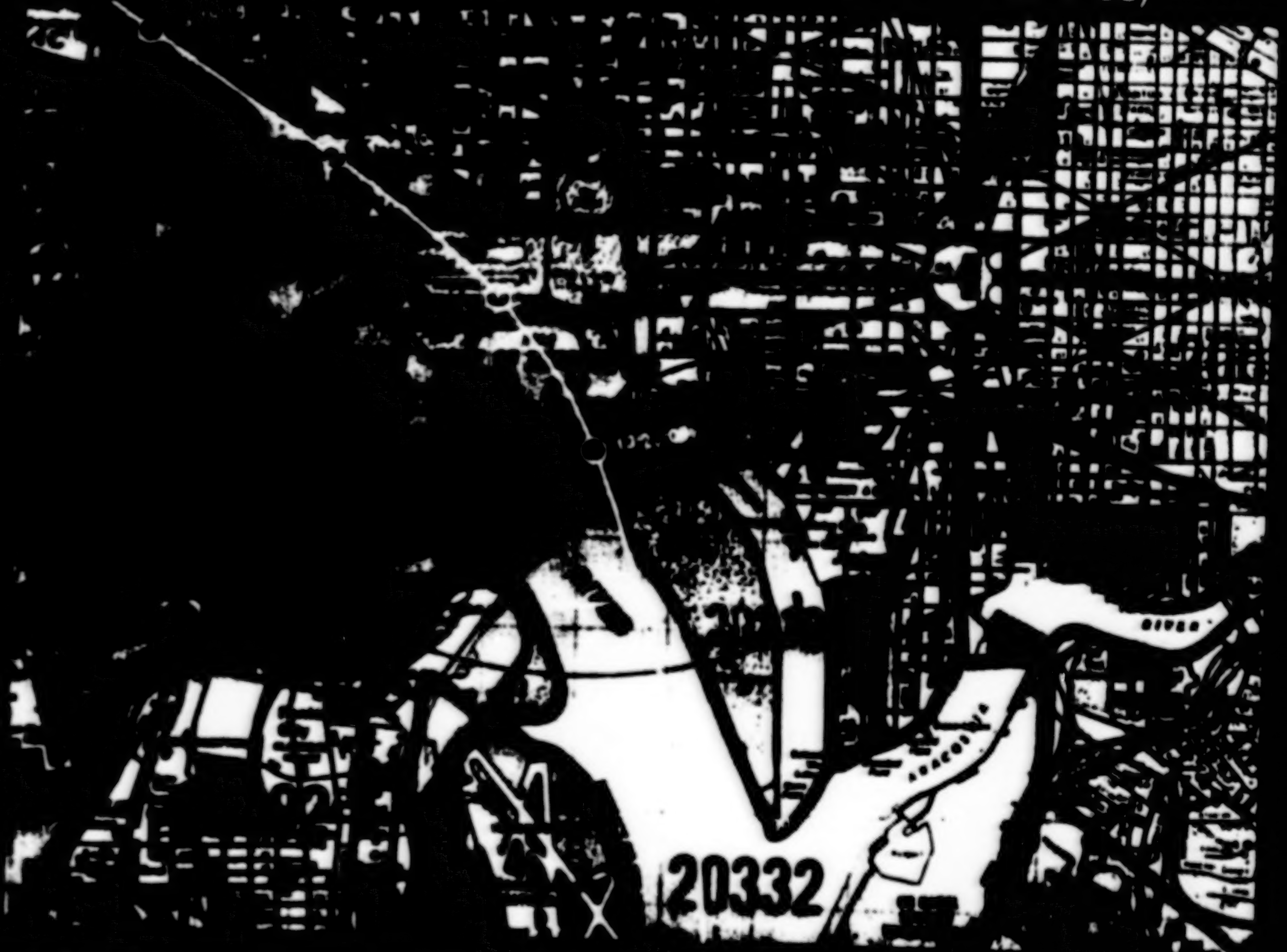

ORIGINAL PAGE IS
OF POOR QUALITY

The approach to Washington National initially followed a 3° glidslope. The approach followed the Potomac and deviated slightly, reaching about 600 feet over the river next to the runway.

Altitude Profile During Approach

(Washington National Airport)

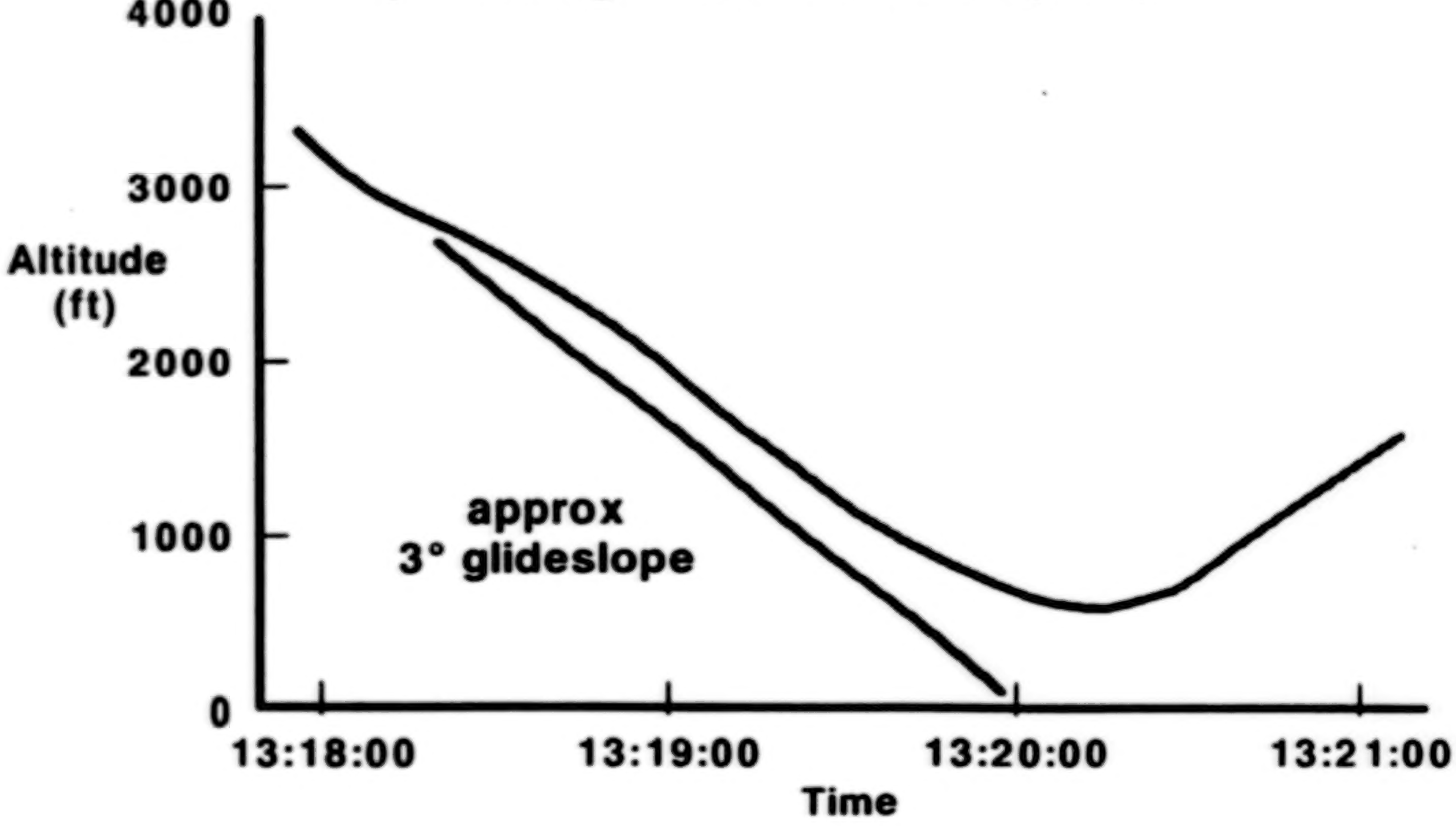

Elevation Bar Scans of Successively Steeper Depression Investigated Impact of Vertically Extensive Urban Clutter

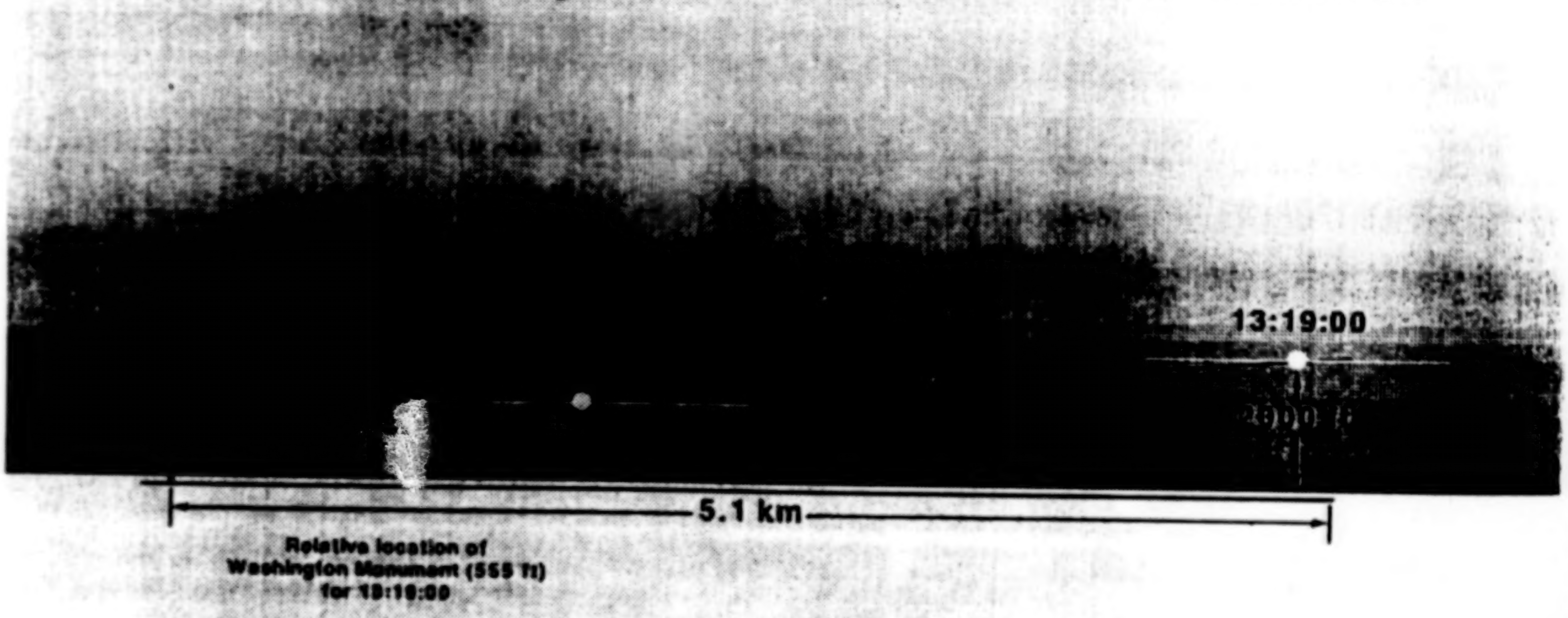
13:19:00
5.1 km
Relative location of
Washington Monument (555 ft)
for 13:19:00

ORIGINAL PAGE IS
OF POOR QUALITY

PRECEDING PAGE BLANK NOT FILMED

Due to an equipment overheating problem, two approaches were conducted on BWI.

The first approach came up the bay and turned west, crossing the Curtis Bay and Marley Creek regions. The data shut-off occurred just short of Glen Burnie and the radio station towers.

The locations and aircraft orientation over the bay provide an excellent opportunity to confidently assess the STAR contributions of ground moving targets or STAR urban discretes. As the Sabreliner turns to the west, the scan illuminates various portions of the Baltimore beltway, I-83 to the north, and portions of Columbia and Northwestern Howard County along I-70.

The second approach was from along the Severn River looking diagonally across northwest Baltimore. Portions of the Baltimore beltway present near radial ground moving traffic perception at times just prior to rush hour.

Approach to BWI

STAE Features

ORIGINAL PAGE IS
OF POOR QUALITY

The first approach to BWI overflew the Cheasepeake Bay and approached from due east. Points of specific interest over land where the approach near the Solley Road power plant and stack and the Glen Burnie downtown area. The sidelobes contain residential traffic in radial geometries.

The second approach to BWI began gathering data about 2 n.miles out over Rt.3, which is a limited access divided highway. Data was collected nearly to touchdown. Interstate traffic was overflown initially. The final stages passed over light commercial business areas and tangential traffic patterns. The instrumented range included the limited access highway on the other side of the airport and the Westinghouse site.

BWI Approach

Detailed Map Features at Unambiguous Range

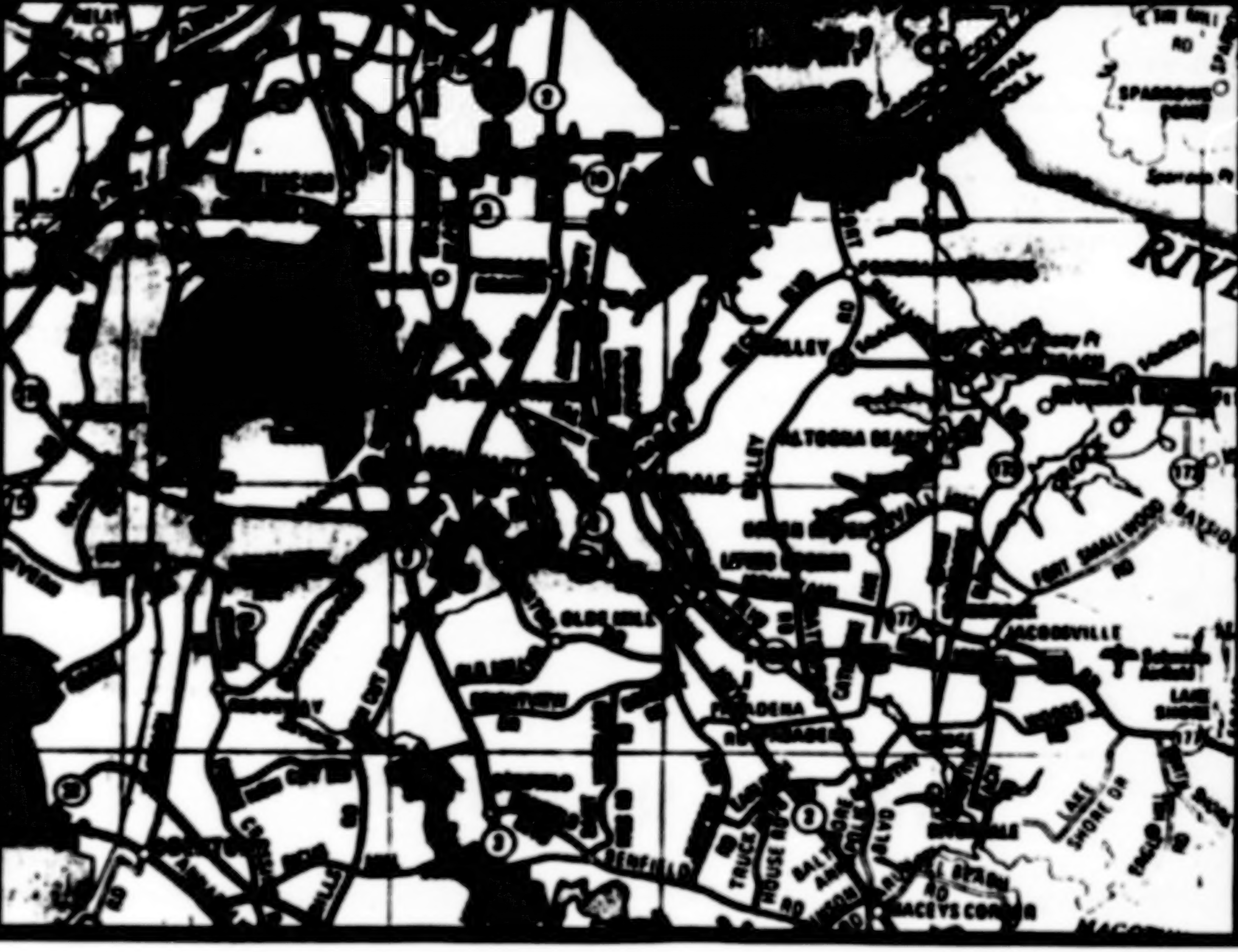
SPARROWS POINT
RIVER
ALTOONA BEACH
FORT SMALLWOOD RD
JACOBSVILLE
PASADENA
LAKE SHORE DR
TRUCK HOUSE RD
BENFIELD
MACEYS CORNER

ORIGINAL PAGE IS
OF POOR QUALITY

Approach to BWI

(Altitude Profiles)

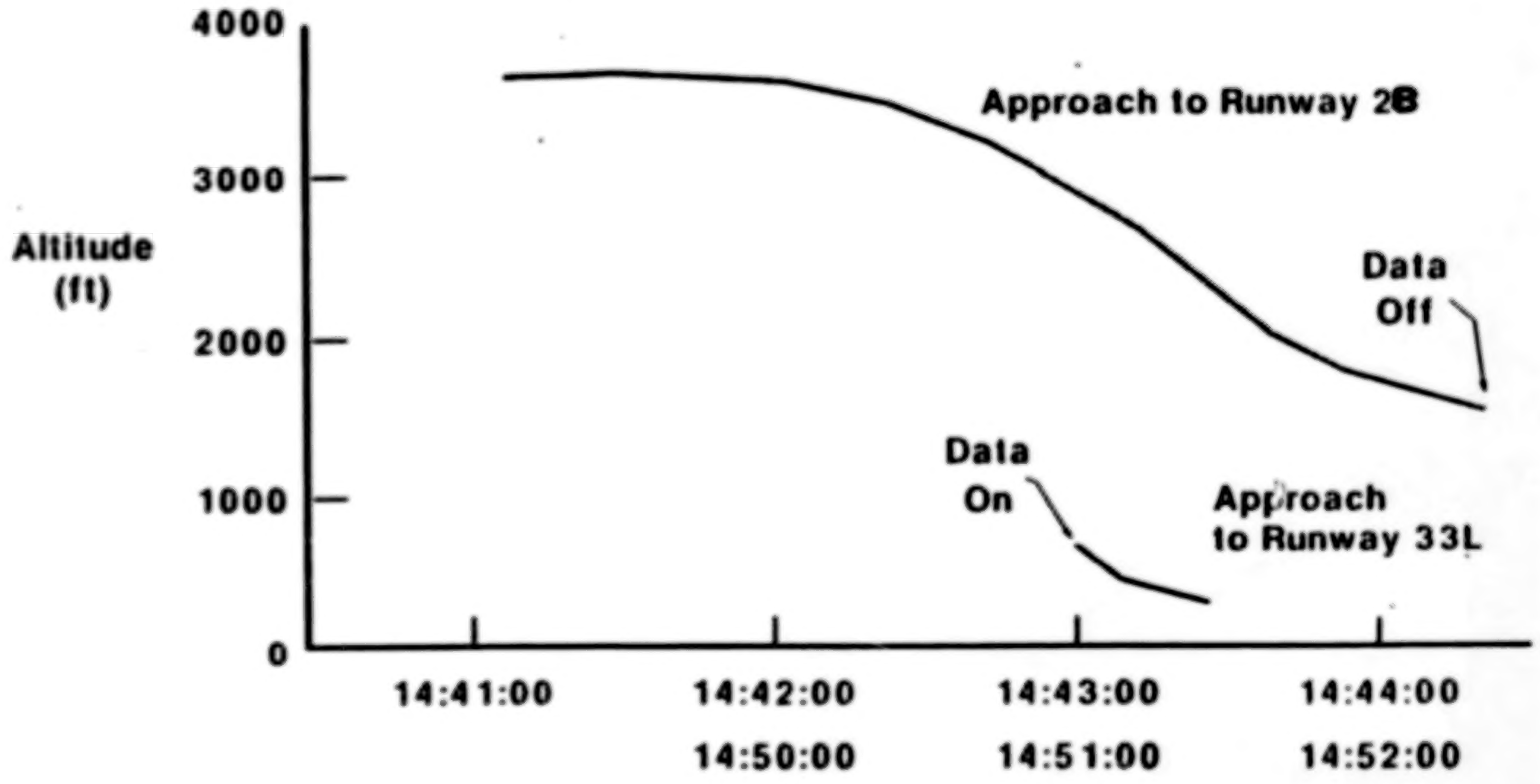

The altitude profiles for the appoaches to BWI contained no significant vertically extending discretes.

- **Westinghouse knows the importance of clutter in radar design**
- **Westinghouse has gathered realistic clutter data**
- **Westinghouse will design for sensitive detection and robust clutter rejection**

1. Westinghouse has conducted a flight test with equipment superior to the experiment to gather data and assess the problems of clutter and ground moving traffic in and around airports.
2. This data furnishes instances of stressing clutter environments in which an airborne radar for the detection of microburst windshear hazards must work in a low false alarm manner.
3. Westinghouse intends to design and produce a superior, cost effective sensor for the detection of low level microburst windshear hazards with sufficient warning time to the pilot for avoidance. Our design will be based for detection of microburst observables according to the NASA-Langley models of "wet" and "dry" microburst at different, key stages of their lifecycles.

Saberliner Flight Test - Questions and Answers

Q: ERNEST BAXA (Clemson University) - Can you comment on clutter spectral characteristics of the Washington, DC overflights? Do you feel that urban clutter will be distinctly differed from non-urban?

A: BRUCE MATHEWS (Westinghouse) - The term "clutter spectral characteristics" to me or to Westinghouse Airborne Radar people means strictly a geometric Doppler sense. So it is really the amplitude distribution of Rayleigh scatterers geometrically in a range gate that sets up the Doppler spectrum for them. What did I expect the amplitude distribution of urban clutter to look like? It was pretty much what we expected I guess. It's the discrete distribution of urban clutter that makes it confounding and that's the difference with non-urban clutter.

Q: WAYNE SAND (NCAR) - What did you learn from these flight tests? Can you maintain a clear screen in these environments?

A: BRUCE MATHEWS (Westinghouse) - We are still looking at that data so I can't really comment very much further on that.

Session X. Airborne Doppler Radar / Industry

N91-24150

Status of Bendix Research
Daryal Kuntman, Bendix

DOPPLER WEATHER RADAR
WITH
PREDICTIVE WINDSHEAR DETECTION CAPABILITY

DARYAL KUNTMAN
BENDIX/KING AIR TRANSPORT AVIONICS DIVISION

OCTOBER 18, 1990

WE ARE...

A DIVISION OF ALLIED-SIGNAL AEROSPACE COMPANY WHICH IS A PART OF ALLIED-SIGNAL CORPORATION.

HAVE BEEN MANUFACTURING AIRBORNE WEATHER RADARS SINCE 1954.

HAVE THE MOST RADARS (OVER 35,000 DELIVERED) ON AIR TRANSPORT TYPE AIRCRAFT FLYING WORLDWIDE.

COMMITTED TO THE DEVELOPMENT OF AIRBORNE WEATHER RADAR WITH FORWARD LOOKING PREDICTIVE WINDSHEAR DETECTION CAPABILITY.

BENDIX/KING ATAD RADARS
IN CURRENT AIRLINE FLEETS

- RDR-1E: MAGNETRON TRANSMITTER NOT SUITABLE FOR WINDSHEAR DETECTION.
- RDR-1F: MAGNETRON TRANSMITTER NOT SUITABLE FOR WINDSHEAR DETECTION.
- RDR-4A: LATEST GENERATION
  SOLID-STATE TRANSMITTER
  FULLY COHERENT
  DOPPLER TURBULENCE DETECTION CAPABILITY

RDR-4A FREQUENCY GENERATION

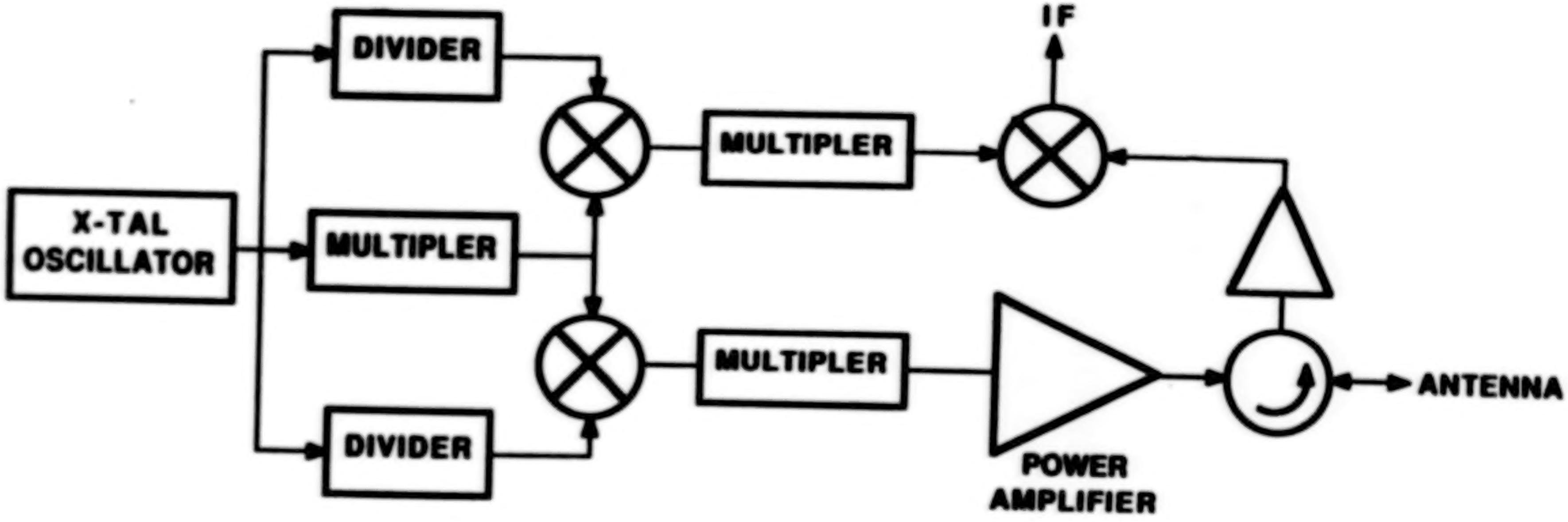
X-TAL OSCILLATOR
DIVIDER
MULTIPLER
DIVIDER
MULTIPLER
MULTIPLER
IF
POWER AMPLIFIER
ANTENNA

PLAN

- TO ADD WINDSHEAR DETECTION CAPABILITY TO THE RDR-4A SYSTEM AS A MODIFICATION.

- CONDUCT FLIGHT TESTS WITH AIRLINES DURING 1991.

MODIFICATIONS

RECEIVER/TRANSMITTER:
- ADD WINDSHEAR DETECTION HARDWARE AND SOFTWARE
- ADD WINDSHEAR MODE CONTROL SOFTWARE
- ADD WINDSHEAR DATA TO THE OUTPUT BUSES

CONTROL PANEL: ADD WINDSHEAR MODE SELECTION CAPABILITY

INDICATOR: ADD WINDSHEAR DATA DISPLAY CAPABILITY

ANTENNA: NO MODIFICATIONS REQUIRED

RDR-4A FUNCTIONAL BLOCK DIAGRAM

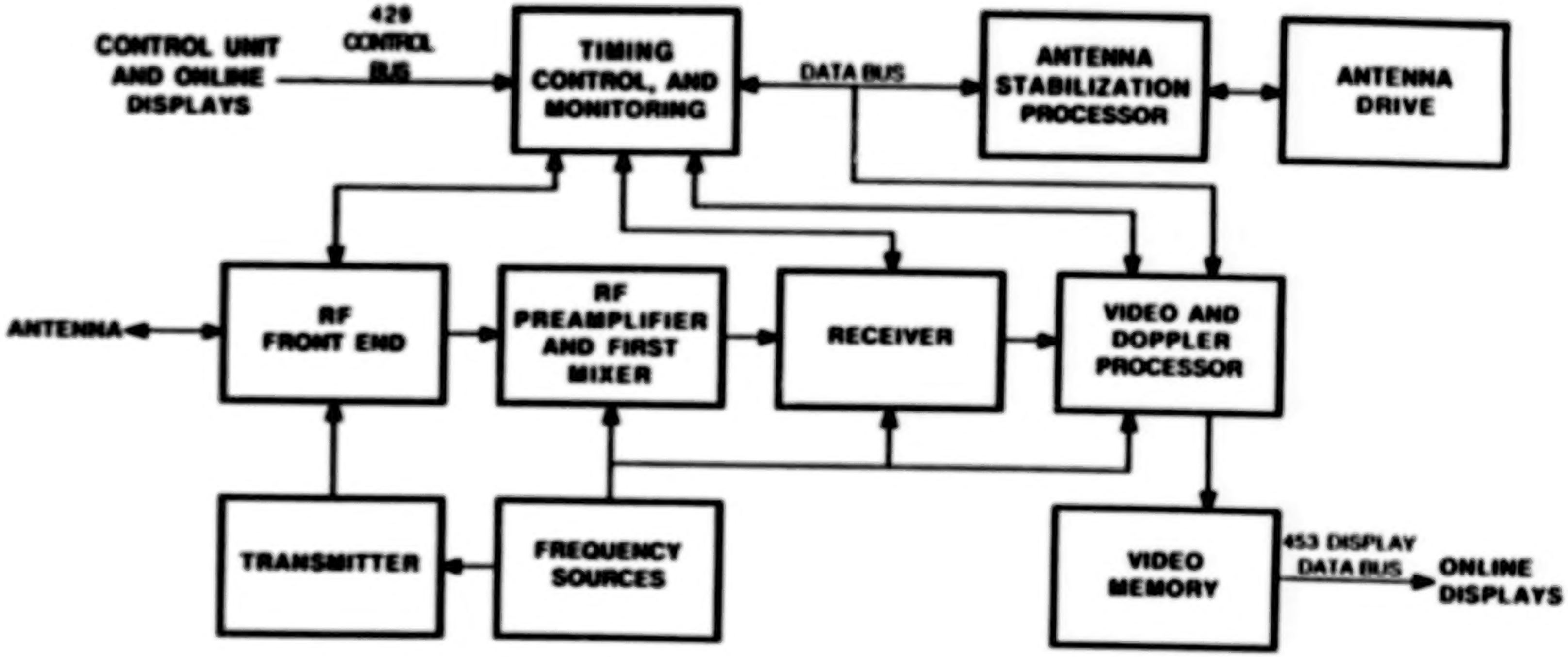
CONTROL UNIT AND ONLINE DISPLAYS
429 CONTROL BUS
TIMING CONTROL, AND MONITORING
DATA BUS
ANTENNA STABILIZATION PROCESSOR
ANTENNA DRIVE
ANTENNA
RF FRONT END
RF PREAMPLIFIER AND FIRST MIXER
RECEIVER
VIDEO AND DOPPLER PROCESSOR
TRANSMITTER
FREQUENCY SOURCES
VIDEO MEMORY
453 DISPLAY DATA BUS
ONLINE DISPLAYS

RDR-4A WITH WINDSHEAR DETECTION

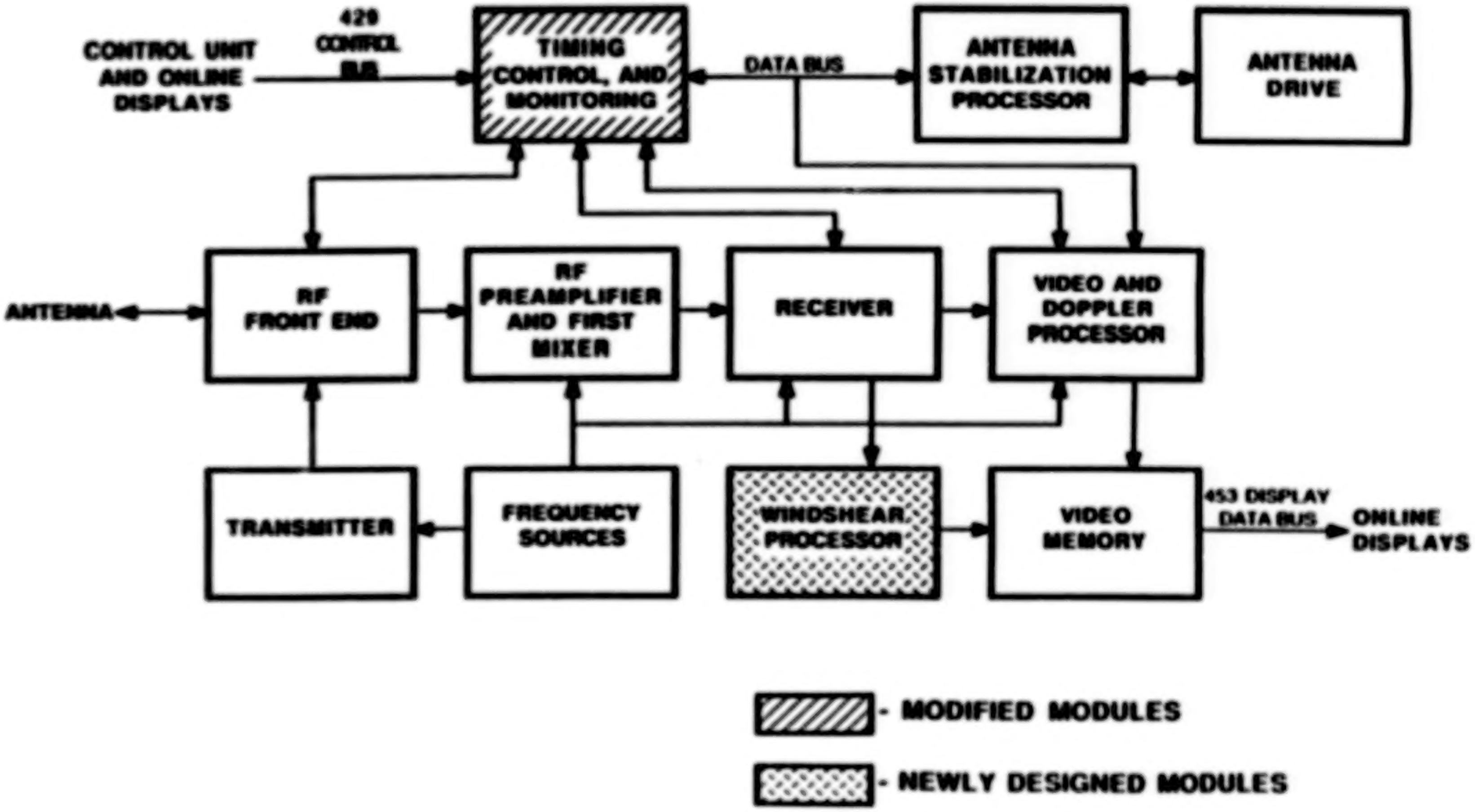
CONTROL UNIT AND ONLINE DISPLAYS
429 CONTROL BUS
TIMING CONTROL, AND MONITORING
DATA BUS
ANTENNA STABILIZATION PROCESSOR
ANTENNA DRIVE
ANTENNA
RF FRONT END
RF PREAMPLIFIER AND FIRST MIXER
RECEIVER
VIDEO AND DOPPLER PROCESSOR
TRANSMITTER
FREQUENCY SOURCES
WINDSHEAR PROCESSOR
VIDEO MEMORY
453 DISPLAY DATA BUS
ONLINE DISPLAYS
▨ - MODIFIED MODULES
░ - NEWLY DESIGNED MODULES

RDR-4A CHARACTERISTICS

	WEATHER AND MAP MODE	TURBULENCE DETECTION	WINDSHEAR DETECTION
TRANSMITTER PEAK POWER	125 W (NOMINAL)		
PULSE WIDTH	6 AND 18μSEC ALTERNATING	6μSEC	2μSEC
PRF	380 Hz	1600 Hz	6000 Hz
MAXIMUM RANGE	320 NMILES	40 NMILES	10 NMILES
OPERATING MODE	PULSED COHERENT		
FREQUENCY	9345 ± 2 MHz		
SYSTEM NOISE FIGURE	5 DB		
ANTENNA SCAN	180°		40°
ANTENNA GAIN	35 DB		
ANTENNA BEAMWIDTH	3.3° ELEVATION 3.4° AZIMUTH		
TILT CONTROL	± 15° MANUAL		AUTOMATIC

ISSUES

TECHNICAL:

- GROUND CLUTTER ELIMINATION
- ESTABLISHMENT OF HAZARD THRESHOLDS
- DEFINITION OF DISPLAY DATA BUS CHARACTERISTICS
- SPECIFYING DATA INPUT REQUIREMENTS
- DEFINITION OF FORM/FIT/FUNCTIONAL REQUIREMENTS (ARINC)

OPERATIONAL:

- MEANS OF SELECTING WINDSHEAR MODE
- DISPLAY MEANS
- AURAL ALERTS
- INTERACTION WITH REACTIVE WINDSHEAR DETECTION SYSTEM

CERTIFICATION:

- ESTABLISHMENT OF A CERTIFICATION CRITERIA SIMILAR TO THE REACTIVE WINDSHEAR DETECTION SYSTEM

ESSENTIAL REQUIREMENTS FOR CERTIFICATION WITHOUT EXTENSIVE FLIGHT TESTS

- ESTABLISHMENT OF PERFORMANCE CRITERIA USING SIMULATED DATA (NASA)
- DEFINITION OF TEST MEANS USING SIMULATED SIGNAL INPUTS (NASA)
- MINIMUM OPERATIONAL REQUIREMENTS (RTCA)
- TSO (FAA)
- ADVISORY CIRCULAR FOR AIRWORTHINESS AND OPERATIONAL APPROVAL (FAA)

Session X. Airborne Doppler Radar / Industry

N91-24151

Status of Collins Research
Roy Robertson, Collins

NASA / FAA

THIRD COMBINED AIRBORNE WINDSHEAR

REVIEW MEETING

OCTOBER 16 - 18, 1990

ROCKWELL INTERNATIONAL

COLLINS AIR TRANSPORT DIVISION

R. E. ROBERTSON

Rockwell International
Collins Air Transport Division

RER 10/16/90

TOPICS

WINDSHEAR RADAR PROGRAM

FUTURE PLANS

WINDSHEAR RADAR PROGRAM

GOALS

- WEATHER RADAR WINDSHEAR DETECTION
    - -- LARGE INSTALLED BASE
    - -- MINIMAL CHANGES TO AIRCRAFT
- USEFUL DETECTION CHARACTERISTICS
    - -- HIGH POD, LOW FAR
    - -- WET AND DRY MICROBURSTS
    - -- ACCEPTABLE CONSISTENT WARN TIMES
- EFFECTIVE FOR TAKEOFF & LANDING
- STAND ALONE OR COMBINED WITH OTHER SYSTEMS

Rockwell International
Collins Air Transport Division

WINDSHEAR RADAR PROGRAM

OVERVIEW

- MODIFICATION TO WXR-700
  - -- FULLY-COHERENT ARCHITECTURE
  - -- UPGRADE SIGNAL PROCESSING
  - -- IMPROVE RF STABILITY
- FLIGHT TEST PLAN
  - -- COMPANY SABRELINER BEGINNING NOV '90
  - -- CONTINENTAL 737 -- APRIL '91 THRU SEPT '91

Rockwell International
Collins Air Transport Division

WINDSHEAR RADAR PROGRAM

TECHNICAL APPROACH

- TIME SHARE WEATHER AND WINDSHEAR DETECTION
  - MAINTAIN WEATHER AVOIDANCE DISPLAY
  - AUTOMATIC ANTENNA POSITIONING FOR W/S SWEEP
  - PROTECTION OVER 30° SECTOR

- EXTRACT VELOCITY PROFILE ALONG FLIGHT PATH
  - DIRECT MEASURE OF HORIZONTAL COMPONENT
  - VERTICAL COMPONENT INFERRED

- HAZARD DETERMINATION
  - SIGNAL DECONTAMINATION / FILTERING
  - HAZARD CALCULATION / THRESHOLDING
  - OUTPUTS AVAILABLE
    - WINDSHEAR ALERT
    - VELOCITY PROFILE VS RANGE
    - HAZARD PROFILE VS RANGE

Rockwell International
Collins Air Transport Division

RER 10/16/90

WINDSHEAR RADAR PROGRAM

DESIGN CONSIDERATIONS

- HAZARD FACTOR ESTIMATION
  - HORIZONTAL VELOCITY COMPONENT
  - ASYMMETRIC EVENTS, MICROBURST LINES
  - DESCENDING MICROBURSTS
- "WORST CASE" EVENTS DRIVE SYSTEM DESIGN
  - VERY DRY, SMALL MICROBURSTS
- PERFORMANCE TRADE-OFFS
  - DETECTION RANGE
  - PROBABILITY OF DETECTION
  - FALSE ALARM RATES

Rockwell International
Collins Air Transport Division

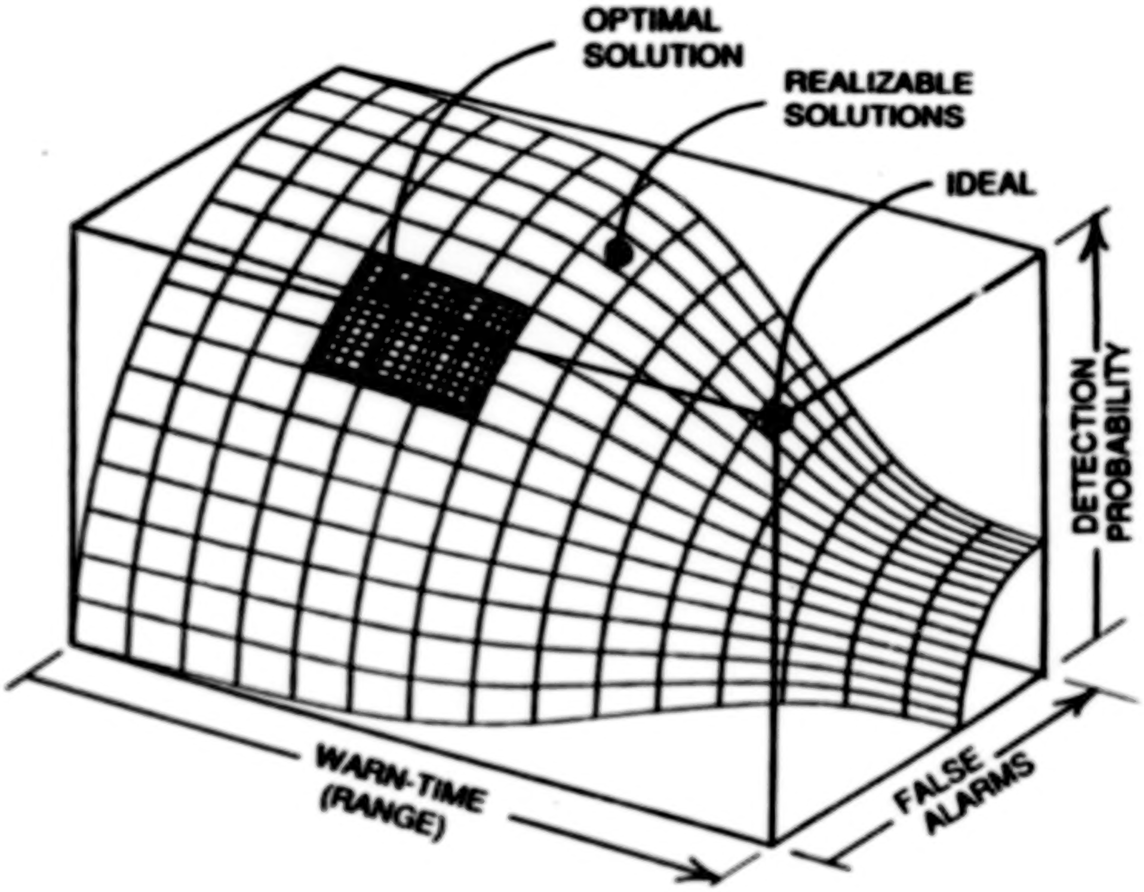
OPTIMAL SOLUTION
REALIZABLE SOLUTIONS
IDEAL
DETECTION PROBABILITY
WARN-TIME (RANGE)
FALSE ALARMS

WINDSHEAR PERFORMANCE TRADEOFFS

RER 10/16/90

Rockwell International
Collins Air Transport Division

WINDSHEAR RADAR PROGRAM

SYSTEM CONSIDERATIONS

- EXECUTIVE ALERT
  - -- AURAL, VISUAL WARNING
  - -- DISCRIMINATE BETWEEN PREDICTIVE/REACTIVE WARNINGS
- GRAPHIC DISPLAY
  - -- INTERPRETIVE DATA
  - -- SITUATION AWARENESS
  - -- AVOIDANCE INFORMATION
- LIMITED INPUT PATH TO PILOT
  - -- HIGH WORKLOAD -- STRESS
  - -- RESTRICTED VISUAL SCAN

Rockwell International
Collins Air Transport Division

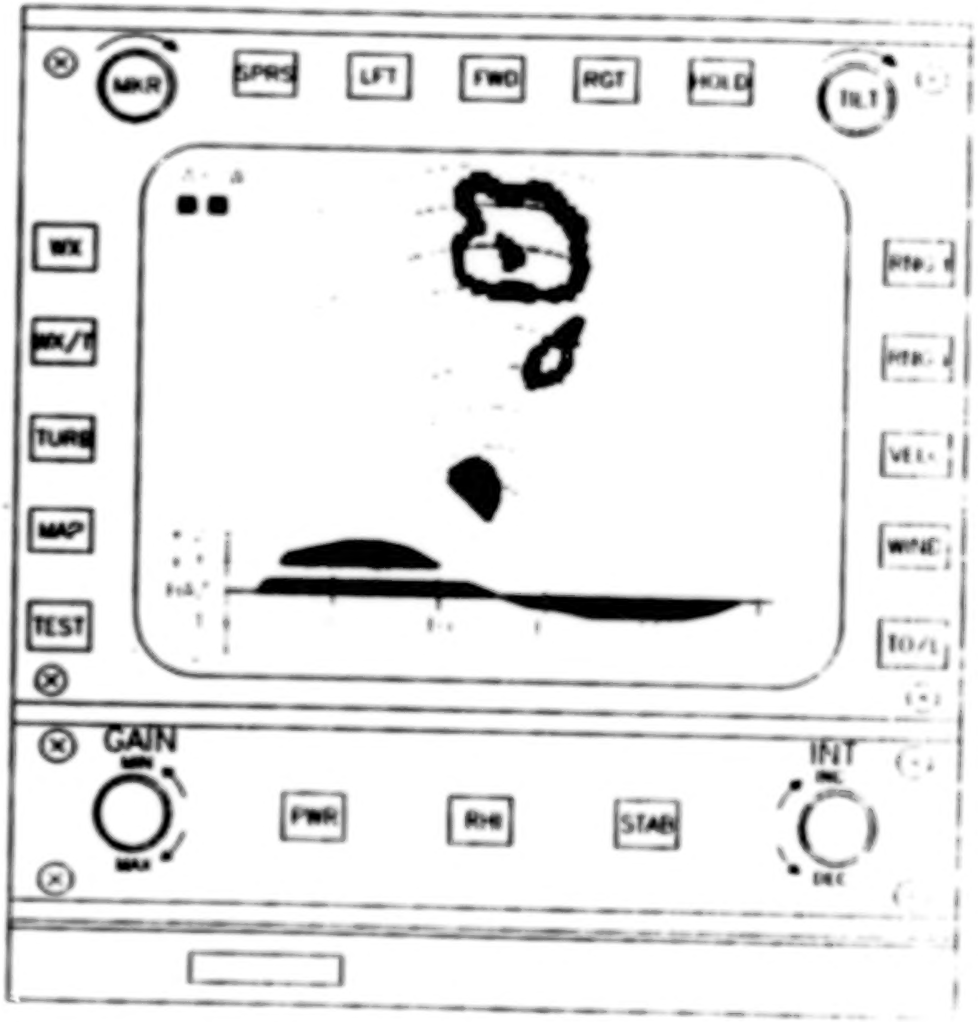
MKR
SPRS
LFT
FWD
RGT
HOLD
TILT
WX
WX/T
TURB
MAP
TEST
VEL
WIND
TO/L
GAIN
MIN
MAX
PWR
RHI
STAB
INT
INC
DEC

WEATHER/WINDSHEAR DISPLAY

Rockwell International
Collins Air Transport Division

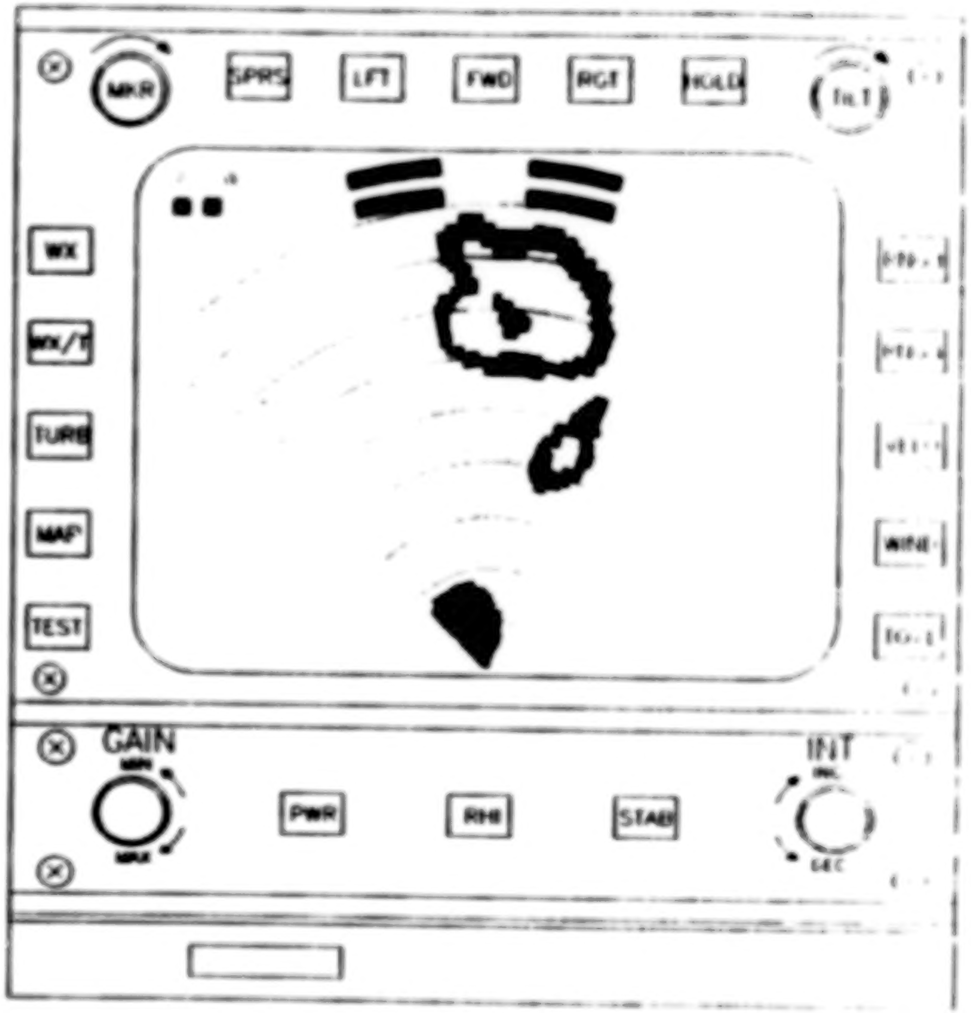
MKR
SPRS
LFT
FWD
RGT
HOLD
TILT
WX
WX/T
TURB
MAP
TEST
GAIN
MIN
MAX
PWR
RHI
STAB
INT
INC
DEC

WEATHER/WINDSHEAR DISPLAY

Rockwell International
Collins Air Transport Division

WINDSHEAR RADAR PROGRAM

CERTIFICATION

- PERFORMANCE REQUIREMENTS NOT DEFINED
  - -- DETECTION RANGE
  - -- POD / FAR
  - -- COVERAGE
- BURDEN OF PROOF REQUIREMENTS
  - -- "INTENDED FUNCTION" CERTIFICATION
  - -- FLIGHT DATA (PENETRATIONS?)
  - -- ANALYSIS / SIMULATION
- STAND ALONE WITHOUT REACTIVE BACKUP

FUTURE PLANS

- MULTI-SENSOR COMBINATIONS
  - -- RADAR / RADIOMETER / REACTIVE
  - -- SIMPLER SENSOR REQUIREMENTS
- ADDITIONAL CAPABILITIES
  - -- CLEAR AIR TURBULENCE
  - -- IMPROVED WINDSHEAR
- CO-OPERATIVE DETECTION
  - -- CROSS ATTENTIVE SENSORS

Rockwell International
Collins Air Transport Division

Status of Collins Research - Questions and Answers

Q: PAUL KELLY (21st Century Technology) - Given the fact that at lower altitudes radar is most susceptible to ground clutter effects and given the fact that microbursts are frequency wet at higher altitudes and dry at lower altitudes, it is obvious that a Doppler based system shows its greatest weakness in the zone in which the information from it is most critical for flight safety. Given the cost of a shear alerting system, airline decision makers will have to be very pragmatic in evaluating competing systems. Does this not illustrate a great need in the industry for some mechanism for codifying and indexing prediction effectiveness on a qualitative and quantitative basis to provide a tool for decision makers in system selection.

A: ROY ROBERTSON (Collins) - The answer is yes. You are correct, the tendency is that radar do act in the direction which you say, low altitude, dry microburst, are difficult environments for the radar to operate. However, I will not say that the radar would be ineffective. We, frankly, are optimistic that radar will still be quite effective in that environment. Your question about the indexing and coding, or method of categorizing the effectiveness of different systems, is a very complicated question. It's the combined effort of everyone at this review meeting to try to determine what effectiveness is and how effective individual sensors are. That involves defining the environmental set as well as the performance of individual sensors. That requires a great deal of data. Analysis can only take that question so far. So until a body of experience is gained on individual predictive sensors, that question cannot be answered. The likely result is that different sensors will excel in different areas. Then it will be up to the airline to perceive what individual properties are more valuable to an airline and that will be different from one airline to another.

PAUL KELLY (21st Century Technology) - There has to be some emphasis on categorizing the degree of effectiveness because we have to do something about giving airline management, which is where the bottom line is, some tool for evaluating competing systems. That's the bottom line that all of our discussions relate to and hence the criticality of our addressing this factor.

ROY ROBERTSON (Collins) - I think that the sum body of knowledge arising from all this effort will certainly move in that direction.

Q: PAUL KELLY (21st Century Technology) - Does the onus for such a code and indexing arrangement not fall on the FAA or is the FAA adopting the position that the initiative will have to come from the industry and expecting the aviation industry to do what it did with the aircraft aging issue when the industry drew up the recommendations and presented them to Sam Skinner for signature?

A: HERB SCHLICKENMAIER (FAA) - You're ahead of me Paul on what the industry did with Sam Skinner. What we've done in this area is as we've done before, work with the industry on what is perceived as a joint industry need. The rationale for the FAA getting together with NASA in the first place, first back in '86 and then again this fiscal year on the new agreement, was to formalize some sort of a structure for conducting the research to look into the questions. But as Roy was saying before, there are some questions in this matter that need to be addressed that are not pertinent to government research. There is not that much expertise quite honestly, at least within the civil aviation side, for the marketing, development and cost effective maintenance and distribution of a piece of avionics into the civil air carrier fleet. I have yet to brief the associate administrator for marketing in the FAA. Those kinds of decisions and questions need to rest with the

Boeings, Douglas, Lockheeds and their customer base. That has as much of an effect on the final design and decision of what the technology is and how it addresses the problem.

Session XI. Airborne Doppler Radar / NASA

PRECEDING PAGE BLANK NOT FILMED

Session X. Airborne Doppler Radar / NASA

N91-24152

Clutter Modeling of the Denver Airport and Surrounding Areas

Steve Harrah, NASA Langley
V. Delnore, Lockheed
R. Onstott, ERIM

CLUTTER MODELING OF THE DENVER AIRPORT AND SURROUNDING AREAS

Steven D. Harrah
NASA Langley Research Center
Hampton, Virginia 23665

Victor E. Delnore
Lockheed Engineering & Science Company
Hampton, Virginia 23666

Robert G. Onstott
Environmental Research Institute
of Michigan
Ann Arbor, Michigan 48107

PRECEDING PAGE BLANK NOT FILMED

Abstract

To accurately simulate and evaluate an airborne Doppler radar as a wind shear detection and avoidance sensor, the ground clutter surrounding a typical airport must be quantified. To do this, an imaging airborne Synthetic Aperture Radar (SAR) was employed to investigate and map the Normalized Radar Cross Sections (NRCS) of the ground terrain surrounding the Denver Stapleton Airport during November of 1988. Images of the Stapleton ground clutter scene were obtained at a variety of aspect and elevation angles (extending to near-grazing) at both HH and VV polarizations.

This presentation will discuss the method of data collection, the specific observations obtained of the Denver area, a summary of the quantitative analyses performed on the SAR images to date, and the statistical modeling of several of the more interesting stationary targets in the SAR database. Additionally, the accompanying moving target database, containing NRCS and velocity information, will be described.

Denver Ground Clutter Observations and Data Collection

V. E. Delnore, Lockheed Engineering & Sciences Company

Outline

Two years ago at the Williamsburg meeting, we described the ground clutter data we were hoping to obtain at Denver the following month. Well, the flight was a success, and now we want to describe the data and some of the analyses that we and the Environmental Research Institute of Michigan (ERIM) have done.

CLUTTER MODELING OF THE DENVER AIRPORT AND SURROUNDING AREAS

Outline

- Basis for Studying Ground Clutter
- Method of Measuring Ground Clutter
- Flight Lines and Observations
- Ground Clutter Statistical Modeling/Analysis
- Results of Statistical Analysis
- Moving Clutter Statistical Modeling/Analysis
- Summary

Basis for Studying Ground Clutter

The motivation here is that we're developing a Doppler radar to be carried on the airplane, looking down along the glide slope, to detect wind shear. But there's a backdrop of ground clutter we must deal with. To suppress the effects of ground clutter, we have to understand its distribution, statistics, and characteristics.

To do this, we flew a Synthetic Aperture Radar (SAR) at Denver -- not to detect wind shear, but to study ground clutter. What we learn about ground clutter from the SAR goes into a computer model of the airport environment as seen by the airborne Doppler radar. Les Britt will describe that to you in the next paper.

CLUTTER MODELING
OF THE DENVER AIRPORT AND SURROUNDING AREAS

Basis for Studying Ground Clutter

- Lack of Historical Near-Grazing Clutter Data
- Simulate Weather Radar Operating in Presence of Ground Clutter
- Understand Airport Clutter Environments

Radar's Eye View of Airport

Here's the approach to 26-Left at Denver.

You can see the runway, but look at all this other stuff around it: tall buildings, mountains, industrial parks, even moving stuff on these highways are railroads.

All reflecting your radar beam and sidelobe energy back up to you, cluttering up you radar screen and increasing the difficulty of any discrimination scheme in your signal processor.

This is what we're trying to sort out. We're not constructing a data base for a subtraction scheme, but instead trying to understand ground clutter so we can process it out in the general case.

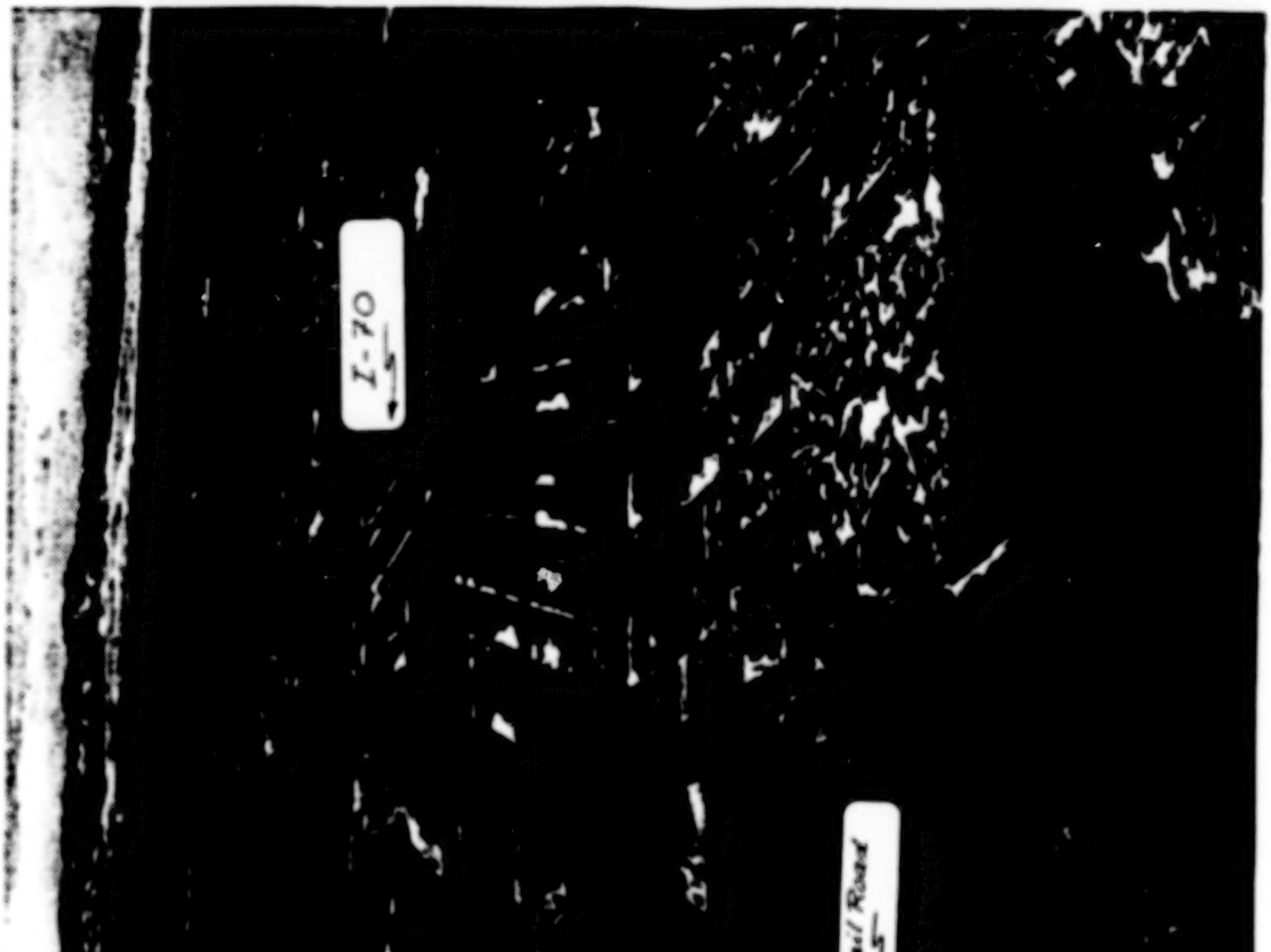
Rocky Mtns
Downtown Denver
Airport 26L
I-70
Rail Road

ORIGINAL PAGE IS
OF POOR QUALITY

CLUTTER MODELING
OF THE DENVER AIRPORT AND SURROUNDING AREAS

Method of Measuring Ground Clutter

- Synthetic Aperture Radar (SAR)
- Down/Cross Range Resolution
- Polarization

PRECEDING PAGE BLANK NOT FILMED

P-3 with SAR

Here is the P-3, at Buckley Air National Guard Base, a few miles southeast of Denver Stapleton, on the morning we flew.

We used an X-band SAR, with its antenna mounted on the belly of a P-3 operated by the Naval Air Development Center.

ORIGINAL PAGE IS
OF POOR QUALITY

C-4

CLUTTER MODELING
OF THE DENVER AIRPORT AND SURROUNDING AREAS

Flight Lines and Observations

- Description of the Denver SAR Images
- Incidence Angles and Polarizations
- Ground Resolution

SAR Swath Geometry

This is the setup we used to map out the ground clutter. We flew several configurations, differing in depression angle and polarization.

The P-3 is shown on the right, with the SAR looking out to its side, and mapping everything within this swath at a resolution of 3 m on the ground.

The usual scheme got us out to a depression angle of about 5 degrees, but for a couple of passes we flew at a lower altitude (all AGL, of course), and got out to 3 degrees. Reflectivity at these near-grazing angles is important, because that's what a real-aperture radar looking down a 3-degree glide slope will be seeing.

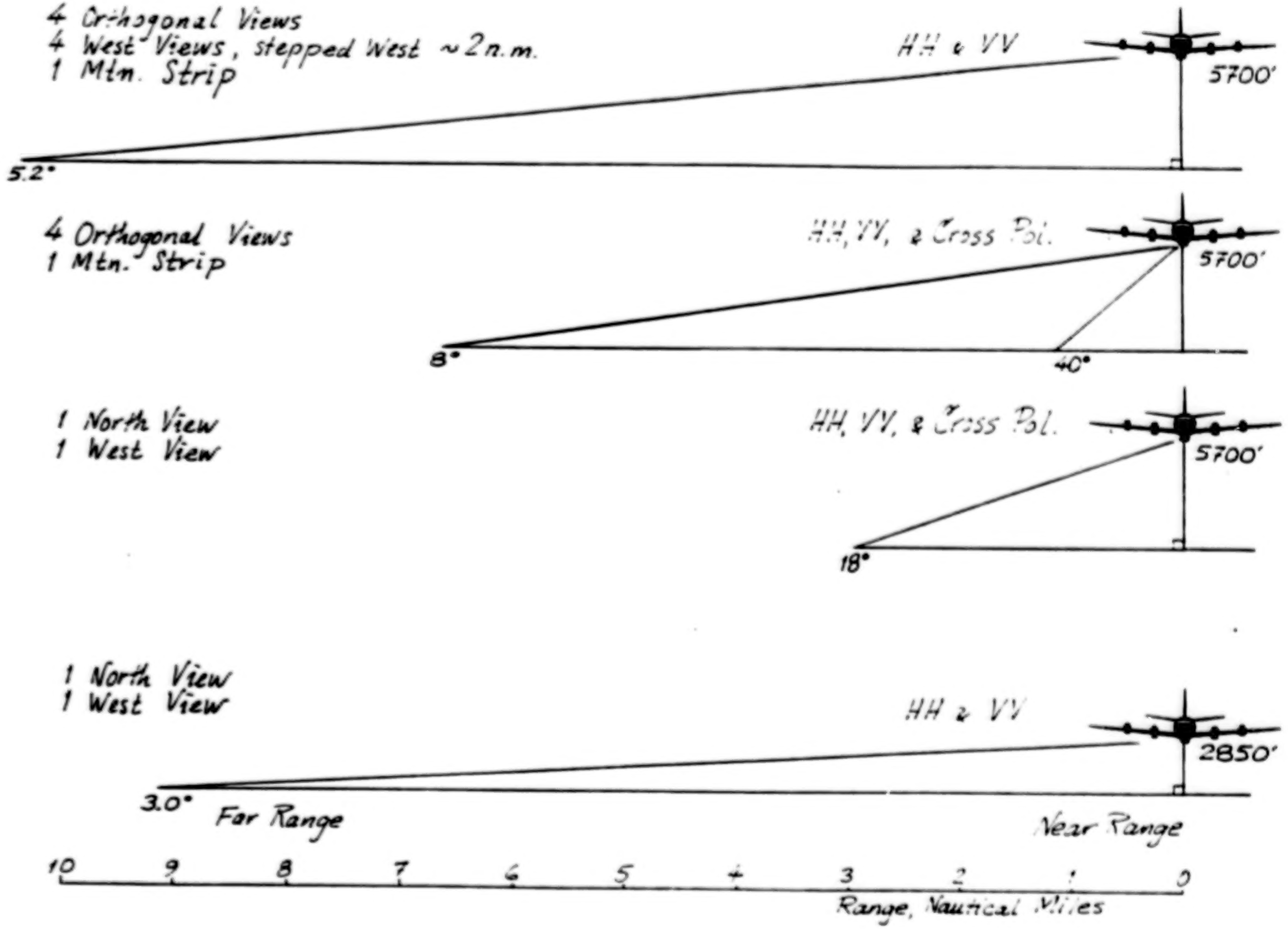
4 Orthogonal Views
4 West Views, stepped West ~2n.m.
1 Mtn. Strip
HH & VV
5700'
5.2°
4 Orthogonal Views
1 Mtn. Strip
HH, VV, & Cross Pol.
5700'
8°
40°
1 North View
1 West View
HH, VV, & Cross Pol.
5700'
18°
1 North View
1 West View
HH & VV
2850'
3.0°
Far Range
Near Range
10
9
8
7
6
5
4
3
2
1
0
Range, Nautical Miles

SAR Swath Widths, Denver '88

ORIGINAL PAGE IS
OF POOR QUALITY

SAR Coverage of Denver Area, Part 1

Here's a perspective sketch of the Denver area: The airport, downtown, the mountains, and Boulder; the marked areas on the ground show some of the areas we mapped. There are orthogonal looks at the same target area (the airport), and the mountain passes.

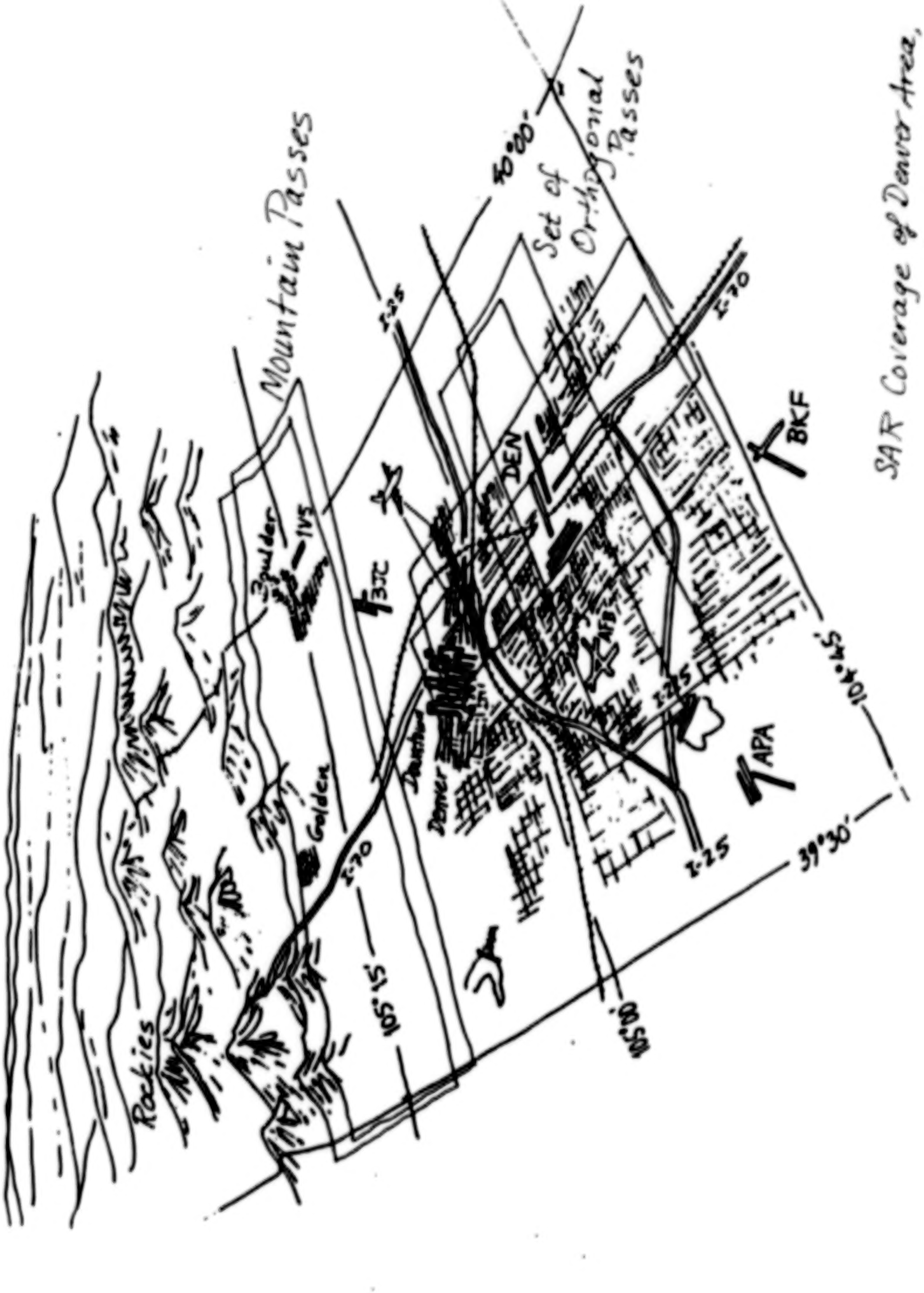
Mountain Passes
Set of Orthogonal Passes
40°00'
I-25
I-70
BKF
DEN
Boulder
IV5
BJC
AFB
Golden
Downtown
Denver
Rockies
105°15'
105°00'
104°45'
39°30'
APA
I-25
I-70

SAR Coverage of Denver Area,
Part 1

ORIGINAL PAGE IS
OF POOR QUALITY

SAR Coverage of Denver Area, Part 2

There are also 4 successive passes, each stepped about 2 1/2 miles over, and all looking in the same direction, so that we see each target at up to 4 different depression angles.

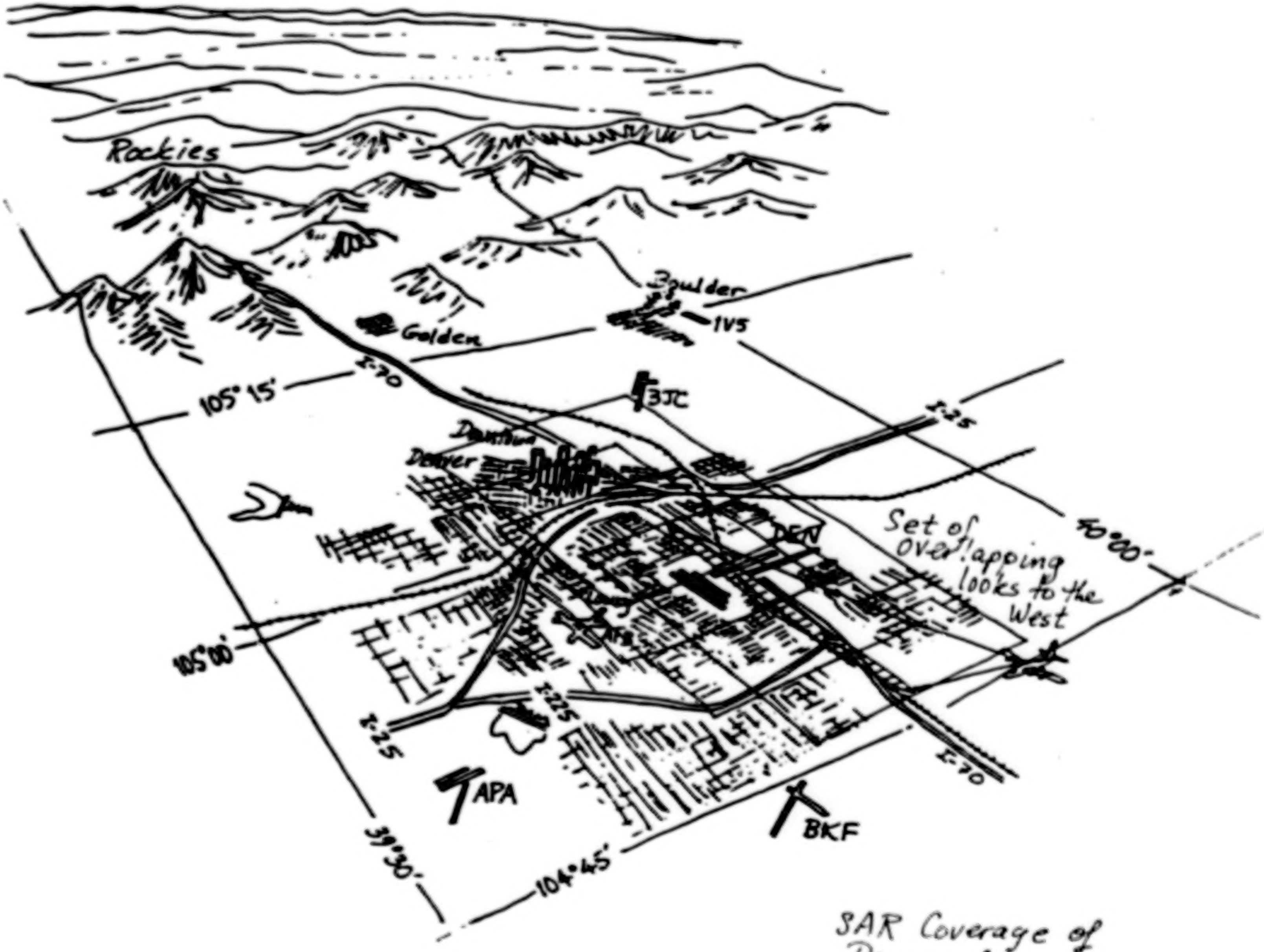
Rockies
Boulder
IVS
Golden
I-70
105°15'
3JC
I-25
Downtown
Denver
DEN
40°00'
Set of overlapping looks to the West
105°00'
I-225
I-25
APA
39°30'
104°45'
BKF
I-70

SAR Coverage of
Denver Area,
Part 2

ORIGINAL PAGE IS
OF POOR QUALITY

SAR Image of Denver Area

Here's some of the processed data:

This is a false-color SAR image, rendered here in gray-scale, at 20 m ground resolution.

The image is corrected for range fall-off, but not normalized to any one depression angle, so what you're seeing is differences in reflectivity due to depression angle and to the target's characteristics.

The airport is the dark area in the center, with its runway areas and passenger terminal. you can see buildings, highways, and lots of clutter sources.

We've identified and cataloged the normalized radar cross section and depression angle of each type of target on several of these images, to model the stationary environment around Denver.

And, using aerial photographs and lots of students, we've estimated the distribution, density, and speeds of car, truck, and train traffic along some of these highways, streets, and railroads.

This gives us moving target information, which we feed into Les' model.

DENVER STAPLETON INTERNATIONAL

HH POLARIZATION

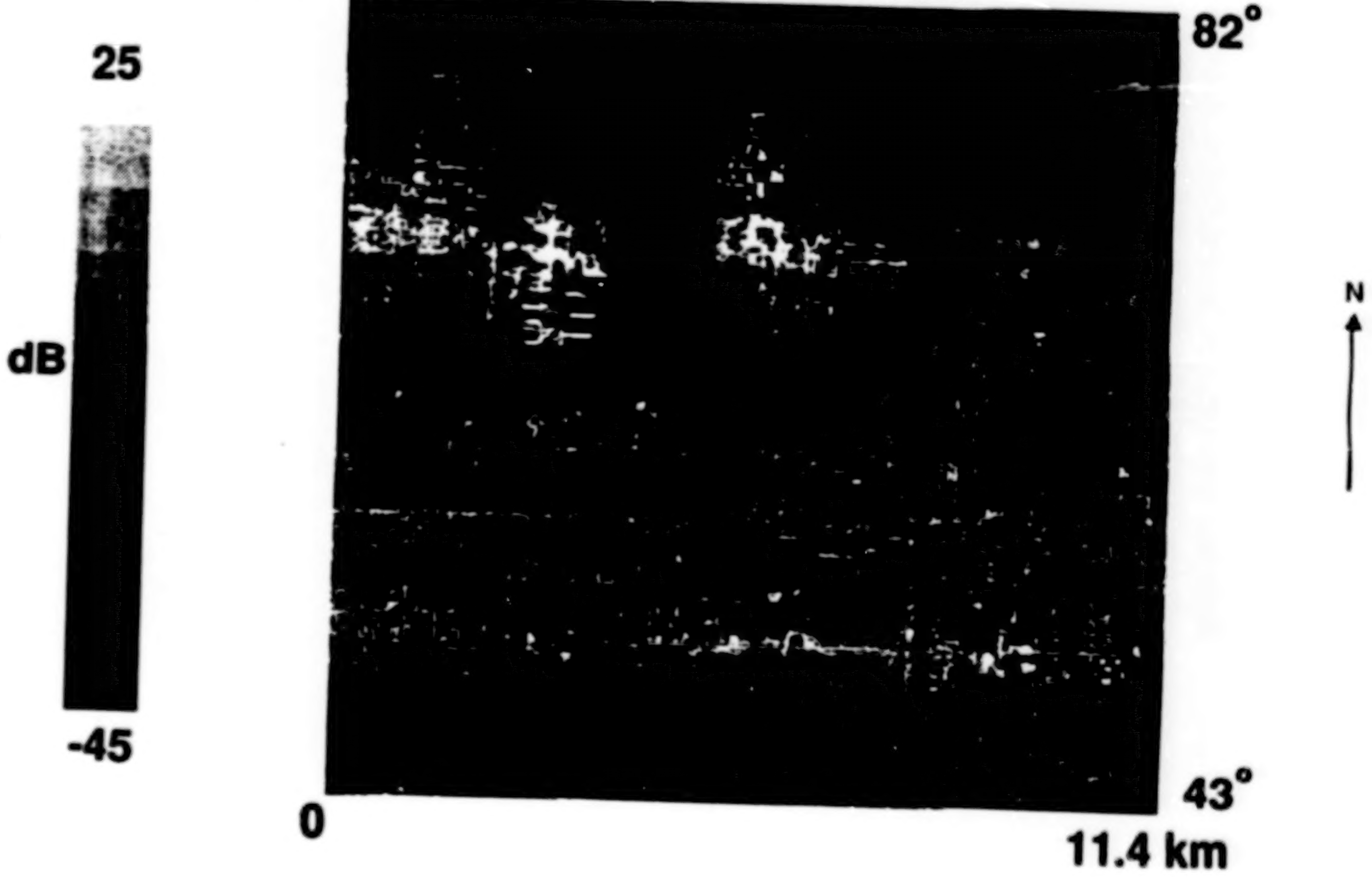
14.3 km
82°
43°
0
11.4 km
25
dB
-45
N

ORIGINAL PAGE IS
OF POOR QUALITY

Statistical Analyses and Ground Clutter Modeling

S. D. Harrah, NASA Langley Research Center

Preliminary Comments

In order to realistically simulate and evaluate the performance of any airborne Doppler radar as a forward looking wind shear sensor, it is imperative to generate an accurate representation of the backscattered ground clutter signal. Researchers at NASA LaRC have developed a robust airborne Doppler radar simulation program, which generates a realistic radar I/Q signal from a complex scattering scene. This scene may consist of weather, stationary ground clutter, and/or moving clutter. The simulation program incorporates a Normalized Radar Cross Section (NRCS) ground clutter database as its source for the ground clutter signal. A Synthetic Aperture imaging Radar (SAR) was employed to measure the backscattered NRCS levels of the terrain surround the Denver Stapleton airport. It should be noted that, all the angles in this section are referred to as incidence angles. The classical definition of incidence angle is the angle measured from the surface normal. Since it is impractical to measure the mean surface normal for each ground cell, the incidence angle referred to here is measured from vertical for each ground cell. It should further be noted that, some authors prefer to use the complement of the incidence angle often called the depression angle.

Ground Clutter Statistical Modeling/Analysis

In this portion of the presentation, I would like to show some of the results of a statistical analysis performed on the Denver Stapleton ground clutter database. The purpose of this analysis may be divided into three categories. First, to validate the backscatter levels observed in the SAR images. Second, to determine any pertinent statistical information which would help in the modeling of ground clutter at high incidence angles. Third, to determine if any statistical properties existed in the Denver ground clutter database which would help in the discrimination of the backscattered ground clutter and weather signals.

To achieve these goals, we analyzed the NRCS levels observed in the Denver ground clutter database to investigate incidence angle and polarization effects and to determine the utility of the spatial Normalized AutoCorrelation Function (NACF). In investigating incidence angle and polarization effects, we generated both full image and sub-image analyses. Some of the specific targets of interest, which we investigated were: the urban environment, isolated tall buildings, and scenes of the Rocky mountains. Some of the statistical parameters generated during the analysis of each image were: the dynamic range (minimum to maximum), the mean, and the variance, of the NRCS levels found in the Denver ground clutter database.

CLUTTER MODELING
OF THE DENVER AIRPORT AND SURROUNDING AREAS

Ground Clutter Statistical Modeling/Analysis

- Investigate Incidence Angle and Polarization Effects
    - Full Image Analysis
    - Specific Targets
        - Urban Environment
        - Tall Buildings
        - Mountains
    - Distributions
        - Min. & Max.
        - Mean & Variance

- Spatial Normalized AutoCorrelation Function (NACF)

Denver Stapleton SAR Image (HH Polarization)

The next two SAR images are grey scale representations of the NRCS values obtain for the Denver Stapleton ground clutter scene. Each image has been calibrated, mapped from slant range to ground range, and corrected for range fall-off. The first image was obtained using HH polarization and the second used VV. The two images were recorded simultaneously using the ERIM SAR. Each image is comprised of thousands of cells, ~20 m X 20 m, in size. The approximate total dimensions of each image and the near and far range incidence angles are reported on each image.

DENVER STAPLETON INTERNATIONAL

HH POLARIZATION

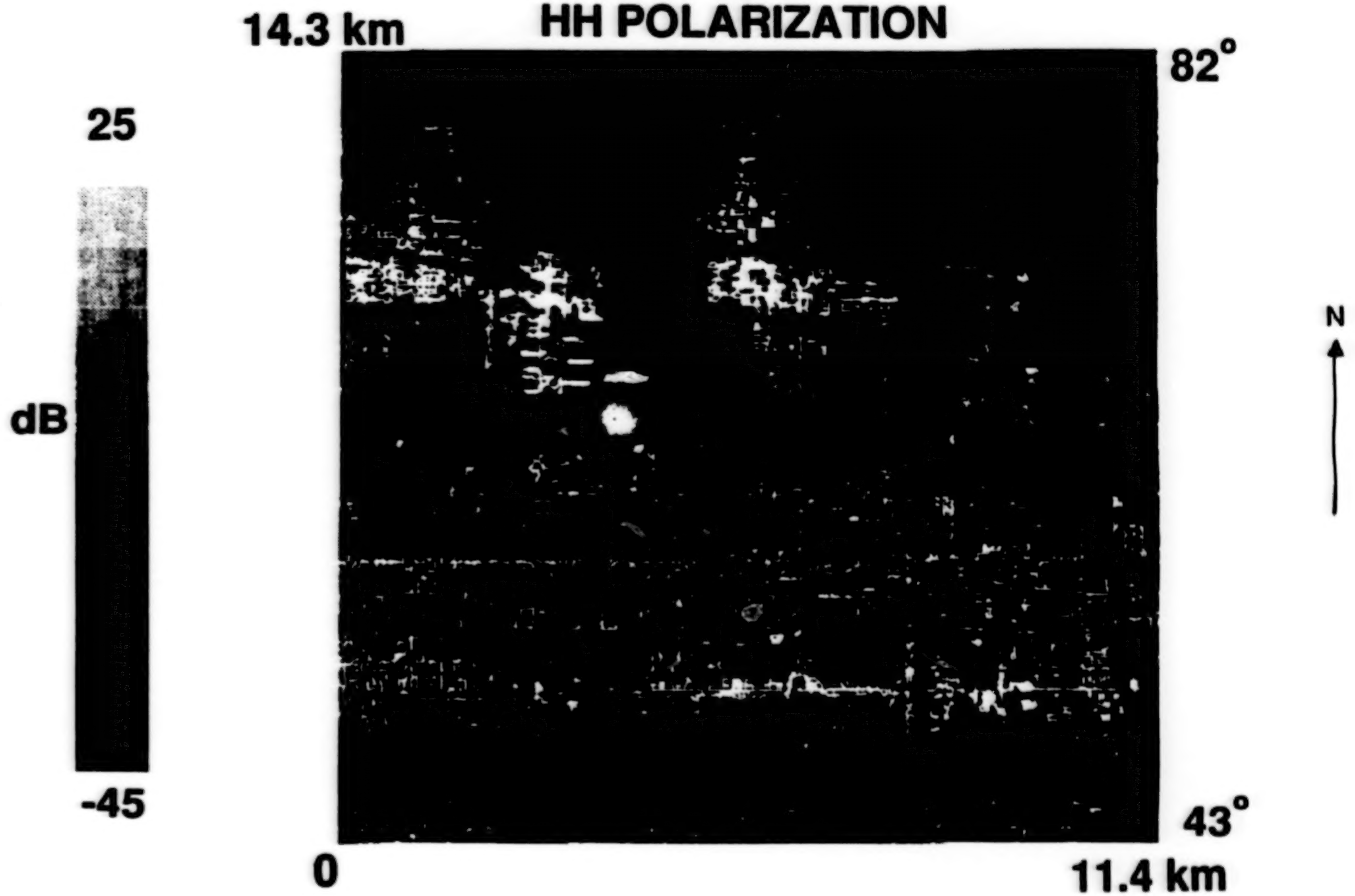
14.3 km
82°
43°
0
11.4 km
25
dB
-45
N

ORIGINAL PAGE IS
OF POOR QUALITY

Denver Stapleton SAR Image (VV Polarization)

Note that , the two images are on a common grey scale; thus, allowing a direct comparison of the intensity for common areas in each image. Because of the rather large quantity of data in each image, as well as, the large dynamic range of the NRCS values, I doubt that these reproduced images will be highly enlightening. Therefore, I would like to remind everyone that, a complete set of SAR images for Denver are available to anyone interested. This data can be obtained on a variety magnetic storage media and in almost any format.

Although some differences can easily be seen in the two images, only through a statistical analysis can the differences be quantified.

DENVER STAPLETON INTERNATIONAL

VV POLARIZATION

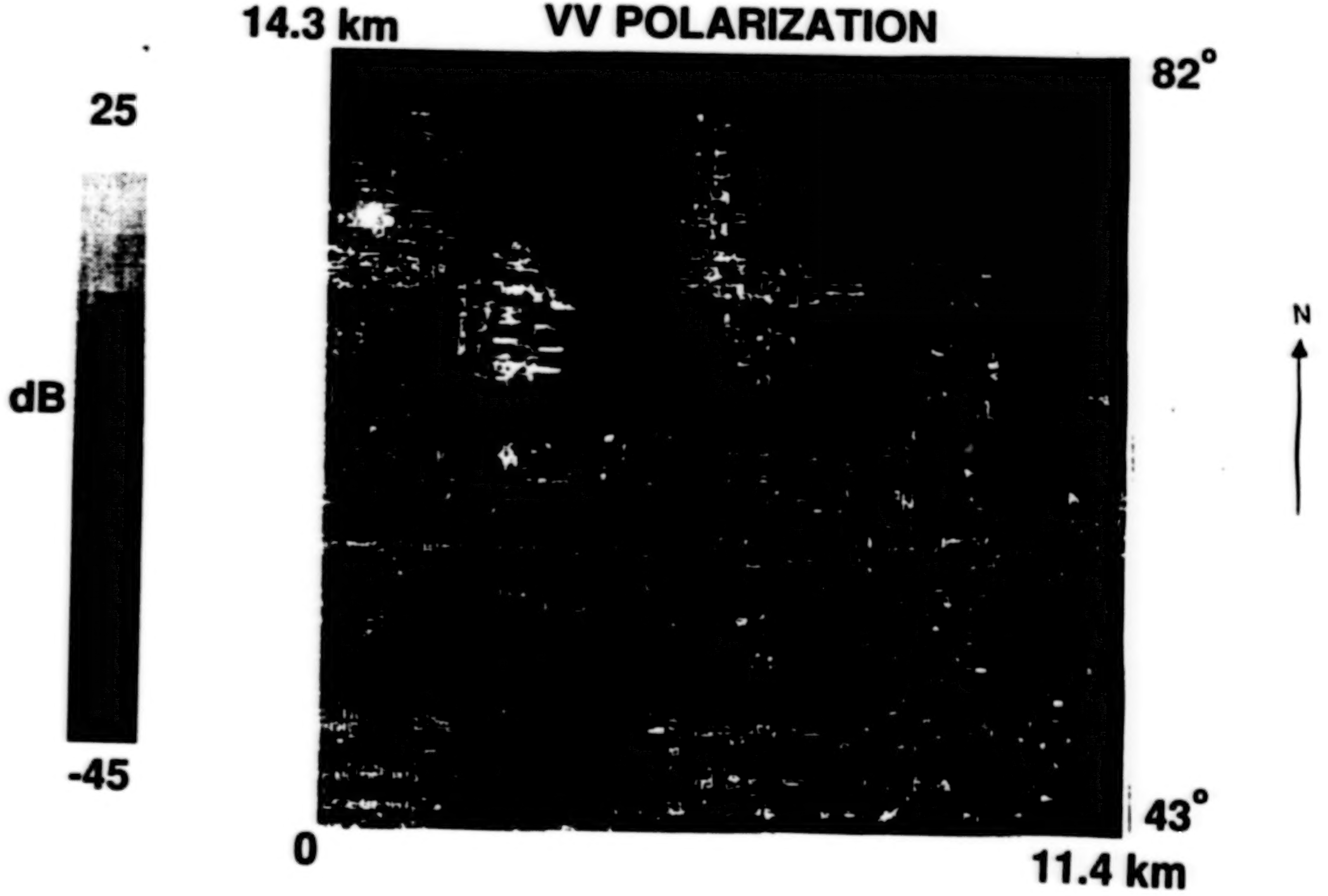
14.3 km
82°
43°
0
11.4 km
N
25
dB
-45

ORIGINAL PAGE IS
OF POOR QUALITY

Histogram of the Denver Stapleton SAR Images

This histogram clearly shows the distribution of NRCS values in the two images. The mean and the standard deviation for each distribution are specified at the top of the plot. From this full image analysis it appears that VV polarization would produce a 10 to 15 dB lower ground clutter return than would HH polarization.

Often HH polarization is used in weather radars, since it gives a slightly larger rain return, typically a few dB. However, this occurs almost exclusively with large rain drop sizes, where the droplets flatten during their descent due to air resistance. But larger drop sizes also produces a larger signal, which in turn reduces the need for using the polarization sensitivity of rain. Since the 10 or 15 dB gained would out weight the 2 or 3 dB lost, the largest Signal-to-Clutter Ratio (SCR) for this clutter scene would be achieved using VV polarization.

Even though these statistics contradict the usual preference of HH polarization for a weather radar, we do not contend that all wind shear radars be built using VV polarization exclusively. Which polarization should be used for wind shear detection and under what circumstances, is still an open question and will be investigated during our flight program. It should be reemphasized that the statistics shown here are for large images consisting of many different scattering types, at very high incidence angles, and are only necessarily representative of this one image. Some images may produce larger VV returns. Image composition is the prime factor for determining which polarization will produce the larger returns.

Since image composition is the prime factor in determining polarization and more importantly in producing the larger SCR, full image analysis can only show the aggregate effect of all the scatterers over the entire image. In order to specify how each scattering type contributes, we divided each image into smaller near-homogeneous sub-images on which we performed the same types of statistical analyses. Because of time, I would like to show you, only a small fraction of the many sub-image results we have obtained, for specific targets of interest.

DENVER STAPLETON INTERNATIONAL AIRPORT

DENVER IMAGES 2 & 6 : (HH) & (VV) POLARIZATIONS
A/C PASS 37 : INCIDENCE ANGLES (43-82)

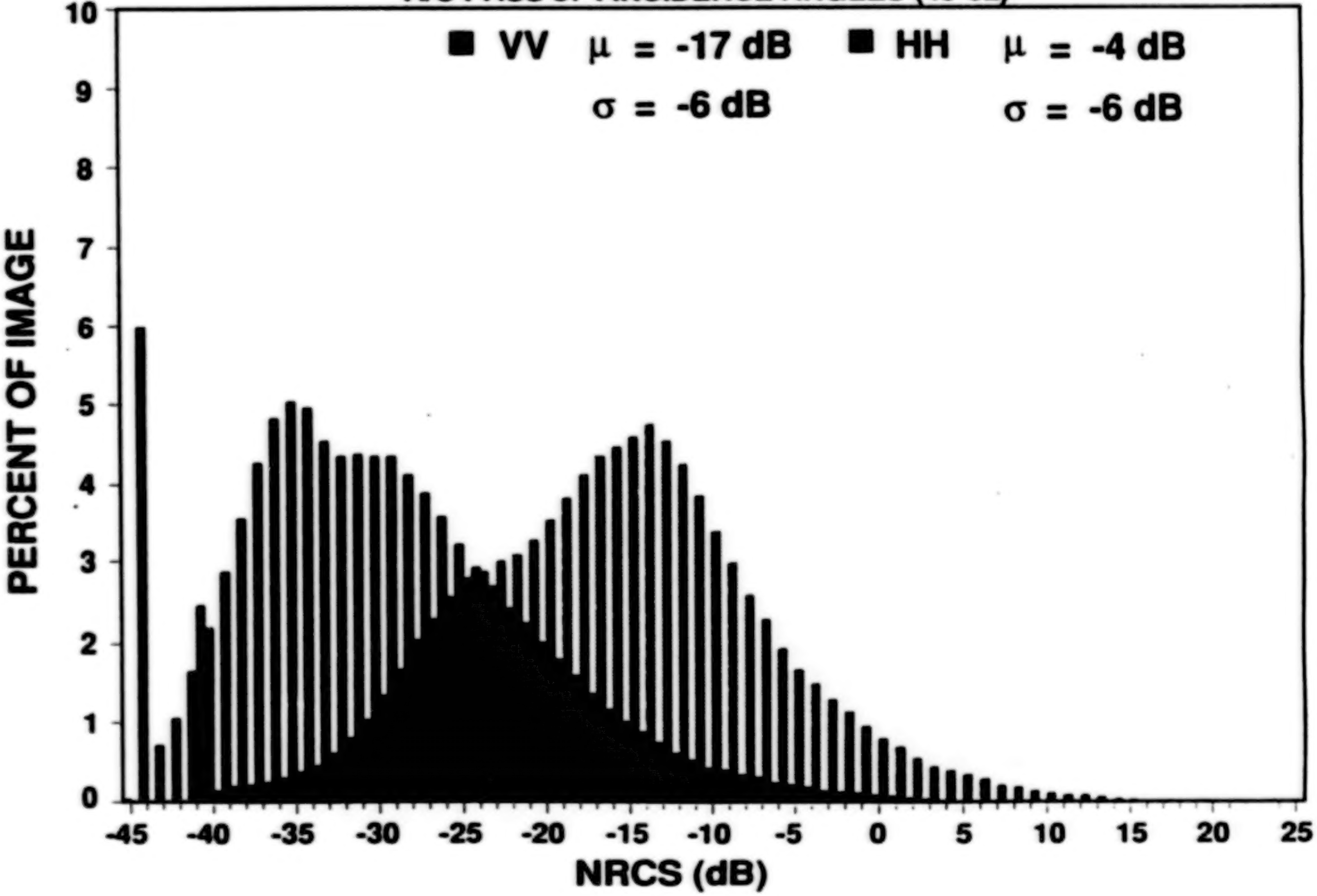

Scattergram of Tall Buildings in the Denver Stapleton SAR Images

Tall buildings, such as those in an urban environments, are primary sources of ground clutter, since they offer a large physical cross section and are constructed of metal and concrete. Also, at incidence angles near-grazing, which would be typical of a wind shear radar during landing, the flat sides of a building will produce a near specular return. Typical NRCS values are shown in the scattergram as a function of incidence angle. These NRCS values were calculated for numerous, isolated, tall buildings present in the SAR images.

This scattergram shows at least two important NRCS features of tall buildings. First, the influence of the incidence angle and the severity of tall building NRCS levels. Second, the insensitivity of the buildings in these images to polarization. In the case of the former, this plot shows that NRCS levels beyond the dihedral angle but 10° or more shy of grazing, produce little return. However, the NRCS can get quite large for near- dihedral or grazing incidence. The scattergram also shows that these buildings are polarization insensitive. So we might not gain any ground clutter suppression by choosing one polarization over another, for images (or environments) consisting of primarily tall buildings.

Although Denver has a number of tall buildings, it should be noted, that these areas do not comprise more than 10% of the total SAR image. Thus one might immediately guess that natural terrain causes the polarization sensitivity. Although natural terrain does account for some of the polarization sensitivity, it is the rural and lightly industrialized areas which seems to make the majority of the contribution.

Ground Clutter
Tall Buildings

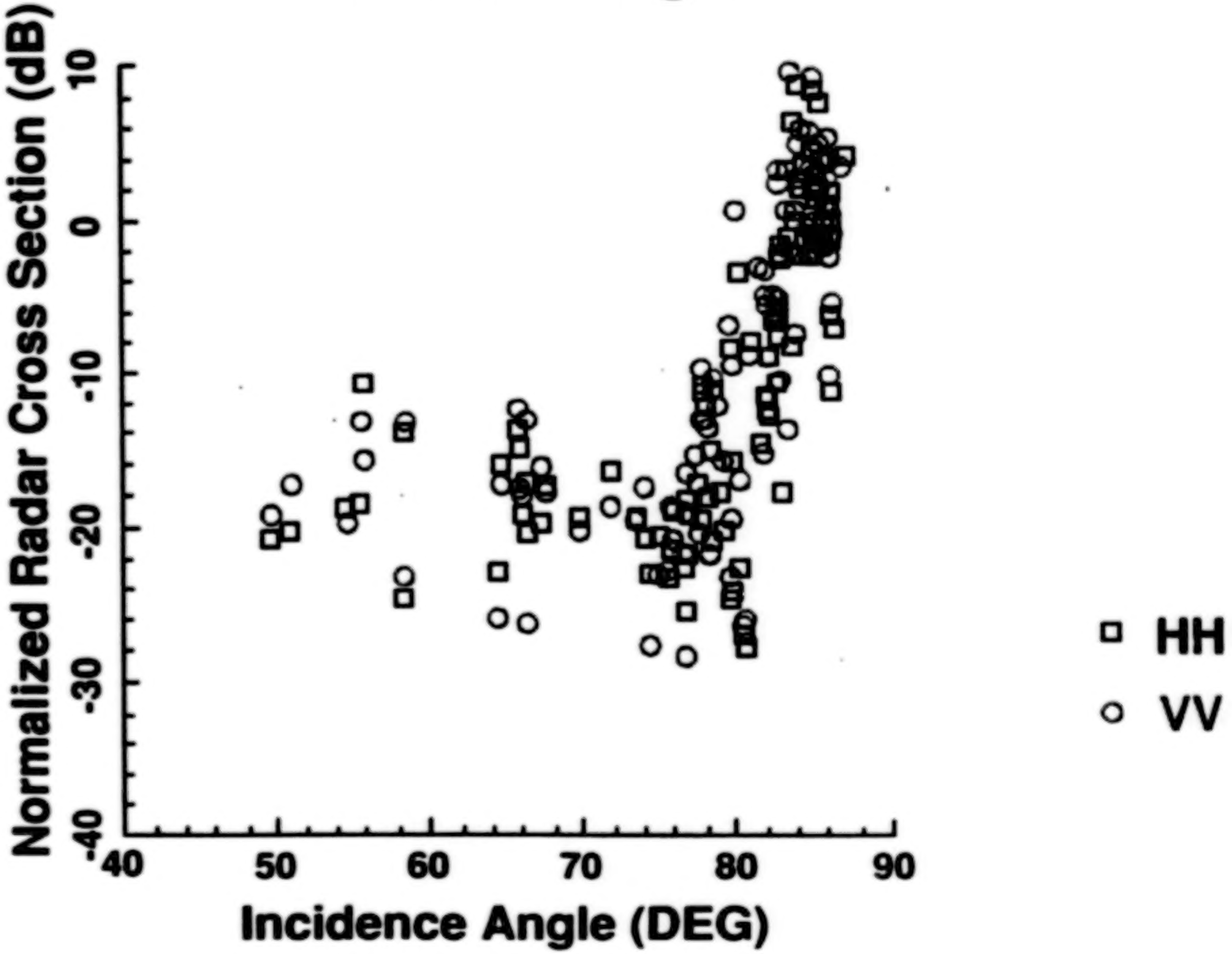

SAR Image of the Denver Central Business District (CBD)

The typical size and consistency of a sub-image is shown in this grey-scale representation of the Denver Central Business District (CBD). It should be recalled that, a sub-image consisted of primarily one type of scattering category. However as often was the case, even small areas contained different type of scatterers; note the several highways crossing this sub-image of the Denver urban scene.

The four westward-looking images of Denver, generated by four aircraft tracks each successively more westward, produced a unique situation. Since each image consisted of significant portions of the previously obtained image, it was possible to compare NRCS levels of the same sub-image at several different incidence angles (elevation) while maintaining roughly the same aspect angle.

CENTRAL BUSINESS DISTRICT

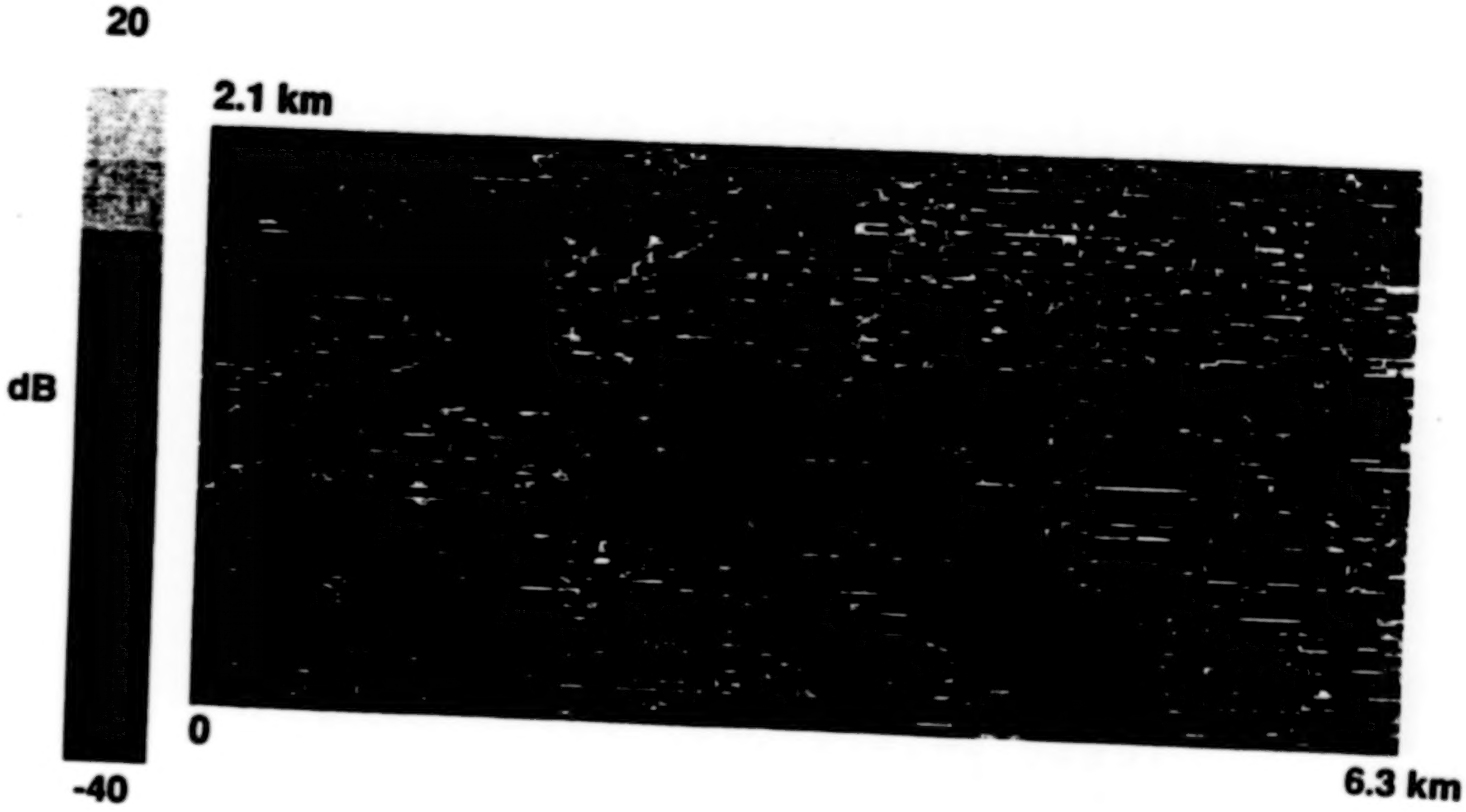
20
dB
-40
2.1 km
0
6.3 km

ORIGINAL PAGE IS
OF POOR QUALITY

Incidence Angle Statistics of the Denver CBD SAR Images

For Denver's CBD we were able to extract three sub-images, each recorded using HH polarization and each covering a different incidence angle range. Statistics were developed for each of the sub-images individually. Shown here are the minimum, mean, and maximum NRCS values for the specific incidence angles occurring in each sub-image.

The procedure used to develop these statistics is as follows. Each full image is analyzed and the location of the specific sub-image is determined. This portion of the image is electronically copied to a file along with its incidence angle information. Thus the statistics are representative of the the same ground area viewed at different elevation angles. Each sub-image is carefully examined to verify that it is comprised of the same location and number of cells as is in the other sub-images. Then the dynamic range and the mean NRCS for each row in each sub-image is determined. Naturally the mean and any other calculated statistics are generated from their linear scale values rather than their logarithmic representation. Since all the cells in a single row are at the same incidence angle, we may plot these statistics versus the incidence angle for each row, to obtain the figure shown here.

This type of graph shows the general trend in the specific clutter category (urban) as a function of incidence angle. The mean NRCS level is nearly constant across the entire range of incidence angles, increasing only ~5 dB around 84°. Note however that, the dynamic range increases some 20 to 30 dB over the range of incidence angles. This information is of great use, for statistically modeling urban ground clutter.

It might further be noted that, this complex, near-homogeneous urban clutter scene does not exactly agree with the previous scattergram plot of isolated, tall buildings (comparing the mean NRCS with those in the scattergram plot). Although agreement is good at the lower incidence angles (~76° - 79°), where the contributions by tall buildings, as suggested by the scattergram plot, is roughly comparable with the mean, the strong NRCS levels of tall buildings at the higher incidence angles does not seem to affect the mean NRCS level significantly. Since each range bin of our radar footprint is much larger than the cell size used in the tall building clutter, we would expect to see NRCS levels more indicative of the mean level rather than the maximum.

DENVER STAPLETON INTERNATIONAL CENTRAL BUSINESS DISTRICT

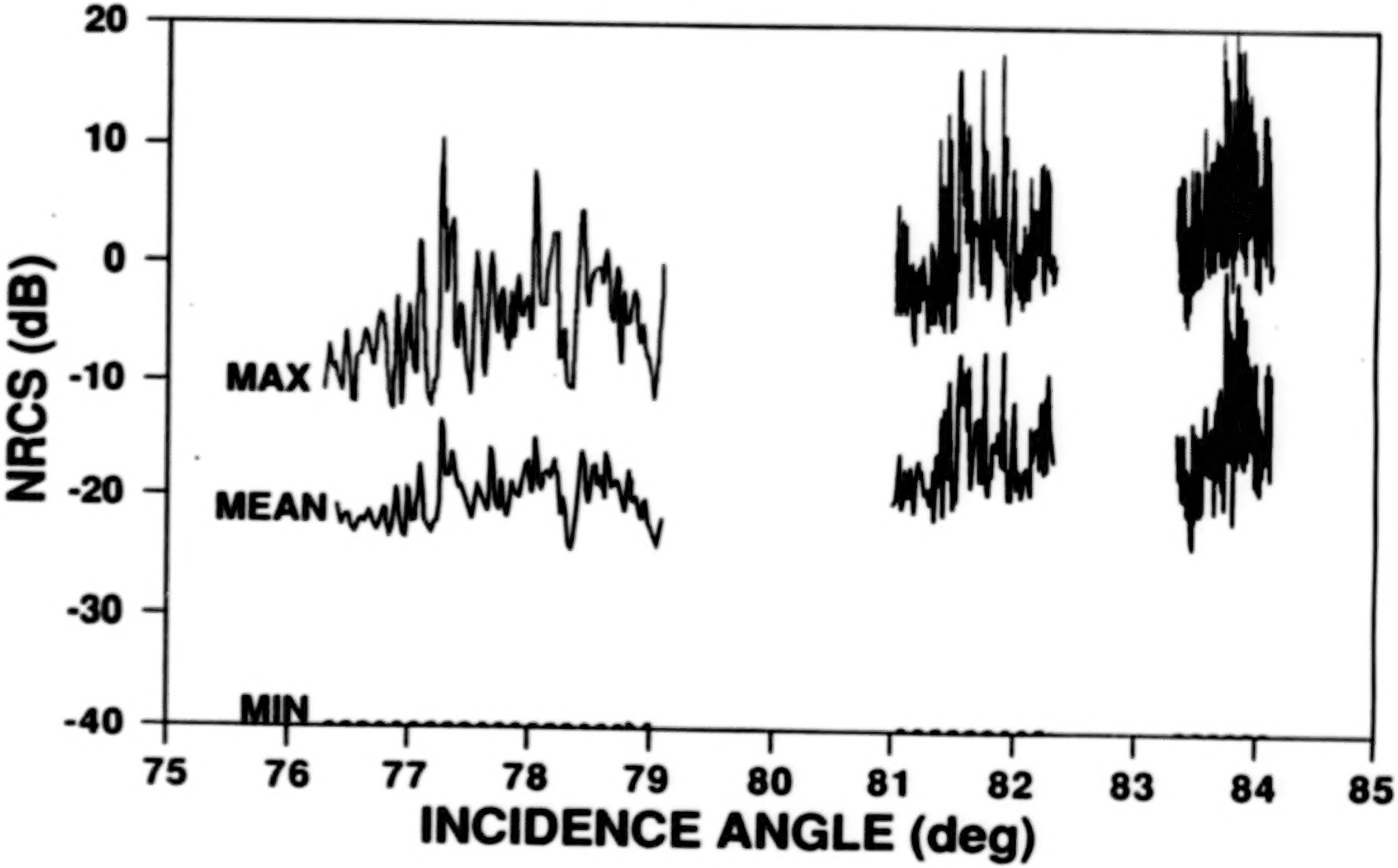

Statistics of the Rocky Mountain SAR Images

Another target of interest was the mountainous areas surrounding Denver. NRCS data was obtain of these areas in order to quantify the second-go-around returns from the mountains. This data was collected for both the "Thrust Feature" and the actual Rocky Mountains themselves. The plots show both typical NRCS levels and incidence angle effects for both types of scatterers. Specifically, the plots show that the only significant NRCS levels are contained in some of the "thrust feature" data; however, since these high levels only occur a low incidence angles, it is not likely that an aircraft's radar will encounter this "thrust feature". Furthermore, it should be noted that the "thrust feature" is a high, directionally dependent (aspect angle) scatterer and because of the aspect views obtained, the NRCS levels shown here should be representative of the largest levels that might be observed for these elevation angles.

Rocky Mountain NRCS Distribution

HH Polarization

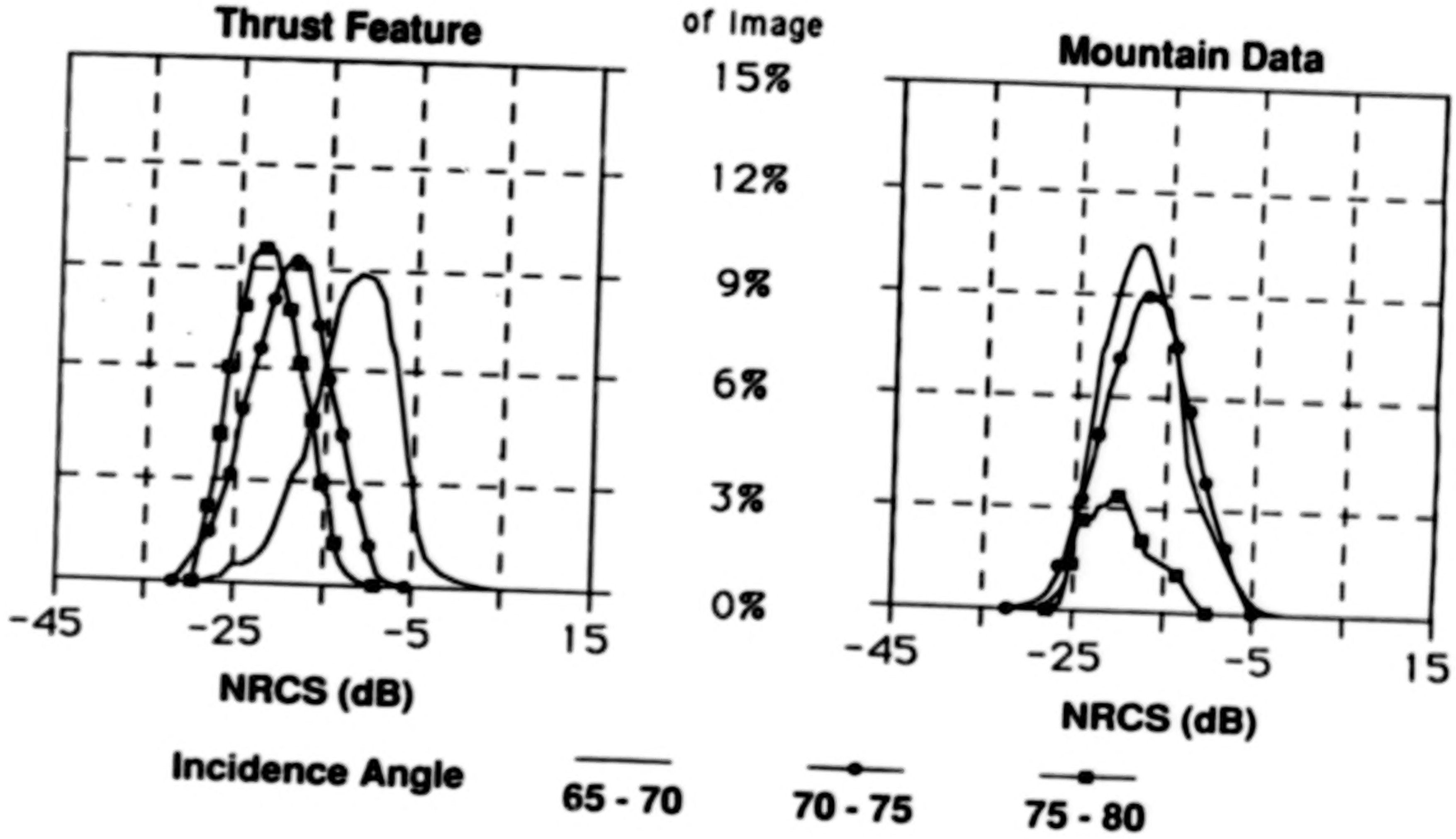

Results of Statistical Analyses Performed on SAR Images

1. The mean NRCS levels, for each scattering category, contained in the Denver Stapleton ground clutter database are consistent with the few available sources of high incidence angle ground clutter data. This conclusion is based upon a literature survey and a comparison with previously obtained ERIM archived SAR images.

2. If a statistical model is incorporated into a computer simulation, rather than a direct measurement of actual NRCS levels, then the variance must be increased with increasing incidence angle. Although empirically derived formulae are often used in statistical models for NRCS ground clutter generation, these formulae typically only describe the variation of the mean NRCS level with incidence angle (i.e., they use a fixed variance). However, it is necessary to also incorporate fluctuations in the second moment statistic (the variance) as a function of incidence angle, if one is to produce a truly realistic, backscattered, ground clutter, radar I/Q sequence.

3. We have found little or no useful levels of the 2-dimensional, spatial, Normalized AutoCorrelation Function (NACF) in the Denver SAR images. Although we have not shown the results of the investigation of the applicability of using a 2D spatial NACF, it should be noted that such an investigation has been pursued. There have been numerous hypotheses suggested, by myself and other researchers, for the failure of such a technique applied to the Denver images. However, I do not feel that I can elaborate on each hypothesis without showing some of the substantiating plots, and since it has been determined that this information would not be appropriate for this level of a technical conference, I will only report this conclusion without the substantiating information.

4. A significant level of polarization sensitivity has been observed during full image analyses. However many of the sub-image analyses of the various targets of interest (primarily consisting of high NRCS ground clutter sources) have shown little or no polarization sensitivity. It appears that the primary factor determining a wind shear radar's polarization is the composition of the ground clutter scene. Different polarization configurations may be necessary in an operational wind shear radar with the choice of polarization based upon the constituent scatterers surround an airport. I believe this is a issue which will only be determined by experience, and at our next meeting I hope to be able to report our finding on this matter.

5. A detailed inspection of the Denver ground clutter database has shown that man-made targets are the only sources of large NRCS ground clutter at near-grazing incidence angles. Natural targets, in general, offer very low NRCS levels compared to man-made targets at the same high incidence angles. Full image and sub-image analyses have been performed in order to isolate and coregister large NRCS sources, thus producing this result.

6. The relative levels of backscattered signal returning as second-go-around from the mountainous terrain surrounding Denver should produce little effect on the performance of a wind shear radar. This too will be investigated during our experimental flights around Denver.

CLUTTER MODELING
OF THE DENVER AIRPORT AND SURROUNDING AREAS

Results of Statistical Analyses Performed on SAR Images

- Mean NRCS Ground Clutter Levels Agree with Literature
- Variance Increases with Increasing Incidence Angle
- Little/No Useful Spatial Correlation Effects
- Some Polarization Sensitivity in Full Image Analyses
- Man-made Targets are the Only Large NRCS Clutter Sources
- Mountain Clutter will Produce Little Effect

Moving Clutter Statistical Modeling/Analysis

For an airborne wind shear radar, removal of a stationary ground clutter signal may be accomplished quite simply, provided that an accurate aircraft velocity can be established. This is because stationary clutter produces a narrow, localized-velocity, spectral signature; thus, filtering only requires a simple notch filter to be implemented in the frequency domain. Moving clutter however can be spread across the entire frequency domain, producing multiple velocity modes within a single range bin. Also, as described earlier, these man-made targets can be a primary source of large NRCS levels. Simply stated, moving clutter can, and should be expected to, exist in nearly every range bin and produce a continually changing, high amplitude, clutter signal across the entire frequency domain, which makes filtering it, the most difficult problem facing an airborne wind shear radar. Although the situation may sound bleak, much progress is being made in this area and will be discussed by Dr. Les Britt in the next presentation.

In order to investigate a variety of signal processing algorithms for moving clutter rejection, moving clutter databases, for the Denver and Philadelphia airports, were created. Also the additional functionality of incorporating moving clutter was added to the NASA airborne radar simulation program. To generate the moving clutter databases, it was necessary to measure certain pertinent parameters. First, all of the roads, highways, and railroad lines, which are to be incorporated, must be measured and coregistered with the SAR image database. Second, all of the various statistics which characterize moving clutter must be measured or analytically derived. These statistics must describe the spatial, RCS, and velocity distributions of the moving clutter image.

CLUTTER MODELING
OF THE DENVER AIRPORT AND SURROUNDING AREAS

Moving Clutter Statistical Modeling/Analysis

- Pertinent Parameters
  - Coregistration
  - Spatial Distribution
  - RCS Distribution
  - Velocity Distribution

- Measurement/Determination of Their Values
  - Inspection of Aerial Photographs
  - NRCS Database and Literature Survey

Aerial Photographs of the Denver Stapleton Area

Aerial photographs of the Denver and Philadelphia areas were examined to establish the locations of all the roads, highways, and railroad lines incorporated in the moving clutter database. This allowed coregistration of the moving and stationary clutter databases. In addition to "mapping out" each of the roads, several other parameters were estimated based upon the examination of these aerial photos. An estimate, of the number of cars, the number of trucks, and the mean speed for each vehicle type, was calculated for each road and highway included in the map.

Based upon these measured parameters, a literature survey, and an intensive interrogation of the SAR images, a statistical model was developed for moving clutter in and around the Denver and Philadelphia airports. Using this model, a random sequence of 10,000 moving targets were generated and used in coordination with the NASA airborne radar simulation program.

DENVER STAPLETON AIRPORT

NOAA SURVEY MAPS

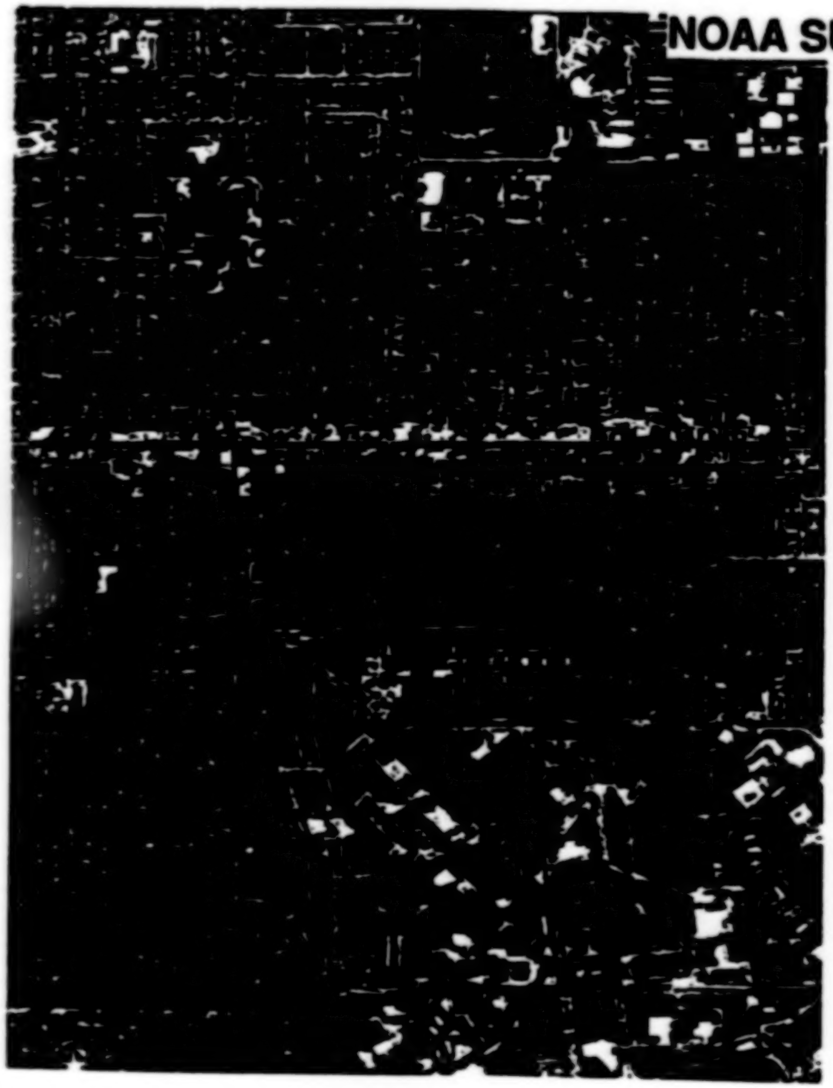

Residential

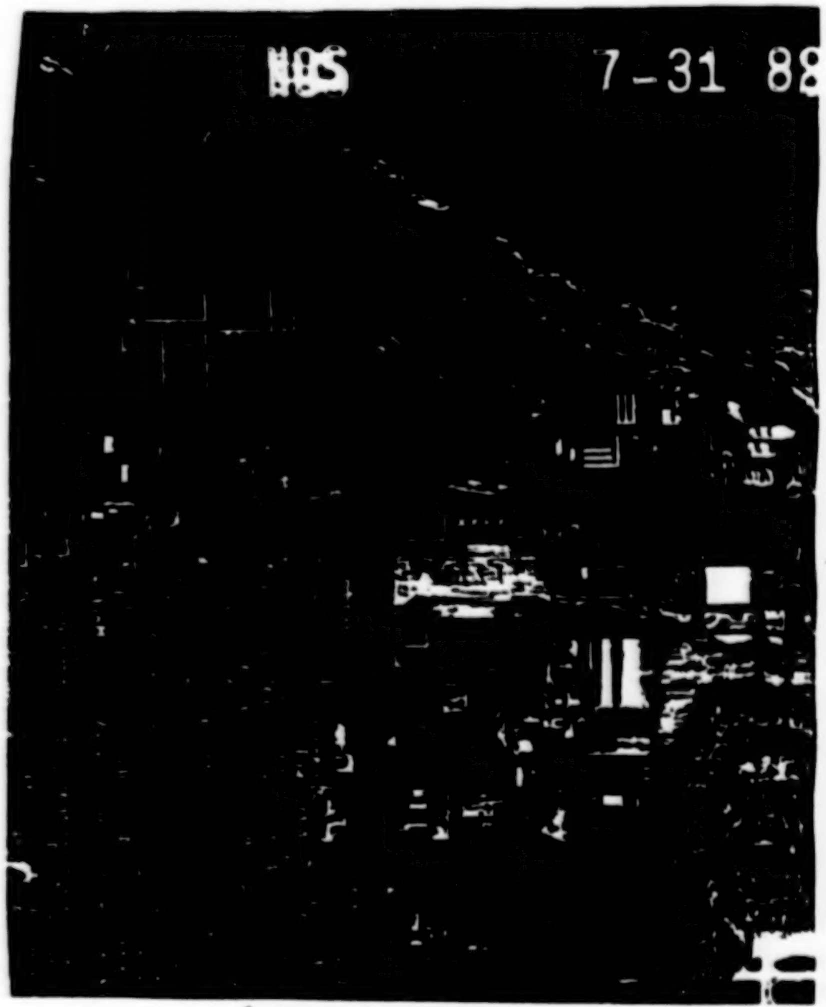

Interstate Highways
Moving Aircraft

ORIGINAL PAGE IS
OF POOR QUALITY

Denver Moving Clutter RCS Map

Shown here is a graphical view of only one of the parameters, RCS, describing the moving clutter database. It might be noted that this plot only shows a few of the major roads and highways in the Denver area. In generating a moving clutter database several parameters must be included, not just RCS. The entire parameter suite used in the simulation program includes: a spatial distribution, an RCS distribution, and a velocity distribution.

Spatial Distribution:
Using the aerial photos and extracted sequences from the SAR images, it was determined that most traffic is distributed uniformly over small stretches of highway. Using the estimated density of cars and trucks for a specific section of highway, a uniformly distributed random sequence of cars and trucks were generated along that road.

RCS Distribution:
Our moving clutter model uses log-normally distributed RCS. This is based primarily on measured observations in the ERIM SAR images of Denver, Philadelphia, and several other, archived, scenes. The RCS mean and standard deviation, respectively, used in our model for the Denver moving clutter was:

Automobiles	+4 & +2 dB
Train Cars	+10 & +2 dB

Velocity Distribution:
Based upon a literature survey, it was determined that traffic velocity primarily follows a normal distribution. An estimated speed limit, based upon the type of road, was used as the mean velocity and the standard deviation was approximately given by 10% of the mean. It should be noted that this parameter must retain a directional quality, if an accurate Doppler signature is to be generated. More simply stated, the moving clutter model must have inwardly and outwardly directed velocities with respect to the radar radial (i.e., positive and negative velocity components).

DENVER MOVING CLUTTER
RCS MAP

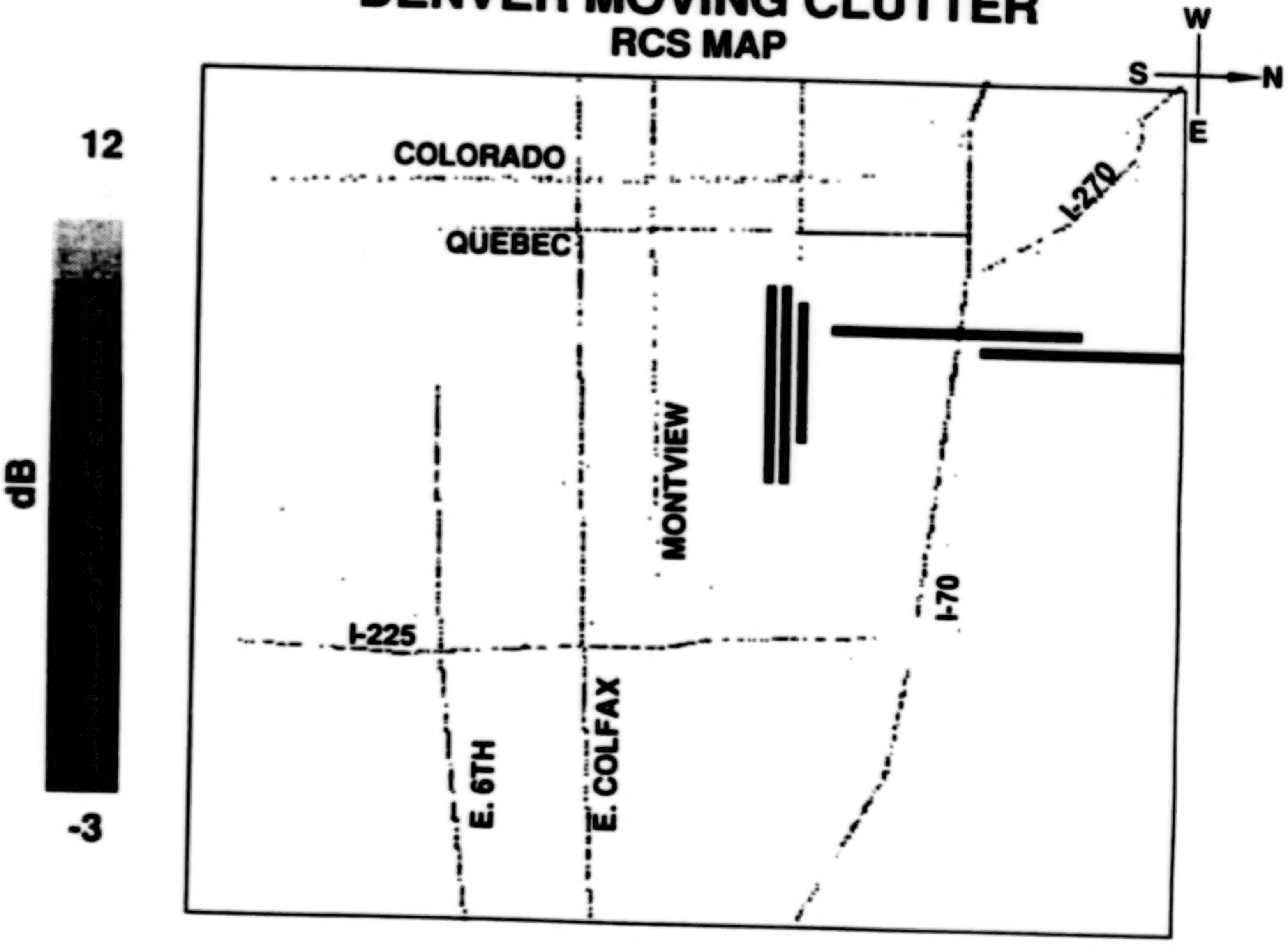
W
S
N
E
12
dB
-3
COLORADO
QUEBEC
I-270
MONTVIEW
I-70
I-225
E. 6TH
E. COLFAX

Statistical Summary of Denver Moving Clutter Database

These two histograms show a statistical summary of the RCS and velocity distributions found in the Denver moving clutter database. Note the mean and standard deviation, for each distribution, is shown at the top of each plot. These histograms represent full image statistics and are generated from over 10,000 moving targets located in the database. Also, the velocity distribution contains moving targets from both interstate highways and residential streets; thus, it is not necessarily representative of the velocity profile on a single street or highway. Note also that, the velocity distribution is in fact only representative of the magnitude of the velocities within the database. As mentioned on the previous page, for an accurate radar simulation the Doppler signature, in a given range cell, will almost always contain both positive and negative velocities (frequencies).

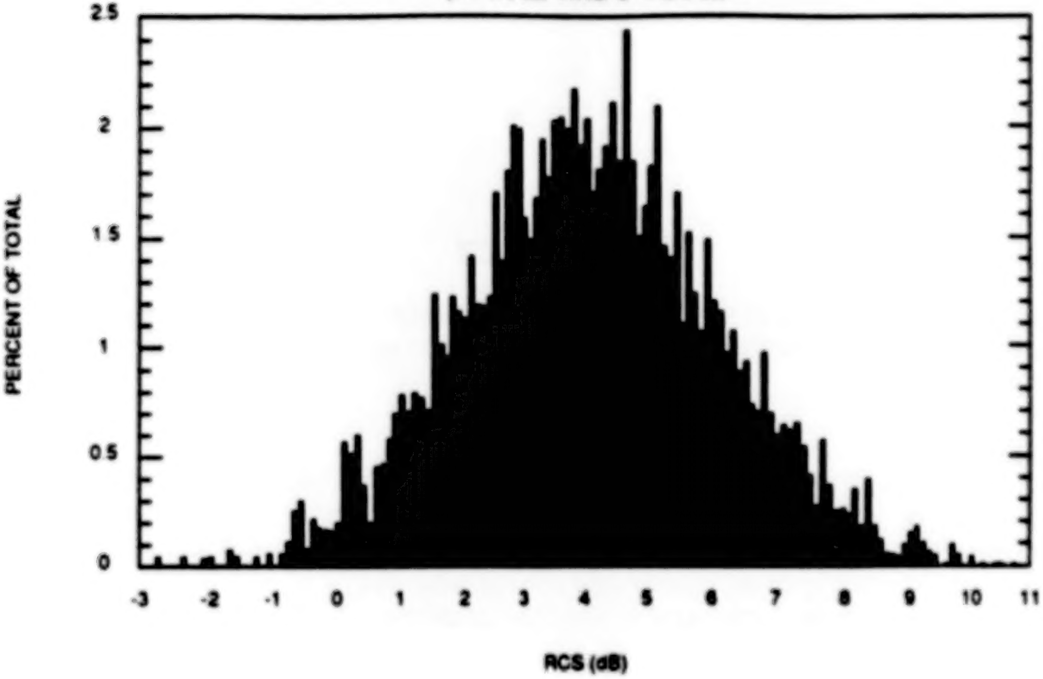

DENVER MOVING CLUTTER DATABASE
RCS DISTRIBUTION
$\mu = 4.0$ dB AND $\sigma = 2.0$ dB

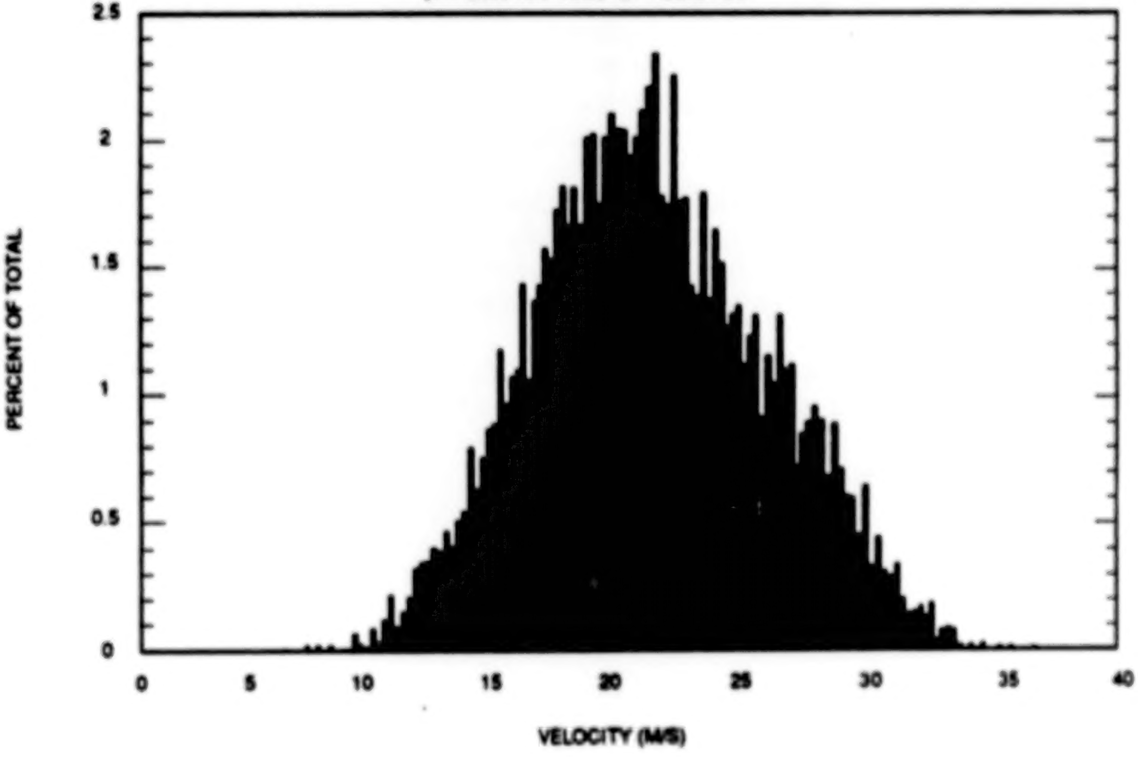

DENVER MOVING CLUTTER DATABASE
VELOCITY DISTRIBUTION
$\mu = 29.6$ m/s AND $\sigma = 23.6$ m/s

Summary

In summary, the benefits of this research can be separated into two categories, general "scientific" knowledge and wind shear radar specific "engineering" information.

Scientific Benefits:
To my knowledge, this data represents the first, non-classified, consistent, very high incidence angle, NRCS ground clutter measurements. Additionally, since the measurements were obtained using a fully polarimetric, high resolution SAR, the NRCS levels in each ground clutter cell are representative of nearly homogeneous scatterers. This allows a measure of the true polarimetric properties of a single particular scatterer.

Engineering Benefits:
Information from these analyses have helped in producing design considerations for the NASA Wind Shear Radar. A few of these are: the need for HH and VV polarization capability to further study polarization and clutter suppression techniques, identification of man-made targets as the only major source of large radar cross section has help in lowering the fear of perpetual radar receiver saturation, and mountain clutter should not produce a significant second-go-around clutter signal thus reducing the necessity for special hardware and software processing algorithms.

Also the incorporation of realistic, high incidence angle, stationary and moving ground clutter data, into the simulation program has lessened the need for modelling. Which can only improve the accuracy and increase the realistic performance of the backbone of this program, the NASA airborne Doppler radar simulation program.

I would like to take this opportunity to remind everyone that, any of this data can be made available, on a wide variety of media and formats, by contacting:
E. M. Bracalente, V. E. Delnore, or S. D. Harrah
NASA Langley Research Center.

CLUTTER MODELING
OF THE DENVER AIRPORT AND SURROUNDING AREAS

Summary

- **Scientific Benefits (Modeling Ground Clutter)**
  - Consistent High Incidence Angle NRCS Ground Clutter Measurements
  - High Resolution Allows for Isolation of Constituent Scatterers
  - Complete Polarimetric NRCS Measurements Recorded Simultaneously

- **Engineering Benefits (Wind Shear Radar Development)**
  - **Hardware/System Design**
    - Some Polarization Sensitivity
    - Man-made Targets are the Only Sources of Large NRCS Clutter
    - Mountain Clutter will Produce Little Effect
  - **Simulation Program**
    - Realistic High Incidence Angle Ground Clutter
    - Enabled the Addition of Moving Clutter

Clutter Modeling of the Denver Airport and Surrounding Areas
Questions and Answers

Q: BRUCE MATTHEWS (Westinghouse) - NASA is and has been collecting an impressive amount and breadth of clutter data. Does this data conform to expectations as available from the literature?

A: STEVE HARRAH (NASA Langley) - I guess the answer is yes in that what we can compare it with we do get good agreement. However, there is a disparity in the models for very high incidence angle radar cross sections of different ground clutter types. With that in mind one has to be careful in just saying yes we agree with literature because literature states two or three different answers. We picked the right one.

Q: BRUCE MATTHEWS (Westinghouse) - Analytic models of various classes of scatterers, such as grass, forests, etc., as functions of grazing angle, wave length, etc. exist and can serve adequately in many, perhaps not all, purposes. Why has NASA chosen an empirical data bank approach rather than connected patches of analytic models?

A: STEVE HARRAH (NASA Langley) - First of all there is some disparity or disagreement among the different models. Secondly and possibly even more importantly, we're trying to account for all of the interactions between, say, cars, trees, grass and different things that one would actually see in the actual operation of a radar. If you simply associate a certain ground patch with grass and another with cars, you can get back the right cross section for each one of them, if they were individual and isolated, but not necessarily show the effect of trees on cars or cars on trees and so forth. So, you don't get all the multipath and all the complicated scattering that would go on if you simply use a analytic approach. From that standpoint the empirical does give us a very realistic look or interpretation of the data, what's actually on the ground. Secondly, the ground areas that we've been looking at are on the order of 10s of kilometers in both down range and cross range direction. It's very difficult to model that amount of data.

EMEDIO BRACALENTE (NASA Langley) - I want to add just some more to that question. Of course one of the things we were primarily concerned about was the urban type clutter around airports and the analytic models associated with buildings, urban environments, and the automobiles along the highways, at grazing angles or low depression or high incidence angles. This is not covered very much in the literature and very difficult to develop analytically. So we felt the only way to really be able to develop a high resolution small area set of individual scatterers representative of urban clutter was to actually take real data and form map, so that when you look at it with a full aperture antenna you sort of collect up a set of multiple scatterers within your beam that are representative of what the radar might see when it was looking at an actual urban clutter environment. That was probably one of the main reasons why we went out empirically rather than trying to do it analytically. In fact we had some effort under way looking at it analytically and it became pretty complicated and difficult to model every little patch in that way because of the lack of data.

Session X. Airborne Doppler Radar / NASA

Radar Simulation Program Up-grade & Algorithm Development
Charles Britt, RTI

N91-24153

RADAR SIMULATION PROGRAM UPGRADE & ALGORITHM DEVELOPMENT

CHARLES L. BRITT, PH.D

Research Triangle Institute
610 Thimble Shoals Blvd.
Suite 203B
Newport News, VA 23606

NASA Contract NAS1-18925

October 18, 1990

Radar Simulation

This is a block diagram of the NASA Radar Simulation program which was discussed extensively at the previous meeting. The radar simulation program is a comprehensive calculation of the expected output of an airborne coherent pulse Doppler Radar system viewing a low level microburst along or near the approach path. Inputs to the program include the radar system parameters and data files that contain the characteristics of the microbursts to be simulated, the ground clutter map, and a discrete target data base which provides a simulation of moving ground clutter. The data bases used in the simulation have been discussed previously.

For each range bin, the simulation calculates the received signal amplitude level by integrating the product of the antenna gain pattern and the scattering source amplitude and phase of a spherical shell volume segment defined by the pulse width, radar range and ground plane intersection. A series of in-phase and quadrature pulses are generated and stored for further processing if desired. In addition, various signal processing techniques are used to derive the simulated velocity and hazard measurements and stored for use in plotting and display programs.

RADAR SIMULATION

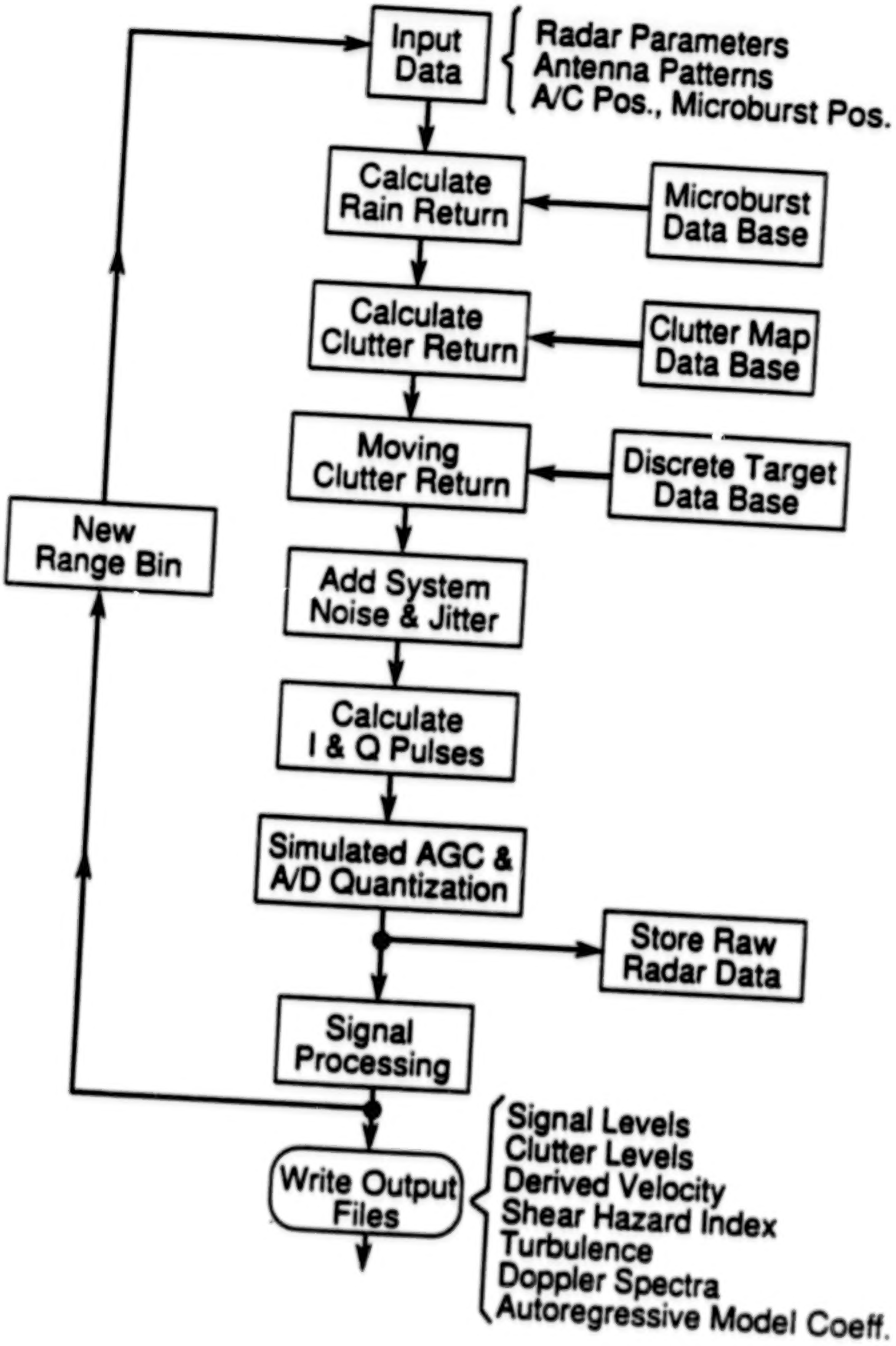

Input Data

Radar Parameters
Antenna Patterns
A/C Pos., Microburst Pos.

Calculate Rain Return

Microburst Data Base

Calculate Clutter Return

Clutter Map Data Base

Moving Clutter Return

Discrete Target Data Base

New Range Bin

Add System Noise & Jitter

Calculate I & Q Pulses

Simulated AGC & A/D Quantization

Store Raw Radar Data

Signal Processing

Write Output Files

Signal Levels
Clutter Levels
Derived Velocity
Shear Hazard Index
Turbulence
Doppler Spectra
Autoregressive Model Coeff.

Airborne Doppler Radar Detection of Microburst Windshear

This view graph shows the situation that has been simulated using the radar simulation program. An aircraft on the glide slope encounters a microburst on the path between the aircraft and the touchdown point. This situation has been selected because it provides the most severe clutter environment for the radar.

AIRBORNE DOPPLER RADAR DETECTION OF MICROBURST WINDSHEAR

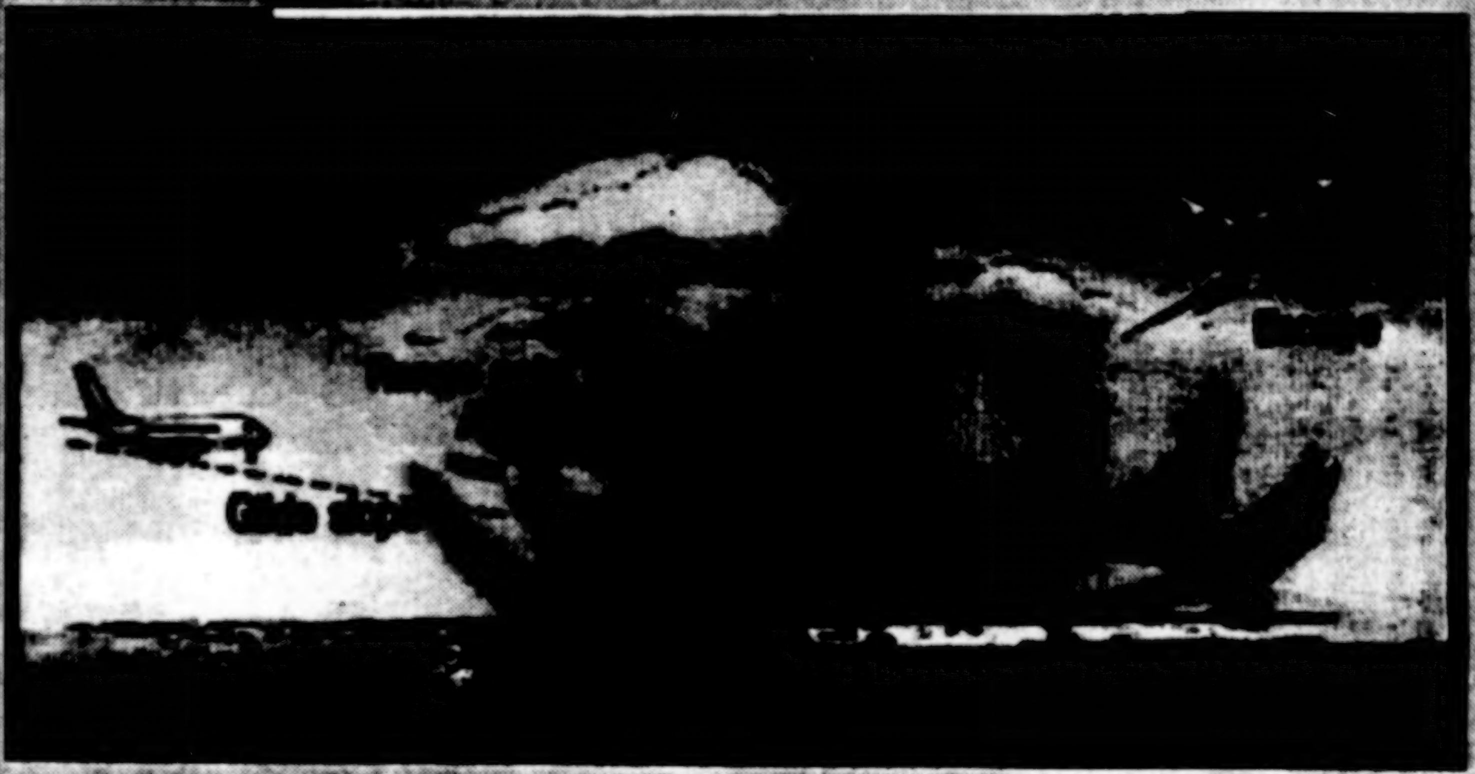
Glide slope

ORIGINAL PAGE IS
OF POOR QUALITY

Measured Wind Velocity

The following view graphs indicate examples of the outputs of the radar simulation program. View graph 3 shows the measured wind velocity plotted versus range-to-touchdown for pulse-pair and spectral average processing. In addition, the "true" wind velocity is plotted for comparison.

MEASURED WIND VELOCITY – m/s

2SIM10R,A11,YIPA,AZ=0,TILT=1,F=9.3

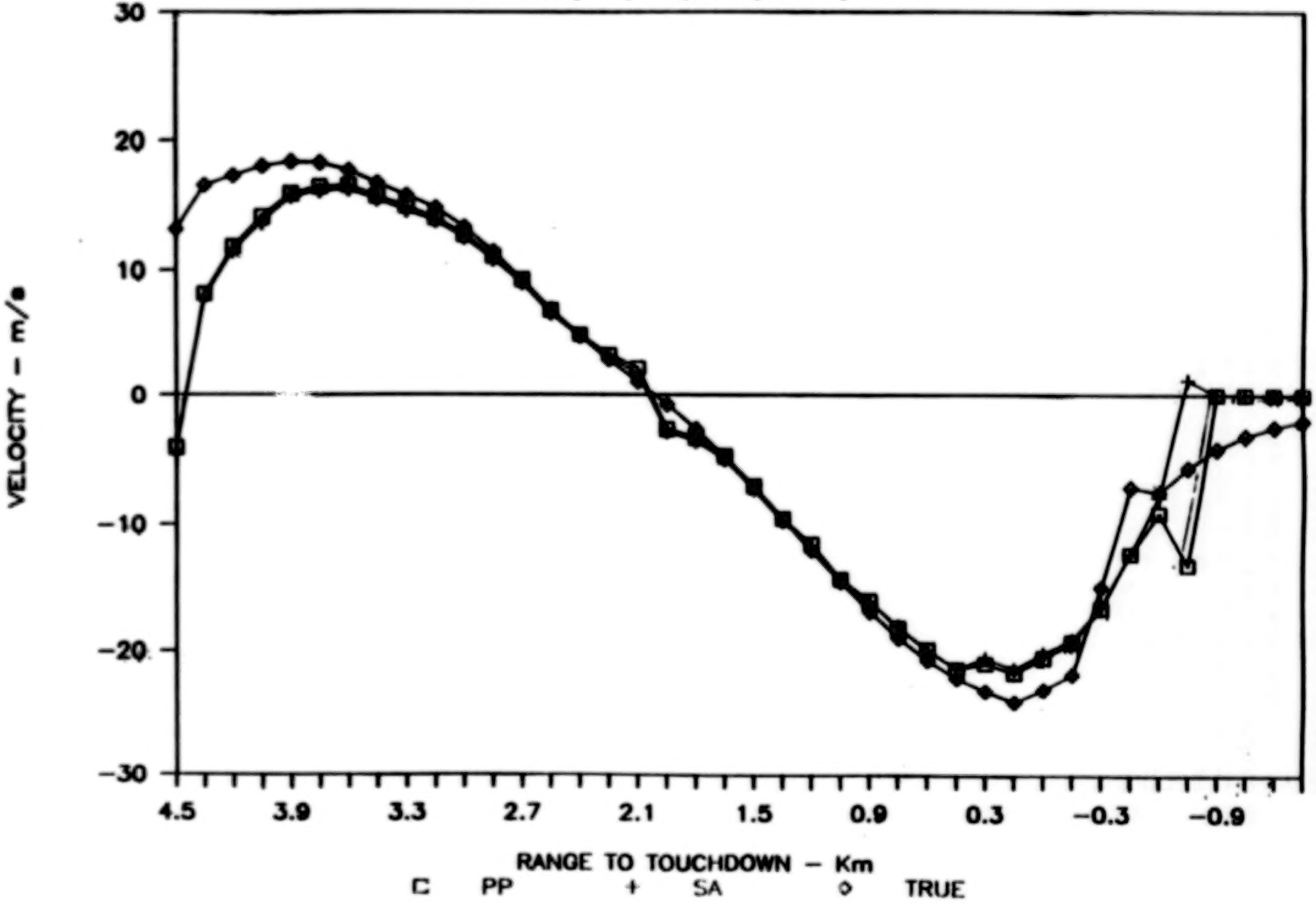

Hazard Factor Vs. Range

View Graph 4 provides another example of the simulation output. In this case the hazard factor is plotted versus range for both pulse-pair and spectral average processing. In addition, true hazard factor and the total hazard factor is plotted. The total hazard factor includes the vertical component of the hazard factor calculation (the vertical component is not measured by the radar).

HAZARD FACTOR VS. RANGE

2SIM10R,A11,YIPA,AZ=0,TILT=1,F=9.3

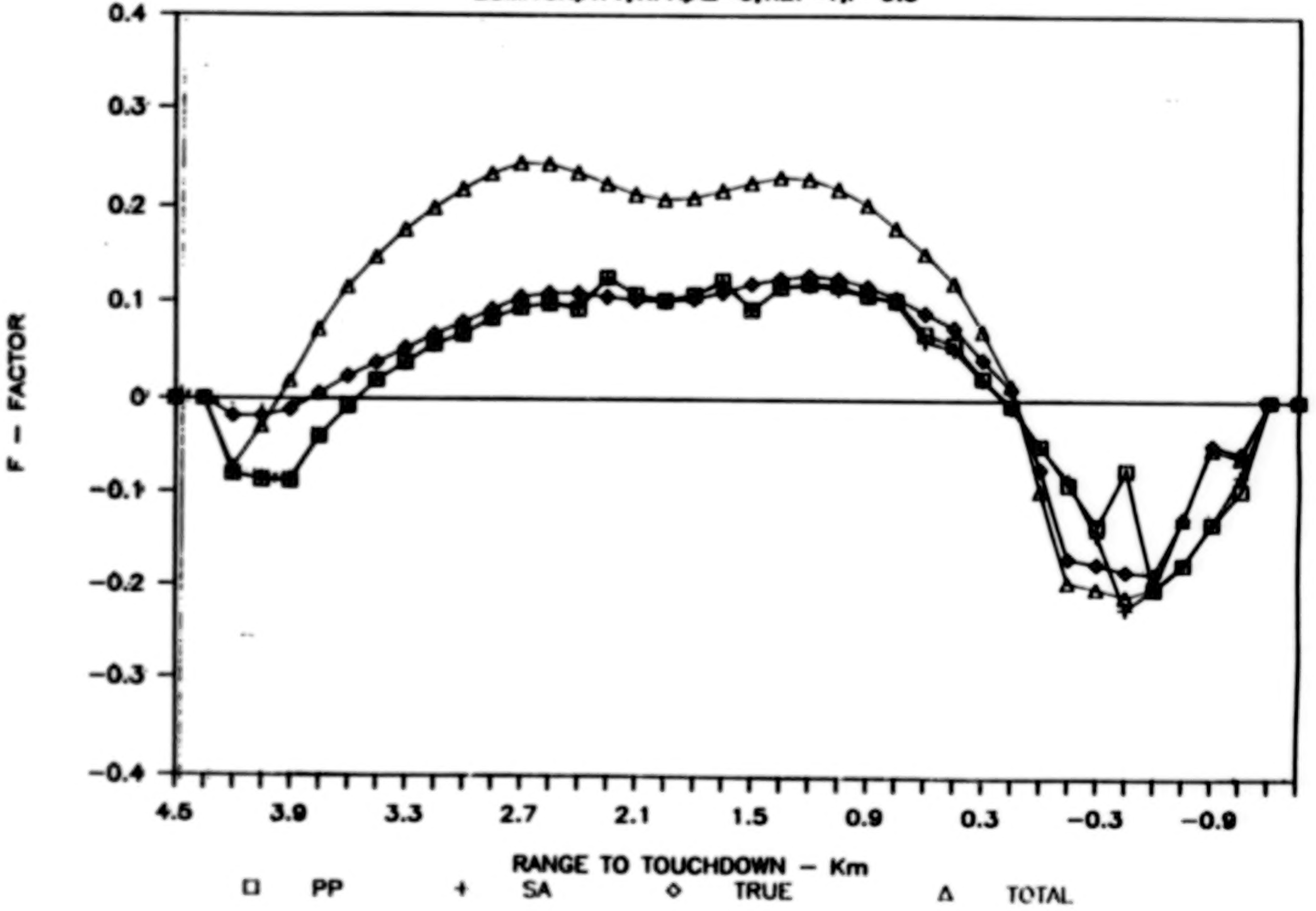

Windshear Radar Display

View Graph 5 shows the examples of simulated sector scans produced by the radar simulation program. A false color display of radar measured velocity and hazard index are shown. The hazard index display clearly shows areas in which the hazard index exceeds a given value.

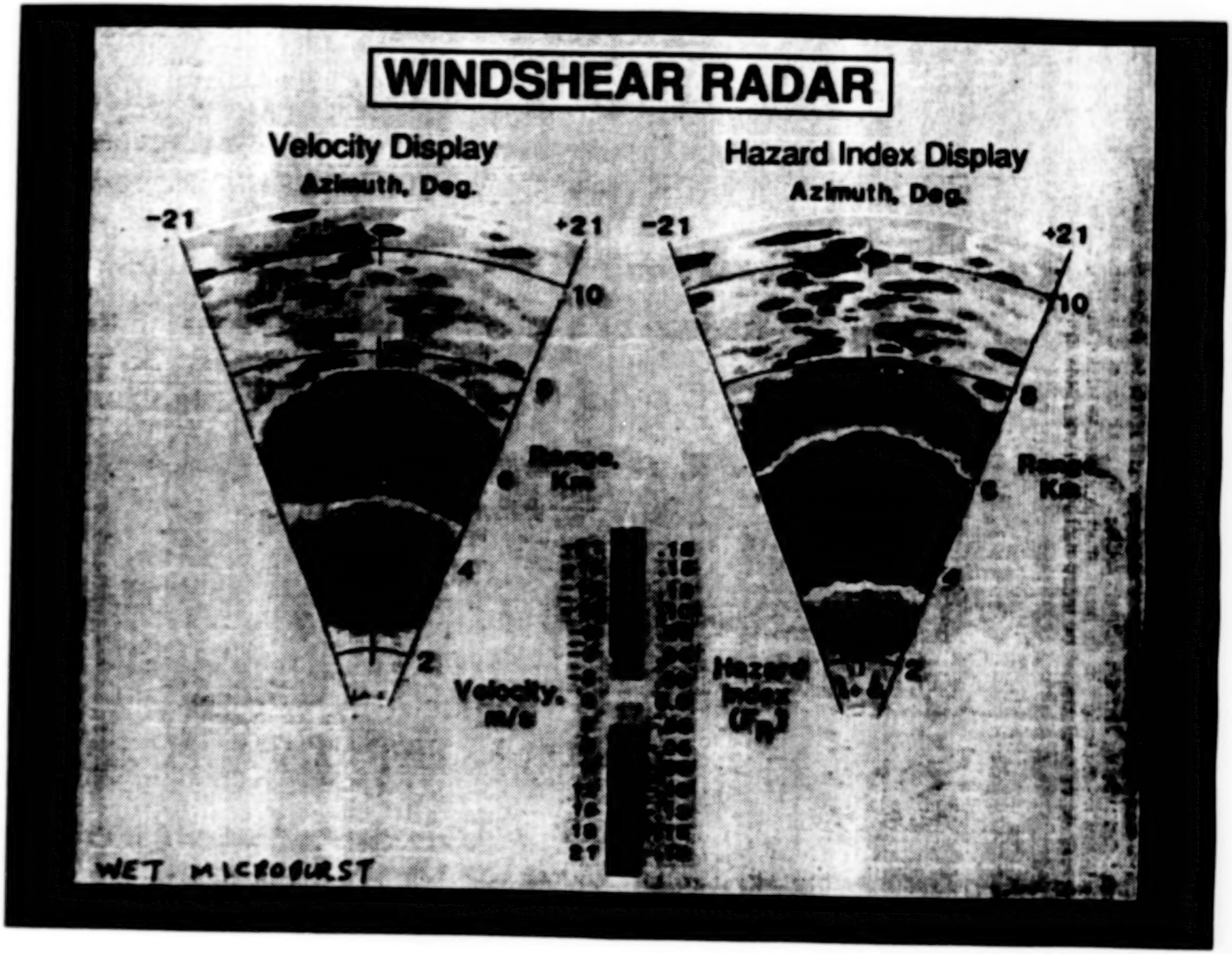

WINDSHEAR RADAR

Velocity Display
Azimuth, Deg.
−21
+21
10
8
6
4
2
Range, Km.
Velocity, m/s
Hazard Index Display
Azimuth, Deg.
−21
+21
10
8
6
4
2
Range, Km.
Hazard Index (F_h)
WET MICROBURST

ORIGINAL PAGE IS
OF POOR QUALITY

Simulation Improvements

View Graph 6 lists the major improvements to the radar simulation program that have been accomplished since the last manufacturers meeting. The major topics to be discussed in the talk include the development of the hazard detection, characterization and threat alarm algorithms and the completion of the hazard display and alarm simulation.

SIMULATION IMPROVEMENTS

- Incorporation of moving ground clutter.
- Simulation of asymmetrical (3-D) microbursts.
- Addition of simulated automatic antenna tilt control.
- Addition of autoregressive model calculations.
- Development of hazard detection, characterization and threat alarm algorithms.
- Completion of hazard display and alarm simulation.

Windshear Radar Alarm Algorithms

View graph 7 indicates the requirements that the windshear radar alarm algorithms must meet in order to provide an alarm to the aircrew. These requirements include detection, characterization of the hazard and evaluation of the threat to the aircraft.

WINDSHEAR RADAR ALARM ALGORITHMS

- Detect hazardous windshear.
- Compute location, extent and motion of hazardous area.
- Evaluate threat to aircraft and provide timely alarm.

Detection of Hazard

View graph 8 indicates the techniques and algorithms used in the simulation (and to be used in the NASA experimental weather radar) to detect a hazardous windshear situation.

DETECTION OF HAZARD

- Independent AGC for each range cell with large dynamic range.
- Range limiting.
- Antenna tilt control.
- Stationary ground clutter filter.
- Weighted least squares hazard estimation.

Weighted Least Squares Hazard Estimator

View graph 9 is a sketch indicating how the weighted least-squares hazard estimation algorithm estimates the slope of a series of velocity measurements in adjacent range bins. The slope of the velocity/range line is proportional to the horizontal component of the hazard factor. The measurements that are used to estimate the least squares line are weighted by the spectral width. It has been observed through simulation that large spectral widths are associated with measurements that contain extensive moving ground clutter and therefore may not be accurate measurements. Weighting the individual velocity measurements in this way tends to improve the estimate of the true hazard.

WEIGHTED LEAST SQUARES HAZARD ESTIMATOR

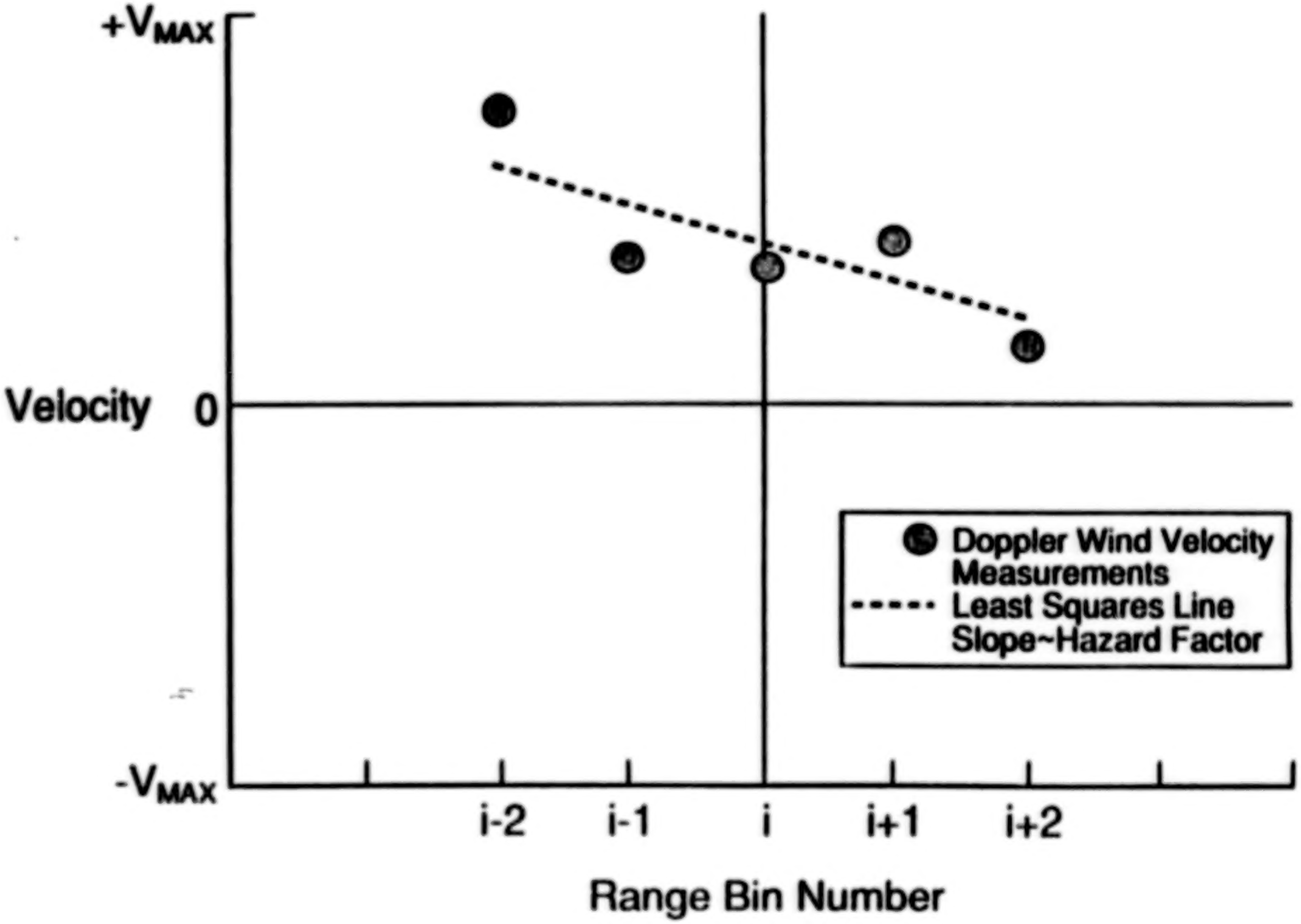

Characterization of Hazard

View Graph 10 indicates the techniques used to characterize the hazard detected by the radar. The size and the centroid of a hazardous area detected by the radar are computed and the centroid is tracked by the radar. An extensive set of track-while-scan algorithms eliminate many false hazard areas due to moving ground clutter by elimination of hazardous areas less than a threshold area and by assuring that a hazardous area exist over several radar scans. This set of algorithms tends to eliminate many false hazard areas (false alarms) due to moving and stationary ground clutter.

CHARACTERIZATION OF HAZARD

- Computation of extent and centroid of hazardous areas.
- Elimination of hazardous areas less than a threshold area.
- Centroids of hazardous areas are tracked by radar.
- Track-while-scan algorithms eliminate many false hazard areas due to moving ground clutter.

Threat Evaluation

After a hazardous area has been detected and tracked, a time-to-closest approach to the aircraft (TAU) is calculated and an alarm to the aircrew is given if the time-to-closest approach is less than a threshold value.

THREAT EVALUATION

- For each confirmed hazard area tracked, a time-to-closest approach (TAU) is calculated.
- Alarm to aircrew is given if the time-to-closest approach is less than threshold value.

Display, Tracking and Alarm Program

This is a simplified block diagram of the display, tracking and alarm program that is used to provide the map displays and simulated windshear alarms. The program uses the data generated by the radar simulation program discussed previously. The program implements the algorithms discussed.

DISPLAY, TRACKING & ALARM PROGRAM

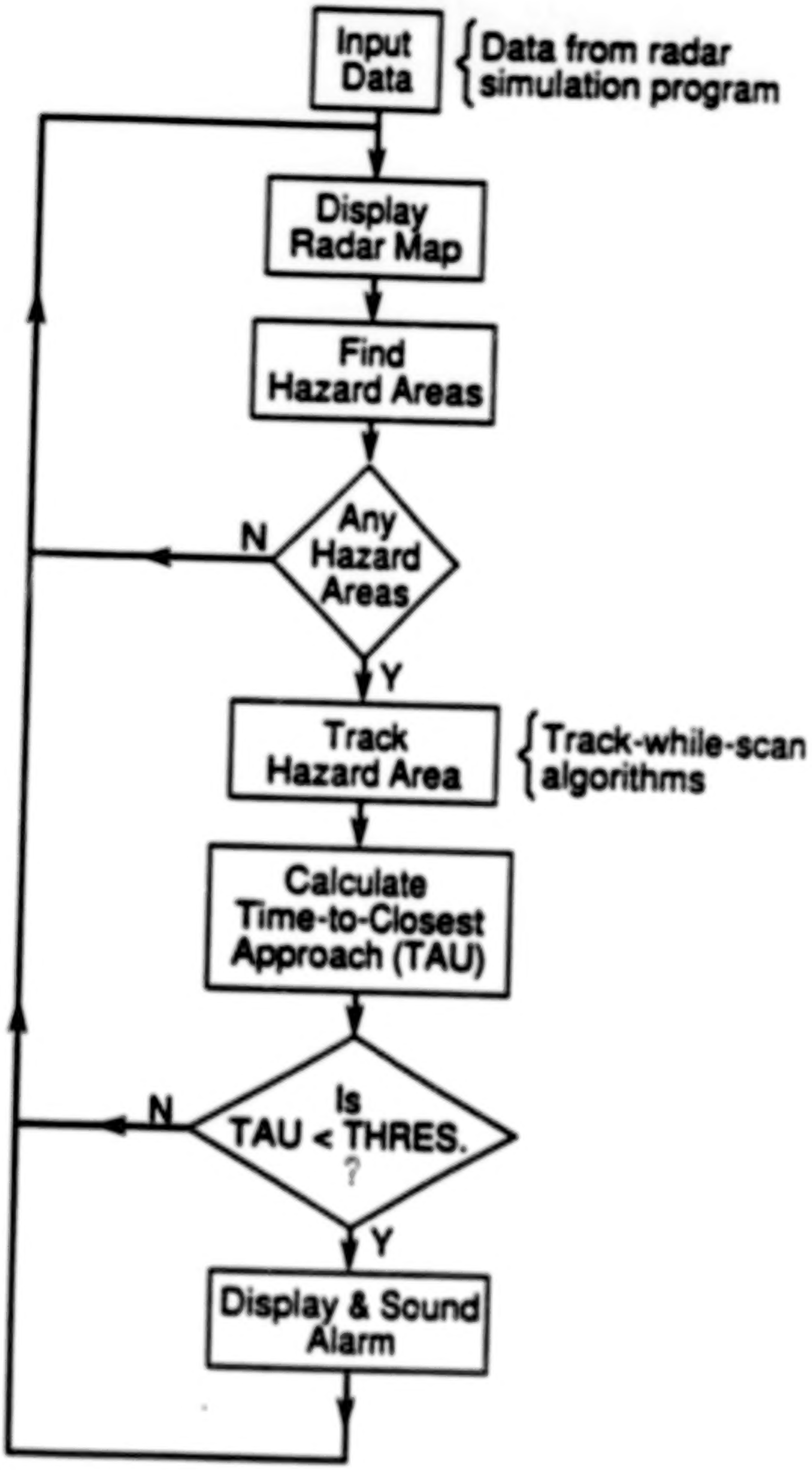
Input Data
Data from radar simulation program
Display Radar Map
Find Hazard Areas
Any Hazard Areas
N
Y
Track Hazard Area
Track-while-scan algorithms
Calculate Time-to-Closest Approach (TAU)
Is TAU < THRES. ?
N
Y
Display & Sound Alarm

Windshear Hazard Display

This is a windshear hazard display generated by the display tracking and alarm program. When all criteria have been met for a hazard alarm, "SHEAR HAZARD" is printed on the screen along with a red ball to indicate the hazard area on the map. A dynamic simulation of this hazard display will be shown on the computer monitor.

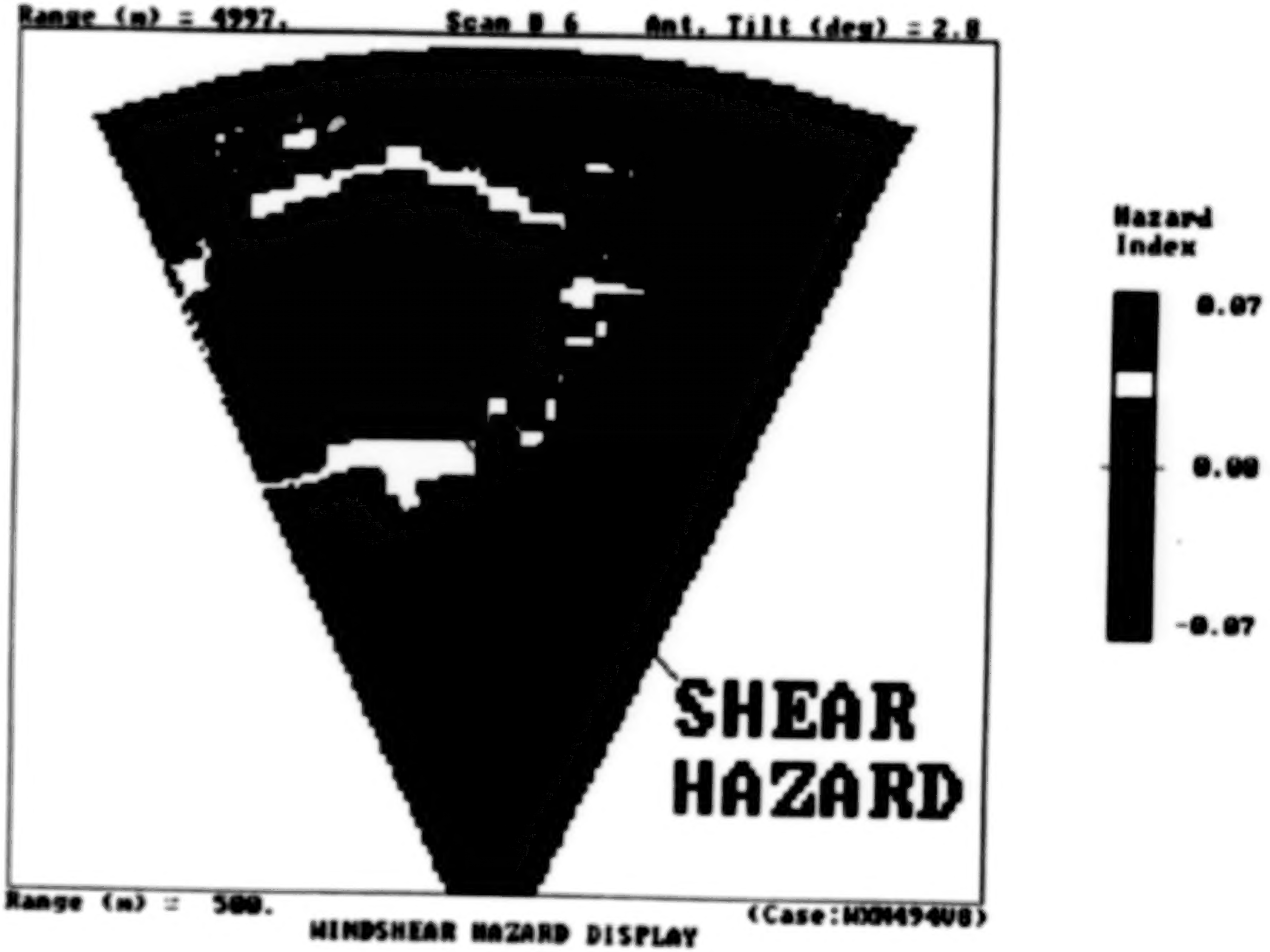
Range (m) = 4997.
Scan # 6
Ant. Tilt (deg) = 2.8
SHEAR
HAZARD
Hazard
Index
0.07
0.00
-0.07
Range (m) = 500.
(Case:HXH494U8)
WINDSHEAR HAZARD DISPLAY

Future Efforts

This view graph indicates some of the efforts that will conducted in the near future. With the development of the NASA experimental radar system it is expected that real ground clutter data will be obtained and will be used in the simulation program in place of the existing ground clutter models. Many alternate algorithms will be developed, such as auto-regressive modeling techniques, and will be investigated using the simulation program.

Additional work is being done to determine a technique for estimation of the vertical component of the hazard index and the incorporation of this component in the alarm algorithms.

FUTURE EFFORTS

- Incorporate real clutter data in simulation.
- Extensive evaluation of alternate algorithms.
- Estimate missed and false alarm performance.
- Improved models of moving and stationary ground clutter.
- Estimation of vertical component of hazard index.

Session X. Airborne Doppler Radar / NASA

N91-24154

Signal Processing Techniques for Clutter Filtering & Wind Shear Detection

Dr. Ernest Baxa, Clemson University
M. Deshpande, VIGYAN Corp.

SIGNAL PROCESSING TECHNIQUES
for
CLUTTER FILTERING
and
WINDSHEAR DETECTION

E. G. Baxa, Jr.
CLEMSON University

3rd CMTAW meeting

Radar Systems Laboratory
Electrical and Computer Engineering
Clemson University

Oct. 18, 1990

Signal Processing Techniques for Clutter Filtering and Windshear Detection

E. G. Baxa, Jr., Clemson University

ABSTRACT

It has been argued that the windshear hazard factor is a sufficient statistic for detecting hazardous windshear conditions. The hazard factor is computed by estimating the spatial gradient of windspeed across the radar sector of coverage. With the airborne Doppler radar, one approach is to use estimates of windspeed within each range resolution cell as a basis for estimating this spatial gradient. Currently, research is directed at understanding how to obtain the best possible estimate of windspeed conditions within a range cell. Conventional pulse-pair processing obtains mean estimates of windspeed. The presence of strong ground clutter in a low altitude airborne radar return can significantly bias these mean estimates. One thrust of this effort has involved use of adaptive clutter rejection filters based upon auto-regressive modelling of the ground clutter returns. This offers the potential for using very simple finite impulse response digital filters to eliminate highly specular ground clutter returns. For situations where the weather return is quite low, e.g., the "dry" microburst, clutter rejection filtering can reduce the weather return signal levels to the extent that the variance of the mean estimates is quite large. Research is involved with using mode estimates, i.e., estimates of the most probable windspeed, in each range cell in determining the hazard factor. An extended Prony algorithm is discussed. It is based upon modelling the radar return as a time series and appears to offer potential for improving hazard factor estimates in the presence of strong clutter returns.

ORIGINAL PAGE IS
OF POOR QUALITY

INTRODUCTION

- Hazard factor proportional to windspeed spatial gradient
- Windspeed gradient can be estimated using a "characteristic" windspeed estimated in each range cell

  MEAN - statistical average
  MEDIAN - middle of ordered frequency content
  MODE - most probable value

- Pulse-pair estimate is a MEAN estimator
- What are the problems with MEAN estimation?
  Are there meaningful alternatives?

PRESENTATION HIGHLIGHTS

- **MEAN** estimates can be biased in low signal-to-clutter ratio environments. Also unstable.
- Clutter rejection filtering may be counter productive in low SCR environments: reduced sensitivity, phase jitter effects
- **MODE** estimation through process modelling from IQ data may overcome problems with bias in the **MEAN** estimates
- Signal/clutter process modelling has limitations in low signal-to-noise environments

FINAL APPROACH SITUATION

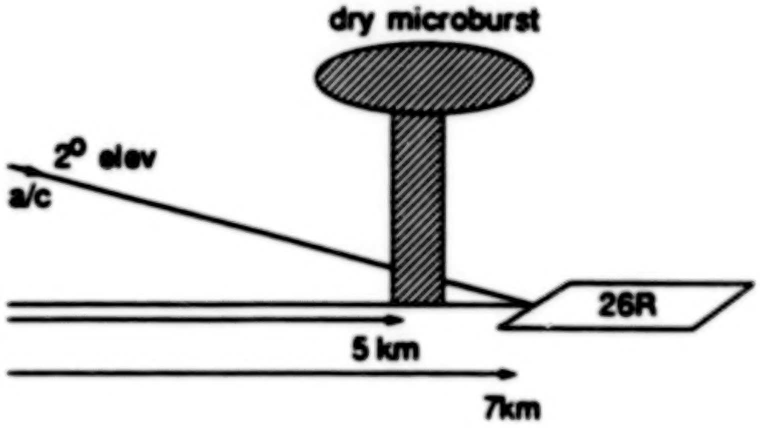

3rd CM/TAW meeting

Radar Systems Laboratory
Electrical and Computer Engineering
Clemson University

Oct. 18, 1990

Notes

Simulated final approach situation with A/C on 3 degree glideslope and radar antenna elevated 2 degrees. Dry microburst in front of Denver runway 26R.

Ground clutter return is based upon SAR data taken at Denver Stapleton airport.

Signal to clutter ratios are on the order of 0 dB in the range cells in which the microburst is present.

DRY MICROBURST

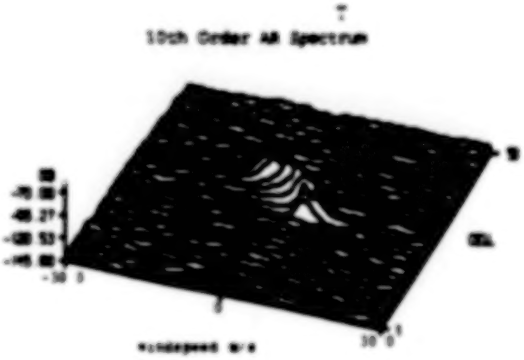

3rd CM/TAW meeting

Radar Systems Laboratory
Electrical and Computer Engineering
Clemson University

Oct. 18, 1989

Notes

Auto-regressive model determined spectrum in each of the fifty range cells with the simulated "dry" microburst without any clutter present. Signal-to-noise ratios in the range cells with the microburst varies from 0 to 30 dB.

Note: zero windspeed corresponds to zero Doppler relative to the ground speed of the aircraft. Positive windspeed corresponds to winds toward the aircraft and negative is away from the aircraft. Range cells are 150 m.

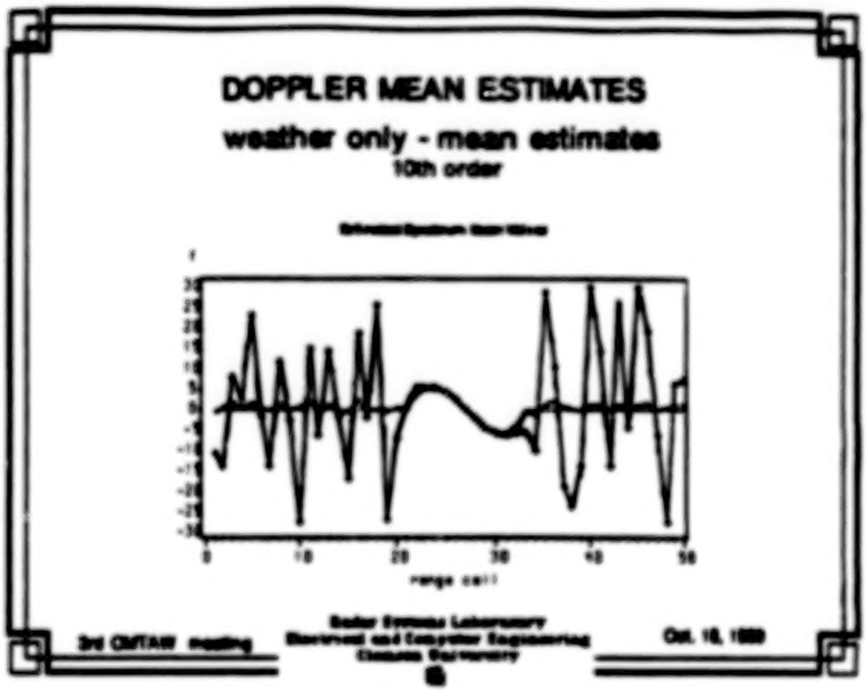

DOPPLER MEAN ESTIMATES

weather only - mean estimates

10th order

3rd CMTAW meeting

Radar Systems Laboratory
Electrical and Computer Engineering
Clemson University

Oct. 16, 1990

Notes

Mean windspeed estimates considering simulated "dry" microburst without ground clutter. Five different mean estimates are used:

1. pulse-pair computed in the time domain
2. pulse-pair computed in the frequency domain using an AR spectrum estimate
3. Fourier domain mean estimate
4. AR spectrum domain mean estimate
5. First order AR model pole estimate

Note: The microburst appears in range cells 20-33 (approximately). Some estimates of mean have been edited to zero outside this range based upon estimated signal to noise ratio in return.

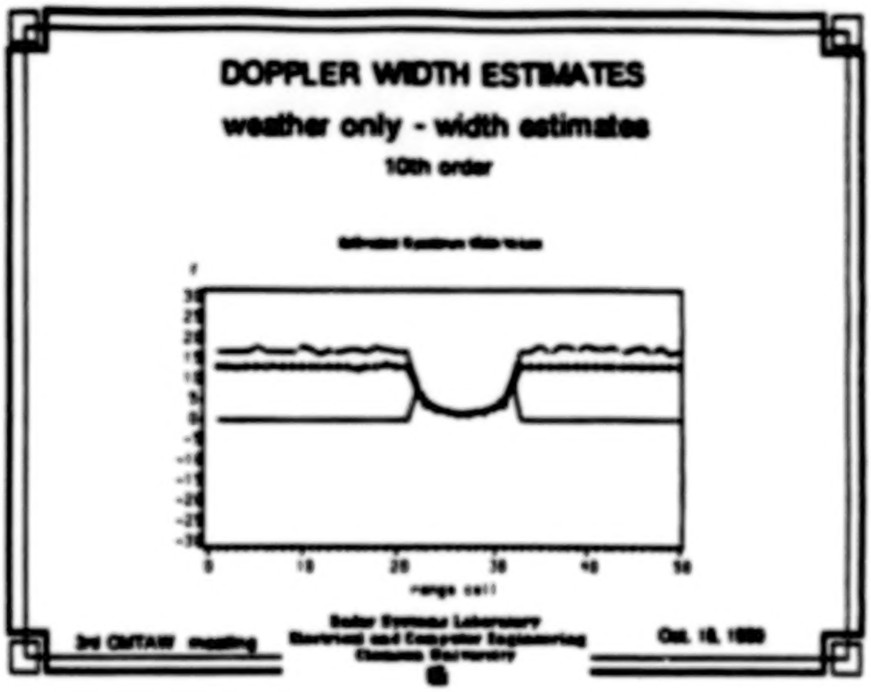

DOPPLER WIDTH ESTIMATES

weather only - width estimates

10th order

3rd CMTAW meeting

Radar Systems Laboratory
Electrical and Computer Engineering
Clemson University

Oct. 18, 1990

Notes

Width estimates for the situation in the previous slide. Four different width estimators have been used:

1. pulse-pair width computed in the time domain.
2. pulse-pair width computed in the AR spectrum frequency domain.
3. AR spectrum standard deviation
4. First order AR model coefficient

Note: Some width estimates for range cells outside those containing the microburst have been edited to zero because of low signal to noise ratio estimates.

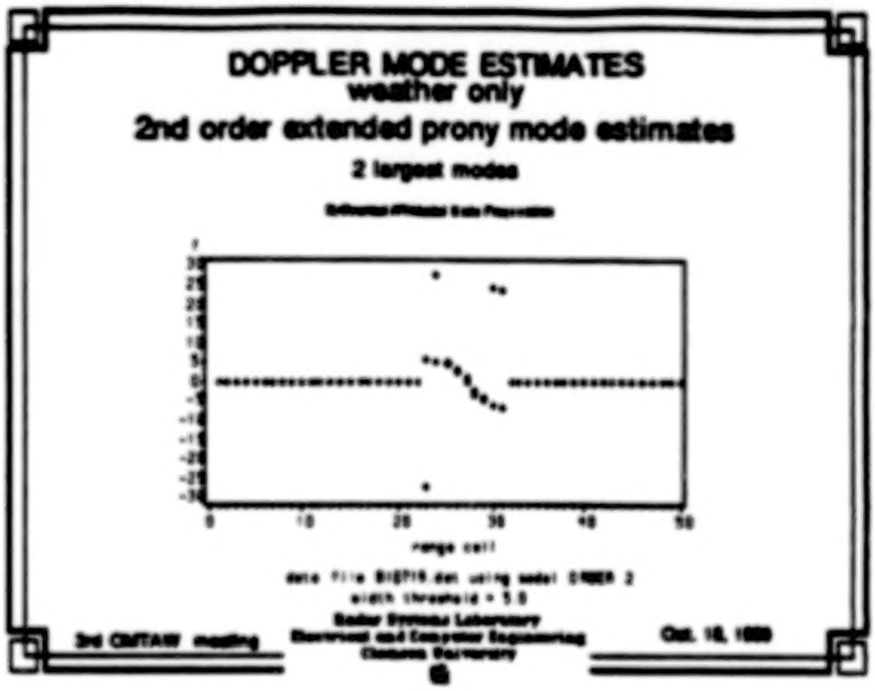

DOPPLER MODE ESTIMATES
weather only
2nd order extended prony mode estimates
2 largest modes

[illegible]

data file DIST19.dat using model ORDER 2
width threshold = 5.0

3rd CMTAW meeting

Radar Systems Laboratory
Electrical and Computer Engineering
Clemson University

Oct. 16, 1989

Notes

Spectrum mode estimates using an extended PRONY algorithm based upon a second order AR model of the data. Outliers are caused by insufficient model order.

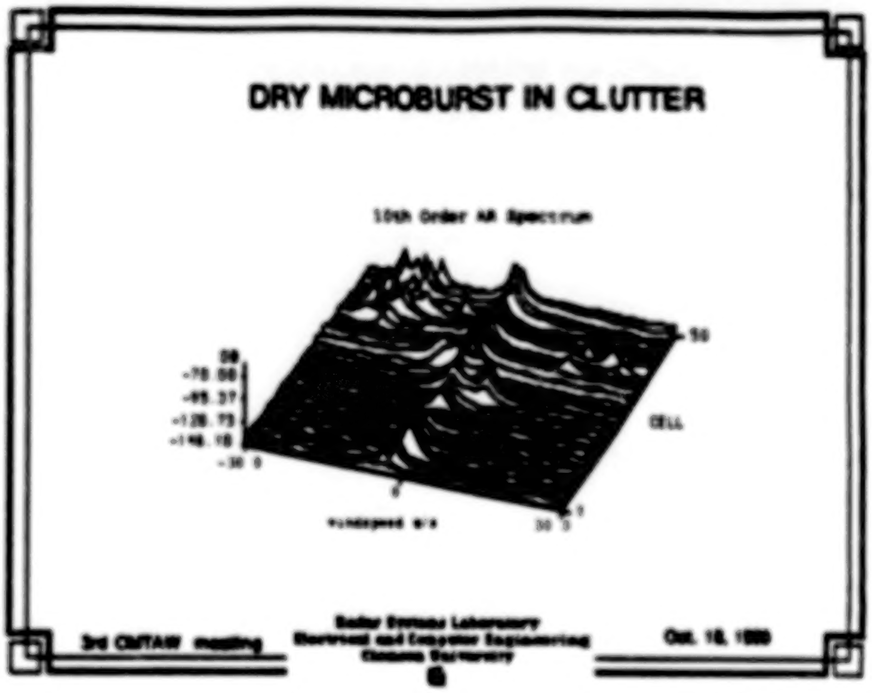

DRY MICROBURST IN CLUTTER

3rd CMTAW meeting

Radar Systems Laboratory
Electrical and Computer Engineering
Clemson University

Oct. 18, 1990

Notes

AR model determined spectrum in each of the fifty range cells with the "dry" microburst and ground clutter present in the return. No clutter rejection filtering is used. Ground clutter in the range cells 40-50 in the negative Doppler region is associated with an interstate highway included in the simulation. Signal to clutter ratios are on the order of 0 dB.

Note that the microburst can still be identified.

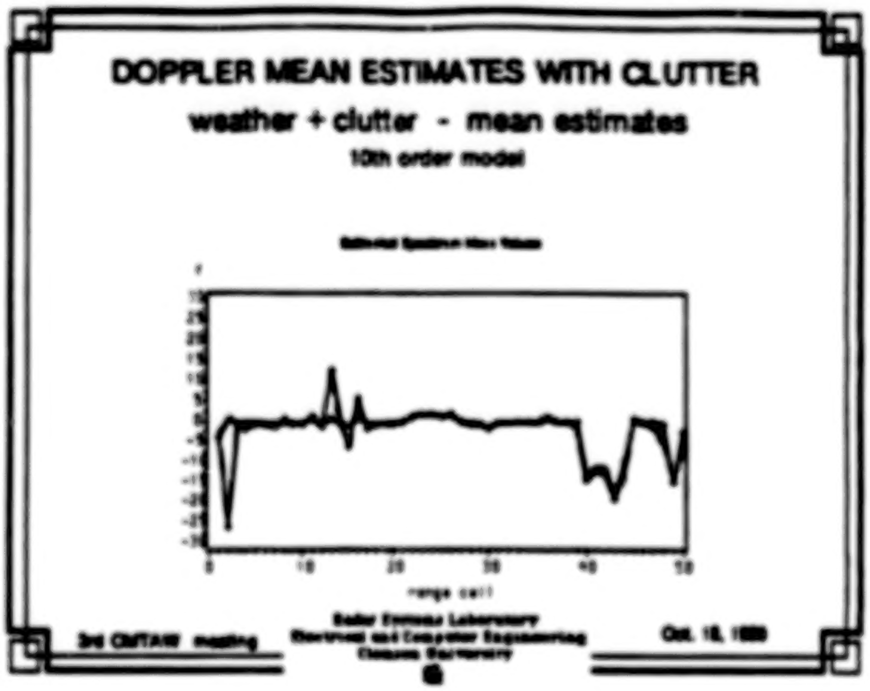

DOPPLER MEAN ESTIMATES WITH CLUTTER

weather + clutter - mean estimates

10th order model

3rd CMTAW meeting

Radar Systems Laboratory
Electrical and Computer Engineering
Clemson University

Oct. 18, 1990

Notes

Mean estimates without clutter rejection filtering for the situation depicted in the previous slide. The same five estimators used proviously are included. Again some of the mean estimates have been edited to zero based upon signal to noise ratio estimates of the return.

Note that the clutter biases the mean estimates in the range cells 20-33 so that the presence of the mocroburst is no longer evident.

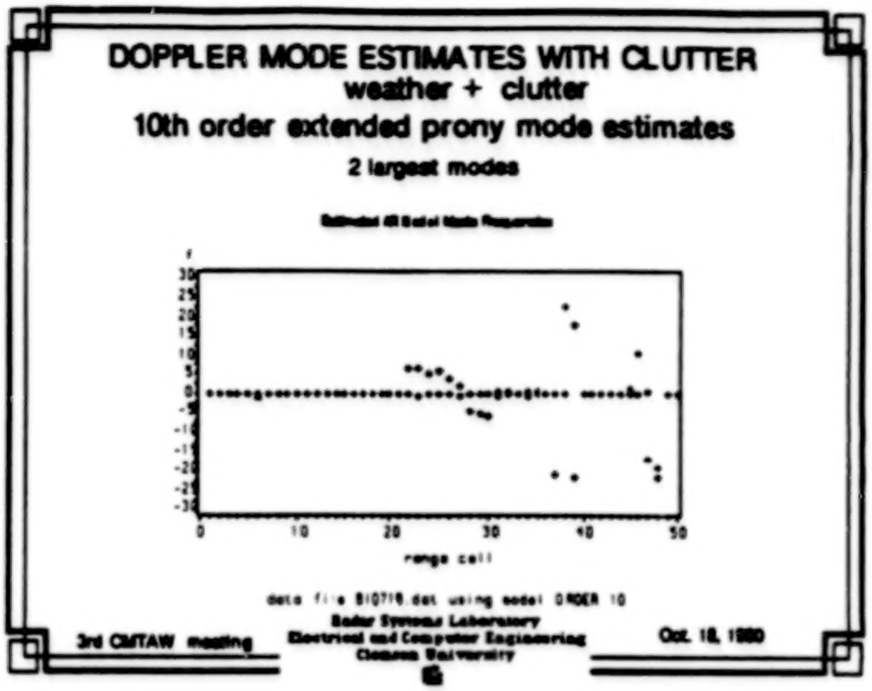

DOPPLER MODE ESTIMATES WITH CLUTTER

weather + clutter

10th order extended prony mode estimates

2 largest modes

data file 810719.dat using model ORDER 10

3rd CMTAW meeting

Radar Systems Laboratory
Electrical and Computer Engineering
Clemson University

Oct. 18, 1990

Notes

Spectrum mode estimates using an extended PRONY algorithm based upon a tenth order AR model of the data. Only the two strongest modes within each range cell are retained. Outliers are caused by the presence of discrete clutter (e.g. interstate highway)

Note that the microburst spectrum modes are clearly identifiable even though no clutter rejection filtering has been done.

DRY MICROBURST WITH OPTIMAL CLUTTER FILTER

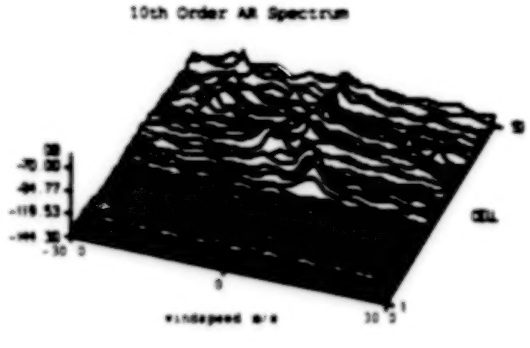

3rd CMTAW meeting

Radar Systems Laboratory
Electrical and Computer Engineering
Clemson University

Oct. 16, 1990

Notes

AR model determined spectrum in each of the fifty range cells with the radar return pre-processed with an optimum clutter rejection filter in each range cell. The filter in each range cell is based upon a tenth order AR model generated FIR filter which is adaptively determined using simulated clutter-only data for the situation depicted earlier.

Note the mocroburst is clearly present and some of the discrete clutter in later range cells is not completed eliminated.

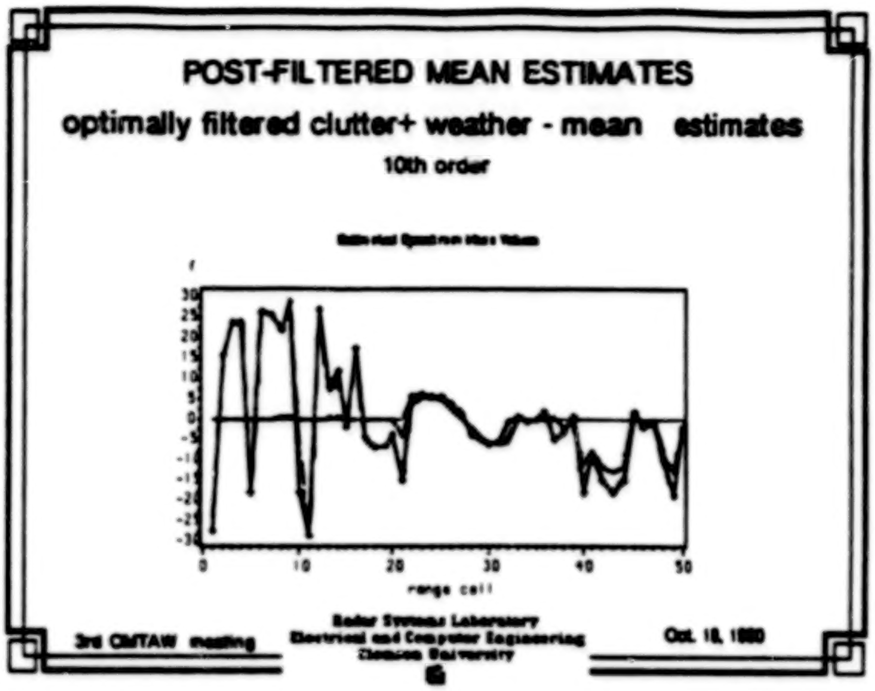

POST-FILTERED MEAN ESTIMATES

optimally filtered clutter+ weather - mean estimates

10th order

3rd CMTAW meeting

Radar Systems Laboratory
Electrical and Computer Engineering
Clemson University

Oct. 18, 1990

Notes

Mean estimates with optimum clutter rejection filtering. The same five mean estimators used previously are compared. Again some of the mean estimates have been edited to zero because of low signal to noise ratio estimates.

Note that the microburst can be clearly identified.

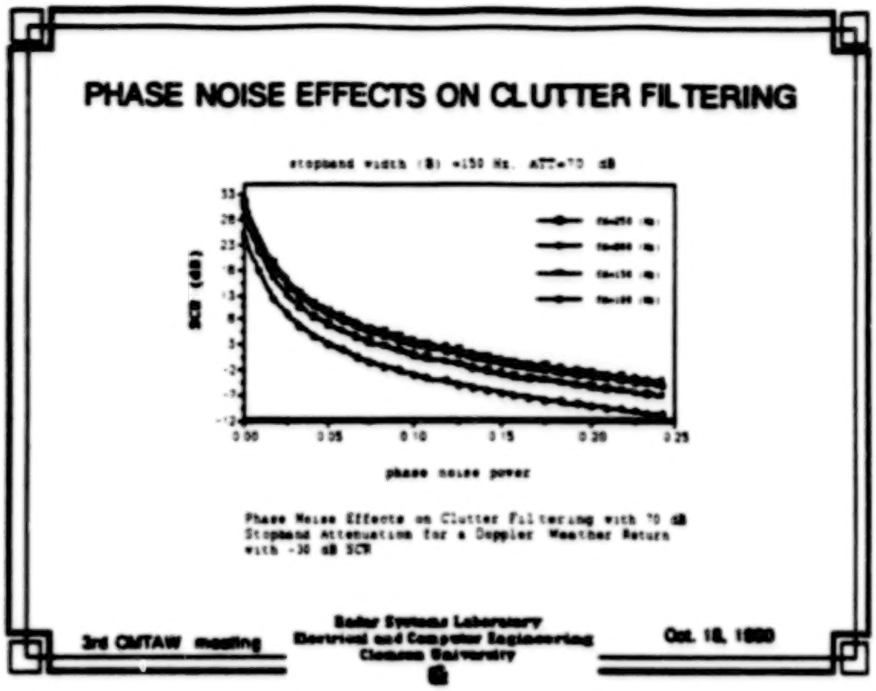

PHASE NOISE EFFECTS ON CLUTTER FILTERING

Phase Noise Effects on Clutter Filtering with 70 dB Stopband Attenuation for a Doppler Weather Return with -30 dB SCR

3rd CMTAW meeting

Radar Systems Laboratory
Electrical and Computer Engineering
Clemson University

Oct. 18, 1990

Notes

Radar system pulse-to-pulse phase jitter is analyzed in the presence of the low signal to clutter ratio situation.

Here an ideal notch filter centered at zero Doppler with a stopband width of 150 Hz and 70 dB stopband attenuation is analyzed. The prefiltered signal to clutter ratio is held to -30 dB and the weather mean Doppler is varied from 100 to 250 Hz. As the phase jitter noise is increased the clutter spectrum is spread to the point that the rejection filter will not provide enough signal to clutter ratio gain for reliable pulse pair processing.

SUMMARY

- Characterization of windspeed within a radar range resolution cell can be severely limited by ground clutter returns
- Low level weather returns will present the greatest challenge in Hazard detection
- Signal processing needs include a variety of algorithms and may require super-computer processing loads for real time implementation

3rd CMTAW meeting

Radar Systems Laboratory
Electrical and Computer Engineering
Clemson University

Oct. 18, 1990

Notes

Characterization of ground clutter returns in initial flight tests will be of paramount importance.

A suite of signal processing algorithms will be needed to improve confidence in hazard detection

Airborne radar will be important for hazard detection but should be integrated with other sensor types.

Bibliography

1. E. G. Baxa, Jr. and J. Lee, "The Measurement of Windspeed Gradient with Low PRF Radar, "Proc. Southeast. Symp. on Sys. Theory, SSST-88, Charlotte NC, March 1988.
2. J. Lee and E. G. Baxa, Jr., "Preliminary Analysis of Windshear Detection Signal Processing Considering Doppler Weather Radar," Radar Systems Laboratory TR No. 8, Research Triangle Institute subcontract 4-414U-3042 under NASA contract NAS1-17639, Clemson University, September 1988.
3. E. G. Baxa, Jr., "Resolution of the STUSE Algorithm Used in Spectrum Estimation," Radar Systems Laboratory TR No. 9, NASA grant NAG-1-928, Clemson University, December 1988.
4. J. Lee and E. G. Baxa, Jr., "Pulse-pair Spectral Estimates in the Presence of Radar Oscillator Phase Jitter," Proc. 21st Southeast. Symp. on Sys. Theory, Florida State University, Tallahassee, March 1989.
5. W. T. Davis and E. G. Baxa, Jr., "Effects of Filtering on Estimating Spectral Moments of Meteorological Doppler Spectra," Proc. 21st Southeast. Symp. on Sys. Theory, Florida State University, Tallahassee, March 1989.
6. W. T. Davis, "The Effects of Clutter-rejection Filtering on Estimating Weather Spectrum Parameters," Radar Sys. Lab. TR no.10, NASA LaRC grant NAG-1-928 and NGT-70055, Clemson University, July 1989.
7. E. G. Baxa, Jr., "On Implementation of the Discrete Fourier Transform - The STUSE Algorithm for Spectral Estimation," IEEE Trans. on Acoust., Speech, and Sig. Proc., vol. 37, no. 11, pp.1763-1765, November 1989.
8. B. M. Keel, "Adaptive Clutter Rejection Filters for Airborne Doppler Weather Radar Applied to the Detection of Low Altitude Windshear," Radar Sys. Lab. TR no.11, NASA LaRC grant NAG-1-928, Clemson University, December 1989.
9. B. M. Keel and E. G. Baxa, Jr., "Adaptive Least Square Complex Lattice Clutter Rejection Filters Applied to the Radar Detection of Low Altitude Windshear," Proc. 1990 IEEE Int. Conf. Acoust., Speech, Sig. Proc., pp.1469-1472, Albuquerque, N.M., April 1990.
10. J. Lee,"Analysis and Improved Design Considerations for Airborne Pulse Doppler Radar Signal Processing in the Detection of Hazardous Windshear," Radar Sys. Lab. TR no.12, NASA LaRC grant NAG-1-928, Clemson University, May 1990.
12. J. Lee and E. G. Baxa, Jr., "Phase Noise Effects on Turbulent Weather Radar Spectrum Parameter Estimation," Proc. 1990 IEEE Int. Radar Conf., pp.345-350, Arlington, VA, May 7-10, 1990.
13. E. G. Baxa, Jr. and J. Lee, "The Pulse Pair Algorithm as a Robust Estimator of Turbulent Weather Spectral Parameters using Airborne Pulse Doppler Radar," (submitted to IEEE Trans. on Aerspace and Elect. Sys.), September 1990.

Estimation of Radial WindSpeed

Manohar D. Deshpande
Vigyan Inc., Hampton

Estimation of Radial WindSpeed:

- From the I and Q data. the mean radial windspeed is determined using Covariance and Spectral domain approaches.
- Here we study the performance of each of these techniques under varying signal to noise ratio.

Covariance Method:

If $R(\tau)$ is the covariance function of the received sequence then the mean Doppler frequency $\hat{f}_d$ can be estimated by

$$\hat{f}_d \equiv \frac{1}{2\Pi T_r} \mathrm{Arctan}\left(\frac{\mathrm{Im.}(R(T_r)}{\mathrm{Re}(R(T_r)}\right)$$

The mean radial wind speed is then obtained as

$$\hat{v}_p = \frac{\lambda}{2} \hat{f}_d$$

PRECEDING PAGE BLANK NOT FILMED

Spectral Estimation Methods:

If $S(f)$ is the spectral density of the sequence then $\hat{f}_d$ can be estimated by using

$$\hat{f}_d = \frac{\sum_{i=-N/2}^{N/2} f_i \, S(f_i)W(f_i)}{\sum_{i=-N/2}^{N/2} S(f_i)W(f_i)}$$

where $W(f)$ is the weighting function introduced to suppress the stationary ground clutter which is centered around zero Doppler frequency.

The spectral density $S(f)$ is determined using following methods.

(1) **Periodogram Method**

(2) **Forward-Backward Linear Prediction Method**

(3) **Eigenvector method**

(4) **MUSIC Method**

The performance of these methods when the signal to noise ratio is varied between 10 dB to -5 dB.is studied

From these results it may be concluded that Covariance method under severe SNR performs better than other methods.

IGINAL PAGE IS
OF POOR QUALITY

WEATHER RADAR MODEL

VELOCITY

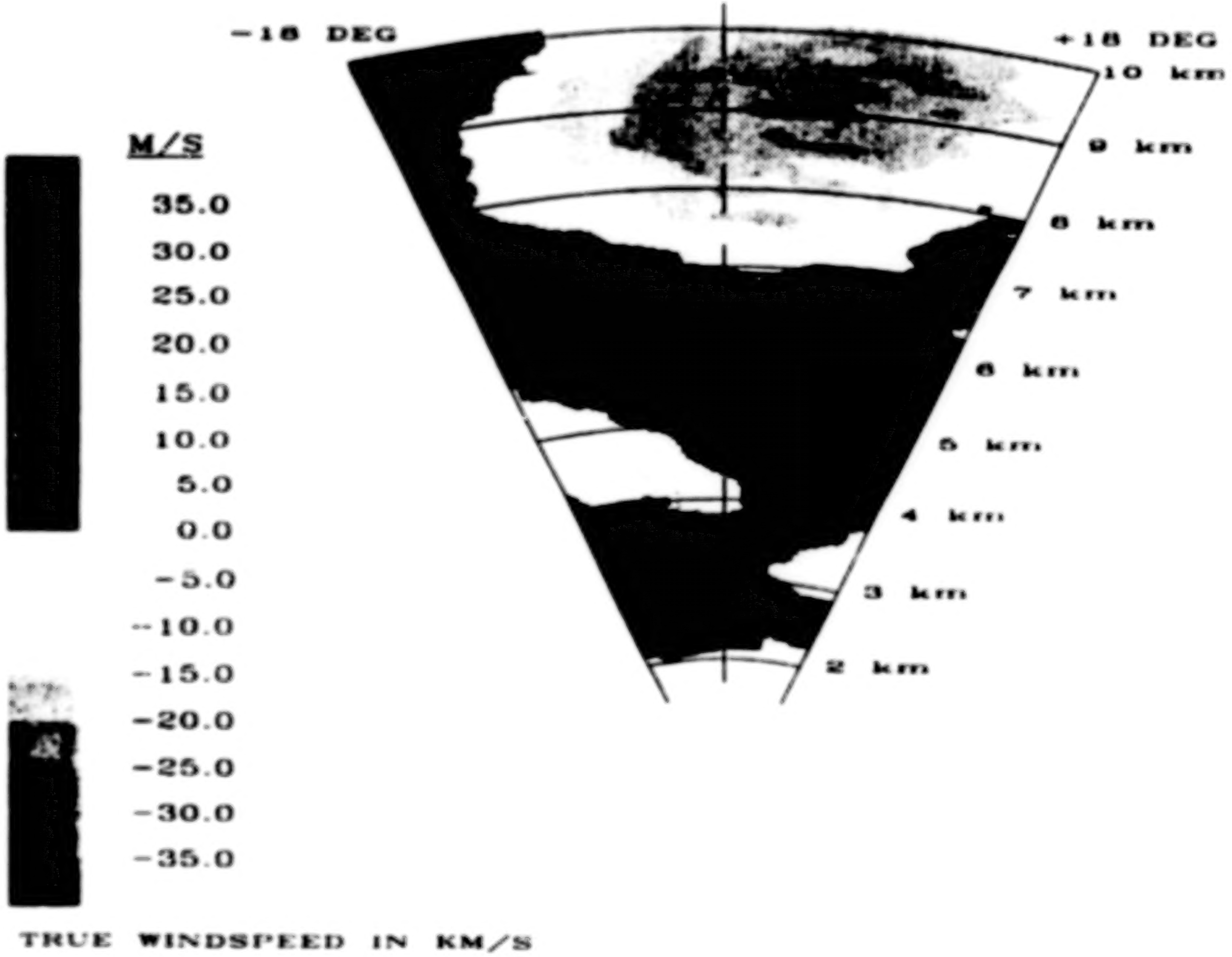

ORIGINAL PAGE IS
OF POOR QUALITY

WEATHER RADAR MODEL
VELOCITY

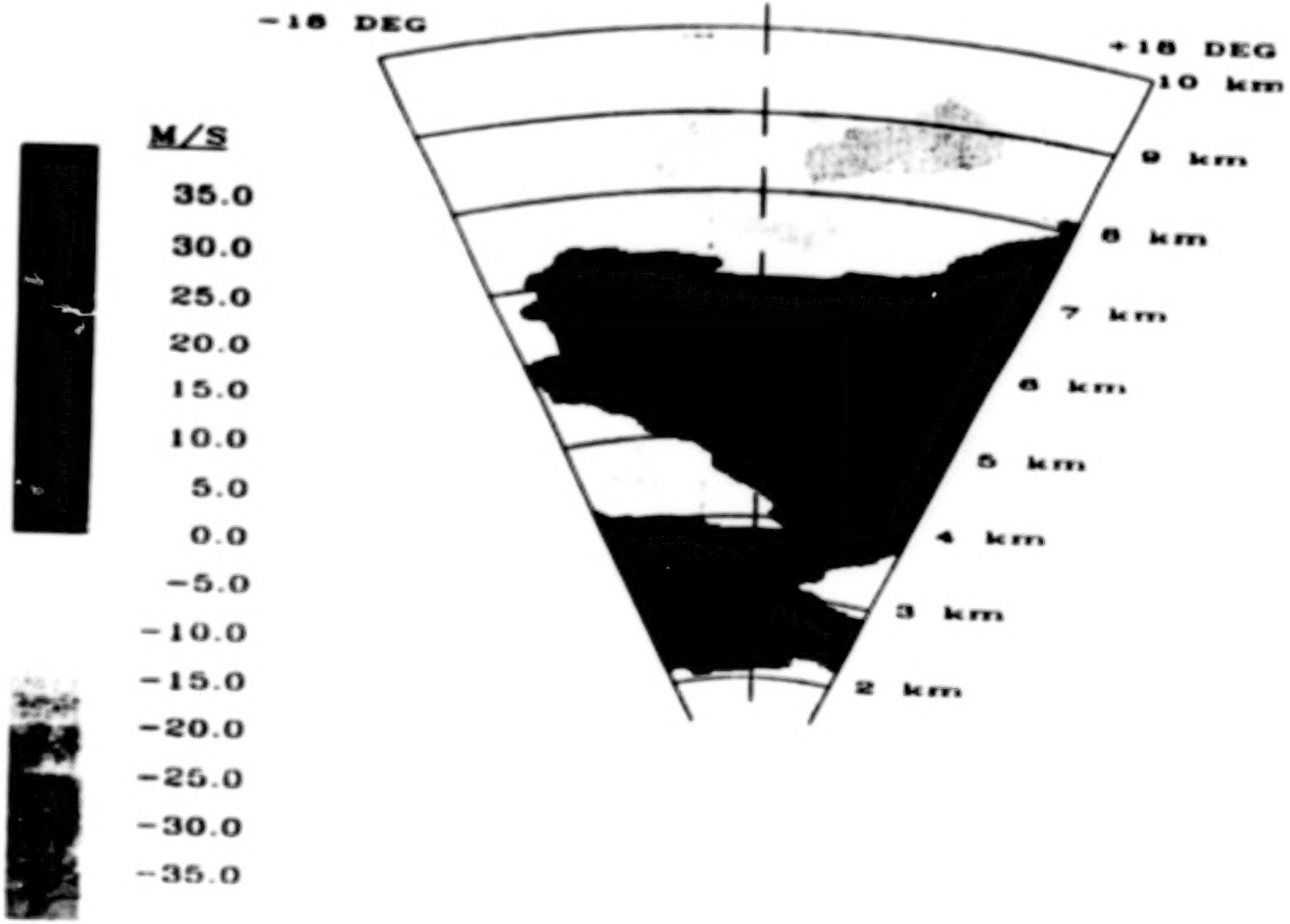

PULSE PAIR PROCESSOR METHOD (SNR=INFINITY)

ORIGINAL PAGE IS
OF POOR QUALITY

WEATHER RADAR MODEL
VELOCITY

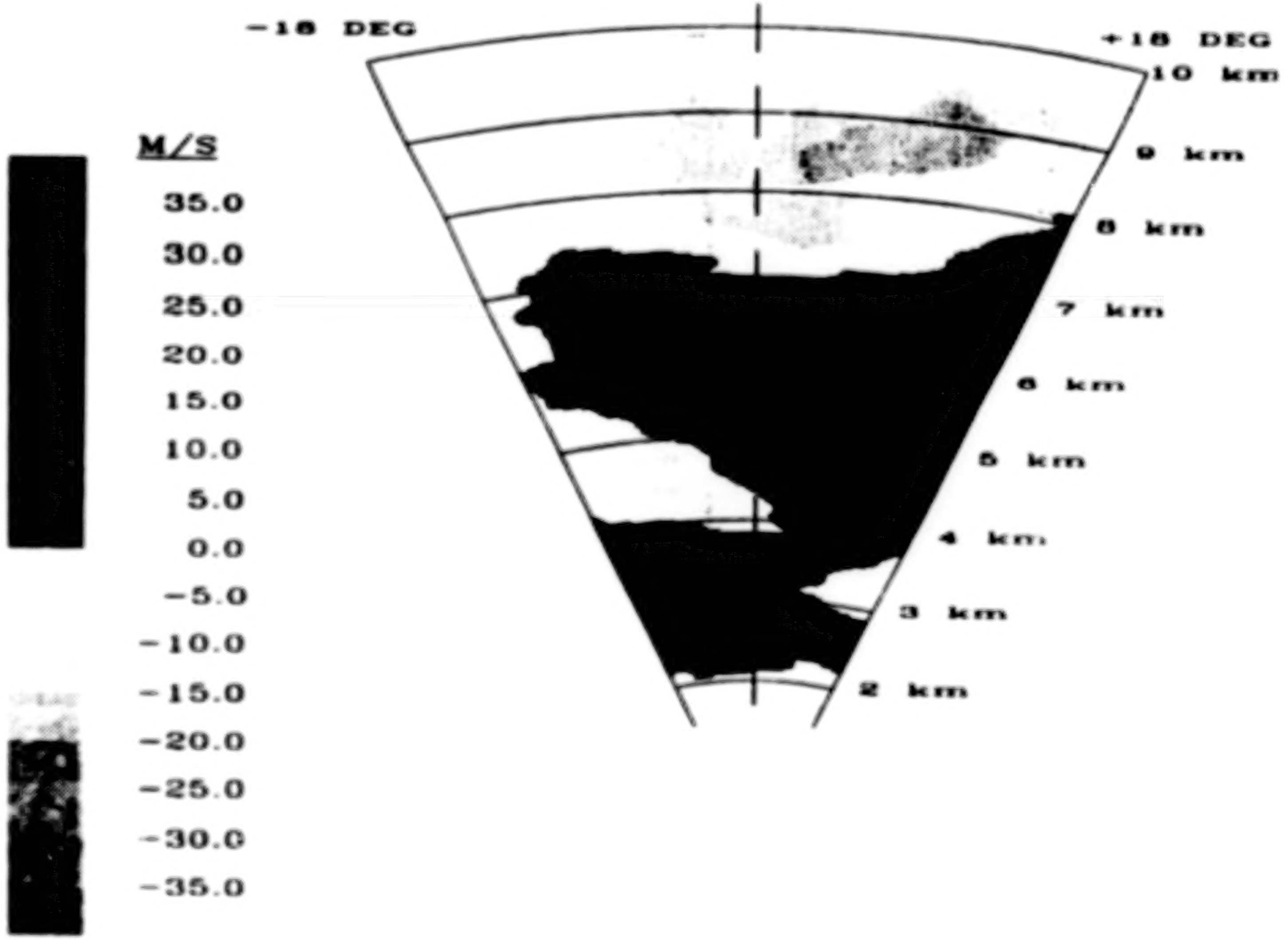

PULSE PAIR PROCESSOR (SNR=10DB)

ORIGINAL PAGE IS
OF POOR QUALITY

WEATHER RADAR MODEL

VELOCITY

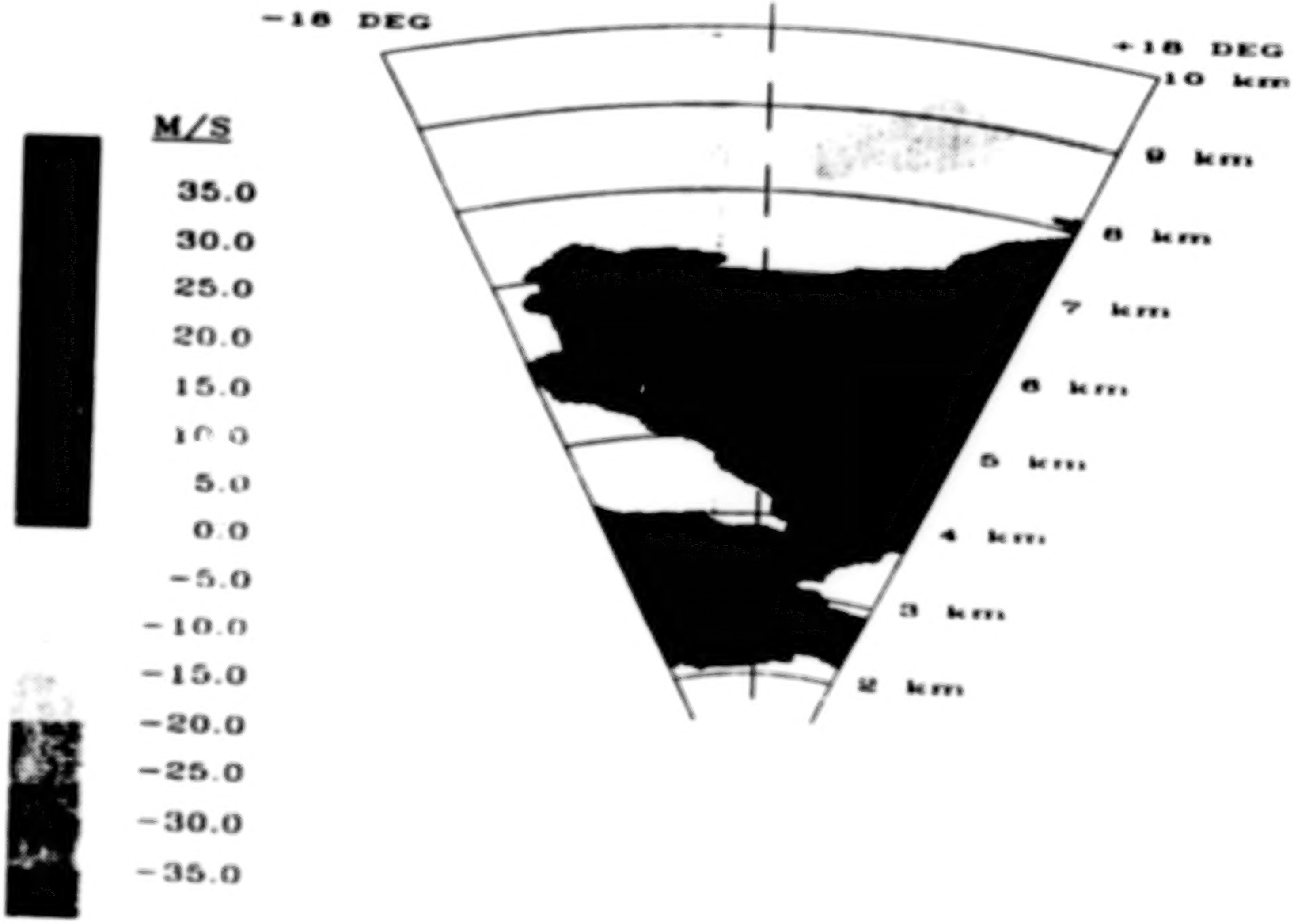

PULSE PAIR PROCESSOR (SNR=5DB)

ORIGINAL PAGE IS
OF POOR QUALITY

ORIGINAL PAGE IS
OF POOR QUALITY

C-5

WEATHER RADAR MODEL
VELOCITY

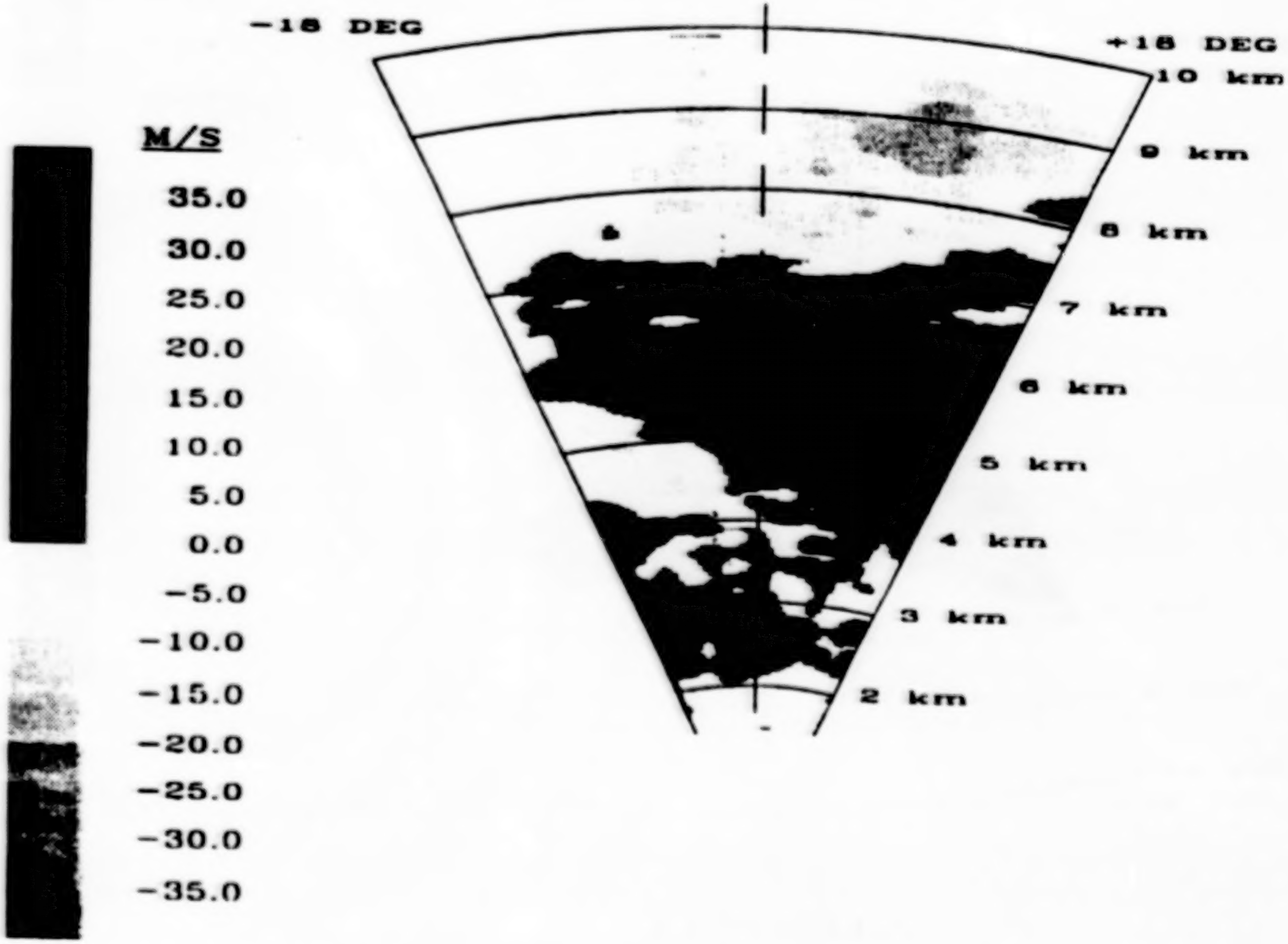

PULSE PAIR PROCESSOR (SNR=−5DB)

WEATHER RADAR MODEL
VELOCITY

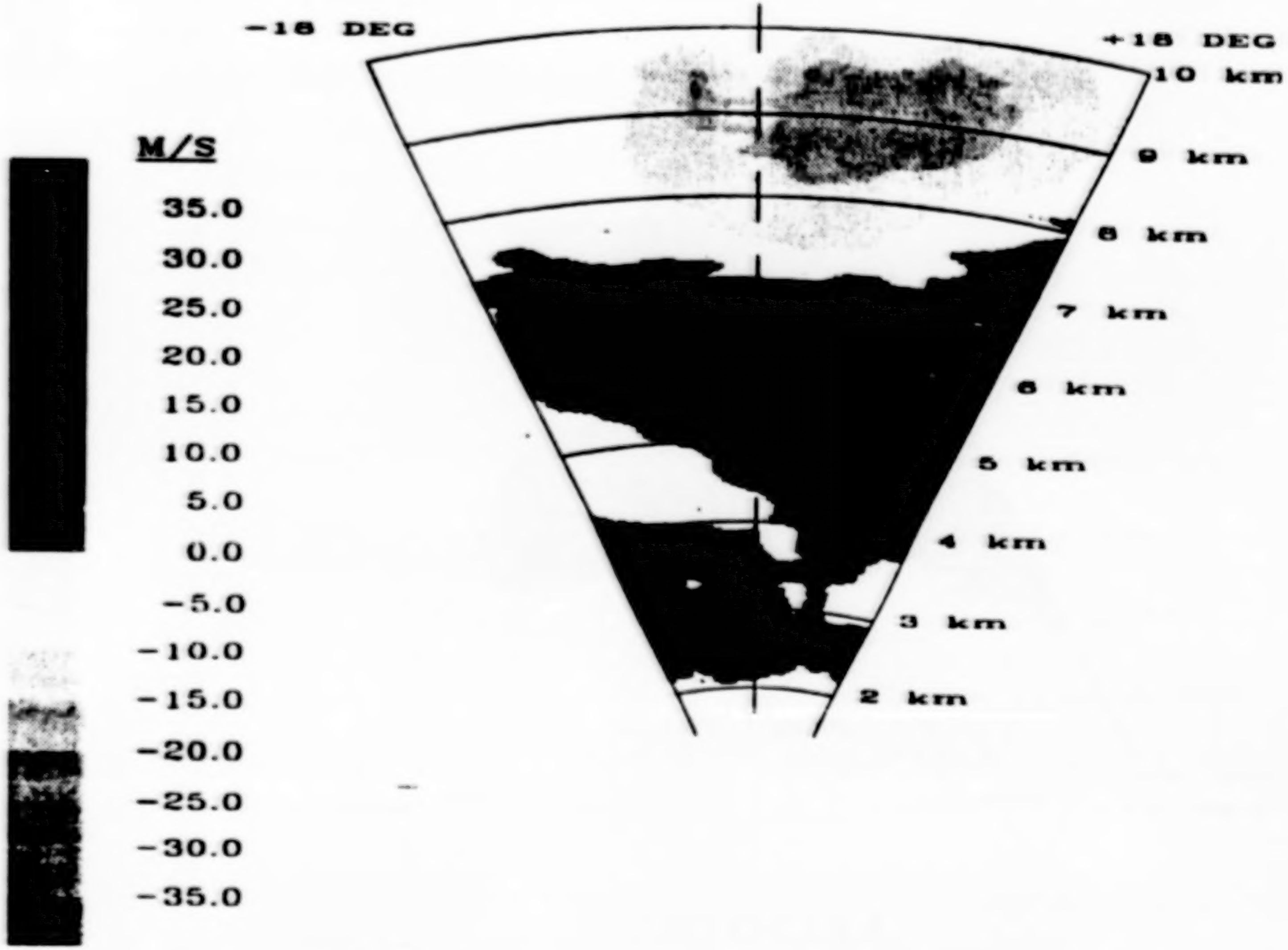

LINEAR PREDICTOR METHOD (SNR = INFINITY)

ORIGINAL PAGE IS
OF POOR QUALITY

WEATHER RADAR MODEL

VELOCITY

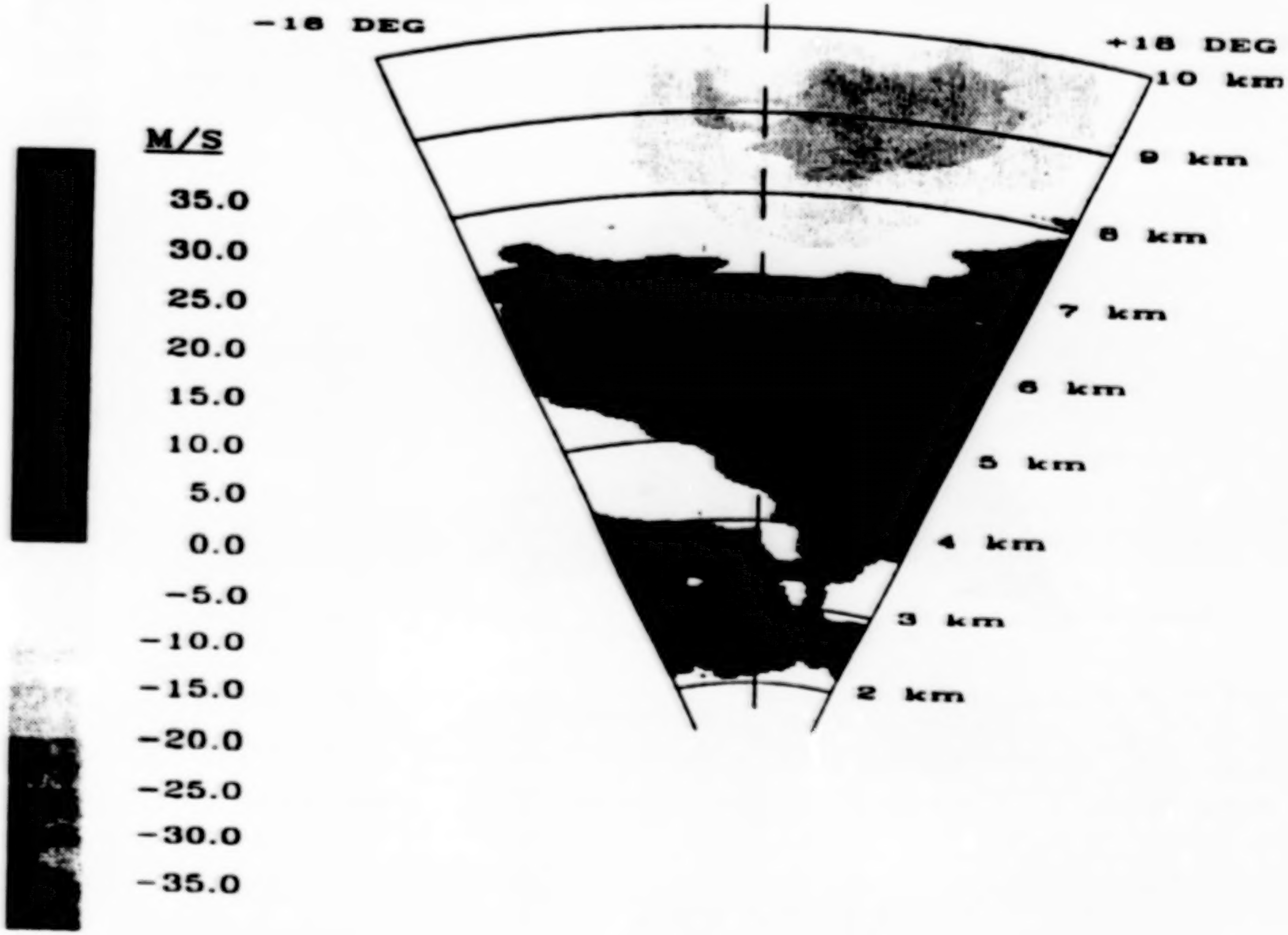

FB LINEAR PREDICTION METHOD(SNR=10DB)

ORIGINAL PAGE IS
OF POOR QUALITY

WEATHER RADAR MODEL

VELOCITY

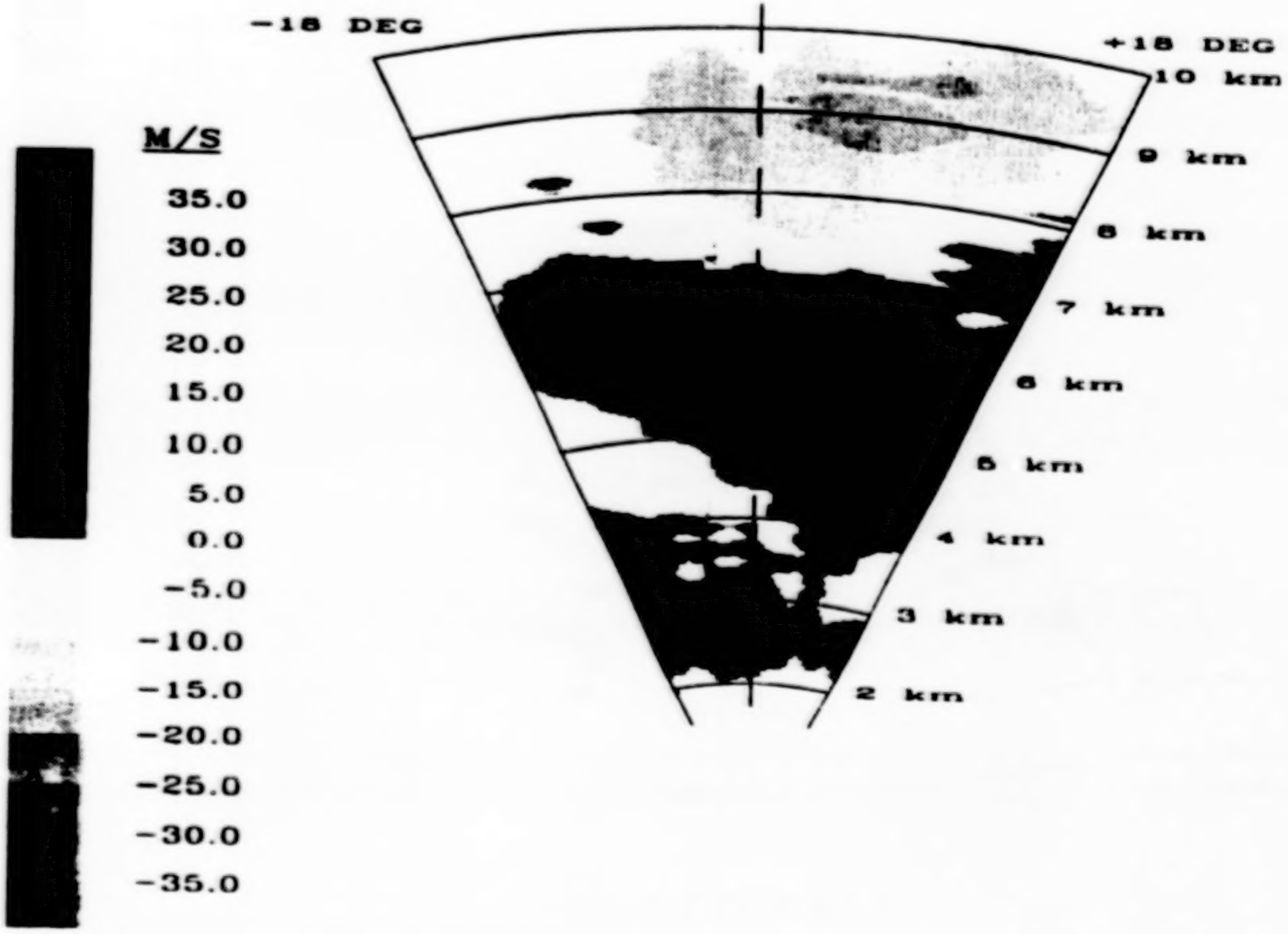

FB LINEAR PREDICTION METHOD(SNR=5DB)

ORIGINAL PAGE IS
OF POOR QUALITY

WEATHER RADAR MODEL
VELOCITY

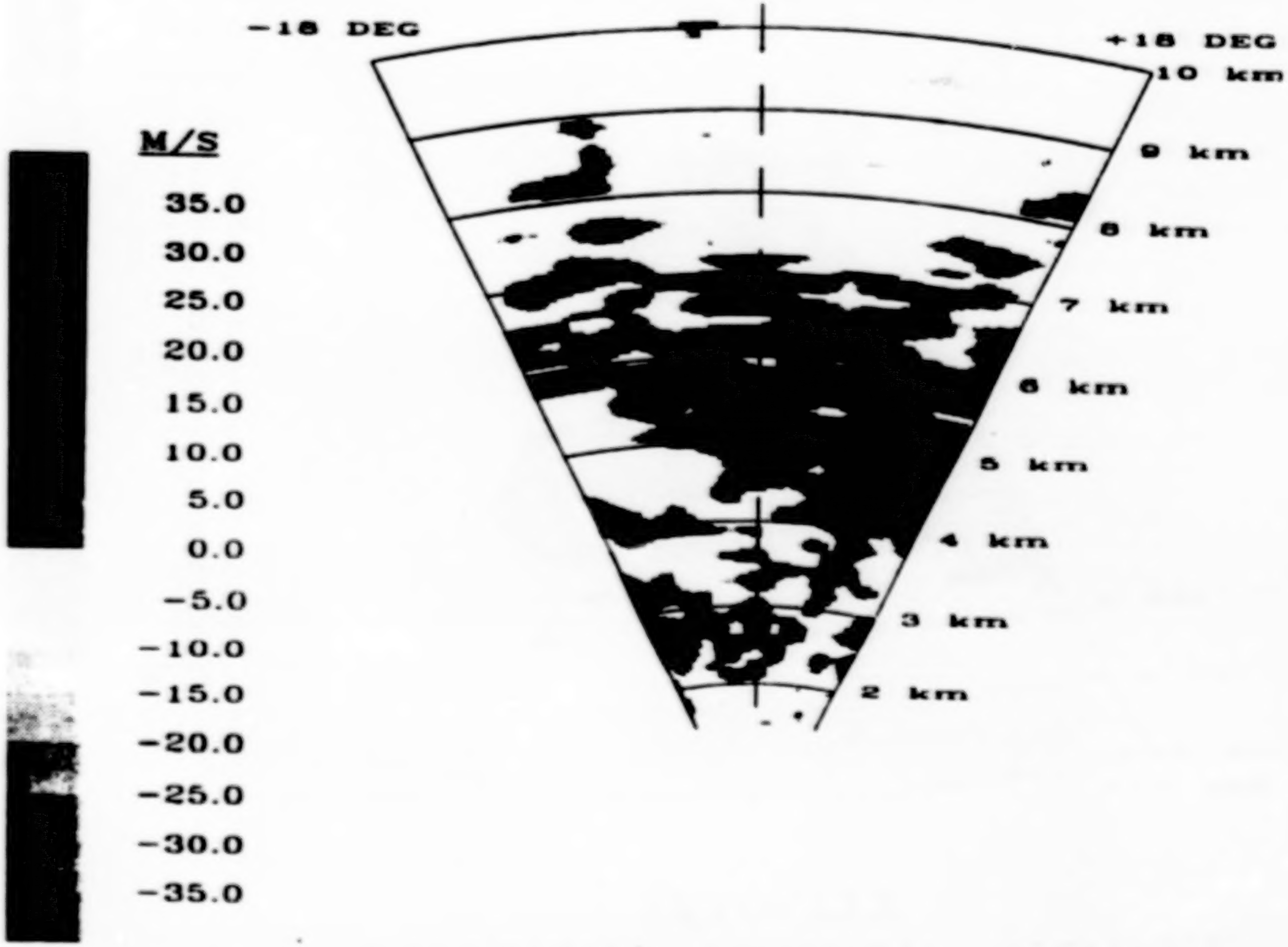

FB LINEAR PREDICTION METHOD (SNR=-5DB)

ORIGINAL PAGE IS
OF POOR QUALITY

WEATHER RADAR MODEL
VELOCITY

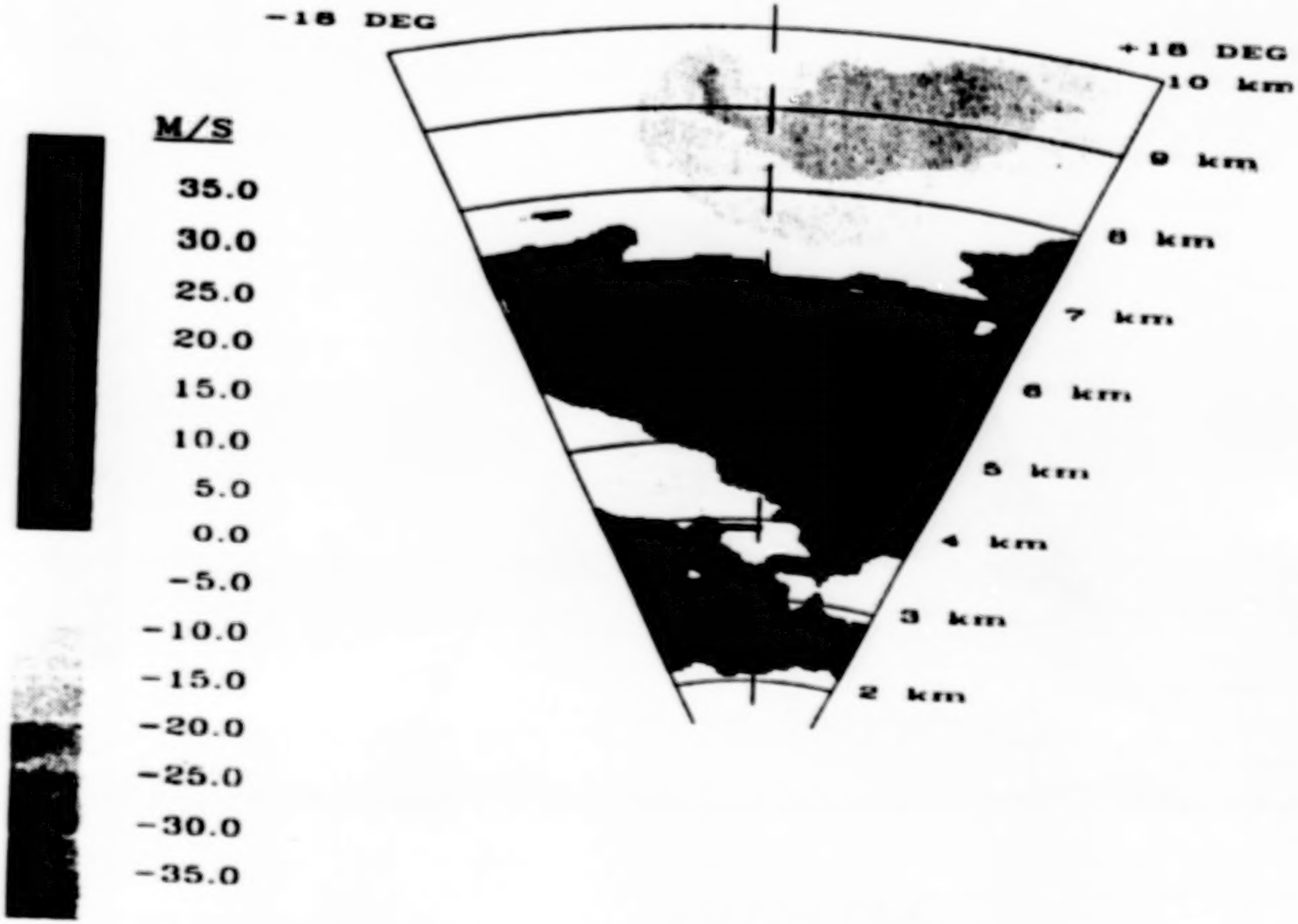

EIGENVECTOR METHOD (SNR = INFINITY)

ORIGINAL PAGE IS
OF POOR QUALITY

WEATHER RADAR MODEL
VELOCITY

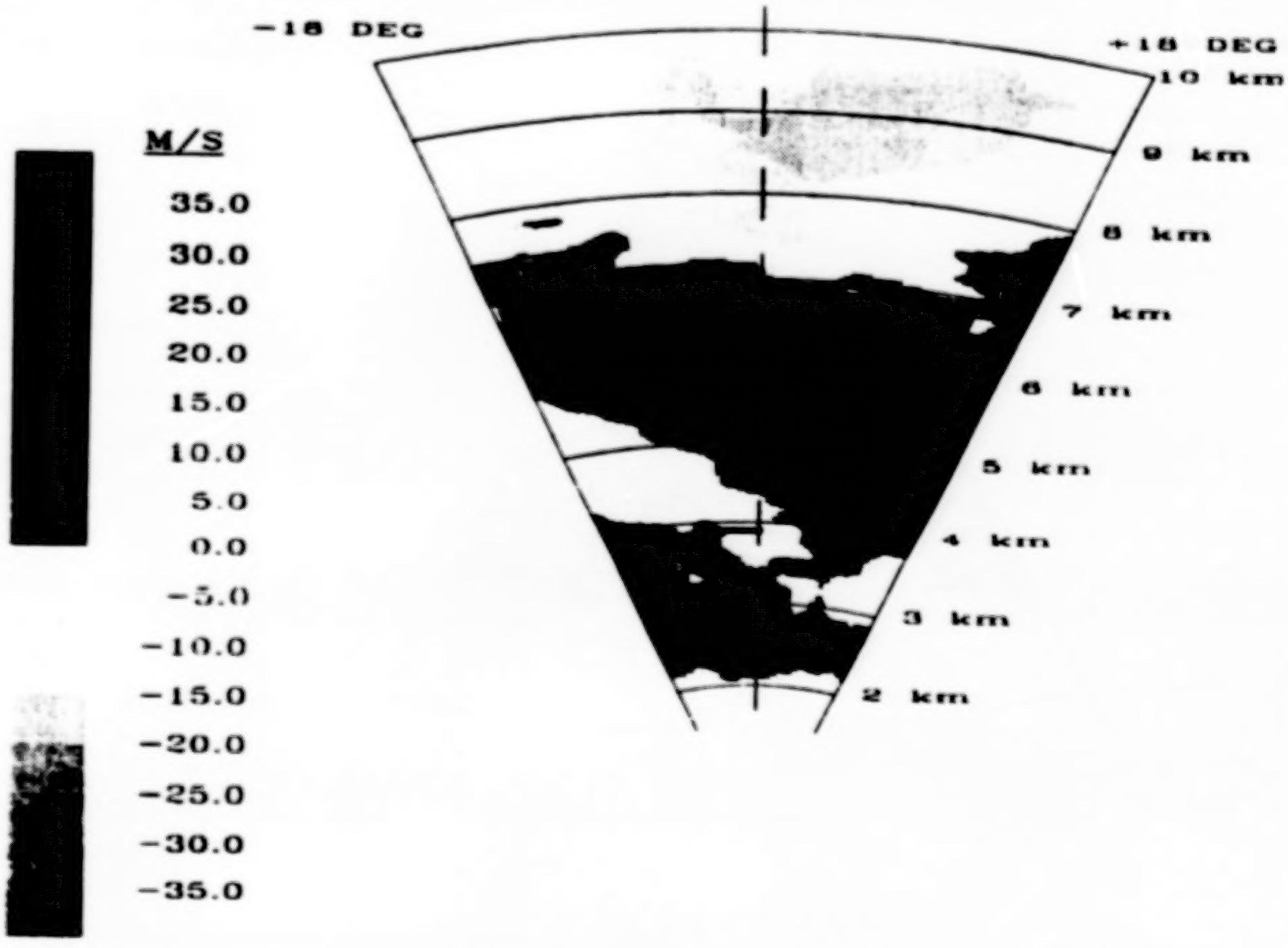

EIGEN-VECTOR METHOD(SNR=10DB)

ORIGINAL PAGE IS
OF POOR QUALITY

WEATHER RADAR MODEL

VELOCITY

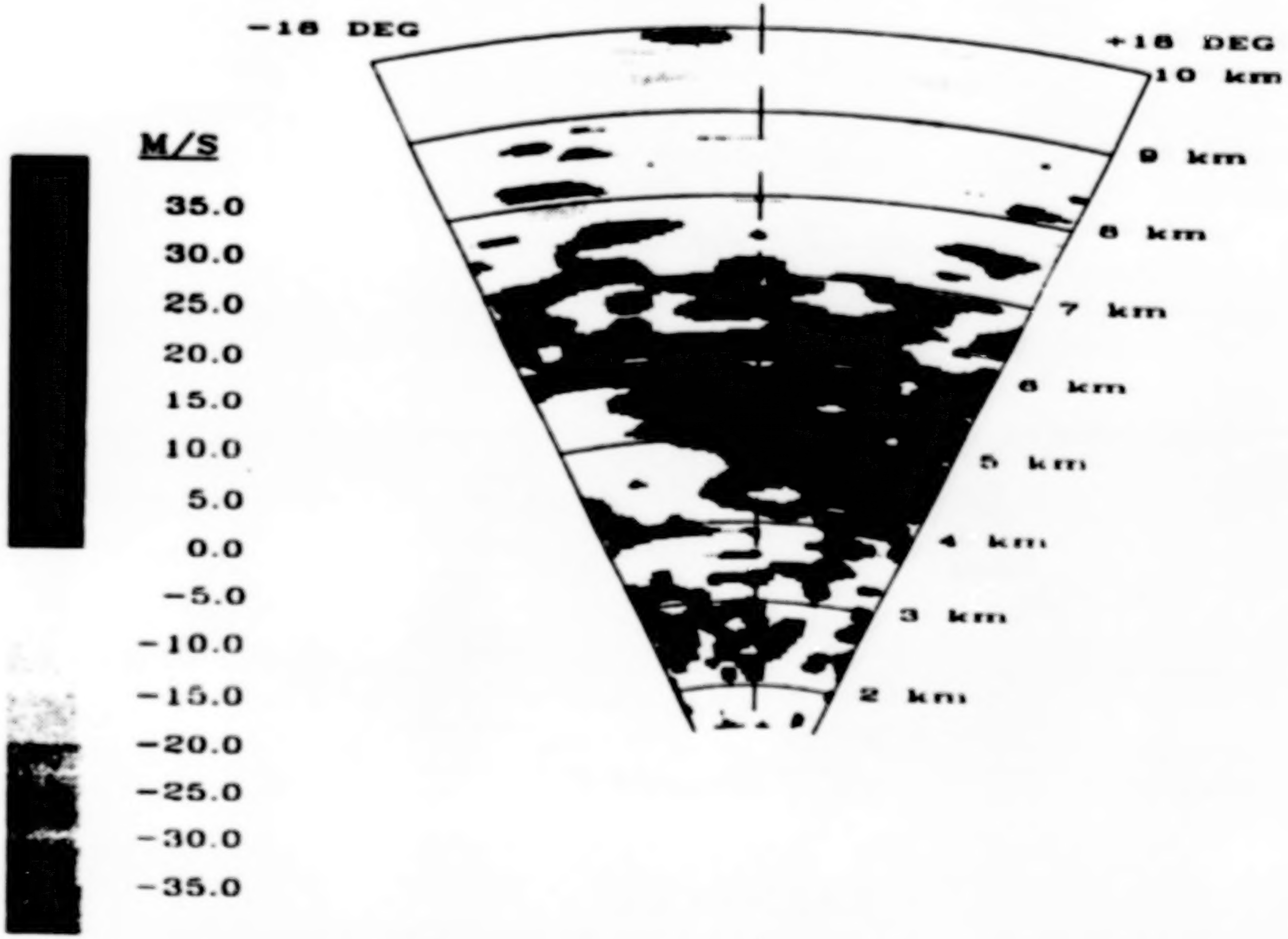

EIGENVECTOR METHOD (SNR=-5DB)

ORIGINAL PAGE IS
OF POOR QUALITY

WEATHER RADAR MODEL

VELOCITY

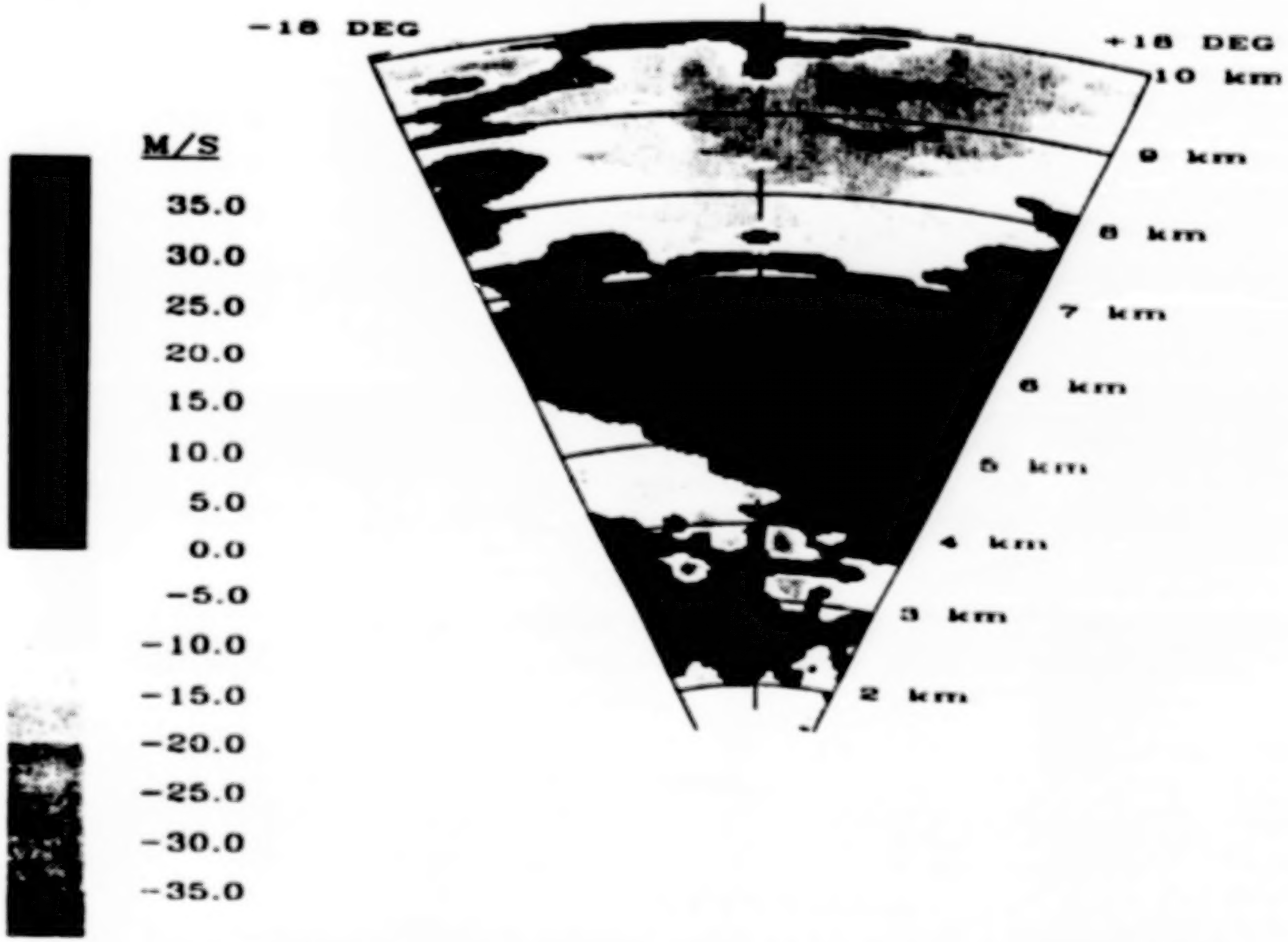

MUSIC METHOD (SNR = INFINITY)

ORIGINAL PAGE IS
OF POOR QUALITY

WEATHER RADAR MODEL

VELOCITY

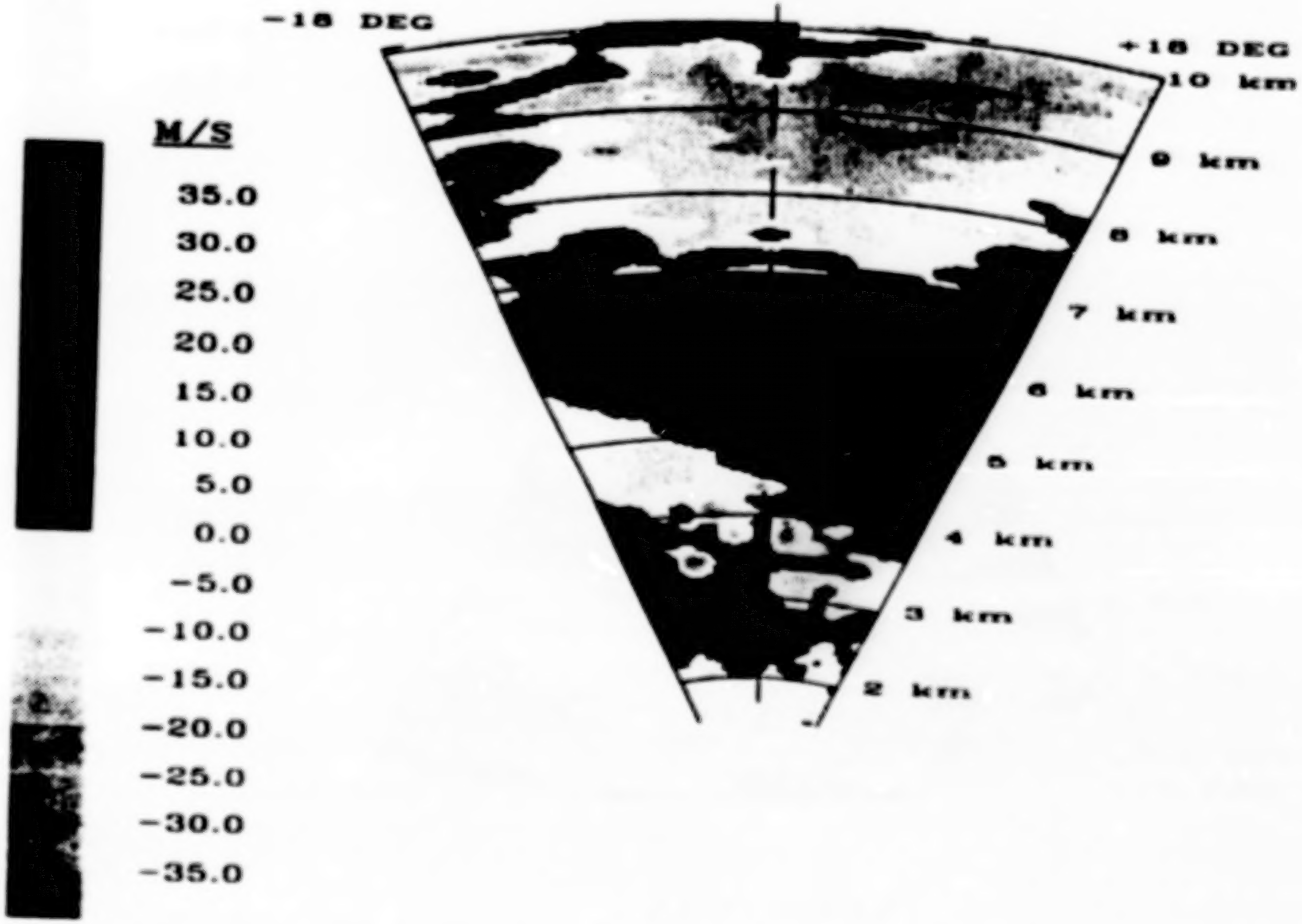

MUSIC METHOD (SNR=10DB)

ORIGINAL PAGE IS
OF POOR QUALITY

WEATHER RADAR MODEL
VELOCITY

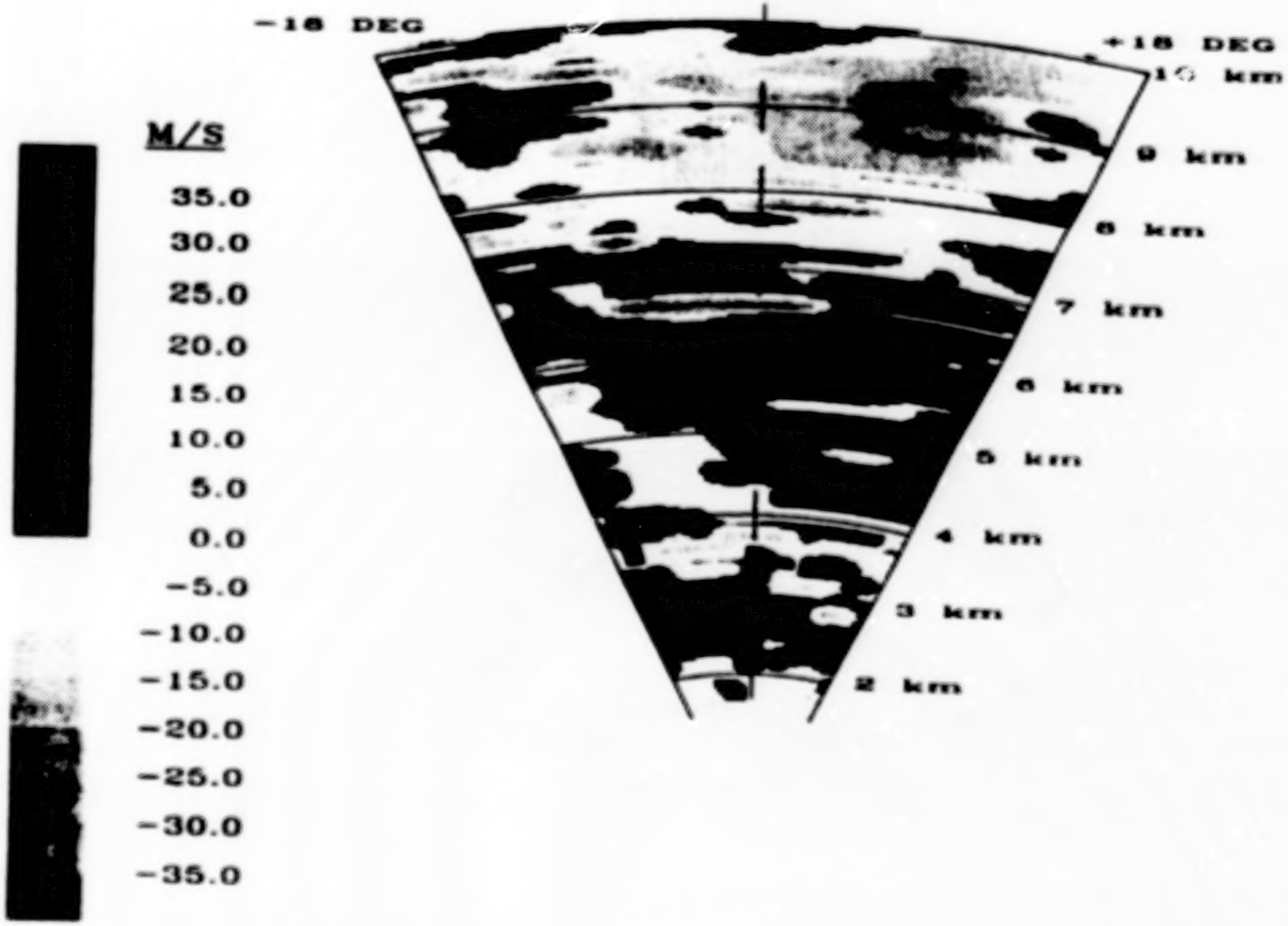

MUSIC METHOD (SNR=5DB)

ORIGINAL PAGE IS
OF POOR QUALITY

WEATHER RADAR MODEL
VELOCITY

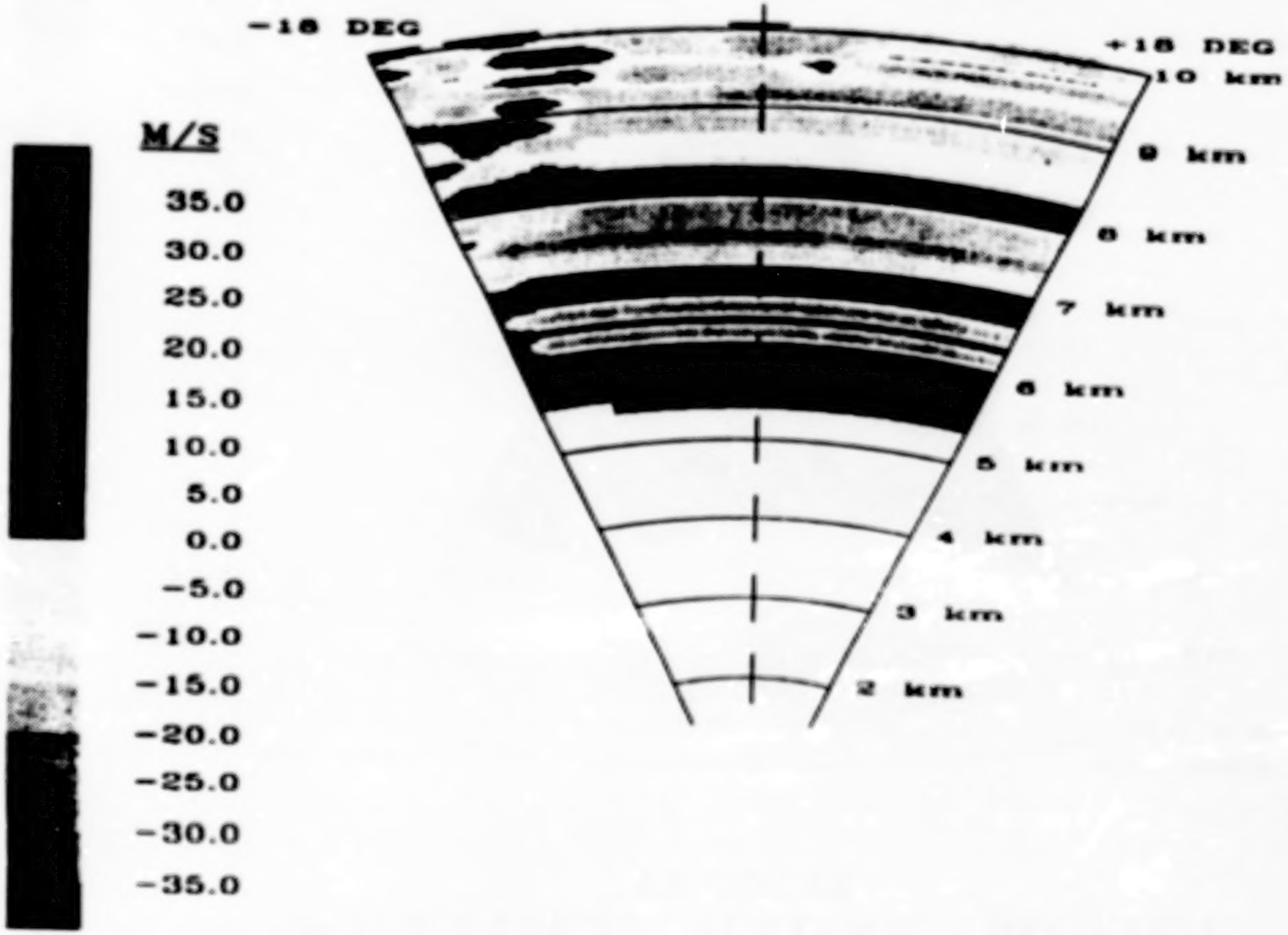

MUSIC METHOD (SNR=−5DB)

ORIGINAL PAGE IS
OF POOR QUALITY

WEATHER RADAR MODEL

VELOCITY

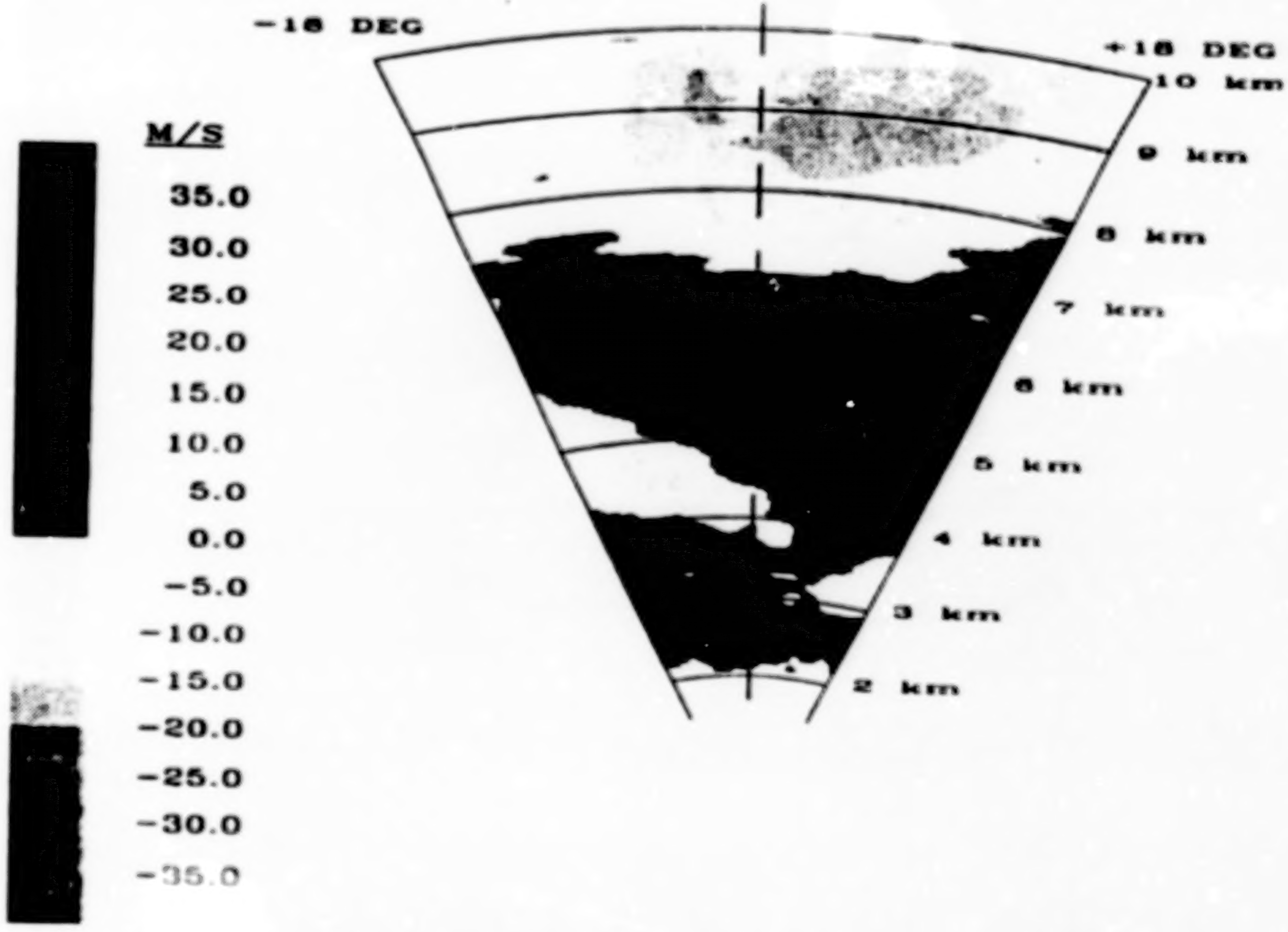

PERIODOGRAM METHOD (SNR=INFINITY)

ORIGINAL PAGE IS
OF POOR QUALITY

WEATHER RADAR MODEL
VELOCITY

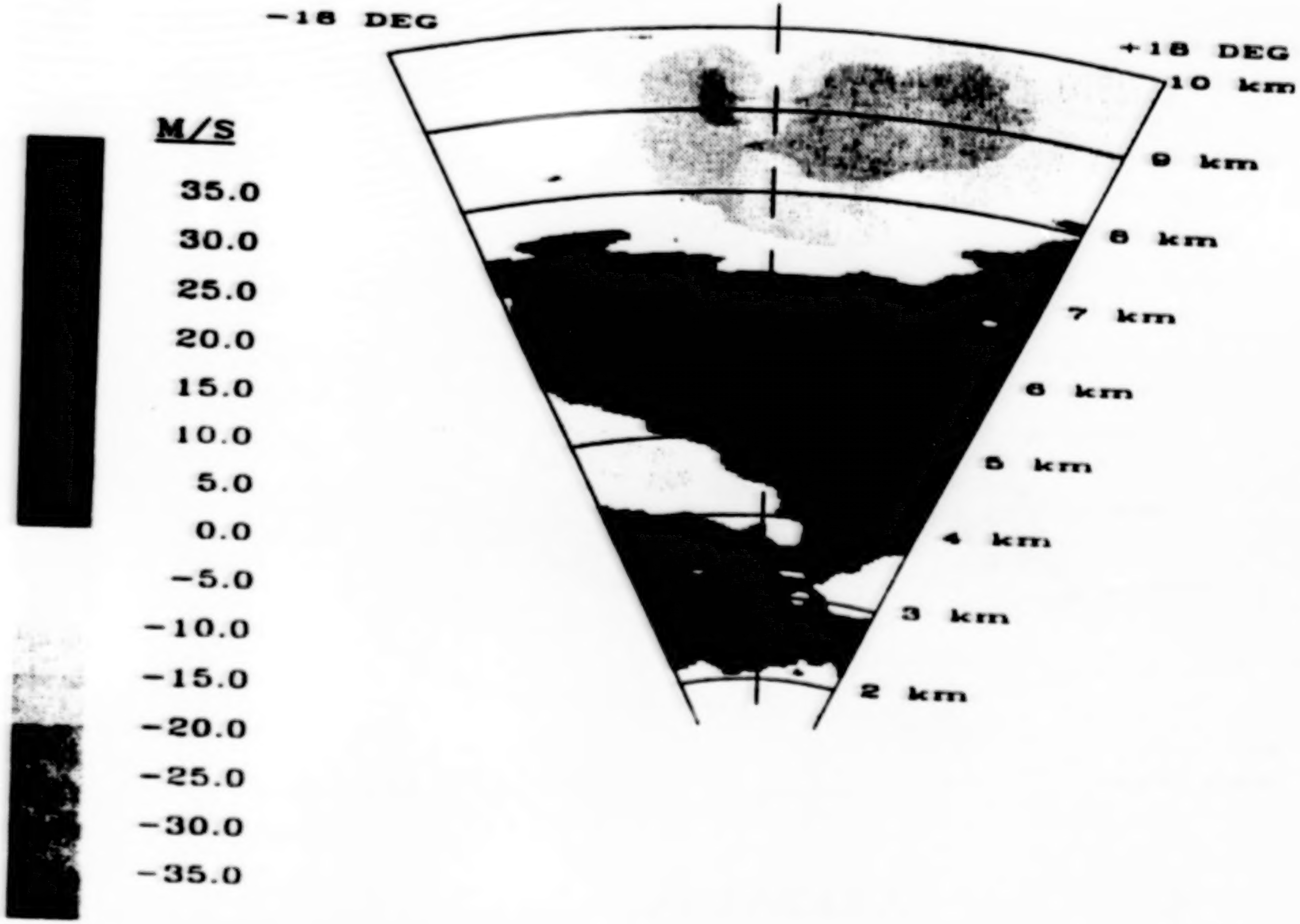

PERIODOGRAM METHOD (SNR=10DB)

ORIGINAL PAGE IS
OF POOR QUALITY

WEATHER RADAR MODEL
VELOCITY

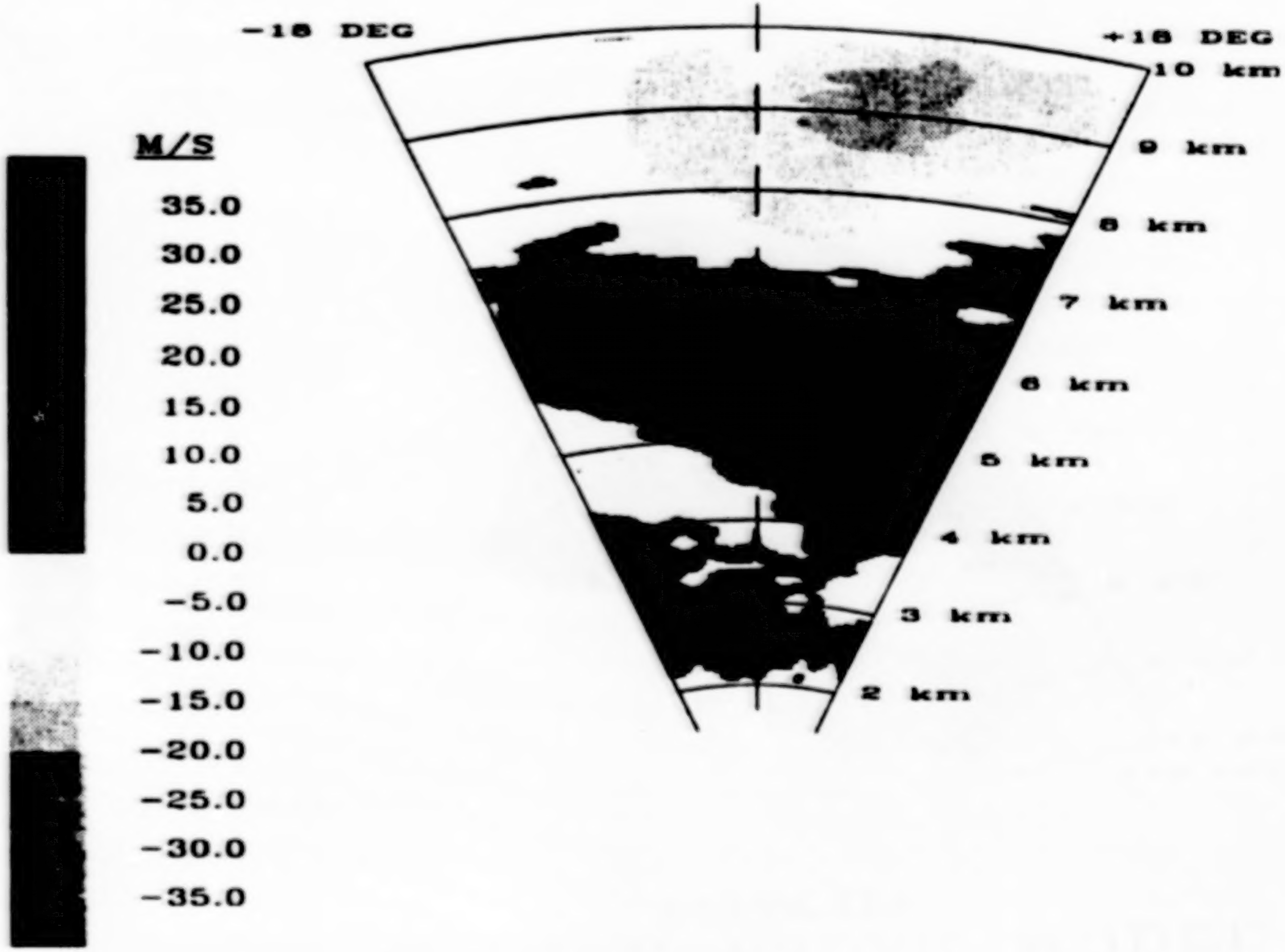

PERIODOGRAM METHOD (SNR=5DB)

ORIGINAL PAGE IS
OF POOR QUALITY

WEATHER RADAR MODEL
VELOCITY

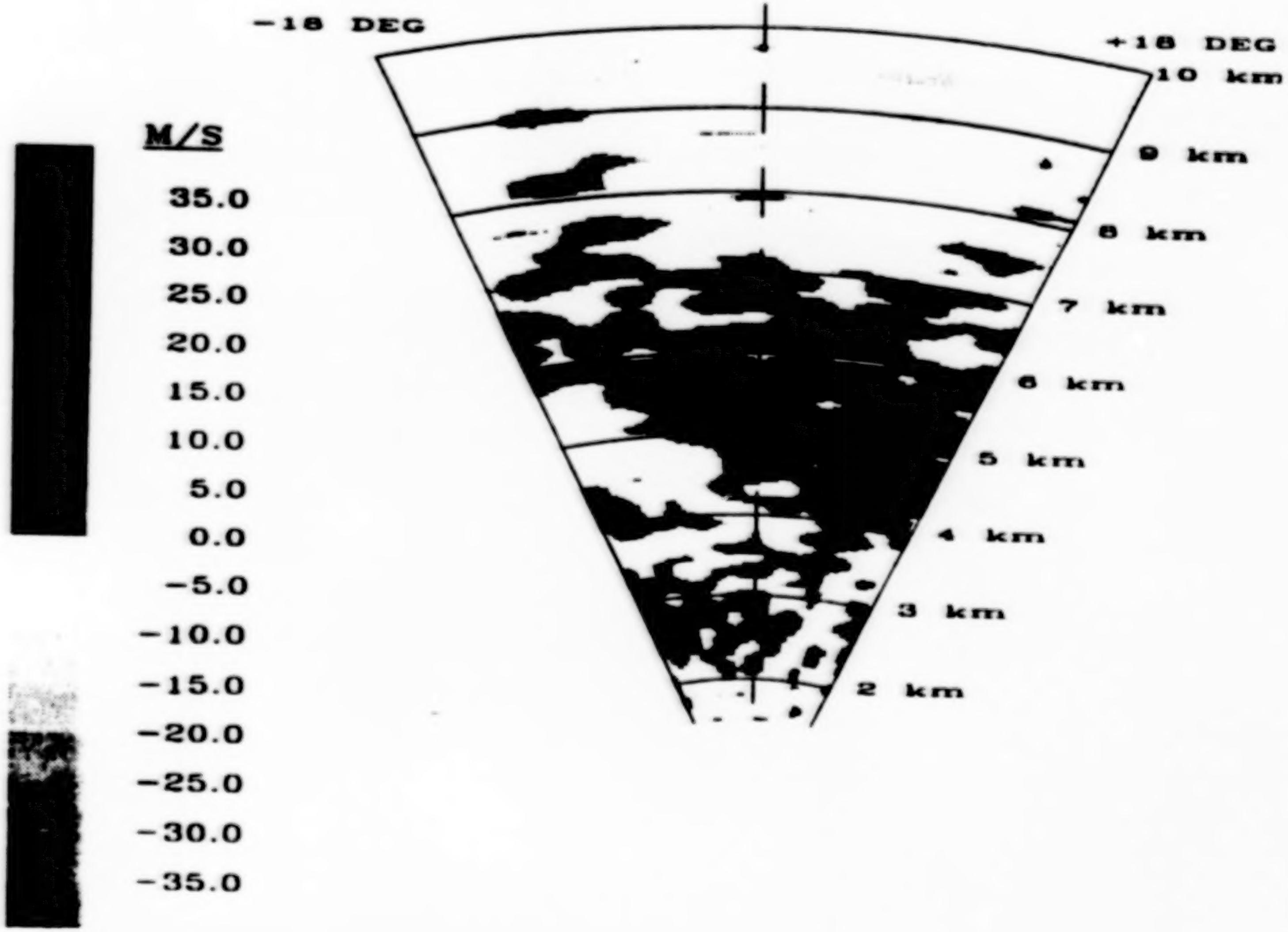

PERIODOGRAM METHOD (SNR=-5DB)

Session X. Airborne Doppler Radar / NASA

N91-24155

Airborne Radar Simulation Studies of the Denver July 11, 1988 Microburst

Charles Britt, RTI
E. M. Bracalente, NASA Langley

AIRBORNE RADAR SIMULATION STUDIES OF THE DENVER JULY 11, 1988 MICROBURST

E. M. Bracalente NASA Langley Research Center

C. L. Britt, Research Triangle Institute (RTI)

On July 11, 1988 5 United Airline (UAL) aircraft had inadvertent encounters with a microburst that struck Denver Stapleton airport. Four of these aircraft experienced severe wind shear during final approach to 26L&R runways, and had to execute emergency missed approach recovery procedures to escape the hazard, barely avoiding a fatal accident. The question was asked, what would an Airborne Doppler Radar with wind shear detection capability had seen if it had been available on these aircraft. Would the radar have detected the microburst with sufficient warning time to allow the pilot to avoid the severest portion of the microburst. To answer these questions a simulation study was conducted using the Radar simulation program described by C. L. Britt of RTI in the second presentation of this session (SESSION XI AIRBORNE DOPPLER RADAR/NASA). The July 11 microburst data base generated by the NASA Microburst Wind Shear Model (developed by Fred Proctor of MESO INC.) was used in the radar simulation along with the Denver stationary and moving clutter maps described in the first presentation of this session.

In the simulation program a wind shear detection Doppler radar was placed in UAL 395 and 236 aircraft and flown along their landing flight paths. The microburst was placed at the appropriate location and intensity corresponding to each aircraft landing approach time. A baseline set of radar design parameters, which will be described later, were used in the simulation. Output display information and wind shear detection processing was produced as the aircraft approached the microburst. The following charts present information on the results of this simulation study.

ORIGINAL PAGE IS
OF POOR QUALITY

PRECEDING PAGE BLANK NOT FILMED

DENVER JULY 11 U-BURST AT TIME PERIOD D49 (VELOCITY PLOT)

The upper plot shows an X-Y horizontal cross section, at 100 m altitude, of wind vectors for the microburst (U-B) that struck Denver Stapleton airport on July 11 1988. The gray shade contours indicate wind speed (scale on left) in meters per second (m/s), and the arrows show wind direction. The wind direction vectors are shown every 200 m. The Y-axis runs north, the X-axis east. The lower plot shows a vertical cross section (altitude, Z vs X distance) through the U-B along the A/C flight path. The altitude resolution is approximately 80 meters. The down draft wind vectors and divergent outflow wind vectors at low altitude can easily be seen.

The data for this plot was generated by the NASA U-B wind shear model. Actual measured meteorological data prior to the storm are used as inputs to the model. The structure of the storm and wind fields resulting from the model, and shown here, compare very close to the actual U-B that occurred on July 11, as confirmed by ground based Doppler radar, and reconstructed winds using recorder data from the A/C that encountered the storm. This plot is for simulation time D49, corresponding to the actual time associated with the position of UAL flight 395.

The center of the U-B is approximately 2.2 kilometers (KM) (1.2 nautical miles (NM)) east and .5 KM (.25 NM) south of runway 26L. The airport runways are indicated on the figure. The arrows in the U-B show the strong out flow divergence with severe velocity wind shear.

The microburst intensity and location are shown here about a minute after it descended to the ground at about the time UAL 395 was at 1200 feet approaching runway 26L. UAL 395 is shown in the figure as it approaches the storm 7 KM (3.8 NM) from touch down (TD) and 4.8 KM (2.6 NM) from the center of the U-B.

Approximately one minute later UAL 395 was at the center of the storm and came within 75 feet of the ground and .5 miles short of the runway TD before it was able to gain altitude and escape the U-B.

DENVER MICROBURST: JULY 11 (D49)
(X−Y) WIND FIELD PLOT: (ALT = 100M)
UAL 395

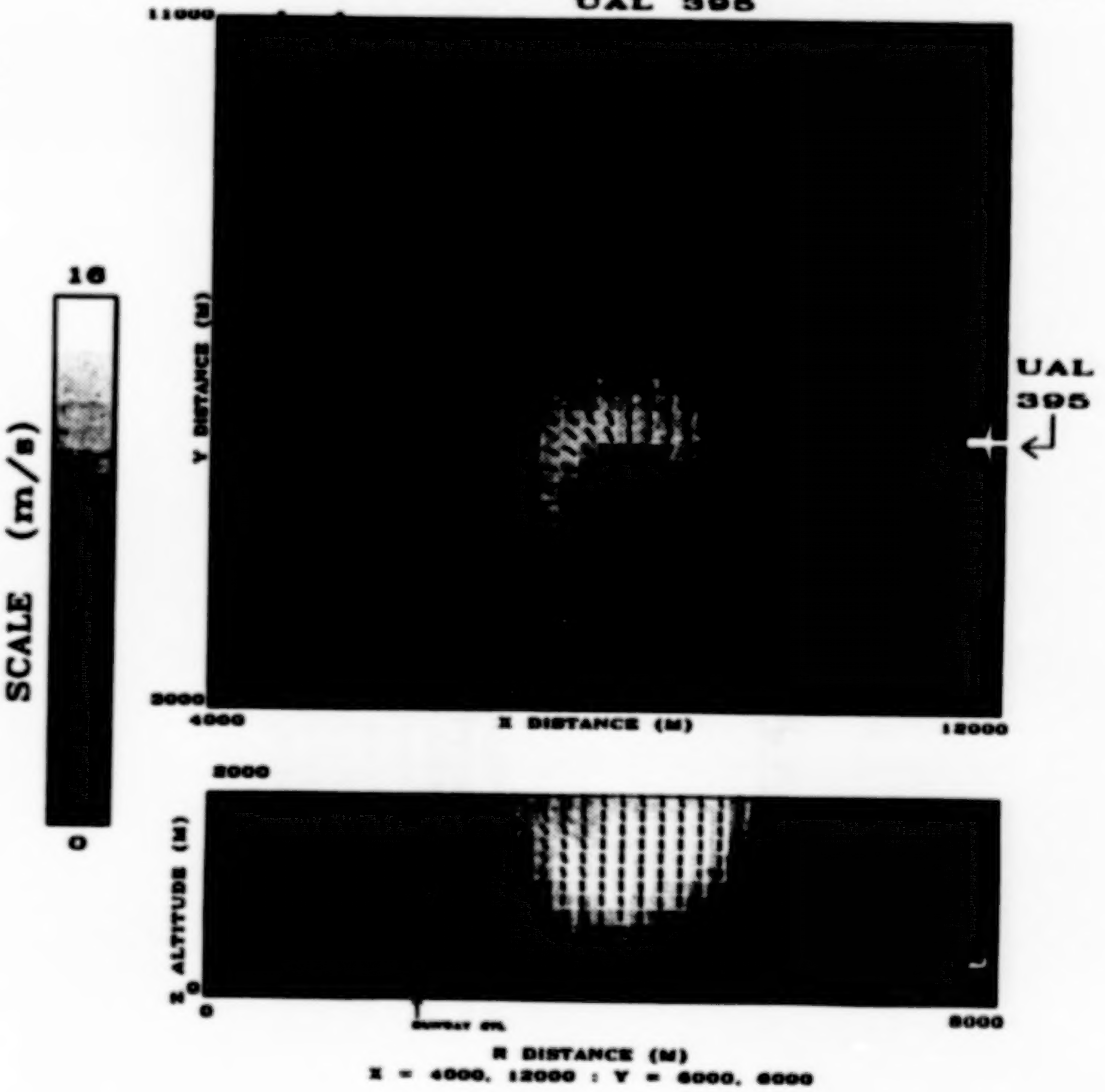

ORIGINAL PAGE IS
OF POOR QUALITY

DENVER JULY 11 U-BURST AT TIME PERIOD D49 (REFLECTIVITY PLOT)

This plot is identical to the D49 velocity plot except the gray shade contours indicate the reflectivity levels in Dbz that existed in the microburst. Within the major portion of the microburst outflow region the reflectivity levels range from 0 to 20 Dbz. This microburst is considered a relatively dry microburst. The reflectivity levels are 3 orders of magnitude lower then the levels experienced in the Dallas-Fort Worth microburst of 1985. These lower levels of reflectivity present a more difficult problem for the radar to detect especially in the presents of severe ground clutter.

DENVER MICROBURST: JULY 11 (D49)
(X–Y) RADAR REFLECTIVITY: (ALT = 100M)
UAL 395

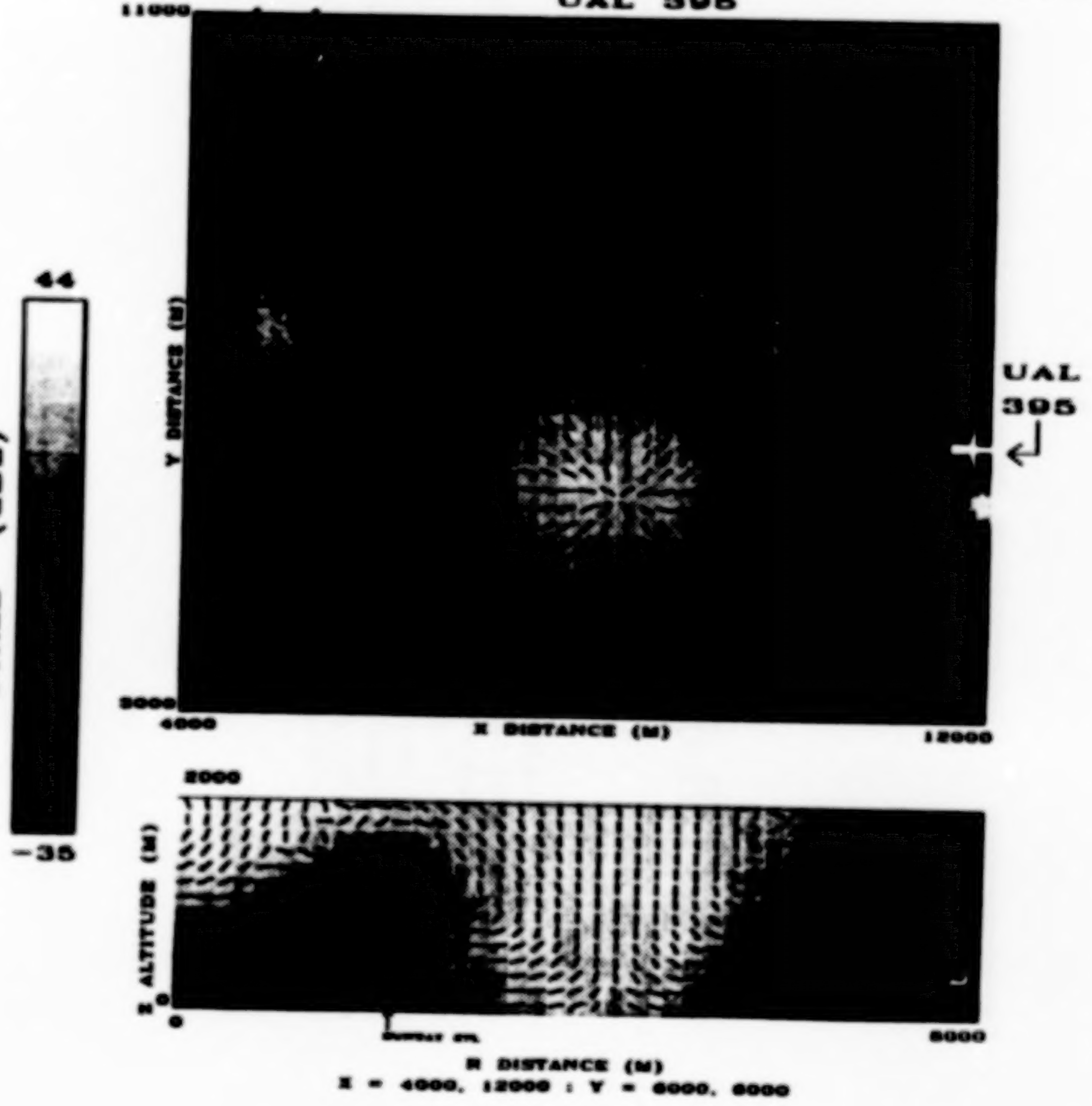

ORIGINAL PAGE IS
OF POOR QUALITY

DENVER JULY 11 U-BURST AT TIME PERIOD D51 (VELOCITY PLOT)

This figure shows the velocity contours of the U-B 2 minutes later in its development from time period D49. At this time the storm has grown in size and intensity , as seen in the figure, and has moved slightly east to 2.3 KM (1.2 NM) from the runway. The location of UAL 236 which was following behind UAL 395 is shown in the figure 4.5 KM (2.7 NM) from the U-B. One minute later UAL 236 was located near the center of the U-B approximately 2 KM (1.1 NM) from TD and 150 m (492 ft) above the ground before it began to gain altitude. A portion of a second smaller microburst can be seen NW of the main microburst.

DENVER MICROBURST: JULY 11 (D51)

(X–Y) WIND FIELD PLOT: (ALT = 100M)
UAL 236

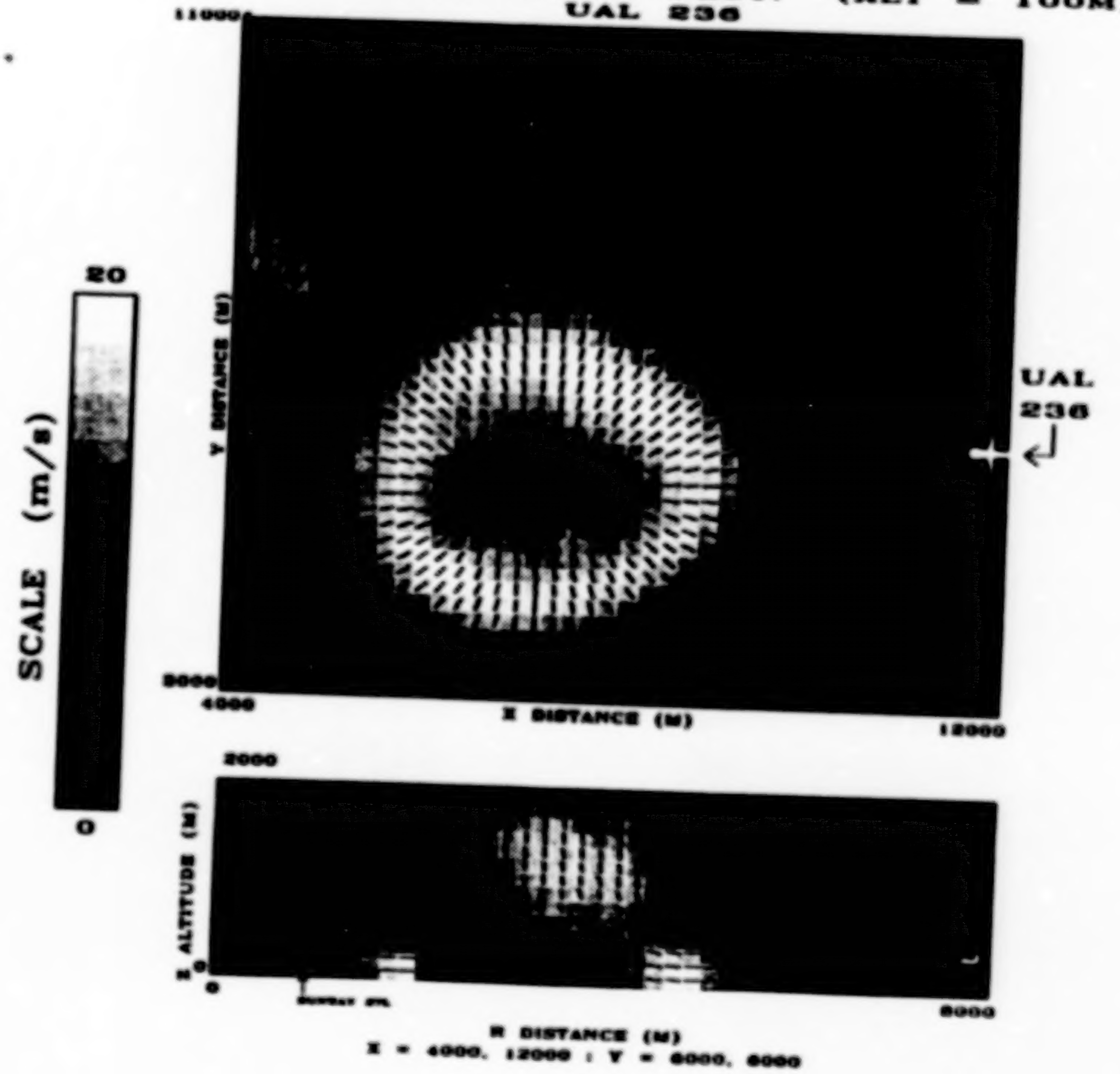

ORIGINAL PAGE IS
OF POOR QUALITY

DENVER JULY 11 U-BURST AT TIME PERIOD D51 (REFLECTIVITY PLOT)

This plot is identical to the D51 velocity plot except the gray shade contours indicate the reflectivity levels in Dbz that existed in the microburst. Within the major portion of the microburst outflow region the reflectivity has increased a little to levels ranging from 0 to 23 Dbz.

DENVER MICROBURST: JULY 11 (D51)

(X–Y) RADAR REFLECTIVITY: (ALT = 100M)

UAL 236

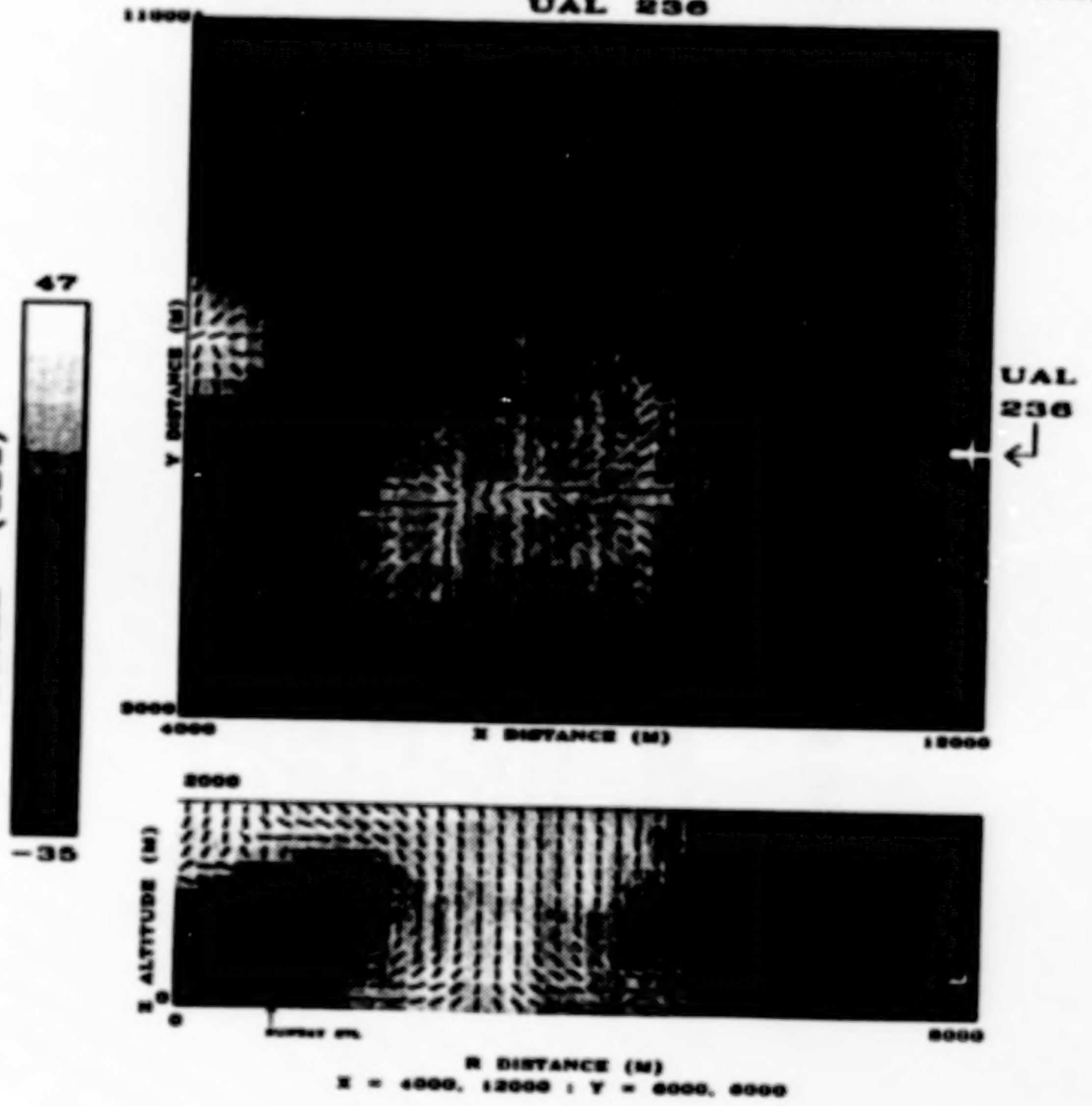

ORIGINAL PAGE IS
OF POOR QUALITY

RADAR BASELINE OPERATING PARAMETERS FOR HAZARD DETECTION

Using the radar simulation program, a set of radar displays of the wind shear hazard that would be seen by a Doppler radar located on board UAL 395 & 236 a/c were produced.

A set of parameters were chosen for the operation of the wind shear detection radar. These parameters are listed on the accompanying chart. The weighted least squares hazard detection and hazard tracking algorithms described in the second presentation of this session were utilized in the simulation runs. In addition a variable antenna tilt was employed to keep the 3 Db point of the main beam hitting the ground 8 km in front of the aircraft. In the simulation program as the aircraft is moved along the glide slope the antenna is scanned over a 42 deg. sector every 3 sec., with the radar sampling a .5 to 5 km range in front of the aircraft. The data is processed to velocity and wind shear information. The horizontal hazard index (F-Factor) is derived and tracked by the radar. If the hazard, area, and alarm thresholds are all exceeded an alarm is sounded to the pilot. The next sets of figures show sample displays of data generated by the radar, illustrating the effects of moving ground clutter and its reduction using antenna tilt.

BASELINE PARAMETERS FOR RADAR HAZARD DETECTION

o FREQUENCY -------------------- X-BAND

o PULSE WIDTH -------------------- .96 usec (144 m)

o PRF -------------------- 3755

o TRANSMITTER POWER -------------------- 200 w

o FLAT PLATE ANTENNA, BEAMWIDTH ---------- 3.5 deg

o ANTENNA SECTOR SCAN -------------------- 42 deg

o TIME TO SCAN SECTOR -------------------- 3 sec

o RANGE COVERAGE IN FRONT OF A/C ---------- 5 Km (2.7 NM)

o VARIABLE ANT TILT: 3 DB INTERCEPT ----- 8 Km

o HORIZONTAL HAZARD INDEX THRESH ------- .07

o HAZARD ALONG TRACK DIMENSION ------ 900 m (10 s)

o AREA THRESHOLD -------------------- .65 SQ.KM (.2 SQ.MI)

o ALARM THRESHOLD -------------------- 40 sec

o SCANS FOR VALID TRACK -------------------- 3

RADAR WIND VELOCITY CONTOUR DISPLAY U-BURST D49; ANTENNA TILT = 0 DEG

With the A/C approx. 3.3 km (1.8 NM) from the center of the storm a velocity display as shown in this figure was produced.

The radar is scanning +/- 21 degrees in azimuth, and covers a half to 5 km range or approx. 60 sec in front of the A/C. The velocity scale is show on the right in m/s.

The negative velocities, in the dark region approximately 2 km from the a/c, are winds toward the A/C i.e. head winds. These winds correspond to the leading edge of the U-burst, and are about –15 m/s (30 K). At a greater range near the center of the storm the horizontal velocity is zero as shown by the medium gray area. This is followed by the positive velocities corresponding to the outflow on the other side of the u-burst (+12 m/s). These produce tail winds to the A/C. This sudden change in direction of wind flow at these magnitudes will produce a wind shear which will severely effect the performance of the A/C.

The radar can only measure the radial or horizontal outflow velocities from the U-burst. It can not sense the down-flow velocity. This down-flow which is at a maximum at the center of the U-burst also produces a wind shear which effects the performance of the A/C.

Also shown in this display, on either side of the U-B are a significant number of velocity contours produced by clutter returns from moving vehicles on the roads and interstates surrounding Stapleton airport. The antenna in this case was set at a 0 deg. tilt relative to the glide slope. This tilt angle produces the worse case clutter returns. To reduce the clutter the antenna needs to be tilled up. A tilt of three deg. is shown in a later display. However, it is of interest to see how well the weighted least squares hazard algorithm would perform in detecting the U-B hazardous area in the presence of this severe clutter. The next chart shows the results.

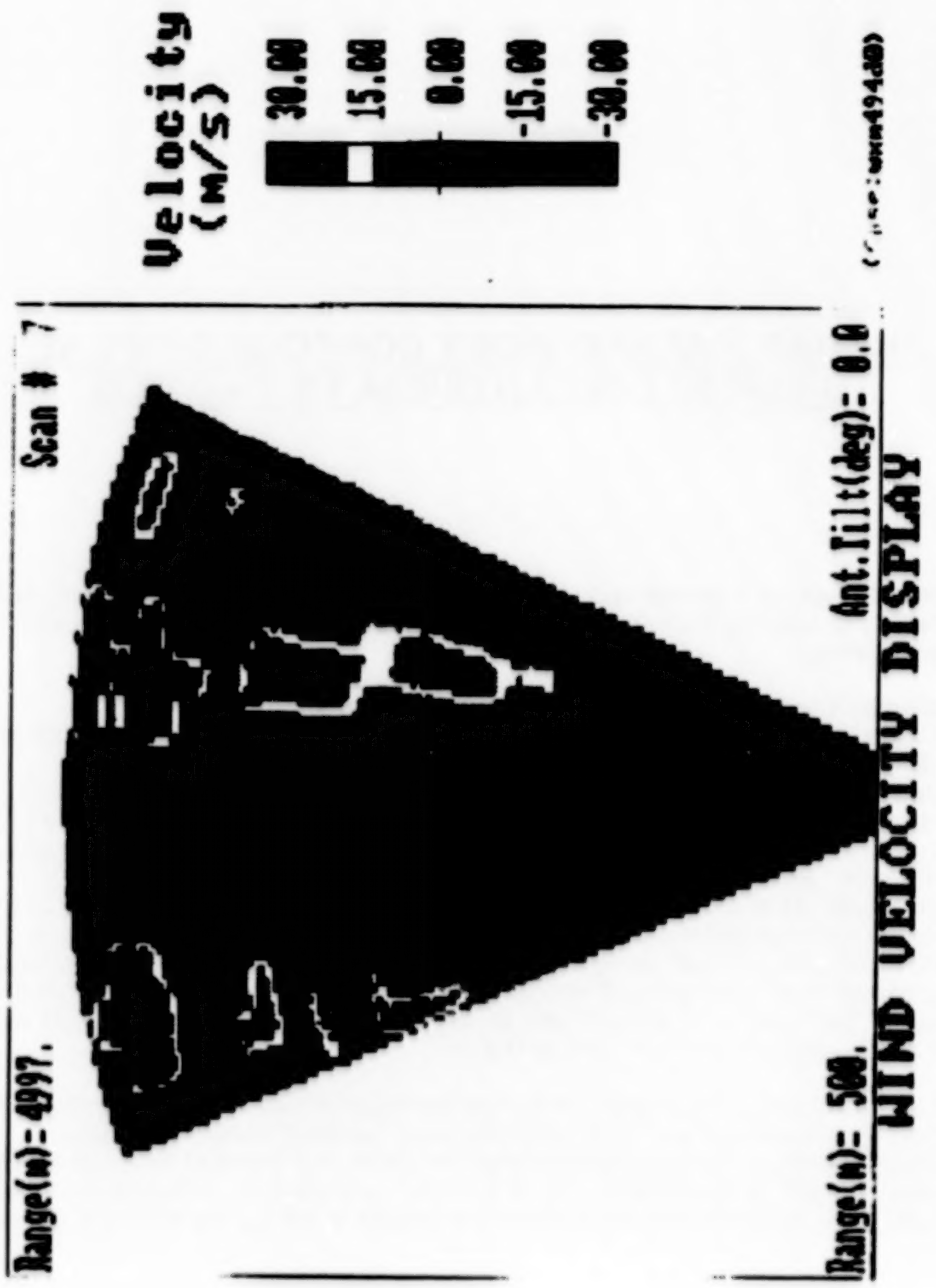

ORIGINAL PAGE IS
OF POOR QUALITY

RADAR HAZARD INDEX CONTOUR DISPLAY
U-BURST D49; ANTENNA TILT = 0 DEG

Before information is presented to the pilot the radar performs additional data processing to assess the wind shear hazard associated with any wind velocity measurements.

This display shows contours of the horizontal wind shear hazard index associated with the previous wind speed measurements for an antenna tilt of 0 deg. The hazard index relates the effect of wind shear on a loss in A/C performance. It is derived from the spatial rate of change in wind velocity, i.e. wind shear in m/s per m, multiplied by the A/C velocity and divided by the force of gravity. The index is a measure of the spatial wind shear's effect on the A/C performance. Positive indexes indicate a loss of performance on the A/C. Negative indexes will produce a performance increase. If the total index — i.e. sum of the vertical and horizontal component — exceeds a positive .1 over a large area or time interval, severe performance degradation will occur to the A/C and is considered hazardous if encountered at low altitudes. We see from this display, of the horizontal component alone, that a large area of hazardous wind shear exists about 3.3 km in front of the A/C.

It can be noted from the display that very few hazard indexes where generated by the moving ground clutter. The weighted least squares hazard algorithm weighted them out. Unfortunately it also weighted out some of the U-B hazardous area near the center of the U-B. To reduce this problem the antenna must be tilted up. The next two displays show the results of tilting the antenna up by 3 deg.

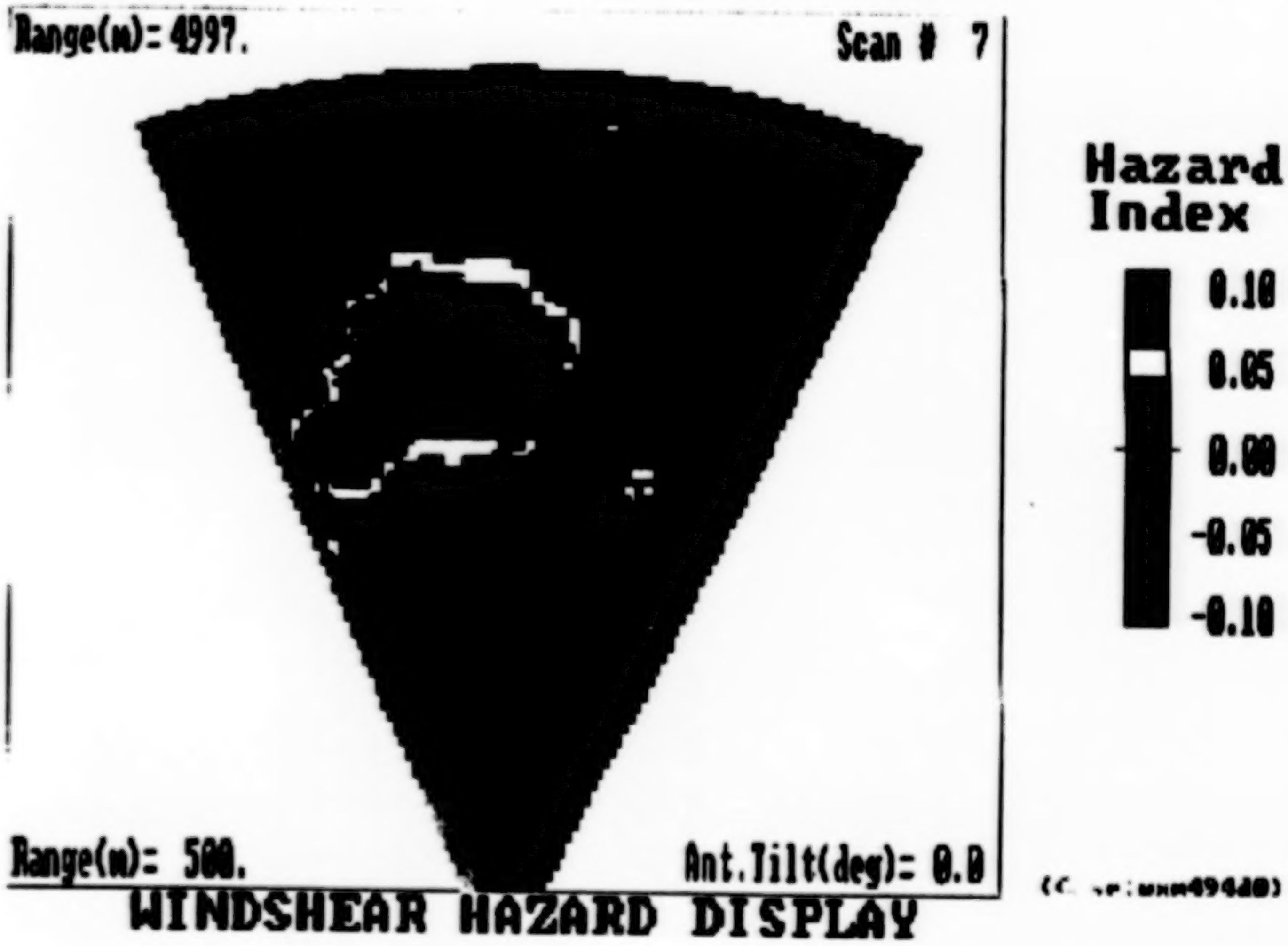

ORIGINAL PAGE IS
OF POOR QUALITY

RADAR WIND VELOCITY CONTOUR DISPLAY
U-BURST D49; ANTENNA TILT = 3 DEG

This display shows the velocity contours of U-B D49 at the same time interval as the previous velocity plot. In this case the antenna is tilted 3 deg. above the glide slope. Note, in comparison to the 0 deg tilt case, the significant reduction in the moving ground clutter signatures. Also a larger portion of the U-B velocity signature is discernible. The next figure shows the hazard index display produced by processing this velocity information.

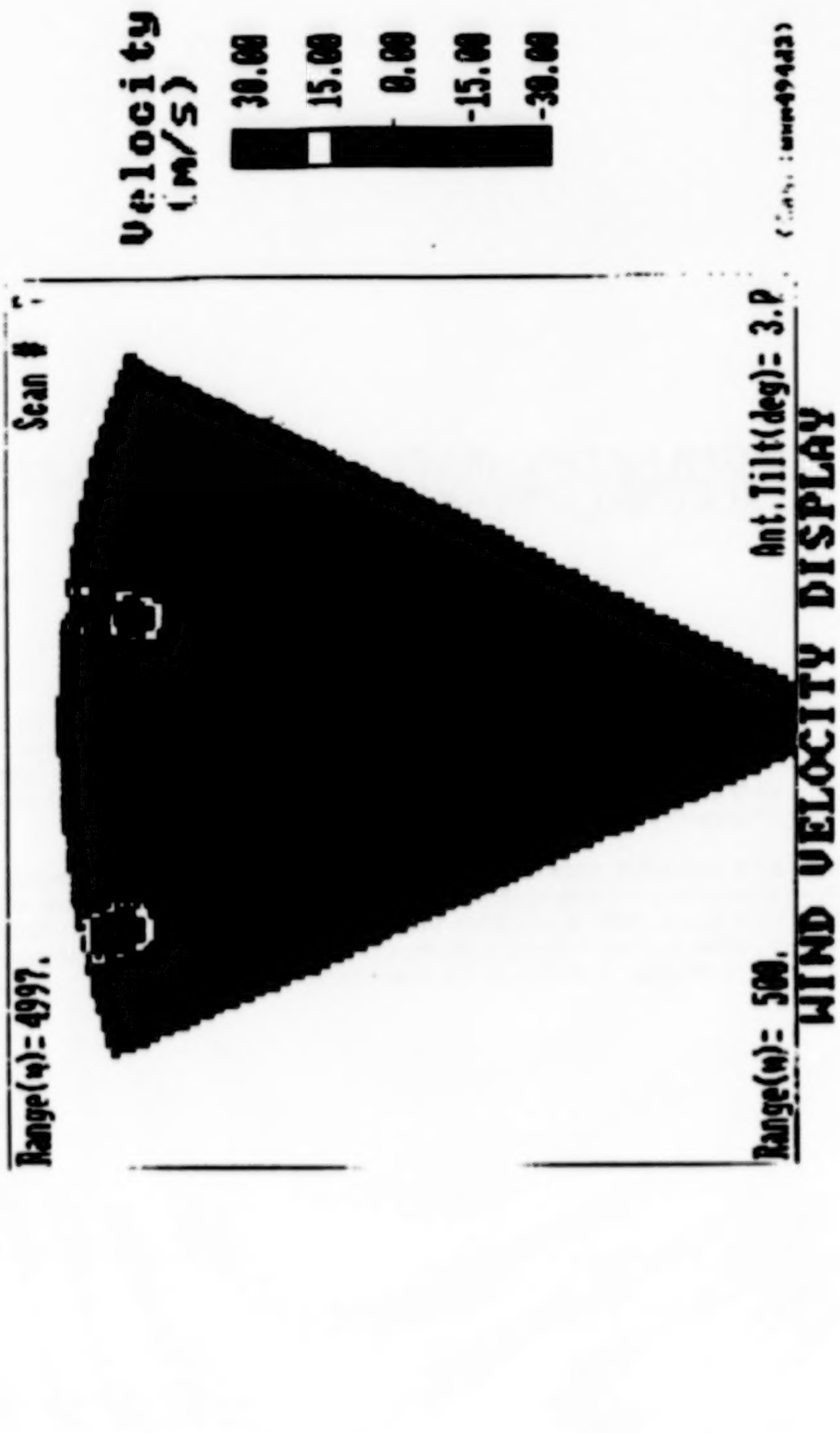
Velocity
(m/s)
30.00
15.00
0.00
-15.00
-30.00
Scan #
Range(m)= 4997.
Range(m)= 500.
Ant.Tilt(deg)= 3.0
WIND VELOCITY DISPLAY

ORIGINAL PAGE IS
OF POOR QUALITY

RADAR HAZARD INDEX CONTOUR DISPLAY
U-BURST D49; ANTENNA TILT = 3 DEG

This display shows contours of the horizontal wind shear hazard index associated with the previous wind speed measurements for an antenna tilt of 3 deg. In this case a much larger portion of the U-B hazard area is produced. Note that two small hazard areas, near the outer portion of the display, are produced by the moving ground clutter targets that were not removed during the hazard algorithm processing.

After the radar identifies hazardous areas within a scan display it performes additional processing to assesses the size and amplitude of these areas, tracks the hazardous areas, determines if the various thresholds have been exceeded and then provides a shear hazard warning to the pilot. A sample of a shear hazard warning display is shown in the next figure.

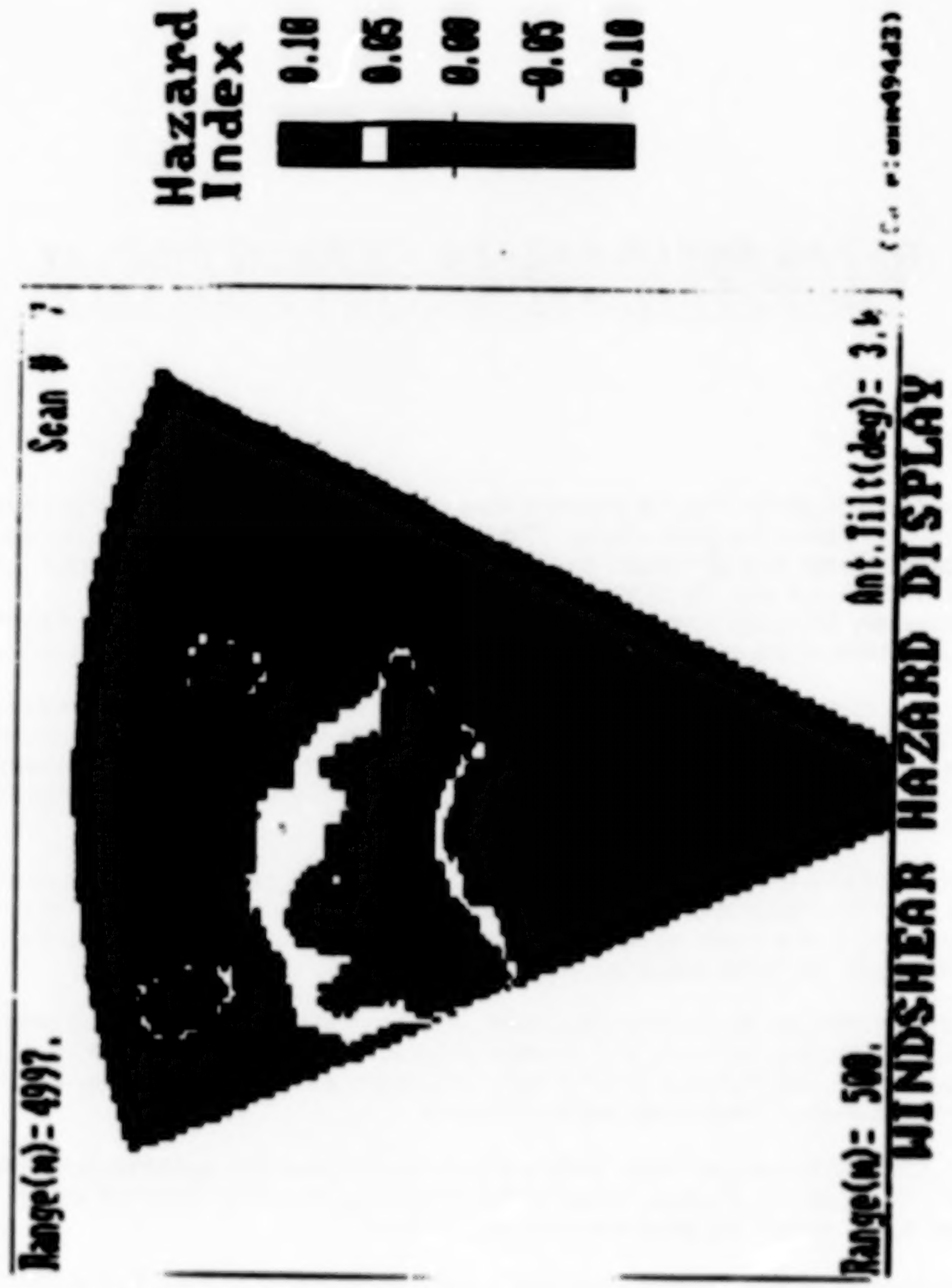

ORIGINAL PAGE IS
OF POOR QUALITY

RADAR SHEAR HAZARD WARNING DISPLAY
U-BURST D49; ANTENNA TILT = VARIABLE

During the simulation run the antenna was continuously scanned as the a/c was progressing along the glide slope. The radar continued to process and evaluate the hazard threat and produced an alarm when the a/c was 40 sec (approx. 3.4 km) in front of the a/c. To minimize the clutter returns the antenna was continuously tilted up from the glide slope, as a function of a/c altitude, keeping the 3 Db point of the main beam hitting the ground 8 km in front of the aircraft.

Positive horizontal hazard indices of .07 or larger that occur over an area of .65 square Km (diameter of .9 km or flight time of about 10 seconds) or greater were set as thresholds for defining hazardous areas. The radar tracked the hazardous areas and produced a shear hazard warning display if they occurred within 40 seconds of the A/C's approach.

A sample of this type display is shown in the ajoining figure. The dark gray area in the display, at about 3.3 KM range, with the dark circle indicates a severe hazard area, and a shear hazard warning has been sounded. At this time the pilot should begin his missed approach procedures.

UAL 395 continued its landing approach until it actually entered the U-B before the pilot began his recovery and missed approach procedure. UAL 395 continued descending to 100 ft above ground level before the a/c was able to gain altitude and continue the missed approach procedure.

If UAL 395 had a Doppler radar with wind shear processing capability on board the a/c, the pilot could have executed the missed approach procedure much sooner and avoided the severest part of the storm.

A simuliar set of simulations were conducted on the flight of UAL 236 as it approached U-B D51. A similar warning display was produced by the radar 40 seconds prior to encounter.

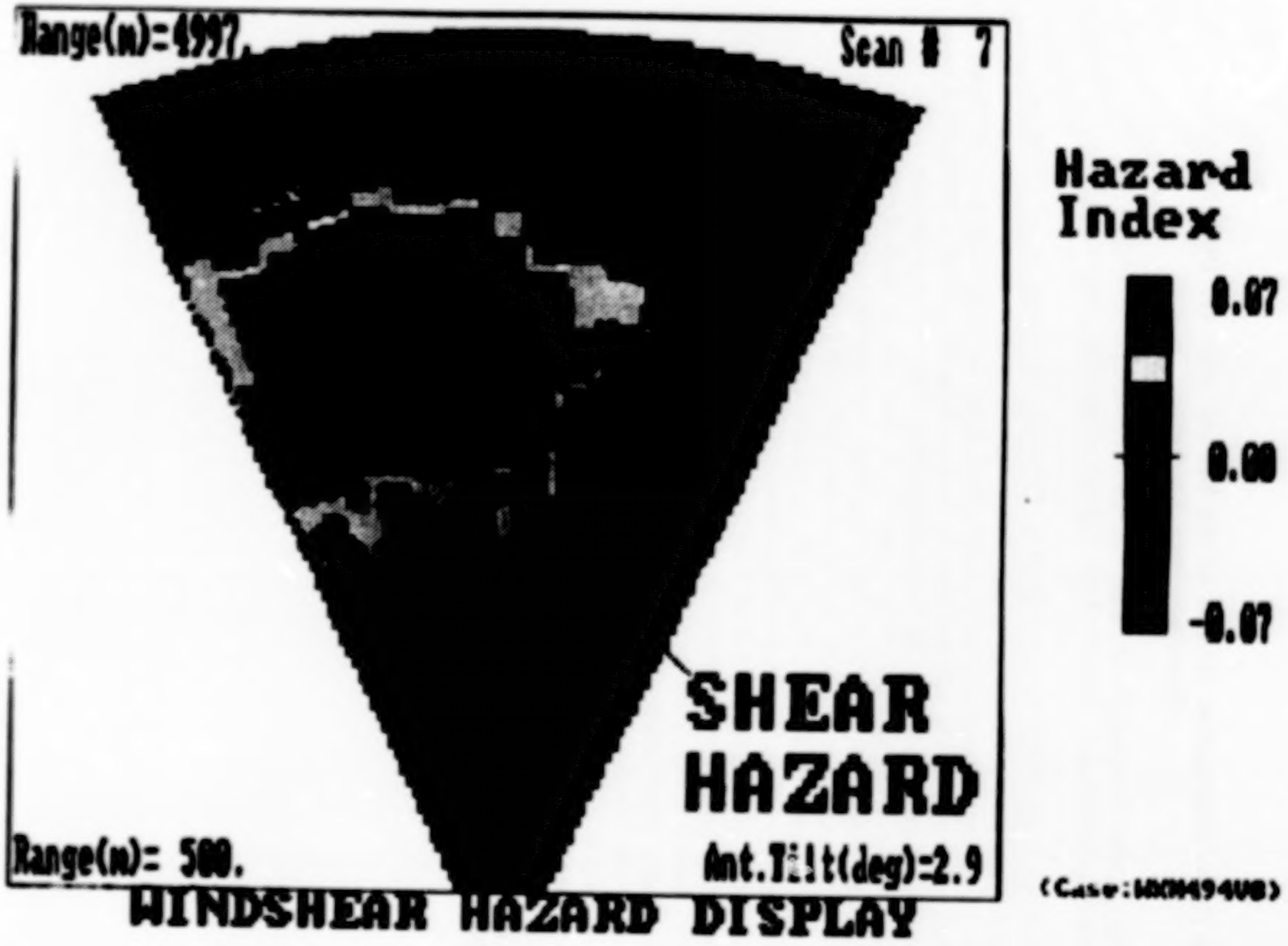

ORIGINAL PAGE IS
OF POOR QUALITY

Airborne Radar Simulation Studies of the Denver July 11, 1988 Microburst Questions and Answers

Q: RUSSELL TARG (Lockheed) - At what rain rate does water build up degrade performance of weather radar - red out? How will rain effect wind shear radar?

A: EMEDIO BRACALENTE (NASA Langley) - If the rain rate builds up, of course, we get a much stronger back scatter return signal for the radar to operate on. We also get attenuation, but at these frequencies and over the short ranges we're talking about the back scatter actually increases a little bit faster than we get the attenuation. Over large ranges the attenuation could become critical, if the heavy rain existed over very large portions of the range. When we ran the simulation for the Dallas/Ft. Worth case, which had extremely heavy rains in it, probably in the 8 to 10 inches per hour rate, we saw attenuation which we incorporate in the simulation program. But, it was not sufficient to decrease the back scatter signal. We still had a very strong signal noise ratio. In fact we ran that even up at the KU ban where the attenuation is much heavier and still were able to see through it. So in general, we don't think attenuation of rain rates are going to have an effect. Actually, we prefer to have the rains a little bit heavier because we have a stronger signal to work with. There is the question of heavy rain on the radome and those effects have been addressed off and on. In general the microburst type phenomenon tends to occur in an atmosphere where we're not encountering rain initially. We're looking forward and since we're trying to protect over the 5 to 10 kilometer range we don't think there will be any degradation due to heavy rains. Exactly at what level buildup it would take to completely degrade performance, you're probably talking about extremely heavy rains which probably are up in the tens of inches per hour. They don't usually exist over a very large extent so the attenuation is still going to be small.

Session X. Airborne Doppler Radar / NASA

N91-24156

Description, Characteristics, & Testing of the NASA Airborne Radar
W. R. Jones, NASA Langley
O. Altiz, Rockwell International
P. Schaffner, NASA Langley
J. H. Schrader, RTI
H. J. C. Blume, NASA Langley

Description, Characteristics, and Testing of the NASA Airborne Radar

by

W.R. Jones, NASA Langley
O. Alitz, Rockwell International
P.R. Schaffner, NASA Langley
J.H. Schrader, Research Triangle Institute
J.H.C. Blume, NASA Langley

PRECEDING PAGE BLANK NOT FILMED

Description, Characteristics, and Testing of the NASA Airborne Radar

W. R. Jones, NASA Langley; O. Alitz, Rockwell International;
P. R. Schaffner, NASA Langley; J.H. Schrader, RTI;
and H. J. C. Blume, NASA Langley

ABSTRACT

The NASA/FAA Airborne Wind Shear Program has as its objective the development and demonstration of technology for low altitude wind shear risk reduction through airborne detection, warning, and avoidance. This paper presents the description of a coherent radar scatterometer and its associated signal processing hardware which have been specifically designed to detect microbursts and record their radar characteristics. Radar parameters, signal processing techniques and detection algorithms, all under computer control, combine to sense and process reflectivity/clutter/microburst data. Also presented is the system's high density, high data rate recording system. This digital system is capable of recording many minutes of the in-phase and quadrature components and corresponding reciever gains of the scattered returns for selected spatial regions, as well as other aircraft and hardware related parameters of interest for post-flight analysis.

Description, Characteristics, and Testing of the NASA Airborne Radar

I. Introduction
A. Block diagram of combined system
B. Aircraft test configuration
C. System Capabilities
II. Rockwell/Collins radar modifications
A. WXR-700XN, Basic Research Radar
B. WRT-701XN Receiver/Transmitter Characteristics
C. WXI-711 Indicator special features
III. NASA/Langley scatterometer system
A. Experimental system signal flow
B. I&Q system diagram
C. Data recording
D. Real-Time Display Processing
IV. Status

Experimental Radar System Block Diagram

This block diagram shows the complete Wind Shear radar system. The top row of blocks shows the pilots standard system and a proposed auxiliary display of information from the experimental radar. The second row is the flat-plate antenna which is mounted in the nose of the aircraft. The lower section consists of the modified research weather radar unit from Rockwell/Collins and the NASA/Langley developed and built subsystem comprising control and display computers, system interfaces to the aircraft (DATAC), the I/Q detectors, timing circuits and data recording system.

Experimental Radar System Block Diagram

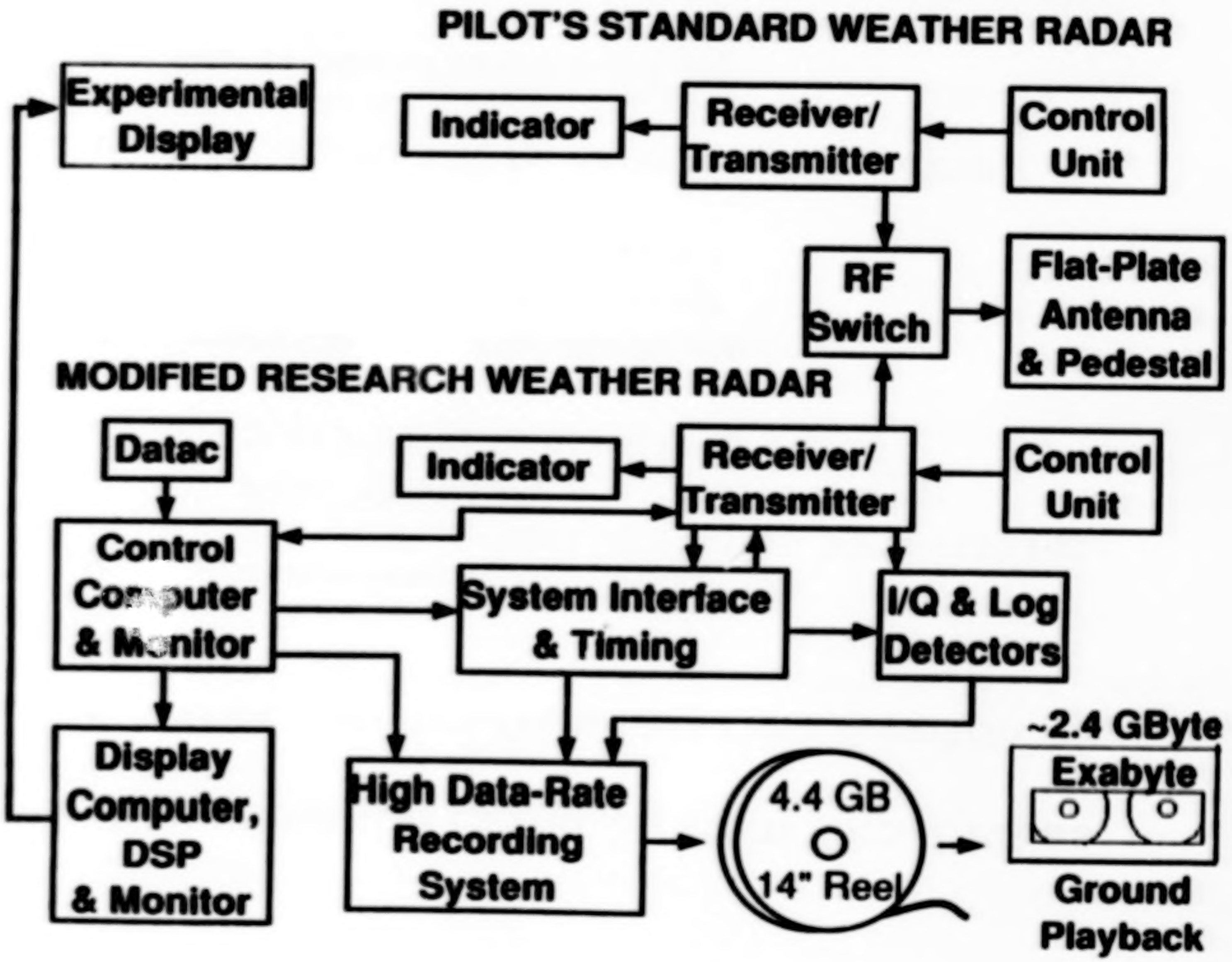

PILOT'S STANDARD WEATHER RADAR
Experimental Display
Indicator
Receiver/ Transmitter
Control Unit
RF Switch
Flat-Plate Antenna & Pedestal
MODIFIED RESEARCH WEATHER RADAR
Datac
Indicator
Receiver/ Transmitter
Control Unit
Control Computer & Monitor
System Interface & Timing
I/Q & Log Detectors
Display Computer, DSP & Monitor
High Data-Rate Recording System
4.4 GB
14" Reel
~2.4 GByte
Exabyte
Ground Playback

Experimental Radar System Capabilities

- Independent Data Frames 128 Pulse Repetition Periods per Frame

- Selectable Transmitter Parameters
    - PRF (Will use 9581, 4791, 3755, 2395, 1198 Hz)
    - Pulse Width (Will use ~ 1, 2, 4, or 8 μs)
    - Dual X-Band Transmit Frequencies

- Selectable Antenna Parameters
    - Scan Pattern (az, el, az/el)
    - Scan Rate (3 Frames/1.5°)

- Independent AGC for each Range Bin (>60 dB)

- Fast I.F. Gain Control (<0.5 μs)

Experimental Radar System Capabilities
Continued

- Selectable Range Bin Sampling of up to 124 bins to be recorded and processed out of 81 to 843 (depending on PRF & pulse width) available from R/T unit
- Capability of skipping 0, 1, 2, or 3 Range Bins for each one selected
- "Second Range Mode" in which every other transmit pulse is inhibited in order to study effects of range aliasing

Wind Shear Experimental Radar - Functional Block Diagram

This block diagram shows the major functional components of the NASA/Langley Experimental Radar in some detail. The Rockwell/Collins modified R/T unit has analog and digital interfaces to the remainder of the system. The analog outputs from the R/T unit consist of the Coherent Reference (COHO ref.), used to lock the phase of the 3rd local oscillator (3rd LO) for the 3rd IF in the NASA I/Q Detector, and the 1st IF (mislabeled 1st RF Out on the diagram) which provides the "video" signal to the I/Q Detectors. Digital output lines from the R/T carry the clock signal (used to synchronize an 8 phase clock in the NASA portion of the system), the Frame Trigger (Trig.) which denotes the start of a new 128 pulse frame of data, and the Inhibit (Inhib.) signal which indicates when alternate transmit pulses are being inhibited in the Range Alias mode. Communications between the R/T unit and the NASA control computer are carried out over ARINC 429 (control) and ARINC 453 (data) serial busses. The control computer also houses a number of other interface cards. A DATAC interface card used to acquire data from the aircraft data systems. A GPIB/IEEE-488 interface card provides for control of the Programmable Low Pass (anti-aliasing) Filters and the Programmable Pulse Generator used for tape recorder timing. A DSP card and an associated interface card implement digital bin-to-bin Automatic Gain Control (AGC) using averages (for each bin) of the log detector output over a portion of each frame to calculate attenuator settings for the next frame. The Sample/Write control circuit generates timing signals to clock data into FIFO buffers and to insert "line sync" word patterns in the I&Q digital data stream at the beginning of each line of data corresponding to the set of returns from a single transmit pulse. The Tape and Processing I&Q buffers are organized in a ping-pong arrangement where the A buffers are filled first, followed by the B buffers. Digitized data flows to the Tape and Processing FIFOs in parallel. While the B buffers are being clocked out to tape (based on signals from the Read Control circuit) or read by the Display Processing Computer, the A buffers are being filled with digitized data from the A/D converters. The auxiliary Data FIFO and a similar FIFO hosted in the Display Processing Computer are simultaneously filled with data by the Control Computer. This auxiliary data includes aircraft data from the DATAC system, hardware status and control words, Collins R/T information from ARINC 429 (Control) and ARINC 453 (Data) bus interfaces, and bin-to-bin AGC log channel averages. This data is clocked out to tape at the beginning of each frame of 128 pulses.

WINDSHEAR EXPERIMENTAL RADAR-FUNCTIONAL BLOCK DIAGRAM

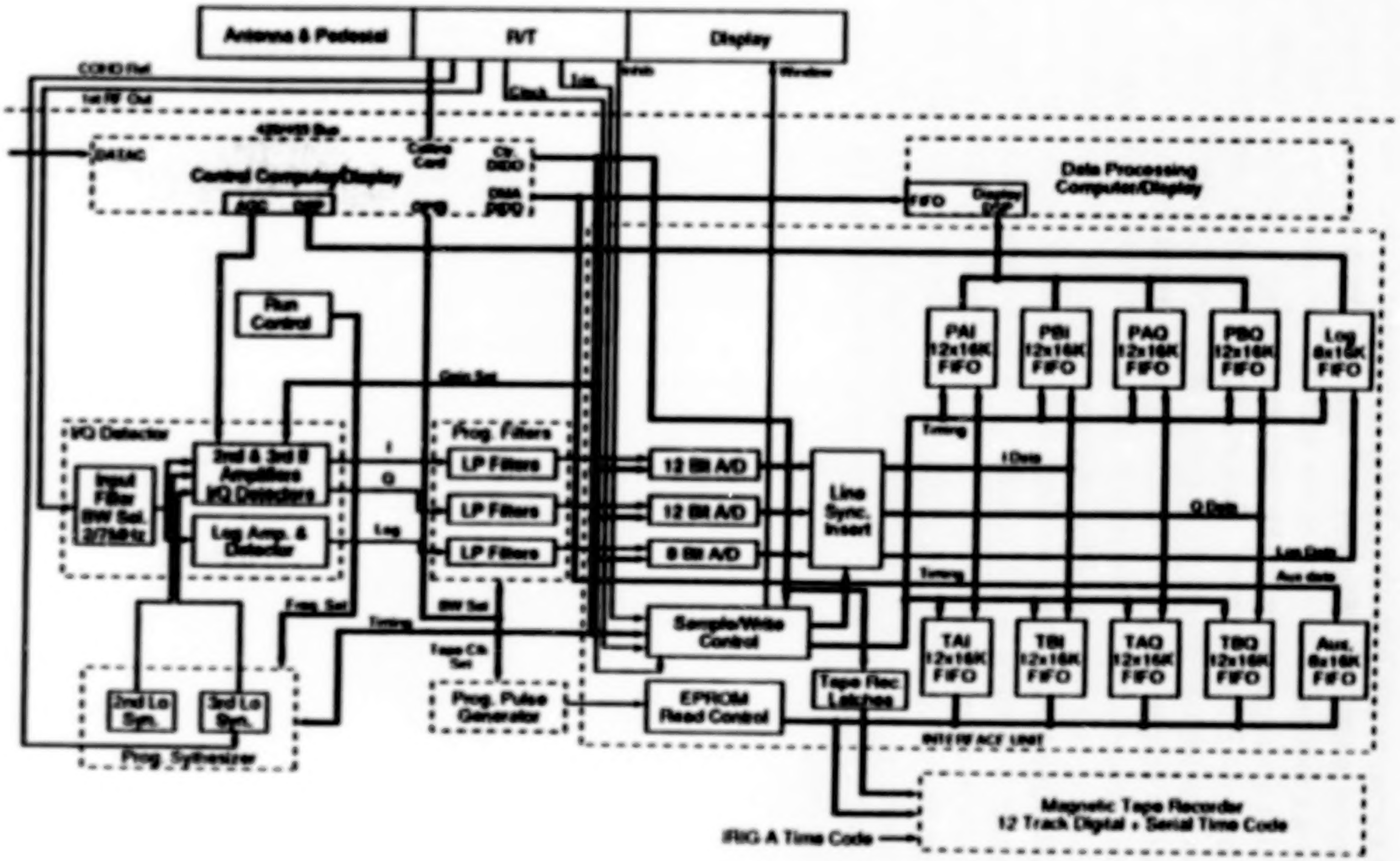
Antenna & Pedestal
R/T
Display
COHO Ref
1st RF Out
Clock
Window
Control Computer/Display
DATAC
Data Processing
Computer/Display
FIFO
Run
Control
Gain Set
I/Q Detector
Input
Filter
BW Sel.
2/7MHz
2nd & 3rd If
Amplifiers
I/Q Detectors
Log Amp. &
Detector
I
Q
Log
Prog. Filters
LP Filters
LP Filters
LP Filters
12 Bit A/D
12 Bit A/D
8 Bit A/D
Line
Sync.
Insert
PAI
12x16K
FIFO
PBI
12x16K
FIFO
PAQ
12x16K
FIFO
PBQ
12x16K
FIFO
Log
8x16K
FIFO
Timing
I Data
Q Data
Log Data
Aux data
Freq. Sel
Timing
BW Sel
Tape Clk
Sel
Sample/Write
Control
TAI
12x16K
FIFO
TBI
12x16K
FIFO
TAQ
12x16K
FIFO
TBQ
12x16K
FIFO
Aux.
8x16K
FIFO
2nd Lo
Syn.
3rd Lo
Syn.
Prog. Synthesizer
Prog. Pulse
Generator
EPROM
Read Control
Tape Rec
Latches
INTERFACE UNIT
Magnetic Tape Recorder
12 Track Digital + Serial Time Code
IRIG A Time Code

W/S Radar Waveguide & Component Location Aboard Test Aircraft

The Experimental Windshear Radar System components are distributed in several locations in the NASA/Langley 737 aircraft. The Antenna and Pedestal are mounted behind a radome in the nose of the aircraft. This assembly is fed by waveguide routed through a waveguide switch located near the pilot's Standard Weather Radar unit in the nose E&E compartment. This waveguide switch is controlled by the pilot and allows switching between the Standard and Experimental R/T units. The unused system's output is fed to a Dummy Load to prevent unwanted radiation into the interior of the aircraft. The pilot's Indicator (Display) and Control units are interfaced to the Standard R/T via ARINC 429 and 453 buses. The experimental R/T unit and 2 KW High Power Amplifier Unit are located aft of the cockpit in the galley area. Another waveguide switch, controlled by the Experimental R/T unit, switches the HPAU in and out of the system as requested by the experimenters at the dual bay Wind Shear Radar Experiment Station located near the tail in the aft cabin. Connections from the Experiment Station to the Experimental R/T unit include ARINC 429 and 453 buses, and coaxial cables carrying 1st IF, Coherent Reference, and monitor signals.

W/S RADAR WAVEGUIDE & COMPONENT LOCATION
Aboard Test Aircraft

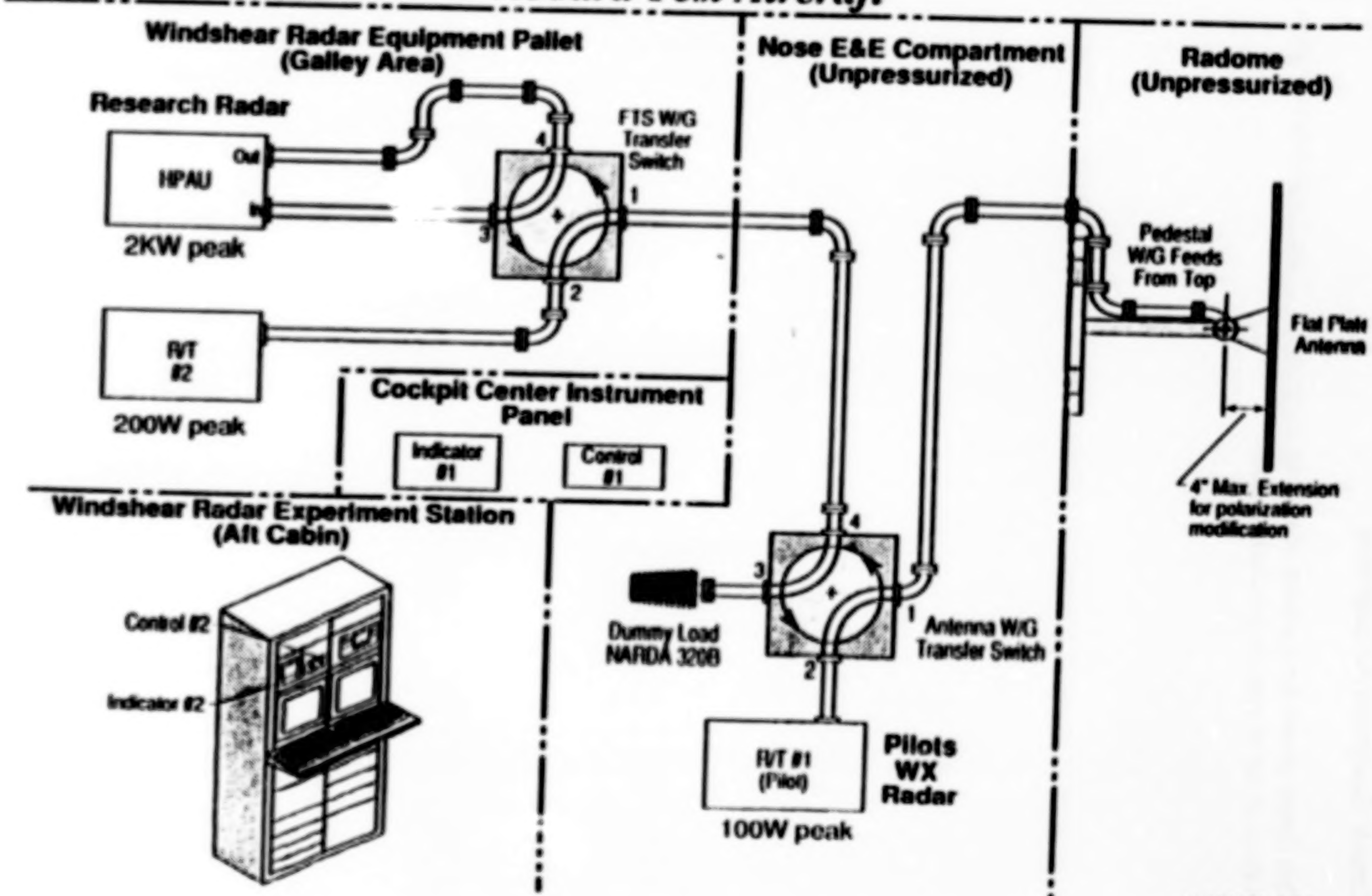
Windshear Radar Equipment Pallet (Galley Area)
Research Radar
HPAU
Out
In
2KW peak
R/T #2
200W peak
FTS W/G Transfer Switch
1
2
3
4
Cockpit Center Instrument Panel
Indicator #1
Control #1
Windshear Radar Experiment Station (Aft Cabin)
Control #2
Indicator #2
Nose E&E Compartment (Unpressurized)
Dummy Load NARDA 320B
Antenna W/G Transfer Switch
R/T #1 (Pilot)
Pilots WX Radar
100W peak
Radome (Unpressurized)
Pedestal W/G Feeds From Top
Flat Plate Antenna
4" Max. Extension for polarization modification

Console Equipment Arrangement

This figure shows the location of various components of the Experiment Station portion of the system in the dual bay rack.

WINDSHEAR RADAR FLIGHT EXPERIMENT

Console Equipment Arrangement

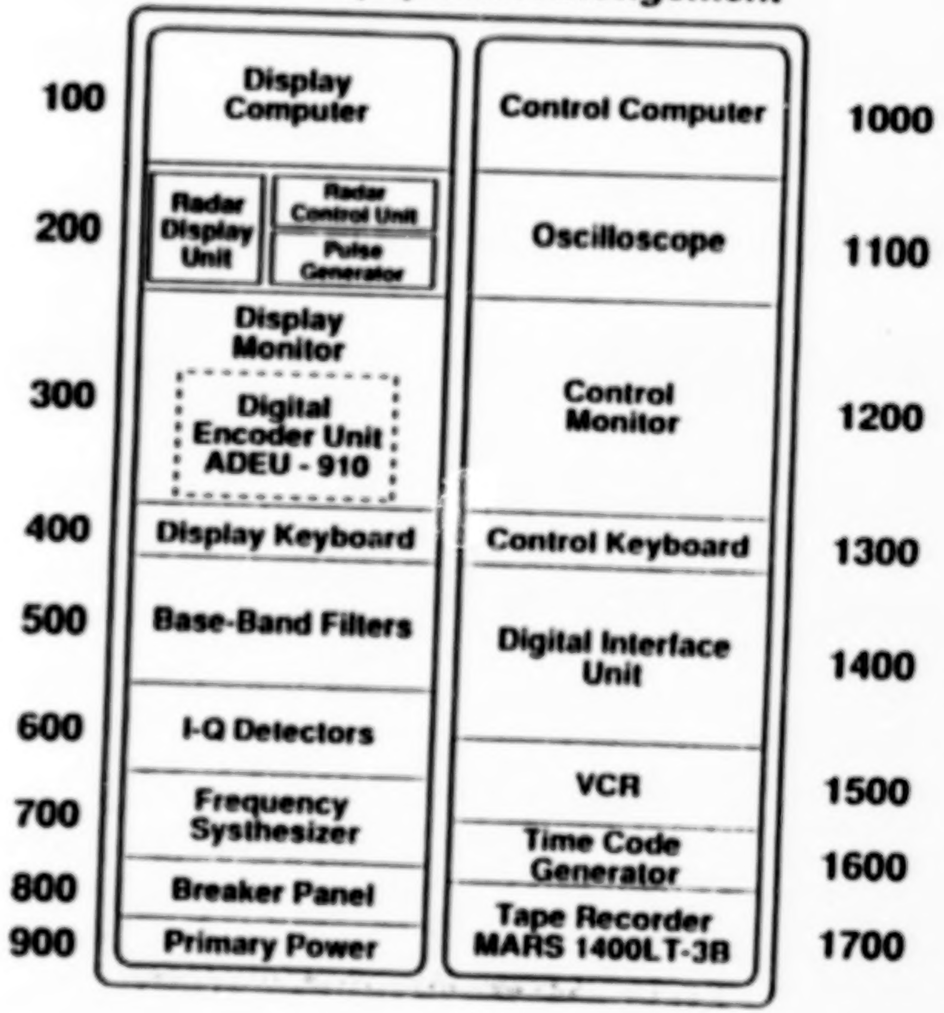

100 Display Computer

200 Radar Display Unit | Radar Control Unit | Pulse Generator

300 Display Monitor | Digital Encoder Unit ADEU - 910

400 Display Keyboard

500 Base-Band Filters

600 I-Q Detectors

700 Frequency Systhesizer

800 Breaker Panel

900 Primary Power

Control Computer 1000

Oscilloscope 1100

Control Monitor 1200

Control Keyboard 1300

Digital Interface Unit 1400

VCR 1500

Time Code Generator 1600

Tape Recorder MARS 1400LT-3B 1700

105 0507 001 0/1 A

WXR 700 XN Research Radar System

This block diagram shows the Rockwell Collins supplied modified Weather Radar system components. This system can operate as a stand-alone radar but will generally be operated as an integral part of the NASA/Langley Experimental Wind Shear Radar system.

BLOCK DIAGRAM, WXR700XN RESEARCH RADAR SYSTEM

ROCKWELL INTERNATIONAL, COLLINS

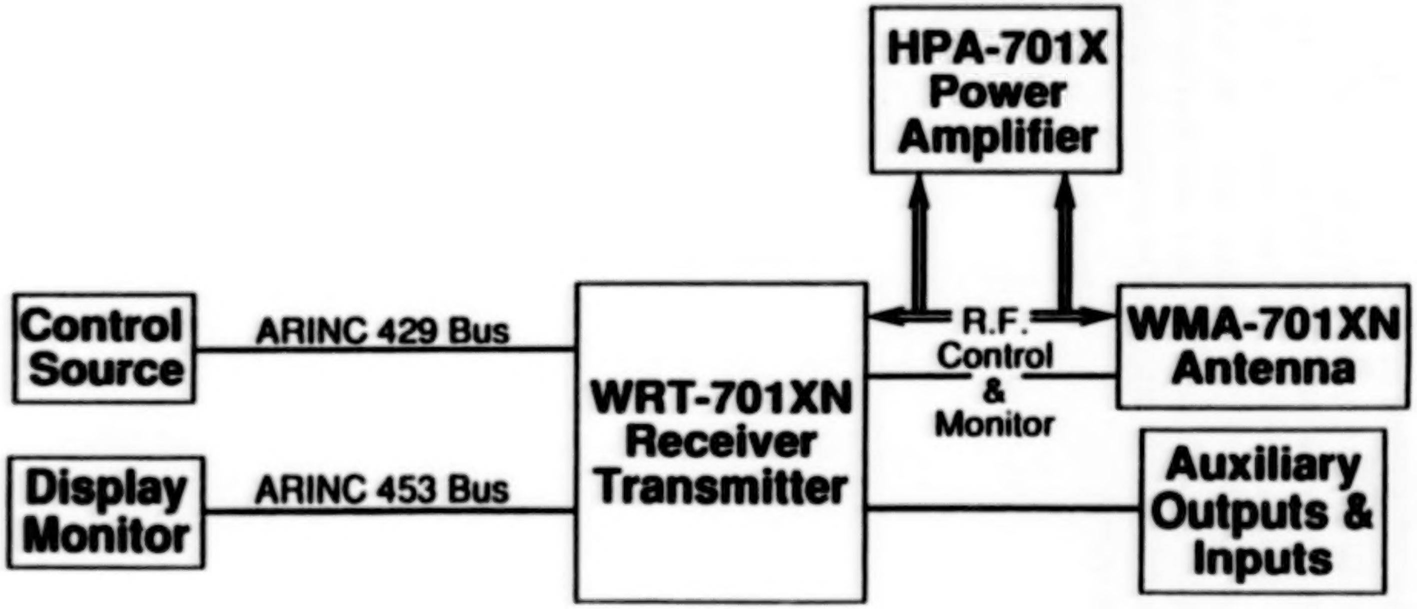

HPA-701X Power Amplifier

Control Source

ARINC 429 Bus

Display Monitor

ARINC 453 Bus

WRT-701XN Receiver Transmitter

R.F.

Control & Monitor

WMA-701XN Antenna

Auxiliary Outputs & Inputs

WRT 701 XN Receiver/Transmitter

This simplified block diagram illustrates the internals of the Collins R/T unit and the interfaces which allow it to be integrated as a component of the NASA/Langley system. The AC Attitude control is an ARINC 429 bus, separate from the ARINC 429 Control bus driven by the Control Computer, which supplies roll and pitch information used to be used by the R/T unit in compensating for effects of aircraft motion on antenna pointing. The First Intermediate Frequency output (erroneously shown as an input) provides to signal input to the NASA/Langley developed portion of the system. A coherent reference is also provided as an output in order to allow coherent detection to be employed to generate In-phase and Quadrature components of the radar return.

SIMPLIFIED BLOCK DIAGRAM, WRT 701XN RECEIVER TRANSMITTER

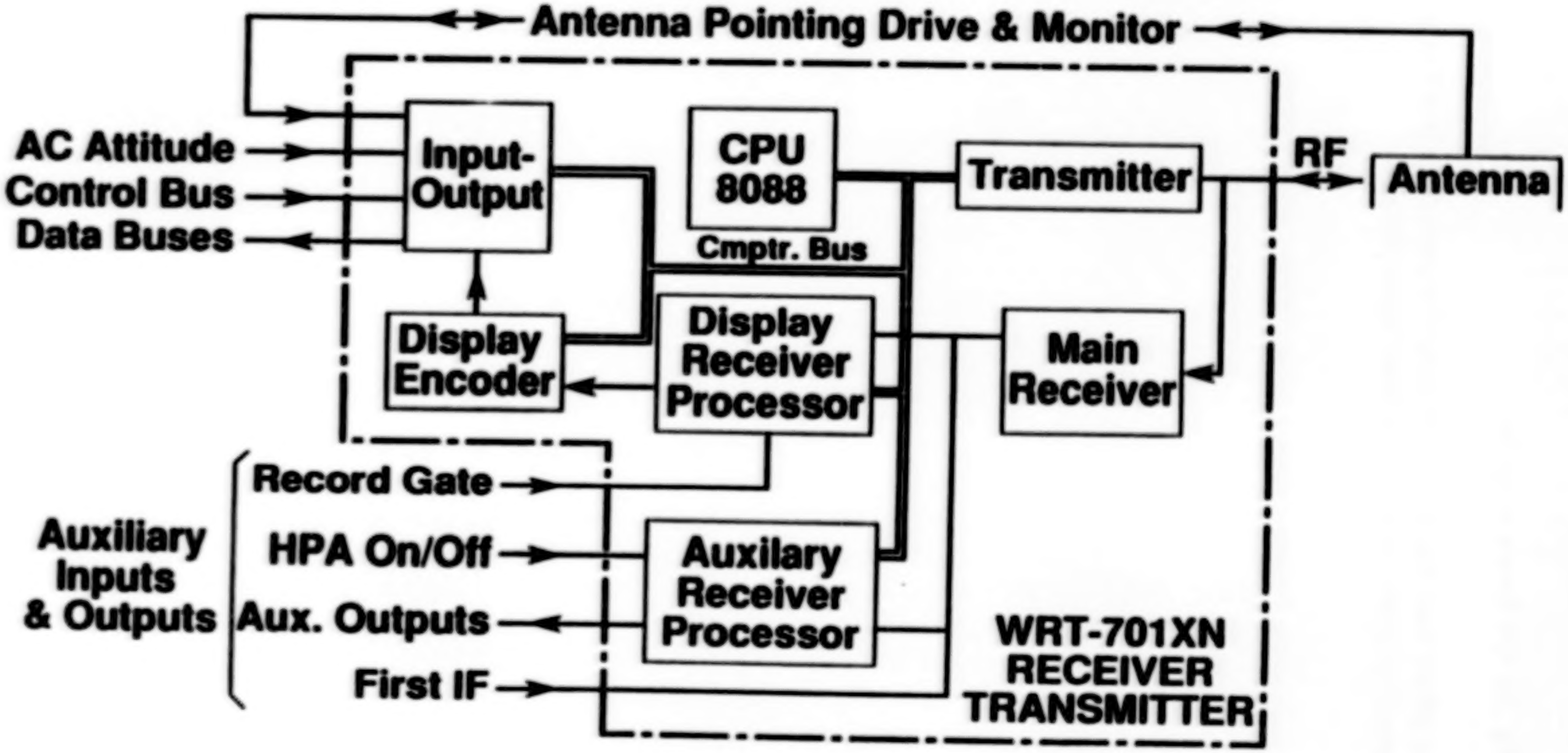
Antenna Pointing Drive & Monitor
AC Attitude
Control Bus
Data Buses
Input-Output
CPU 8088
Transmitter
RF
Antenna
Cmptr. Bus
Display Encoder
Display Receiver Processor
Main Receiver
Auxiliary Inputs & Outputs
Record Gate
HPA On/Off
Aux. Outputs
First IF
Auxilary Receiver Processor
WRT-701XN RECEIVER TRANSMITTER

HPA 701 XN Power Amplifier

The HPAU traveling wave tube amplifier provides a 10 dB or greater increase in transmitted power to provide greater signal strength.

HPA-701XN POWER AMPLIFIER

- Traveling wave tube amplifier.
- Amplifies WRT transmit output.
- 2650 Watts peak.
- Provides receive signal path, antenna to WRT.

WMT 701 XN Antenna

The antenna is the same flat plate unit supplied with Collins' Standard Weather Radar but a n additional rotational joint has been added to the positioner to allow a 90 degree rotation of the antenna to provide either horizontal or vertical polarization in order to allow investigation of any polarization effects which might aid in separating signals resulting from weather from those produced by ground clutter.

WMT-701XN ANTENNA

- Flatplate radiator with supporting pedestal.
- Pointing is controlled by the computer in the WRT-701XN receiver transmitter.
- Stabilized with aircraft attitude inputs.
- Selectable horizontal or vertical polarization.

Research System Detector (simplified) Block Diagram

The NASA system incorporates synchronous detection to provide In-phase and Quadrature components of the radar signal. A log detector is used to drive a Digital Signal Processing card, implementing a feed forward bin-to-bin digital Automatic Gain Control system which sets three programmable attenuators in the I&Q signal path in order to minimize system noise and keep the signal within the dynamic range of the 12 bit A/D converters.

RESEARCH SYSTEM DETECTOR BLOCK DIAGRAM

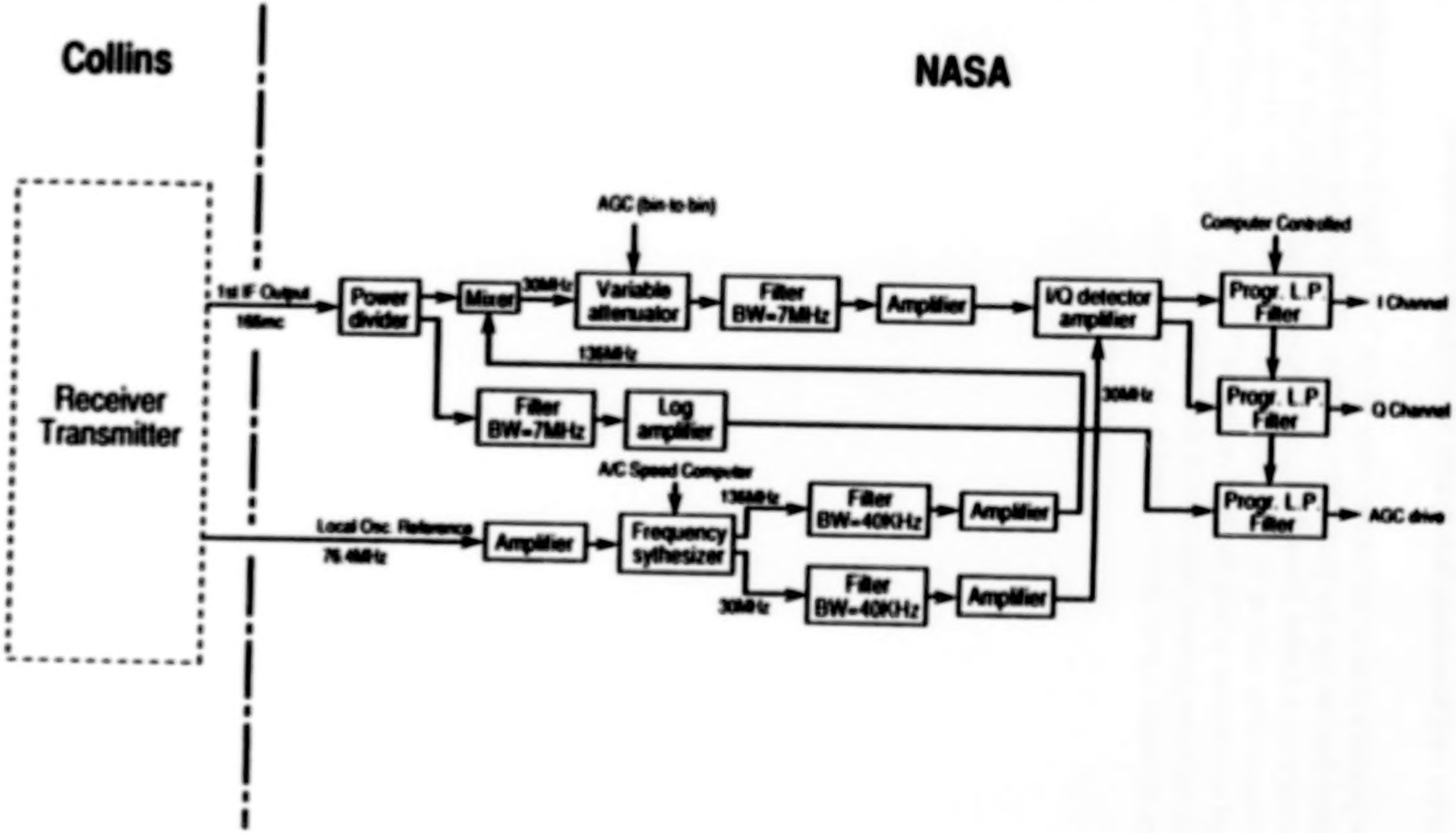
Collins
NASA
Receiver
Transmitter
1st IF Output
166mc
Power divider
Mixer
30MHz
AGC (bin-to-bin)
Variable attenuator
Filter BW=7MHz
Amplifier
I/Q detector amplifier
Computer Controlled
Progr. L.P. Filter
I Channel
136MHz
Filter BW=7MHz
Log amplifier
30MHz
Progr. L.P. Filter
Q Channel
A/C Speed Computer
Local Osc. Reference
76.4MHz
Amplifier
Frequency sythesizer
136MHz
Filter BW=40KHz
Amplifier
30MHz
Filter BW=40KHz
Amplifier
Progr. L.P. Filter
AGC drive

Display and Recording Subsystems Simplified Block Diagram

The primary goal of the current stage of the Wind Shear Radar Experiment is to collect data on tape for post-flight analysis. The I&Q and AUX data streams are recorded on a Kodak Datatape 1" 14 track tape unit providing up to 4.4 GBytes of storage at data rates up to 1.6 million 12 bit digital words per second. One channel is used in direct or analog mode to record an IRIG-A (10 KHz carrier) time code signal used to locate desired segments of data on playback. The last channel is used by the tape recorder's error detection and correction circuitry.

Display & Recording Subsystems Simplified Block Diagram

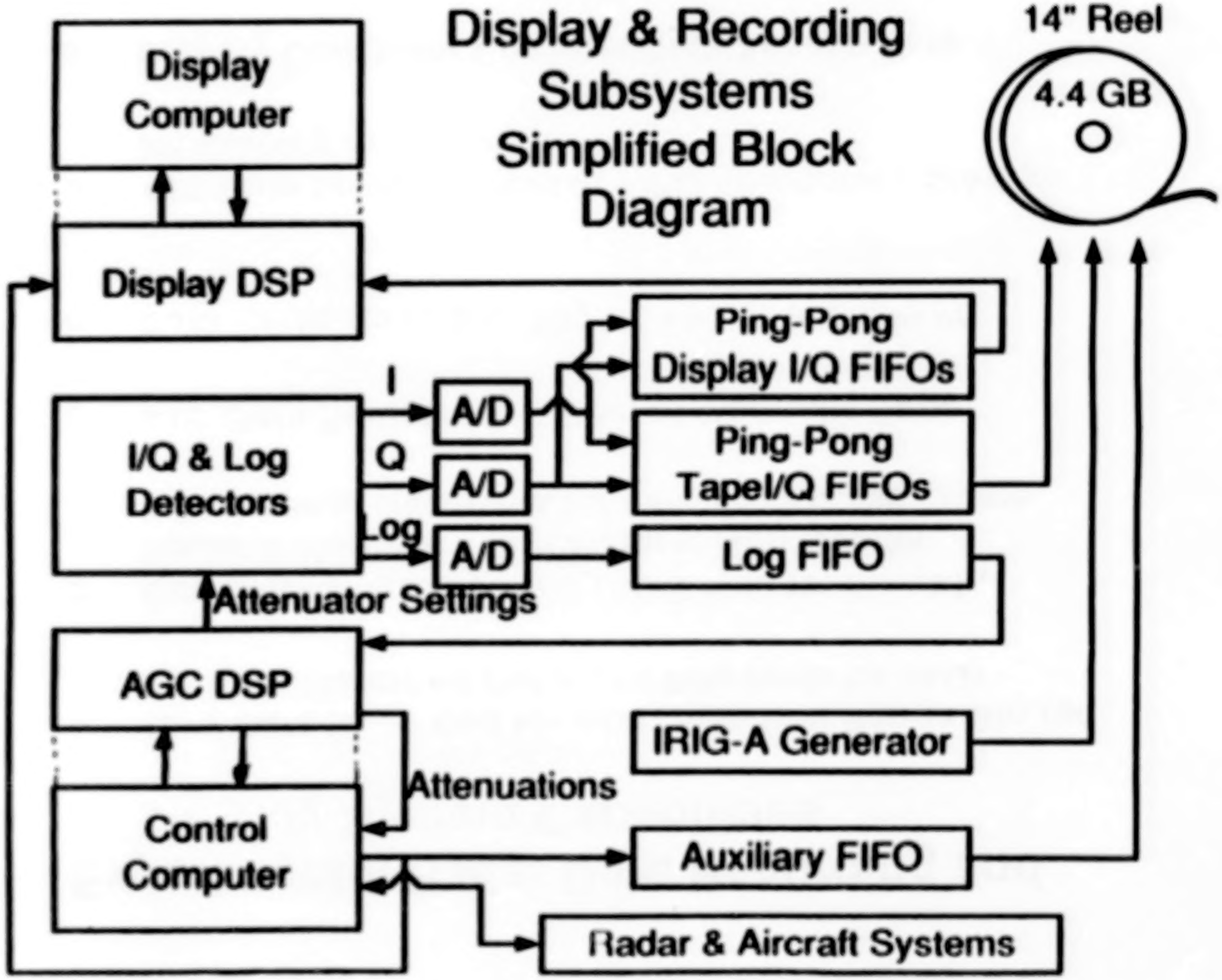
14" Reel
4.4 GB
Display Computer
Display DSP
Ping-Pong Display I/Q FIFOs
I
Q
Log
A/D
A/D
A/D
I/Q & Log Detectors
Ping-Pong TapeI/Q FIFOs
Log FIFO
Attenuator Settings
AGC DSP
IRIG-A Generator
Attenuations
Control Computer
Auxiliary FIFO
Radar & Aircraft Systems

Experimental Radar Data Recording and Display System Capabilities

- Raw Data Recorded for each Selected Range Bin for every Transmitted Pulse (12 Bits each for I&Q)
- Complete Auxiliary Data (AGC values; Aircraft, Radar & Hardware Parameters; Run Header Information) Recorded for every 128 pulse Frame
- >10^9 Data Samples/14" Reel of Magnetic Tape
- Data Rates up to 2.4 MBytes/sec or 800,000 I/Q samples/sec
- 16K Data Samples Held in FIFO Temporary Storage for Display Processing
- Display Computer Controls Data Access Rate

Wind Shear Data Playback Process

A Compaq 386/20 AT compatible computer is used to play back data from the 14 track flight tapes at a ground based playback station. The data is dumped to a 500 MByte hard disk at a continuous 50,000 word/second rate. Each disk full of data is transferred to an 8mm Exabyte Cassette Tape in a format which can be read by the Interactive Systems Corporation UNIX based analysis software. On the UNIX system the data is then loaded into an Informix database system where it can be accessed by analysts.

Windshear Data Playback Process

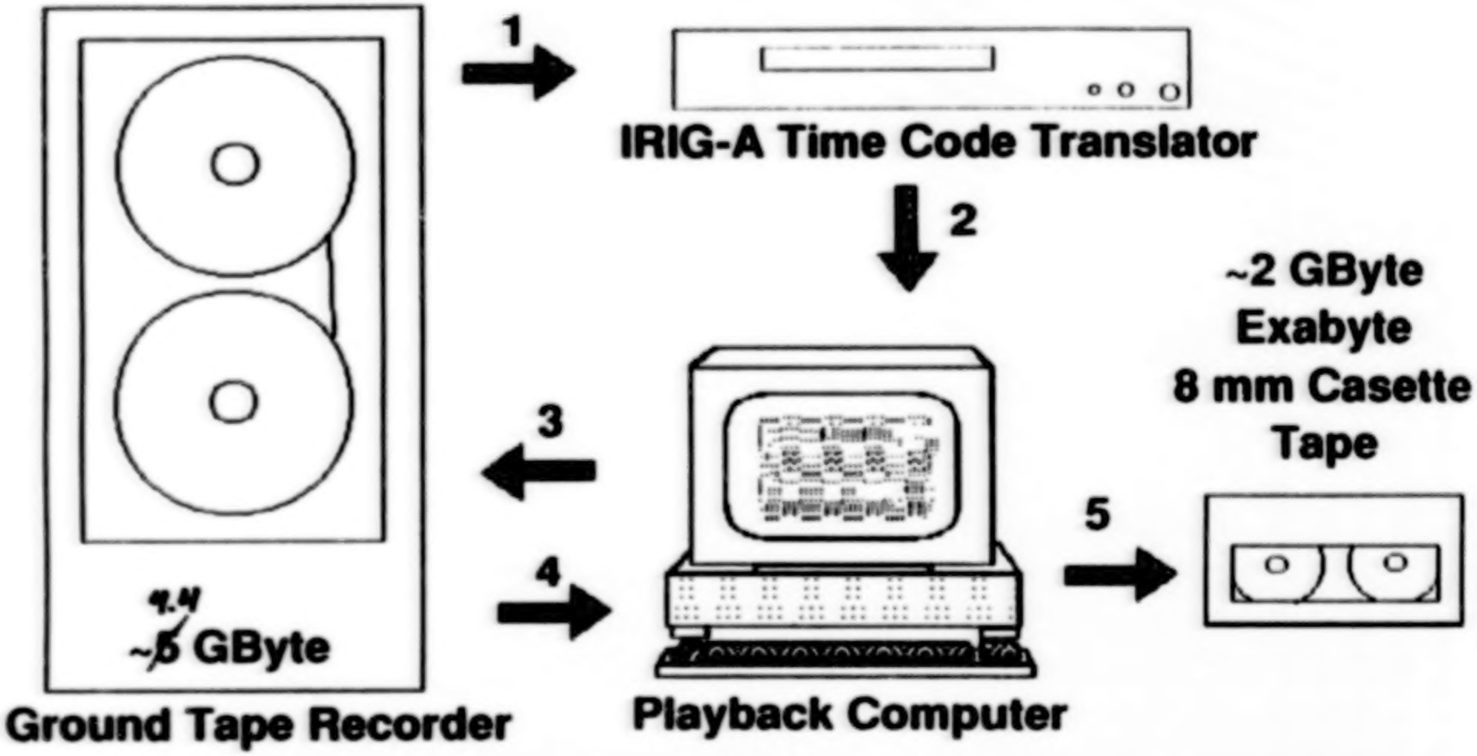
1
IRIG-A Time Code Translator
2
~2 GByte
Exabyte
8 mm Casette
Tape
3
4
5
4.4
~~~5~~ GByte
Ground Tape Recorder
Playback Computer

1 Serial Time Code (IRIG-A, 10 KHz Carrier - direct channel)
2 Time Code Translator produces digital output to computer
3 At time determined by flight log, computer initiates dump
4 12 bit flight data (I&Q and Auxiliary) to 16 bit words on disk
5 Disk file to 8mm Exabyte Tape for analysis system use
~~~

Real-Time Display Processing

A quick-look real-time display has been implemented as part of the Experiment Station on the aircraft. This system consists of a Data Translations DT7020 DSP board hosted in a Texas Microsystems B386 20 MHz rack mounted PC/AT compatible system. The DT7020 card is loaded with data acquisition and processing routines by the 80386 host processor. The DSP board acquires data from the I&Q Processing FIFOs, via a DT-Connect parallel interface, and from the Auxiliary data stream provided by the Control Computer. This data is processed in a continuous loop and the processed data is available to a program running on the host which can then provide a variety of display formats. This system is a valuable diagnostic tool and will aid in effectively using the system to collect data for later analysis. In a later stage of the program a more powerful real-time computer system is planned in order to demonstrate wind shear hazard detection in real time using more sophisticated algorithms than are possible on the DSP board.

Real-Time Display Processing

AT-386 Host

DT-7020 DSP Card

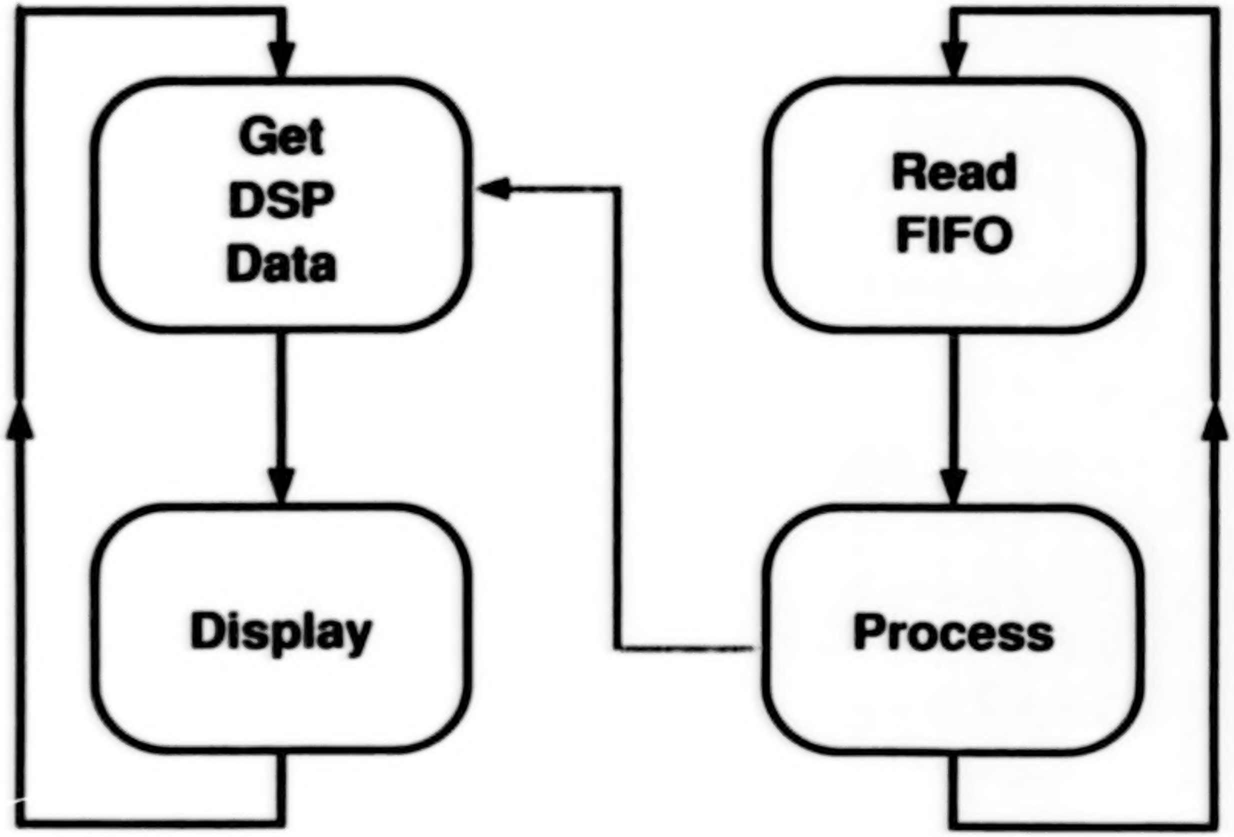

Get DSP Data

Display

Read FIFO

Process

Experimental Radar Real-Time Display
Operational Modes

- Derived Velocity vs Range along range line, with or without doppler filter
- Received Power vs Range along range line, in dBm or dBz
- FFT of 6 selected Range Bins across 1 frame of 128 pulses
- Color map of velocity/range over full azimuth scan, with or without doppler filter
- Color map of hazard/range over full azimuth scan
- Color map of hazard/range over full azimuth scan with wind shear tracking and alarm algorithms included (demonstration mode)

NASA Experimental Radar
Status

- Radar system is currently undergoing the final stages of component testing and integration in the laboratory at NASA Langley.

- After the completion of system integration, operational testing will performed with the antenna system installed on the roof of Building 1299 at Langley. Weather and ground targets will be used as available. During this period, development of real-time and analysis software will continue.

- It is planned to install the system on the Langley 737 aircraft in early January 1991 and begin flight testing, calibration, and clutter and weather data collection.

QA

OVERVIEW
OF THE
WXR-700XN RESEARCH RADAR SYSTEM
PART OF THE
NASA AIRBORNE RESEARCH RADAR SYSTEM

PRESENTED BY

ROCKWELL INTERNATIONAL - COLLINS

OCTOBER 16-18, 1990

CONTENTS

WXR-700XN RESEARCH RADAR SYSTEM

- CONTROL SOURCES
- DISPLAY MONITOR
- HPA-701XN POWER AMPLIFIER
- WMT-701XN ANTENNA
- WRT-701XN RECEIVER TRANSMITTER

FIGURES

FIGURE 1 BLOCK DIAGRAM, WXR-700XN RESEARCH RADAR SYSTEM

FIGURE 2 AIRCRAFT CONTROL AND DISPLAY SUBSYSTEM

FIGURE 3 GROUND CONTROL AND DISPLAY SUBSYSTEM

FIGURE 4 SIMPLIFIED BLOCK DIAGRAM: WRT-701XN RECEIVER TRANSMITTER

ROCKWELL INTERNATIONAL, COLLINS

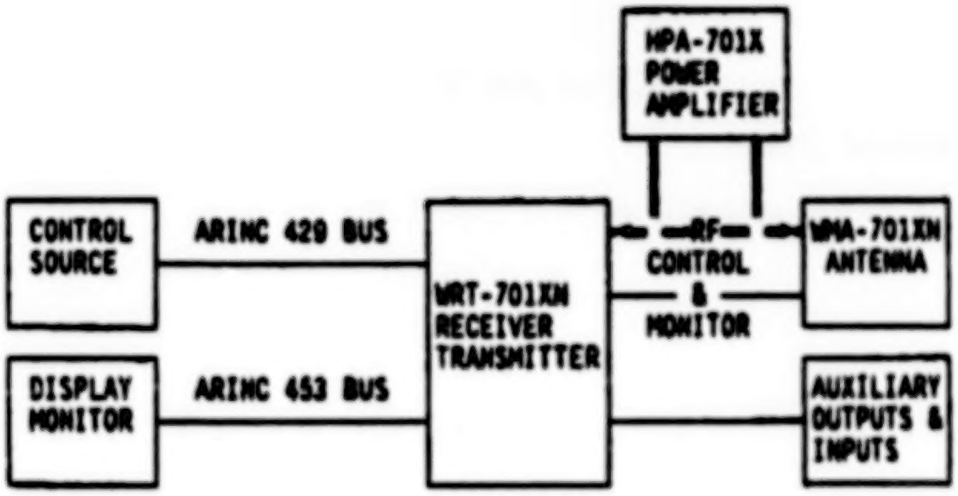
HPA-701X
POWER
AMPLIFIER
CONTROL
SOURCE
ARINC 429 BUS
WRT-701XN
RECEIVER
TRANSMITTER
RF
CONTROL
&
MONITOR
WMA-701XN
ANTENNA
DISPLAY
MONITOR
ARINC 453 BUS
AUXILIARY
OUTPUTS &
INPUTS

FIGURE 1 BLOCK DIAGRAM, WXR-700XN RESEARCH RADAR SYSTEM

WXR-700XN RESEARCH RADAR SYSTEM (FIGURE 1)

CONTROL SOURCES

TEST COMPUTER (IBM COMPATIBLE) AND CDIO-701XN COMPUTER INTERFACE CARD WITH NASA OR COLLINS SOFTWARE IN COMPUTER (FIGURE 2).

COLLINS WDP-701 WEATHER DISPLAY PROCESSOR USED IN CONJUNCTION WITH A PERSONAL COMPUTER SYSTEM AND COLLINS SOFTWARE. (FIGURE 3)

DISPLAY MONITOR

WXI-711 INDICATOR (FIGURE 2)

COLOR RGB TV MONITOR USED WITH WDP-701 (FIGURE 3)

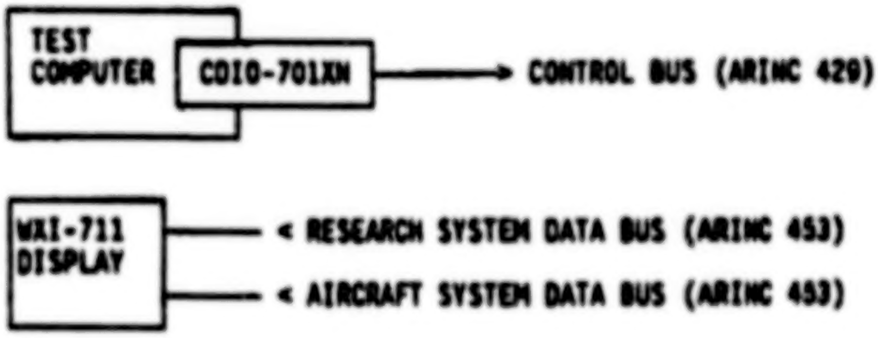
TEST COMPUTER
CDIO-701XN
CONTROL BUS (ARINC 429)
WXI-711 DISPLAY
< RESEARCH SYSTEM DATA BUS (ARINC 453)
< AIRCRAFT SYSTEM DATA BUS (ARINC 453)

FIGURE 2 AIRCRAFT CONTROL AND DISPLAY SUBSYSTEM

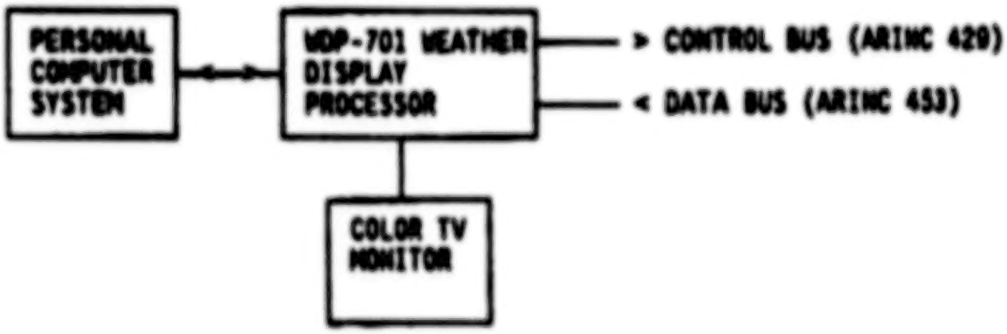
PERSONAL COMPUTER SYSTEM
WDP-701 WEATHER DISPLAY PROCESSOR
> CONTROL BUS (ARINC 429)
< DATA BUS (ARINC 453)
COLOR TV MONITOR

FIGURE 3 GROUND CONTROL AND DISPLAY SUBSYSTEM

HPA-701XN POWER AMPLIFIER

TRAVELING WAVE TUBE AMPLIFIER

AMPLIFIES WRT TRANSMIT OUTPUT

2650 WATTS PEAK

PROVIDES RECEIVE SIGNAL PATH, ANTENNA TO WRT

WRT-701XN ANTENNA

FLATPLATE RADIATOR WITH SUPPORTING PEDESTAL

POINTING IS CONTROLLED BY THE COMPUTER IN THE WRT-701XN RECEIVER TRANSMITTER

STABILIZED WITH AIRCRAFT ATTITUDE INPUTS

SELECTABLE HORIZONTAL OR VERTICAL POLARIZATION

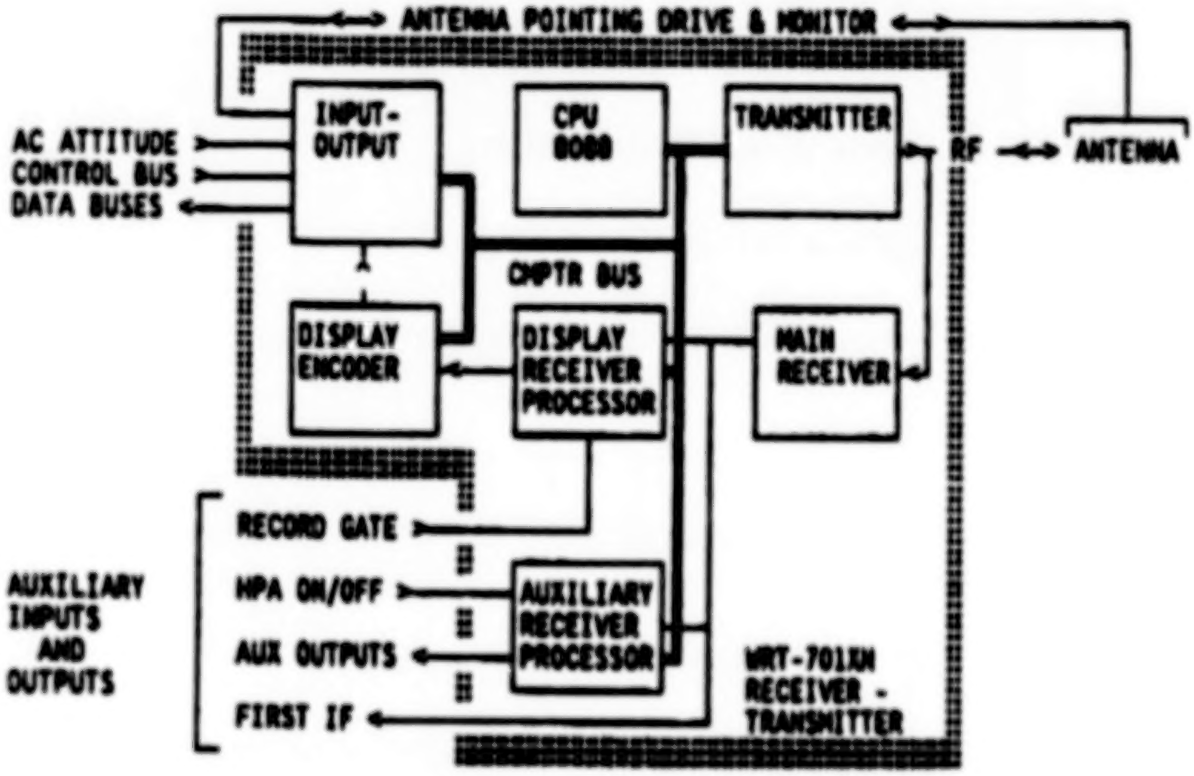
ANTENNA POINTING DRIVE & MONITOR
AC ATTITUDE
CONTROL BUS
DATA BUSES
INPUT-OUTPUT
CPU 8080
TRANSMITTER
RF
ANTENNA
CMPTR BUS
DISPLAY ENCODER
DISPLAY RECEIVER PROCESSOR
MAIN RECEIVER
RECORD GATE
AUXILIARY INPUTS AND OUTPUTS
HPA ON/OFF
AUX OUTPUTS
FIRST IF
AUXILIARY RECEIVER PROCESSOR
WRT-701XN RECEIVER - TRANSMITTER

FIGURE 4 SIMPLIFIED BLOCK DIAGRAM, WRT-701XN RECEIVER TRANSMITTER

WRT-701XN RECEIVER TRANSMITTER (FIGURE 4)

CONTROL BUS INPUT (ARINC 429 BUS) ESTABLISHES THE OPERATING CONFIGURATION.

INTERNAL COMPUTER (8088 CPU) CONFIGURES THE SYSTEM VIA THE COMPUTER BUS.

TRANSMITTER - SELECT FREQUENCY, PULSE WIDTH PRF, LOW OR HIGH PEAK POWER

DISPLAY RECEIVER PROCESSOR - BANDWIDTH, RANGE, GAIN, STC, AND MODE (WEATHER, MAP, VELOCITY, ...)

DISPLAY ENCODER - SELECT ENCODING BASED UPON OPERATING MODE

AUXILIARY RECEIVER PROCESSOR - SELECT GAIN, INITIAL STC FOR MATCHED BANDWIDTH, STC SLOPE 0, 6 OR 9 dB/OCTAVE

ANTENNA - SETS UP AND EXECUTES REQUESTED POINTING ROUTINES, USES AIRCRAFT PITCH & ROLL TO COMPUTE POINTING POSITION, ISSUES DRIVE COMMANDS AND MONITORS ANTENNA POSITION.

DATA BUS OUTPUTS (ARINC 453 BUS) PROVIDE HARDWARE CONFIGURATION VERIFICATION, FAULT MONITORING AND RADAR TARGET DATA FOR DISPLAY.

[CONTINUED]

WRT-701XN RECEIVER TRANSMITTER (FIGURE 4)

AUXILIARY INPUTS:

HPA ON/OFF

RECORD GATE

AUXILIARY OUTPUTS; (* NASA PROCESSOR INPUTS)

* FIRST IF

* TRANSMIT SYNC

* 2ND RANGE SYNC

* 4 MHz CLOCK

* COHERENT REF OSCILLATOR

WRT XMIT PEAK POWER MONITOR

AUX SECOND IF STC

AUX SECOND IF RANGE VIDEO

AUX SECOND IF QUADRATURE (Q) RETURN

AUX SECOND IF IN-PHASE (I) RETURN

HPA POWER ENABLE

HPA STANDBY/OPERATE

HPA VIDEO GATE

HPA 777.7 MHz REFERENCE

HPA PHASE DETECTOR

HPA PEAK POWER MONITOR

GENERAL QUESTIONS AND ANSWERS

Q: SCOTT GRIFFITH (Allied Pilots Association) - In view of present FAA regulatory requirements, what economic incentives do the airlines have to explore new wind shear measurement technologies i.e., predictive and/or combined systems?

A: GUICE TINSLEY (FAA) - The expected benefit from predictive systems would be safety benefits and the expanded capabilities resulting from the detection of clear air turbulence. However, there is a long term economic benefit resulted from improved safety.

Q: FRANK DREW (Lockheed Austin Division) - Has the FAA committed to regard current reactive systems as compliant once predictive systems are real and affordable? If not, what kind of reaction time will the industry be given once predictive systems are real and affordable?

A: GUICE TINSLEY (FAA) - It is impossible to clearly forecast the future. However, based on past experience and assuming no catastrophic events that would require change of the wind shear equipment rule, both reactive and predictive systems are allowed and considered in compliance with the rule.

Q: ED LOCKE (Thermo Electron Technologies) - Will there be any new LIDAR device R & D funding available in '91 and '92 for better and cheaper LIDAR concepts?

A: ROLAND BOWLES (NASA Langley) - There is not likely to be any out-of-house funding. There is the possibility of in-house funding to accelerate the 2 micron work. We also would want to leverage that 2 micron work against space applications which is another significant need from a NASA perspective, other than just airborne wind shear detection.

Q: WALT OVEREND (Delta Airlines) - How are we to reconcile that all of the airline aircraft or a great majority will be equipped with reactive wind shear systems? For a fleet of 450 airplanes the cost will be, or is, $25 to $30 million dollars. Research efforts are now far behind the requirements established some 5 years ago.

A: ROLAND BOWLES (NASA Langley) - NASA can't reconcile that. You, the industry, perhaps have something to say about that. I think that the way to answer this is that the FAA in showing a great deal of flexibility and has decided to waiver the equipment rule for four U.S. carriers. Frank Tullo from Continental stated who those people were. That gives an additional period of time for the technology to mature, for you guys to get out and work and see what can be put in the marketplace that will satisfy a requirement for predictive wind shear detection. My feeling is that we've got 8 months to write a TSO for this equipment, if we ain't got it in 8 months, forget it. I think what we need to do is write an aviation system requirement and the sensor technology that fits will surface. It's a question of performance for acceptable cost. Our program in NASA is to get out and make those kinds of measurements, with systems that represent at least the class of technology that is on the horizon, and to provide that data uniformly to the industry and you make your decisions.

Q: PAT ADAMSON (Turbulence Prediction Systems) - Will you give me that Doppler radar is inferential and is not a direct measure of velocity?

PRECEDING PAGE BLANK NOT FILMED

79-80

A: ROLAND BOWLES (NASA Langley) - We've been arguing about this. I have made many comments that one of the things that was difficult to grasp was the inferential nature of an IR device in terms of estimating a wind. From my view point, the impedance match there is not very clear. But the physics now are supporting that kind of inferential measurement. It's got to be validated over a whole range of atmospheric conditions and other things. I'd like to get the radar and the laser people into this because I have often said that these are direct measurement devices and Pat argues that they are still inferential. You've got to understand pretty carefully the motion of the raindrop as it's forced by the wind. It has its own dynamics. And the aerosol, who knows what it's doing. Are pulse Doppler active measurement devices direct measurement devices or is there still some inferential nature to the characteristic of the measurement?

BRUCE MATTHEWS (Westinghouse) - I'm not going to exactly treat the question but I'm going to try to take it somewhere. The idea of inference may not be as direct as you've stated your question here. I think in a more general sense all sensors are going to make some inference about the hazards along the glide slope and that may be more the point. Roland was talking yesterday about the antenna beam being lifted as the airplane came down in altitude. That means that the radar is going to be pointing its main beam in a path near where the airplane is going to fly. It's going to infer what the hazard is along that glide slope from measurements made near the expected trajectory of the airplane. That will be an inference. Categorically that seems just as much an inference as the IR is making about a down draft inferred from temperature applying to the glide slope of the airplane.

UNKNOWN - If we understand the question right, the question is can we get a direct measure of the wind velocity. As the wind is coming down there is this a down draft which before it hits the ground, starts spreading out. Now, how long will it take before the rain drops pick up the velocity of the wind? We did some studies that showed that the time constant was of the order of 2 or 3 seconds. So the rain drops are following the wind velocity very closely. So based on that, I would say that the radar would give a direct measure.

PAT ADAMSON (Turbulence Prediction Systems) - Not to carry this too far, but with Doppler you've got the size of the volumetric sample, the pulse repetition frequency which determines the aliasing, and the turbulence or the vortex within the bin that's measured. I'm not saying it's not a good estimate, I don't mean that and I haven't argued that at all. But it is by no means a direct measurement of the velocity of the winds. It's a mean estimate of the spectral distribution returned to the receiver. Over most cases that's probably pretty good. I have a real problem with direct measurement with any remote sensor. It is not a direct measurement. It's an inference based on some physical principle. There are a lot of errors as we saw on the talk just a little while ago. As you get low signal to noise those inferences and those assumptions tend to go down.

Q: RICHARD DOBINSKY (Sky Council) - There are three basic techniques that are being discussed to detect wind shear; radiometric techniques, laser and radar. Are there any other techniques, and if so elaborate on these.

A: ROLAND BOWLES (NASA Langley) - There has been work done by the French on sound detection and ranging, large low frequency, infra-sound. We've done some work at the center on infra-sound. We can sit at Langley Research Center and listen to the shuttle take off at the Cape using low frequency sound. I think that is beyond the scope of what we're trying to do in our program. Typically you would think they would be ground based, so it's FAA's problem.

Q: RICHARD DOBINSKY (Sky Council) - Please summarize the trade off comparisons, strengths and weaknesses of each of the three detection techniques.

A: ROLAND BOWLES (NASA Langley) - That's what the conference has been all about over the last several years. My view is they are all going to work to some degree. I think some circumstantial evidence is now being developed along those lines. If things go according to the plan Mike Lewis laid out, we're going to have a lot to say about these at the next conference. I would like to point out one other thing. If you listened carefully you could see a little bit of an anomaly in some of the questions I was raising with regard to reactive systems. We raise questions about wether the people who operate them and have certified them really have a convincing case that can be made about their validity. That's an open question. I do believe it is possible to engineer devices and that the industry has engineered devices that make very good energy change measurement systems for airplanes. Reasonable men can then debate at what level of energy change we annunciate alerts and how do we trade it off. In NASA's program, we're not building a reactive warning system, we're building a reactive measurement system for airplane energy change that will become a standard by which we try to assess, to some degree, the validity of our forward look devices. It seems to me that it is imperative in our program that we establish that what a forward look sensor sees at time t the airplane will experience at $t+\tau$ seconds, where τ is positive. If not, the whole concept of prediction is flawed. You would have to make decisions on information that would not be a reliable indicator or trend setter for what would happen to you if you elected to continue. It's just fundamental. I think the Orlando experiment is the first ever a demonstration that that hypothesis may be true for one particular electro-optical technique. That's a winner. In other words, reactive systems when properly implemented should satisfy Newton's law and I'm going to stay with Newton. He hasn't been wrong yet if you treat him right.

Q: RICHARD DOBINSKY (Sky Council) - Can you choose an optimum configuration or technique to focus R & D upon?

A: ROLAND BOWLES (NASA Langley) - In other words, what will be NASA's criteria to reject a technology. Within the time and money we've got to work the program, if it don't work we're going to reject it. It's got to provide measurement performance that at least satisfies what we would consider a success criteria for measurement performance. I think all three of these technologies are going to work to some degree. There is always going to points on the envelope where you can fool the instrument perhaps. But then that raises the question of how many missed alert are too much and how many nuisance alerts are too much? I think an example for us to learn from is the trials and tribulations that the TDWR guys have gone through. They've done a remarkable job of sorting that out. Look at what they're doing, they're getting out in the field year in and year out and collecting data. It's the only way you can refine answers to those kinds of questions. You've got to get out and collect data.

Q: SUSAN KIM (Boeing) - With regards to the extension obtained requested by the four airlines what happens if when the extension period is up, the new forward looking technology is not defined sufficiently to equip those aircraft which don't have wind shear alerting systems? (Will they then be required to equip with reactive systems while the forward looking effort continues?)

A: HERB SCHLICKENMAIER (FAA) - As I understand it, if at the end of the evaluation period there does not seem to be "sufficient progress", then the program for that wavered airline turns into a reactive schedule starting up as if it happened on that date.

ROLAND BOWLES (NASA Langley) - I would like to make a comment on that. Given the current cost of money, that policy could save somebody a fair amount of bucks. One might wonder why some or all of the airlines didn't leap in.

Q: **MIKE TAYLOR (Boeing)** - Can the airborne Doppler radar distinguish between a microburst event and a tornado?

A: **STEVE CAMPBELL (MIT Lincoln Laboratory)** - It is worth noting that the TDWR in our test bed and I believe also the Mile High radar, have been running a prototype tornado vortex signature algorithm. One problem you have running that is, of course, that you have very few data points. There were some tornadoes out in Denver in 1987 or '88. In fact, as one of the microburst algorithm developers I was proud to announce that we detected some of those tornadoes as microbursts as well. I would think you should be able to do it with a technique similar to what's done for the TVS algorithm.

UNKNOWN - From a cockpit perspective, a tornado has a classic signature on a weather radar. I don't think that Doppler is really necessary for that, assuming we keep weather radar in the aircraft.

ROLAND BOWLES (NASA Langley) - We should never take weather radar out of the cockpit, I'll agree with you there.

CLOSING REMARKS

ROLAND BOWLES (NASA Langley) - There is a lot of sensitivity about stand alone forward look versus not stand alone. My feeling is, and I've always said it, many people have said it, and I've heard myself say it many times, "reactive systems technology is non throw away". Policy gets in the question here at some point. But it's non throw away technology. That doesn't mean that there may not end up a predictive technology that may stand alone. What gets involved here is corporate policy, airline operations, how industry wants to respond to it, a lot of different things. I think progress is being made in all three areas of the sensor technology. I think what can be done by an appropriate synthesis of the ground based technology, as LLWAS and TDWR gets integrated, and how we can move those kinds of products to the flight deck to the benefit of both operations and safety, the prospects are very bright in that. I think the point is our task is simple for the next year. We're going to put these sensors on. We've decided what they are. The hardware is being cut. This is the last big funding bulge in our program because hardware tails off next year and then it's mainly operating the airplane, making measurements and hopefully doing a thorough analysis and presentation of results to you, the industry. The course is set for us, a lot of work to be done on the NASA side. I still would feel that somehow a process has to be put together to really write down the aviation system requirement for predictive systems. We can't linger on that one. It's got to be done here in the next 8 to 10 months.

I appreciate all of you coming. I think it has been a good conference. By the way there were 188 people cumulative, not maybe 188 in a room at any one given instant, but most of them, some of them stayed in the bar a lot. This has been a real good turn out. It's been the largest turn out of any of these conferences to date. I think the one thing that encourages me is that at the first meeting a few years ago, NASA and the FAA were doing all the talking by and large. Now we're to the point where, if you looked at the agenda carefully, there was a 50/50 split between industry speaking and other government agencies speaking and people like NCAR and Lincoln Labs. Perhaps next time it will even be dominated by an industry response. The problem is really one where we owe you technical answers to well understood and well posed technical questions. But eventually its marketplace dynamics and manufacturers willing to bite the bullet , take the risk, build and certify, that's going to do it.

PAT ADAMSON (Turbulence Prediction Systems) - From the industry standpoint, I just want to reemphasize that if we're not active we will not have predictive sensors. It's going to take more than the government side or the NASA side or the FAA side. It's going to take the people that are in this room and others to not go home and forget and say, well somebody else will deal with it. It needs to be dealt with if you want predictive sensors. The product is driven by whether you can sell it. The retrofit market is one of the incentives for people like myself and others to get into this thing. So we've got to get after this problem. Not just not talk about it but do something about it.

ROLAND BOWLES (NASA Langley) - One final precaution here. You know we've declared victory at least twice or so on this problem and it always comes back. We ought to be very careful here, with the capital investment we've all made in this, not to declare victory prematurely and walk away from it. I think that this time we ought to have some answers that ought to stand the test of time.

HERB SCHLICKENMAIER (FAA) - I harken back to when I was one of the advisors in the National Academy of Sciences review of low altitude wind shear, coming down to a place in Tidewater, Virginia, where they kind of know something about airplanes, and

85,86

talking with an expert panel of people on the airplane side of the problem. There were heads of research organizations that were giggling at the concept in 1982 and '83 of remotely detecting a hazardous wind shear phenomena. I'll humbly submit there was still the question on the table of what does hazardous mean. There were questions about the size, there were questions about the concept. A program was borne in '86 where we finally sat down and decided to just answer the question that the National Research Council posed. If radar won't work then we'll write that up. Over the course of time we were fortunate enough to expand our horizon and take a look at the technologies available from LIDAR and infrared. We are now to the point where the last question in a conference on airborne wind shear detection technology is not will, but can the airborne Doppler radar distinguish between a microburst and a tornado. There's an inference there that we've already solved the problem. We've come a tremendous way and as Roland has indicated there is more to go. Yes, I have been associated with other programs where success was declared early and came back to have to eat those words. You're going to make this work. It's a safety program that I think we can pull the national resources together to address. And, barring certain shortfalls in travel funds I trust that we and the rest of the FAA will be able to partake wholeheartedly in this very exciting and last venture in aviation safety. Thank you very much.

PAUL KELLY (21st Century Technology) - Herb, I think I speak for everybody when I say we'd like to ask you and Roland to communicate to your respective chains of command the appreciation and gratitude of all of us who have attended this conference. We have been real impressed with the material that's been presented and we want you to know that you guys, in our opinion, did a very good job. We want also not to forget all your staff and the Bionetics personnel who assisted you. We are really very grateful and you are to be wholeheartedly commended.

Appendix - List of Attendees

PRECEDING PAGE BLANK NOT FILMED

89-92

THIRD COMBINED MANUFACTURERS' AND TECHNOLOGISTS' AIRBORNE WIND SHEAR REVIEW MEETING

OCT 16 - 18, 1990

Mr. David Aalfs
Electrical and Computer Engineering
Clemson University
Clemson, SC 29634-0915
803-656-3190

Mr. H. Patrick Adamson
Turbulence Prediction Systems
3131 Indian Road
Boulder, CO 80301
303-443-8157

Msr. Bernard Ades
Direction Generale de l'Aviation Civile
DGAC/SFACT/P
246 rue Lecourbe
75732 Paris CEDEX 15
FRANCE
33-140434264

Mr. Orville J. Alitz
Rockwell International
Collins Air Transport Div.
M/S 124-111
400 Collins Road, NE
Cedar Rapids, IA 52498
319-395-3885

Mr. Farzin Amzajerdian
Litton Aero Products
Mail Station 6
6101 Condor Drive
Moorpark, CA 93021-2699
805-378-2643

Dr. Willard W. Anderson
NASA Langley Research Center
Guidance and Control Division
MS 479
Hampton, VA 23665-5225
804-864-1718

Mr. Zachary Applin
NASA Langley Research Center
Hampton, VA 23665-5225

Capt. Ed Arbon
Flight Safety Foundation
2200 Wilson Blvd., Suite 500
Arlington, VA 22201-3306
703-522-8300

Mr. P. Douglas Arbuckle
NASA Langley Research Center
MS 489
Hampton, VA 23665-5225
804-864-4072

Mr. Yves Aurenche
ONERA
Service DES/80
BP M072
92322 Chatillon Cedex
FRANCE
33-45-34-75-01

Mr. Sheldon Baron
BBN Systems & Technologies
10 Moulton Street
Cambridge, MA 02138
617-873-3235

Dr. Joseph J. Barrett
Allied-Signal Inc.
P.O. Box 1021R
Morristown, NJ 07960
201-455-5149

Mr. John A. Bartlom
Smiths Industry
255 Great Valley Parkway
Malvern, PA 19355
215-296-5000

Mr. James Bash
Honeywell, Inc.
MS 2G27ES
P.O. Box 21111
Phoenix, AZ 85036-1111
602-869-6493

Mr. C. Don Bateman
Sundstrand Data Control, Inc.
15001 N.E. 36th Street
P.O. Box 97001
Redmond, WA 98073-9701

Prof. Ernest G. Baxa, Jr.
Electrical and Computer Engineering
Clemson University
Clemson, SC 29623-0915
803-656-5900

Mr. Rod Benoist
Litton Aero Products
MS 6
6101 Condor Drive
Moorpark, CA 93021-2699
805-378-2018

Ms. Gaudy M. Bezos
NASA Langley Research Center
Subsonic Aerodynamics Branch
MS 286
Hampton, VA 23665-5225
804-864-5083

Mr. Cleon Biter
National Center for Atmospheric Research
Research Applications Program
P.O. Box 3000
Boulder, CO 80307-3000
303-497-8437

Dr. David L. Bjorndahl
Litton Aero Products
MS 12
6101 Condor Drive
Moorpark, CA 93021-2699
805-378-2004

Mr. L. Thomas Bleasdale
Manager, Marketing RF Products
Honeywell
P.O. Box 21111
Phoenix, AZ 85036
602-869-2396

Mr. Jean Louis Boulay
ONERA
Service OP
BP M072
92329 Chatillon cedex
FRANCE

Dr. Roland L. Bowles
NASA Langley Research Center
Vehicle Operations Research Branch
MS 156A
Hampton, VA 23665-5225
804-864-2035

Mr. Emedio M. Bracalente
NASA Langley Research Center
MS 490
Hampton, VA 23665-5225
804-864-7975

Mr. Ruy L. Brandao
Allied-Signal Aerospace Co.
Bendix/King Air Transport Avionics Div.
2100 NW 62nd. Street
Fort Lauderdale, FL 33309
305-928-3408

Mr. James R. Branstetter
Federal Aviation Administration
FAA/ADS-142
NASA Langley Research Center
MS 250
Hampton, VA 23665-5225

Mr. Philip Brockman
NASA Langley Research Center
MS 468
Hampton, VA 23665-5225
804-864-1554

Mr. Raymond S. Calloway
NASA Langley Research Center
Mail Stop 471
Hampton, VA 23665-5225
804-864-1679

Dr. Steven D. Campbell
MIT Lincoln Laboratory
MS HW-16
244 Wood Street
P.O. Box 73
Lexington, MA 02173-0073
617-981-3386

Mr. Thomas G. Campbell
NASA Langley Research Center
Antenna & Microwave Research Branch
MS 490
Hampton, VA 23665-5225
804-864-1772

Mr. Bryan Campbell
NASA Langley Research Center
Subsonic Aerodynamics Branch
MS 286
Hampton, VA 23665-5225

Mr. Ralph Cokeley
Lockheed Aeronautical Systems Company
Dept 98-10, Bldg 608, Plant 10
1011 Lockheed Way
Palmdale, CA 93550
805-572-2452

Msr. Philippe Conti
Dassault Aviation
Flight Test
B.P. 28
13801 Istres Cedex
FRANCE
42-56-91-10

Mr. Robert C. Coston
NASA Langley Research Center
MS 493
Hampton, VA 23665-5225
804-864-1413

Mr. H. Leslie Crane
MITRE Corporation
MS W376
7525 Colshire Drive
McClean, VA 22102
703-883-7243

Ms. Lucille H. Crittenden
Research Triangle Institute
610 Thimble Shoals Blvd.
Suite 203B
Newport News, VA 23606
804-864-1776

Mr. James Daily
Honeywell, Inc.
MS N30303
2111 N. 19th Avenue
Phoenix, AZ 85027
602-869-1758

Mr. John B. Carocari
BENDIX/KING
Allied-Signal Inc.
400 N. Rogers Road
Olathe, KS 66062-1212
913-782-0400

Ms. Rachel Colleu
Aerospatiale
E/DET/SY/AVIC
316 Route de Bayonne
31060 Toulouse Cedex 03
FRANCE
011-33-61-937404

Mr. Larry Cornman
National Center for Atmospheric Research
Research Applications Program
P.O. Box 3000
Boulder, CO 80307-3000
303-497-8439

Mr. Norman L. Crabill
Aero Space Consultants
105 Inland View Dr.
Newport News, VA 23603-1431
804-887-9339

Dr. Jeremiah F. Creedon
NASA Langley Research Center
Flight Systems Directorate
MS 113
Hampton, VA 23665-5225

Mr. Harold Curtis
Kollsman
403 Sage Bluff Circle
San Antonio, TX 78216
512-494-5652

Mr. Ernie Dash
ST Systems Corporation
1919 Commerce Drive, Suite 100
Hampton, VA 23666-4269
804-825-0292

Dr. Victor E. Delnore
Lockheed Engineering & Sciences
NASA Langley Research Center
MS 490
Hampton, VA 23665-5225
804-864-1812

Mr. Lawrence M. Denton
Raytheon
1501 Crystal Dr, # 1028
Arlington, VA 22202
703-415-1177

Mr. Thomas D. Deriso
Delta Airlines Inc.
Hartsfield Airport
Operations Center, Dept 044
Atlanta, GA 30320
404-765-4020

Dr. Manohar D. Deshpande
Vigyan, Inc.
NASA Langley Research Center
MS 490
Hampton, VA 23665-5225
804-864-1774

Mr. Charles Dobbs
Technology Planning, Inc.
51 Monroe Street
Suite 1609
Rockville, MD 20850
301-340-9310

Mr. Alain Donzier
REMTECH
P O Box 2423
Longmont, CO 80502
303-772-6325

Mr. Frank M. Drew
Lockheed Missiles and Space Company, Inc
6800 Burleson Road
Austin, TX 78744-1016
512-386-2188

Dr. Richard N. Dubinsky
Sky Council
689 Indian Road, 3rd Floor
Toronto, Ontario
CANADA
M6P 2E1
416-767-5156

Mr. R. Earl Dunham
NASA Langley Research Center
Flight Research Branch
MS 247
Hampton, VA 23665-5225

Ms. Dana J. Dunham
NASA Langley Research Center
Subsonic Aerodynamics Branch
MS 286
Hampton, VA 23665-5225

Dr. Peter J. Eccles
The MITRE Corporation
Principal Engineer, W194
7525 Colshire Drive
McLean, VA 22102-3481
703-883-7817

Mr. Chester L. Ekstrand
The Boeing Company
M/S 24-23
P.O. Box 2707
Seattle, WA 98124-2207
206-555-6969

Mr. Lawrence J. Englert
Kollsman
2121 Spring Creek Parkway
Suite 220
Plano, TX 75023
214-618-3454

Mr. Carl W. Erickson
Boeing Commercial Airplane Company
MS 47-31
P.O. Box 3707
Seattle, WA 98124-2207

Ms. Kaete S. Erskine
The MITRE Corporation
MS W276
Civil Systems Division
7527 Colshire Drive
McLean, VA 22101
703-883-7298

Mr. Steven A. Faltz
MS 490
NASA Langley Research Center
Hampton, VA 23665-5225
804-864-1850

Dr. W. Michael Farmer
The Bionetics Corporation
4309 Mission Bell
Las Cruces, NM 88001
505-521-1121

Mr. George W. Flathers, II
The MITRE Corporation
MS W376
7525 Colshire Drive
McLean, VA 22102-3481
703-883-6707

Mr. Andres Fraga
Eastern Airlines
Miami International Airport
Miami, FL 33148
305-873-2438

Mr. John F. Garren
NASA Langley Research Center
Flight Management Division
MS 153
Hampton, VA 23665-5225

Mr. K. Scott Griffith
Allied Pilots Association of
American Airlines
12160 Penderview Terrace #1104
Fairfax, VA 22033
703-385-7684

Mr. William A. Guenon, Jr.
Raytheon Company
Suite 1500
1215 Jefferson Davis Highway
Arlington, VA 22202-3256
703-486-5400

Mr. Robert W. Hall, Jr.
Air Line Pilots Association
Engineering & Air Safety
P.O. Box 1169
Herndon, VA 22070-1169
703-689-4205

Mr. Fred Faxvog
Manager of Sensors
Honeywell SRC
3660 Technology Drive
MN 65-2600
Minneapolis, MN 55418
612-782-7704

Mr. Paul B. Forney
Lockheed Missiles & Space Company
Mail Stop 97-20/281
3251 Hanover Street
Palo Alto, CA 94304
415-424-2121

Mr. C. Mikel Gale
American Airlines, Inc.
Avionics Engineering, MD #567
P.O. Box 582809
Tulsa, OK 74158-2809
918-292-2188

Mr. Jeffrey M. Gillberg
Honeywell Inc.
Systems and Research Center
3660 Technology Drive
MN65-2500
Minneapolis, MN 55418
612-782-7572

Mr. Michael H. Grove
Sundstrand Data Control, Inc
15001 NE 36th St
Redmond, WA 98073-9701
206-861-3084

Mr. Gregory P. Haeffele
Boeing Commercial Airplane Group
P.O. Box 3707
MS 7H-92
Seattle, WA 98124-2207
206-865-6425

Prof. R. John Hansman
Massachusetts Institute of Technology
Dept. of Aeronautics & Astronautics
Room 33-115
Cambridge, MA 02139

Mr. Avi Harpaz
SETI Inc.
430 Stump Road
Montgomeryville, PA 18936
215-855-8522

Mr. Steven D. Harrah
NASA Langley Research Center
Antenna & Microwave Research Branch
MS 490
Hampton, VA 23665-5225
804-864-1805

Mr. Michael K. Harris
Lockheed Aeronautical Systems Co.
P.O. Box 551
Bldg 63G, Dept 75-53
Plant A-1
Burbank, CA 91510
818-847-5686

Mr. Tom Henry
220 Daniel Webster Highway
Merrimack, NH 03054
603-886-2291

Mr. Brian Hill
WTKR-TV
720 Boush St
Norfolk, VA

Mr. David A. Hinton
NASA Langley Research Center
Vehicle Operations Research Branch
MS 156A
Hampton, VA 23665-5225
804-864-2040

Mr. Ray Hood
National Aeronautics and Space Admin.
Code RC
Washington, DC 20546
202-453-2745

Mr. Eugene A. Howell
United Technologies Optical Systems
P.O. Box 109660
West Palm Beach, FL 33410-9660
407-775-4299

Dr. R. Milton Huffaker
Coherent Technologies, Inc.
3300 Mitchell Lane, Suite 330
Boulder, CO 80301

Mr. Robert L. Ireland
Resident Representative at Boeing
United Airlines c/o Boeing
Mail Stop 65-34
P.O. Box 3707
Seattle, WA 98124
206-433-4105

Mr. Patrick W. Johnson
American Electronics, Inc.
9332 Annapolis Road
Lanham, MD 20706-3113
301-459-4343

Mr. Claude R. Keckler
NASA Langley Research Center
MS 479
Hampton, VA 23665-5225
804-864-1718

Dr. Wayne H. Keene
Raytheon Company
Electro-Optics/Strategic Systems Dir.
MS 1K9
528 Boston Post Road
Sudbury, MA 01776
508-440-2561

Mr. Roy Koll
Rosemount Aerospace
14300 Judicial Road
Burnsville, MN 55337
612-892-4546

Mr. Paul P. Kelly
21st Century Technology
International Square
1825 Eye Street, N.W.
Suite 400
Washington, D.C. 20006
202-429-2079

Mr. Bruce R. Kendall
NASA Langley Research Center
Antenna & Microwave Research Branch
MS 490
Hampton, VA 23665-5225
804-864-1795

Ms. Susan C. Kim
Boeing Commercial Airplanes
Renton Division Avionics/Flight Systems
P.O. Box 3707
Seattle, WA 98124-2121
206-393-8097

Mr. Michael C. Krause
Raytheon Company
Mail Stop 1655
528 Boston Post Road
Sudbury, MA 01776
508-440-3171

Mr. Kapriel V. Krikorian
M/S RE/R-11 9025
Hughes Aircraft Company
P.O. Box 92426
Los Angeles, CA 90009-2426
213-607-5491

Mr. Daryal Kuntman
Allied-Signal Aerospace Company
Bendix/King Air Transport Avionics Div.
2100 NW 62nd Street
Fort Lauderdale, FL 33309
305-928-3417

Mr. James L. Kurtz
Georgia Tech Research Institute
Radar and Instrumentation Dev. Lab.
Atlanta, GA 30332
404-528-7690

Mr. Julian H. Kushnick
Allied-Signal Inc
PO Box 1021R
Morristown, NJ 07962-1021
201-455-2361

Mr. William G. Laynor
National Transportation Safety Board
TE-2, Rm. 824C
800 Independence Ave., SW
Washington, DC 20594

Msr. Christian Le Roux
DGAC/STNA
246 rue Lecourbe
75738 Paris
FRANCE
33-1-40434849

Mr. James F. Lemon
M/S RE/R-10/12036
Hughes Aircraft Company
P.O. Box 92426
Los Angeles, CA 90009-2426
213-334-3284

Mr. Michael S. Lewis
NASA Langley Research Center
Mail Stop 265
Hampton, VA 23665-5225
804-864-7655

Mr. Edward V. Locke
Thermo Electron Technologies
74 West St.
Waltham, MA 02254-9046
617-622-1378

Mr. James G. Mages
Northwest Airlines, Inc.
E7400
Mpls - St. Paul IAP
St. Paul, MN 55101
612-726-8819

Msr. Jacques Mandle
SEXTANT Avionique, DN
25 Rue J. Vedrines
26027 Valence CEDEX
FRANCE
3375798776

Mr. Bruce D. Mathews
Westinghouse DEC
Box 746
MS 1157
Baltimore, MD 21203
301-765-6236

Capt. Alvah S. Mattox Jr.
Allied Pilots Association
Rt 1 Box 258
Weyers Cave, VA 24486

Mr. Mike H. McClendon
American Airlines
MD 843, Flight Academy
P.O. Box 619617
DFW Airport, TX 75261-9617
817-967-5253

Mr. W. Edward Melson
NASA Goddard Space Flight Center
Wallops Flight Facility
Wallops Island, VA 23337
804-824-1306

Mr. Robert W. Meyer
Raytheon Company
430 Boston Post Road
MS CC10
Wayland, MA 01778
508-440-1018

Mr. Bruce C. Montag
Southwest Research Institute
6220 Culebra Road
San Antonio, TX 78251
512-522-5001

Mr. Sandeep Mulgund
Princeton University
D202 Engineering Quadrangle
Princeton, NJ 08544-5263
609-258-5340

Dr. Loren D. Nelson
OPHIR Corporation
Suite 100
3190 South Wadsworth Blvd.
Lakewood, CO 80227
303-986-1512

Mr. Cornelius O'Connor
MS 343
NASA Langley Research Center
Hampton, VA 23665-5225

Dr. John McCarthy
National Center for Atmospheric Research
P.O. Box 3000
Boulder, CO 80307-3000
303-497-8422

Dr. Burnell T. McKissick
NASA Langley Research Center
Vehicle Operations Research Branch
MS 156A
Hampton, VA 23665-5225
804-864-2037

Capt. William Melvin
Air Line Pilots Association
1101 W. Morton
Denison TX 75020

Mr. Ernest W. Millen
Director
Chancelwyn Research
390 Rivers Ridge Circle
Newport News, VA 23602
804-888-0880

Mr. Samuel A. Morello
NASA Langley Research Center
Flight Management Division
MS 153
Hampton, VA 23665-5225

Mr. Hans Muller
Sundstrand Data Control
PO Box 97001
Redmond, WA 98073-9701
206-891-3069

Mr. A. M. H. Nieuwpoort
Fokker Aircraft B.V.
P.O. Box 7600, Dept. EDAA (S029-32)
Schiphdpyk 231
1117 ZJ Schiphol-Oost
THE NETHERLANDS
31-20-6052149

Mr. Saburo Onodera
Japan Air lines
2-1-1 Hanedakuko Ohta-Ku
Tokyo 144
JAPAN
81-3-747-3357

Ms. Rosa M. Oseguera
NASA Langley Research Center
Vehicle Operations Research Branch
MS 156A
Hampton, VA 23665-5225
804-864-2039

Mr. W. J. Overend
Delta Airlines
C/O Engineering Dept.
Atlanta International Airport
Atlanta, GA 30320
404-765-3103

Mr. Walter W. Patterson
Westinghouse Electric Corporation
MS 1295
P.O. Box 746
Baltimore, MD 21203
301-765-3459

Mr. Bill Peltola
Sundstrand Data Control, Inc.
15001 N.E. 36th Street
P.O. Box 97001
Redmond, WA 98073-9701
206-885-8625

Mr. Jeff Pierro
NASA Langley Research Center
Hampton, VA 23665-5225

Dr. Fred Proctor
MESO, Inc.
28 Research Drive
Hampton, VA 23666
804-865-7800

Dr. Mark A. Richards
Georgia Institute of Technology
GTRI/MAL/SPB/CCRF/5-206
Atlanta, GA 30332
404-528-7711

Mr. Roy E. Robertson
Rockwell International
Collins Air Transport Division
M/S 124-111
400 Collins Road, NE
Cedar Rapids, IA 52498
319-395-1990

Dr. Robert G. Otto
Lockheed Missiles and Space Co., Inc.
O/97-01, 201, 2
3251 Hanover Street
Palo Alto, CA 94304-1191
415-424-2148

Mr. Eric C. Palmer
McDonnell Douglas
3855 Lakewood Boulevard
Long Beach, CA 90846
213-593-3298

Mr. Andy Peczalski
Honeywell
MN 09-B100
10701 Lyndale Ave., S
Bloomington, MN 55420

Mr. Ian W. Philpott
M/S 106-207
Rockwell International
400 Collins Road, NE
Cedar Rapids, IA 52498
319-395-3881

Mr. Greg Piesinger
Honeywell, Inc.
MS 021D4
P.O. Box 21111
Phoenix, AZ 85036
602-869-6168

Mr. Fred Remer
University of North Dakota
Department of Atmospheric Science
P.O. Box 8216
University Station
Grand Forks, ND 58202
701-777-2291

Mr. Terry M. Riley
Serv-Air, Inc.
P.O. Box 6669
Greenville, TX 75403-6669
214-454-2000

Mr. Paul Robinson
Flight Management Division
NASA Langley Research Center
MS 156A
Hampton, VA 23665-5225
804-864-2031

Dr. Donald R. Rogers
Turbulence Prediction Systems
3131 Indian Road
Boulder, CO 80301
303-443-8157

Mr. Robert N. Romine
Lockheed Missiles & Space Company, Inc.
6800 Burleson Road
Austin, TX 78744-1016
512-386-2255

Capt. Brian K. Ryder
United Airlines Flight Center
Stapleton International Airport
Denver, CO 80207
303-780-5201

Mr. Greg Salottolo
National Transportation Safety Board
800 Independence Ave., SW
Washington, DC 20594

Mr. Philip R. Schaffner
NASA Langley Research Center
MS 490
Hampton, VA 23665-5225
804-864-1809

Mr. Blaine Schmidt
E-Systems Engineering
2268 South 3270 West
Salt Lake City, Utah 84119
801-973-4300

Mr. Nelson Seabolt
NASA Langley Research Center
Hampton, VA 23665-5225

Mr. Syed T. Shafaat
Boeing Commerical Airplane Corp
PO Box 3707, MS01-82
Seattle, WA 98124-2207
206-342-3121

Mr. Robert R. Roll
Lockheed Missiles & Space Company
3251 Hanover Street
Palo Alto, CA 94304-1191
415-424-3042

Mr. Robert A. Rosen
M/S RE/R-11/8035
Hughes Aircraft Company
P.O. Box 92426
Los Angeles, CA 90009-2426
213-334-3284

Mr. Samuel P. Saint
Safe Flight Instrument Corporation
Shelter Harbor
Westerly, RI 02891

Dr. Wayne Sand
National Center for Atmospheric Research
Research Applications Program
P.O. Box 3000
Boulder, CO 80307-3000
303-497-8454

Mr. Herbert W. Schlickenmaier
Federal Aviation Administration
ARD-200, Room 712
800 Independence Ave., SW
Washington, DC 20591

Mr. Lyle C. Schroeder
NASA Langley Research Center
MS 490
Hampton, VA 23665-5225
804-864-1832

Mr. Andrew Serrell
Air Safety Foundation
809 Ocean Pines
Berlin, MD 21811

CAPT Samuel L. Shirck
Continental Airlines
CPO G-162
P.O. Box 92044
Los Angeles, CA 90009
213-646-3947

Mr. Bernard B. Silverman
Active EO System Analysis
3075 Rivera Drive
Delray Beach, FL 33445
407-265-3860

Dr. Peter C. Sinclair
Colorado State University
Atmospheric Science Department
Fort Collins, CO 80523
303-491-8679

Mr. Nigel P. Slack
British Aerospace Ltd
Airlines Division
Comet Way
Hatfield, Hertfordshire AL10 9TL
ENGLAND
707-62345-3744

Mr. David Sobota
144 Research Dr
Hampton, VA 23666

Mr. David Soreide
Boeing Corporation
MS 7J-05
P.O. Box 3999
Seattle, WA 98124
206-865-3144

Dr. M. G. Stapelbroek
Rockwell International Corporation
Science Center D/781, 031-BC17
3370-Miraloma Avenue
P.O. Box 3105
Anaheim, CA 92803-3105
714-762-4528

Dr. Leo D. Staton
NASA Langley Research Center
Antenna & Microwave Research Branch
MS 490
Hampton, VA 23665-5225
804-864-1793

Dr. Robert F. Stengel
Princeton University
D202 Engineering Quadrangle
Princeton, NJ 08544-5263
609-258-5103

Mr. Stephen A. Stoll
2805 Warbler Pl
Williamsburg, VA 23185

Mr. Mark E. Storm
ST Systems Corporation
NASA Langley Research Center
MS 474
Hampton, VA 23665-5225

Mr. D. Alex Stratton
Princeton University
D202 Engineering Quadrangle
Princeton, NJ 08544-5263
609-258-5340

Mr. Russell Targ
Lockheed R&D
0/97-01
3251 Hanover Street
Palo Alto, CA 94304
415-424-2436

Mr. Michael W. Taylor
Boeing Commercial Airplane Company
MS 2T-61
P.O. Box 3707
Seattle, WA 98124-2207
207-544-5203

Ms. Despina Tsouka
National Technical University of Athens
Faculty of Civil Engineering
5 Iroon Polytechniou Street
GR 15773 Athens
GREECE
01-777-4085

Mr. Frank Tullo
ATA
G162
7300 World Way West
Los Angeles, CA 90009
213-646-4195

Msr. Jean-Claude Valentin
DGAC/STNA
246 Rue Lecourbe
75732 Paris
FRANCE
33140434934

Mr. Edward J. Vertaschitsch
Boeing Aerospace & Electronics
P.O. Box 3999
MS 7J-65
Seattle, WA 98124-2499
206-865-3983

Mr. Edgar G. Waggoner
NASA Langley Research Center
Subsonic Aerodynamics Branch
MS 286
Hampton, VA 23665-5225

Mr. Craig Wanke
MIT
Room 37-438
77 Massachusetts Ave
Cambridge, MA 02144
617-253-0993

Mr. Howard T. Williams
Gulfstream Aerospace Corporation
M/S D-04
P.O. Box 2206
Savannah, GA 31402-2206
912-964-3224

Dr. Marilyn Wolfson
MIT Lincoln Laboratory
Room HW-25
P.O. Box 73
Lexington, MA 02173-0073
617-981-3409

Mr. John Wright
Continental Airlines
8451 Travelair, Building 8
Houston, TX 77061
713-640-5108

Mr. John Tuttle
Kollsman
5464 Villas Drive
Bonsall, CA 92003
619-945-1873

Mr. Everette E. Vermilion
Sundstrand Data Control, Inc.
15001 N.E. 36th Street
P.O. Box 97001
Redmond, WA 98073-9701

Mr. Dan D. Vicroy
NASA Langley Research Center
Vehicle Operations Research Branch
MS 156A
Hampton, VA 23665-5225
804-864-2022

Mr. Robert Walkinshaw
Bendix/King Air Transport Avionics Div.
P.O. Box 9327
Ft. Lauderdale, FL 33309
305-928-2370

Mr. Norman White
Kollsman Corporation
MS 2-B11-1
220 Daniel Webster Highway
Merrimack, NH 03054
603-886-2685

Mr. Jason Witow
Optical Air Data Systems
9572 Topanga Canyon Blvd.
Chatsworth, CA 91311
818-997-3636

Mr. Daniel L. Woodell
Rockwell International Corp.
Avionics Group
400 Collins Road, NE
M/S 106-207
Cedar Rapids, IA 52498
319-395-3090

Mr. Thomas J. Wright
E-Systems, Inc.
Monter Division
2268 South 3270 West
Salt Lake City, UT 84119
801-974-7275

Mr. John S. Wyler
Smith Industries
255 Great Valley Parkway
Malvern, PA 19355
215-296-5000

Mr. Joe Youssefi
Honeywell
M/C N30D3
21111 N. 19th Avenue
Phoenix, AZ 85027
602-869-1557

Mr. J. Allen Zak
ST Systems Corporation
NASA Langley Research Center
MS 250
Hampton, VA 23665-5225
804-864-6397

Mr. Carl H. Young
Eastern Air Lines, Inc.
Mgr., Flight Test
Bldg. 30, MIAFR
Miami, FL 33148
305-873-7060

Mr. Vincent Zahornasky
Kollsman
M/S 1L04-2
220 Daniel Webster Hwy.
Merrimack, NH 03054-4809
603-595-6040

Mr. Terry Zweifel
Honeywell
M/S N30D3
21111 N. 19th Avenue
Phoenix, AZ 85027
602-869-2979

Report Documentation Page

1. Report No. NASA CP-10060, Part 2 DOT/FAA/RD-91/2-II	2. Government Accession No.	3. Recipient's Catalog No.

4. Title and Subtitle Airborne Wind Shear Detection and Warning Systems - Third Combined Manufacturers' and Technologists' Conference	5. Report Date January 1991
	6. Performing Organization Code
7. Author(s) Dan D. Vicroy; Roland L. Bowles; and Herbert Schlickenmaier, compilers	8. Performing Organization Report No.
	10. Work Unit No. 505-64-12
9. Performing Organization Name and Address NASA Langley Research Center Hampton, VA 23665-52225	11. Contract or Grant No.
	13. Type of Report and Period Covered Conference Publication
12. Sponsoring Agency Name and Address National Aeronautics and Space Administration Washington, DC 20546	14. Sponsoring Agency Code

15. Supplementary Notes

Dan D. Vicroy; and Roland L. Bowles: NASA Langley Research Center, Hampton, Virgin
Herbert Schlickenmaier: Federal Aviation Administration, Washington, DC

16. Abstract

The Third Combined Manufacturers' and Technologists' Conference was hosted jointly by NASA Langley Research Center (LaRC) and the Federal Aviation Administration (FAA) in Hampton, Virginia, on October 16-18, 1990. The meeting was co-chaired by Dr. Roland L. Bowles of LaRC and Herbert Schlickenmaier of the FAA. The purpose of the meeting was to transfer significant ongoing results of the NASA/FAA joint Airborne Wind Shear Program to the technical industry and to pose problems of current concern to the combined group. It also provided a forum for manufacturers to review forward-look technology concepts and for technologists to gain an understanding of the problems encountered by the manufacturers during the development of airborne equipment and the FAA certification requirements. The present document has been compiled to record the essence of the technology updates and discussions which followed each.

17. Key Words (Suggested by Author(s)) Microbursts Wind Shear Aircraft Hazards Doppler Radar Infrared LIDAR	18. Distribution Statement Unclassified-Unlimited Subject Category: 03

19. Security Classif. (of this report)	20. Security Classif. (of this page)	21. No. of pages	22. Price
Unclassified	Unclassified	505	A22

NASA FORM 1626 OCT 86

For sale by the National Technical Information Service, Springfield, Virginia 22161-2171

END

DATE

FILMED

JUL 25 1991